DOPAMINE TRANSPORTER AND GABA RECEPTOR REGULATION OF STRIATAL DOPAMINE RELEASE

Bethan O'Connor

Department of Physiology, Anatomy and Genetics

Oxford-MRC DTP

Balliol College

University of Oxford

Thesis submitted for the degree of

Doctor of Philosophy

Hilary Term 2025

Table of Contents

Statement of Authorship

This thesis does not contain any material that has been accepted for the award of any other degree in any University or other institution. All data represented in this thesis are fully my own work, and where data has been contributed by others their contribution is stated below and in the main text.

The data included in Chapter 3, Section 3.1.2. were collected and analysed by Dr. Emanuel Lopes, a former PhD student and postdoctoral researcher in the laboratory of Prof. Stephanie Cragg. These data are included with Dr. Lopes' full permission and are identified in the corresponding figure legends.

The data included in Chapter 3, Section 3.3.4. were collected and analysed by Sayon Choudhuri, a former FHS pre-clinical medicine student in the laboratory of Prof. Stephanie Cragg. These data are included with Mr. Choudhuri's full permission and are identified in the corresponding figure legends. Data in Section 3.3.4. also includes data from Section 3.1.2., which was collected and analysed by Dr. Emanuel Lopes, as outlined above.

The data included in Chapter 5, Section 5.2.2. were collected by Wenhui Wu, a former research assistant in the laboratory of Prof. Stephanie Cragg. These data are included with Ms. Wu's full permission and are identified in the corresponding figure legends.

The data included in Chapter 5, Section 5.2.7. was in part collected in collaboration with Lucille Duquenoy, a current PhD student in the laboratory of Prof. Stephanie Cragg, whilst establishing voltage indicator imaging as a technique to the laboratory. These data are included with Ms. Duquenoy's full permission and are identified in the corresponding figure legends.

Conference abstracts

O'Connor, B. M., Lopes, E. F., Brimblecombe, K. R., & Cragg, S.J. Convergent regulation of presynaptic short-term plasticity in striatal dopamine release by dopamine transporters and GABA receptors. Monitoring Molecules in Neuroscience (MMiN), Lyon, France, 2022.

O'Connor, B. M., Lopes, E. F., Duquenoy, L., Hao, Y. A., Lee, S., Lin, M. Z., Brimblecombe, K. R., & Cragg, S.J. Convergent regulation of dopamine release by striatal dopamine transporters and GABA receptors. Federation of European Neuroscience Societies (FENS) Forum, Vienna, Austria, 2024.

Publications

Brimblecombe, K. R., Connor-Robson, N., Bataille, C. J. R., Roberts, B. M., Gracie, C., **O'Connor, B.**, Te Water Naude, R., Karthik, G., Russell, A. J., Wade-Martins, R., & Cragg, S. J. (2024). Inhibition of striatal dopamine release by the L-type calcium channel inhibitor isradipine co-varies with risk factors for Parkinson's. European Journal of Neuroscience, 59(6), 1242–1259. https://doi.org/10.1111/ejn.16180

Duquenoy, L.[†], **O'Connor, B.**[†], & Cragg, S. J. (2024). Voltage sensor imaging in a population of dopaminergic axons in the mouse striatum. Protocols.io. https://doi.org/10.17504/protocols.io.rm7vzxp6rgx1/v1

[†] authors are co-first authors and contributed equally to this work

Acknowledgements

I would like to take this opportunity to thank Professor Stephanie Cragg for supporting me to undertake a research project in her laboratory, and for all of the mentorship, guidance, and enthusiasm for science. I would like to thank Dr. Katherine Brimblecombe, for her mentorship and expertise, but also for her on-demand technical support and encouragement, whenever I needed it.

I am thankful for many members of the Cragg laboratory, both past and present, for not only teaching me techniques and giving guidance with experiments, but also for being great friends. I would like to particularly mention Shinil Raina, Jess Livesey, and Lucille Duquenoy, who all started in the Cragg laboratory around the same time as I did, and have made the PhD process so much more enjoyable over the last three and a half years. I would like to thank Lucille Duquenoy for taking the time and effort to establish a new technique with me, and for all of her imaging and coding expertise. I can't say that each other's company kept us sane during the voltage sensor troubleshooting, but at least we were going crackers together! I am grateful to the people who contributed to this project, including Dr. Emanuel Lopes and Sayon Choudhuri.

I would like to thank the Lin laboratory at Stanford University for providing ASAP voltage indicators, and the Wickman laboratory at the University of Minnesota, for providing GIRK2$^{flox/flox}$ mice. I am grateful to the Biomedical Services staff for all of their work regarding animal care and breeding, and I would like to acknowledge the mice used in this thesis. I am immensely appreciative of my previous mentors and lab mates in the Young and España laboratories, for all of the opportunities and guidance that helped me get to where I am today.

I am very grateful for the financial support I received, from the Balliol College Dan Norman Scholarship, the Oxford Medical Research Council Doctoral Training Partnership (Oxford-MRC DTP) and the Department of Physiology, Anatomy and Genetics.

A big thank you to my parents, and sister, who have always supported me and my scientific curiosity, and enabled me to pursue great opportunities, and to my friends in different countries, who are always there for a chat and to hear me complain about experiments.

I am especially grateful for my husband, Nick, who not only took on full-time roles as chef, cleaner, and launderette while I wrote this thesis, but who has been a constant source of support and encouragement in whatever I am doing, and moved to the U.K. and got married just to be with me during this PhD. I'm happy to report I'm almost finished!

Abstract

Mesostriatal dopamine (DA) neurons form extensive axonal arbours in the striatum, where DA signalling plays a key role in basal ganglia function and dysfunction. To understand striatal DA signalling, it is imperative to investigate the diverse, interacting mechanisms that govern DA release and uptake. DA transporters (DATs) have varied, complex roles, not only governing the extracellular lifetime of DA, but also shaping DA release probability and its short-term plasticity. The striatum is enriched in γ-aminobutyric acid (GABA)-containing neurons, where GABA mediates tonic inhibition of striatal DA release and also modestly regulates short-term plasticity. DATs and GABA receptors (GABA-Rs) appear to operate some parallel functions, limiting striatal DA release probability and axonal activation, yet supporting the frequency-dependence of DA release. I investigated whether DATs and GABA-Rs co-operate to determine striatal DA release. Work presented in this thesis used fast-scan cyclic voltammetry and imaging of genetically-encoded fluorescent voltage indicators in mouse striatum *ex vivo* to explore the convergent regulation of DA release by DATs and GABA-Rs, and to test directly whether DATs modulate axonal excitability.

In the dorsal striatum, I found that GABA-Rs support DAT-mediated changes to DA release, without affecting DA uptake, whereas in the ventral striatum, co-operation between DATs and GABA-Rs was not readily apparent. I subsequently explored the contribution of G protein-gated inwardly rectifying K^+ (GIRK) channels to the control of DA release by DATs and GABA-Rs. Finally, I show that DAT-mediated currents modulate axonal membrane potential, in a manner consistent with governing short-term plasticity in DA release. These findings indicate that striatal DA axons integrate signalling from DATs and GABA-Rs to shape axonal excitability and DA output.

Abbreviations

$[Ca^{2+}]_o$	Extracellular Ca^{2+}
$[DA]_o$	Extracellular dopamine
$[K^+]_o$	Extracellular K^+
4-AP	4-Aminopyridine
6-OHDA	6-hydroxydopamine
AAV	Adeno-associated virus
ACh	Acetylcholine
aCSF	Artificial cerebrospinal fluid
AHP	Afterhyperpolarisation
AIS	Axon initial segment
ALDH	Aldehyde dehydrogenase
ASAP5	Accelerated Sensor of Action Potentials version 5 sensor
AUC	Area under the curve
BK	Big conductance Ca^{2+} activated K^+ channel
CaMKI	Ca^{2+}/calmodulin-dependent protein kinase I
CaMKII	Ca^{2+}/calmodulin-dependent protein kinase II
cAMP	Cyclic AMP adenosine monophosphate
ChI	Cholinergic interneuron
cpGFP	Circularly-permuted green fluorescent protein
D_1-like-R	D_1-like dopamine receptor
D_2-like-R	D_2-like dopamine receptor
DA	Dopamine
DAT	Dopamine transporter
DBS	Deep brain stimulation
dDAT	*Drosophila melanogaster* dopamine transporter
DHβE	Dihydro-β-erythroidine
DLS	Dorsolateral striatum
DMS	Dorsomedial striatum
EMCCD	Electron-mutiplying charge-coupled device
EP	Entopeduncular nucleus
EPSP	Excitatory postsynaptic potential
fAHP	Fast afterhyperpolarisation
FOV	Field of view

FSCV	Fast-scan cyclic voltammetry
GABA	γ-aminobutyric acid
$GABA_A$-R	γ-aminobutyric acid A receptor
$GABA_B$-R	γ-aminobutyric acid B receptor
GABA-Rs	γ-aminobutyric acid receptors
GAD	Glutamate decarboxylase
GAT	γ-aminobutyric acid transporter
GIRK	G protein gated inwardly rectifying K^+ channel
GPCR	G protein-coupled receptor
GPe	Globus pallidus externus
GPi	Globus pallidus internus
HCN	Hyperpolarisation-activated cyclic nucleotide-gated channel
hDAT	Human dopamine transporter
hDAT	Human dopamine transporter
HEK	Human embryonic kidney
IK	Intermediate conductance Ca^{2+} activated K^+ channel
IPI	Inter-pulse interval
IPSC	Inhibitory postsynaptic current
IPSC	Inhibitory postsynaptic current
KO	Knockout
LeuT	Leucine transporter
LTCC	L-type voltage-gated calcium channel
mAHP	Medium afterhyperpolarisation
MSNs	Medium spiny neurons
MβCD	Methyl-β-cyclodextrin
NAcC	Nucleus accumbens core
nAChR	Nicotinic acetylcholine receptor
NAcSh	Nucleus accumbens shell
NALCN	Na^+ leak channel
NMDA	N-methyl-D-aspartate
NPA	Nipecotic acid
NSS	Neurotransmitter sodium symporter
P1	First pulse in paired-pulse stimulation paradigm
P2	Second pulse in paired-pulse stimulation paradigm

PD	Parkinson's disease
PIP_2	Phosphatidylinositol-4,5-bisphosphate
PPR	Paired-pulse ratio
PTT	2β-propanoyl-3β-(4-tolyl)-tropane
rDAT	Rat dopamine transporter
rDAT	Rat dopamine transporter
ROI	Region of interest
sAHP	Slow afterhyperpolarisation
SEM	Standard error of the mean
SK	Small conductance Ca^{2+} activated K^+ channel
SM	Sec1/Munc18-like
SNARE	Soluble *N*-ethylmaleimide-sensitive factor attachment protein receptor
SNc	Substantia nigra pars compacta
SNCA-OVX	Mouse model overexpressing human α-synuclein
SNr	Substantia nigra pars reticulata
SNX27	Sorting nexin 27
STD	Short-term depression
STF	Short-term facilitation
STN	Subthalamic nucleus
Synapsin TKO	Synapsin I, II, and III triple knockout
Tetrodotoxin	TTX
TRP	Transient Receptor Potential
VGCC	Voltage-gated Ca^{2+} channel
VGKC	Voltage-gated K^+ channel
VGSC	Voltage-gated Na^+ channel
VMAT2	Vesicular monoamine transporter 2
V_{max}	Maximal DA uptake rate
VTA	Ventral tegmental area

Chapter 1.

Introduction

1.1. Thesis overview

DA in the basal ganglia plays a key role in fundamental processes such as motivation, action selection, and movement. DA neurons originating in the midbrain form vast axonal arbours in the striatum, presenting opportunity for local axonal regulation of DA signalling by diverse interacting mechanisms. A major player in the regulation of DA signalling is the DAT, which not only gates DA uptake, but also modulates initial DA release, and re-release. Release from striatal DA axons is under tonic inhibition by GABA acting at GABA-Rs, yet activity at GABA-Rs can paradoxically support DA re-release. It is currently unclear whether striatal DA axons incorporate information from DATs and GABA-Rs to determine DA output. Exploring these mechanisms not only contributes to our understanding of the healthy brain, but may have implications for disorders such as Parkinson's disease (PD) or substance-use disorders.

In Chapter 3, I use fast-scan cyclic voltammetry to explore the convergent regulation of DA release by DATs and GABA-Rs. In Chapter 4, I use fast-scan cyclic voltammetry and expand this line of enquiry to test the involvement of G protein-gated inwardly rectifying K^+ (GIRK) channels in the control of DA release by DATs and GABA-Rs. In Chapter 5, I use fast-scan cyclic voltammetry and a newly developed genetically-encoded fluorescent voltage indicator, ASAP5 (Hao et al., 2024), to explore whether DATs regulate DA axonal membrane potential and whether this is consistent with the role of DATs in mediating short-term plasticity in DA release. Finally, I test whether GABA-Rs or GIRK channels play a role in modulating DA axonal membrane potential in the striatum.

1.2. The basal ganglia and striatum

1.2.1. Connectivity and function of the basal ganglia

The basal ganglia are a collection of subcortical nuclei, and can be divided into dorsal and ventral divisions (Bolam et al., 2000). The dorsal nuclei consist of the dorsal striatum, globus pallidus externus (GPe) and internus (GPi), subthalamic nucleus (STN) and substantia nigra pars compacta (SNc) and pars reticulata (SNr) (Bolam et al., 2000; Rocha et al., 2023). The GPi in primates is equivalent to the entopeduncular nucleus (EP) in rodents (Bolam et al., 2000; Tepper et al., 2007). The ventral nuclei consist of the ventral striatum, ventral pallidum and ventral tegmental area (VTA) (Bolam et al., 2000). The predominant input to the basal ganglia comes from the cortex and thalamus, and predominant output of the basal ganglia comes from the SNr and GPi (Tepper et al., 2007). The striatum sits in the middle of these structures, receiving cortical and thalamic input and subsequently signalling to the SNc, GPe, GPi and SNr (Tepper et al., 2007; Rocha et al., 2023) (Fig. 1.1). Transmission of information through the basal ganglia occurs through 'direct' and 'indirect' pathways (Albin et al., 1989; DeLong, 1990; Smith et al., 1998). In the 'direct' pathway, information is passed from cortical regions, to the striatum, to the output nuclei, whereas in the 'indirect' pathway, information is passed to the output nuclei through a series of other structures including the GPe and STN (Shink et al., 1996; Bolam et al., 2000). The balance between these two pathways is governed by dopamine (DA) acting at excitatory or inhibitory receptors in the striatum (DeLong & Wichmann, 2007). The basal ganglia nuclei are involved in behaviours such as action selection (Balleine & Ostlund, 2007; Howard et al., 2017), motivation (Mogenson et al., 1980; Wise, 2004) and motor control (Marsden, 1982; Rocha et al., 2023). On the other hand, basal ganglia dysfunction contributes to disorders such as Parkinson's disease (PD; DeLong & Wichmann, 2007), Huntington's disease (Matz et al., 2022), and substance-use disorders (Robinson & Berridge, 1993; Berke & Hyman, 2000).

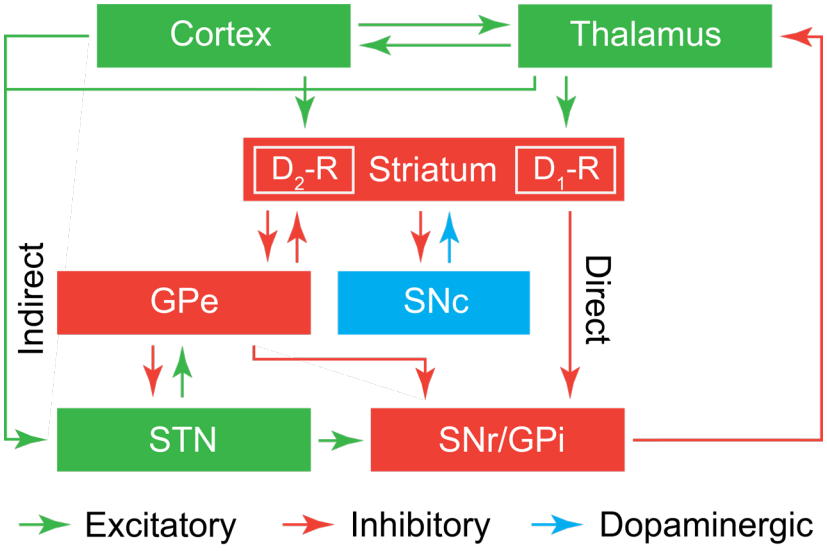

Figure 1.1. Basal ganglia connectivity
Simplified schematic of basal ganglia connectivity. DA in the striatum signals to downstream nuclei through the direct and indirect pathways. Green projections are excitatory glutamatergic projections. Red projections are inhibitory GABAergic projections. Blue projections are DA projections.
D_1-R = DA D_1 receptor containing medium spiny output neurons, D_2-R = DA D_2 receptor containing medium spint output neurons, GPe = globus pallidus externus, SNc = substantia nigra pars compacta, STN = subthalamic nucleus, SNr = substantia nigra pars reticulata, GPi = globus palllidus internus.

1.2.2. Anatomy and composition of the striatum

The striatum, as the main input nucleus of the basal ganglia (E. Benarroch, 2016), is named as such due to the striped (striated) appearance it exhibits, as a consequence of the organisation of grey and white matter (Bamford & Bamford, 2019). The human and non-human primate striatum is anatomically separated into subdivisions, but in rodents this is not the case (Voorn et al., 2004; Obeso et al., 2014). The rodent striatum can, however, be functionally and neurochemically divided along dorso-ventral, ventro-medial, and rostro-caudal axes (Papa et al., 2002; Voorn et al., 2004; Burton et al., 2015; Pirino et al., 2024). Broadly, the major subdivisions of the rodent striatum are the dorsolateral striatum (DLS), dorsomedial striatum (DMS), nucleus accumbens core (NAcC) and nucleus accumbens shell (NAcSh) (Voorn et al., 2004; Burton et al., 2015) (Fig 1.2). The dorsal regions (DLS and DMS) are thought to be critical for goal-driven action selection and habit formation, whilst the ventral regions (NAcC and NAcSh) are involved in reward-based learning, although this is

a simplification, as there appears to be considerable overlap (Voorn et al., 2004; Benarroch, 2016). The striatum can also be neurochemically organised into striosome and matrix compartments, which are thought to, in part, differ in function (Crittenden & Graybiel, 2011; Brimblecombe & Cragg, 2017). Imbalances in signalling between striosome and matrix compartments may contribute to disorders of the basal ganglia (Crittenden & Graybiel, 2011).

Striatal output neurons integrate cortical and thalamic inputs with DA inputs from the SNc and VTA, then signal to downstream nuclei (Gittis & Kreitzer, 2012). Striatal GABAergic output neurons are known as spiny projection neurons, or medium spiny neurons (MSNs), and are divided into those which express D_1-like DA receptors (D_1-like-Rs) or D_2-like receptors (D_2-like-Rs) (Bolam et al., 2000; Gittis & Kreitzer, 2012). MSNs containing D_1-like-Rs are thought to release substance P and dynorphin, in addition to GABA, and form part of the 'direct' pathway, whereas D_2-like-Rs are thought to release enkephalin in addition to GABA, and form part of the 'indirect' pathway (Bolam et al., 2000; Gittis & Kreitzer, 2012). The striatum is predominantly a GABAergic structure, with up to ~98% of neurons being identified as GABAergic in rodents, although the percentage of MSNs in primates is lower (Kemp, 1968; Graveland & Difiglia, 1985; Tepper et al., 2007, 2010). In the rodent striatum, MSNs make up 95% of striatal neurons, with GABAergic interneurons comprising a further 2-3% (Graveland & Difiglia, 1985; Tepper et al., 2010). There are a variety of striatal GABAergic interneuron families, including the parvalbumin positive or fast spiking interneurons, the somatostatin/neuropeptide Y/nitric oxide synthase positive or low threshold spiking interneurons, the calretinin positive interneurons, tyrosine hydroxylase positive interneurons, neurogliaform interneurons, and 5HT3a receptor-containing interneurons (Tepper et al., 2010, 2018). Cholinergic interneurons make up a further 1-2% of the striatal neuron population (Bolam et al., 1984; Phelps et al., 1985; Goldberg & Wilson, 2016). The striatum also contains astrocytes, which functionally interact with several of these neuron types

(Khakh, 2019; Stedehouder et al., 2024). Striatal DA neurons receive not only cortical and thalamic inputs, but also signalling from all of these cell types, to inform striatal output.

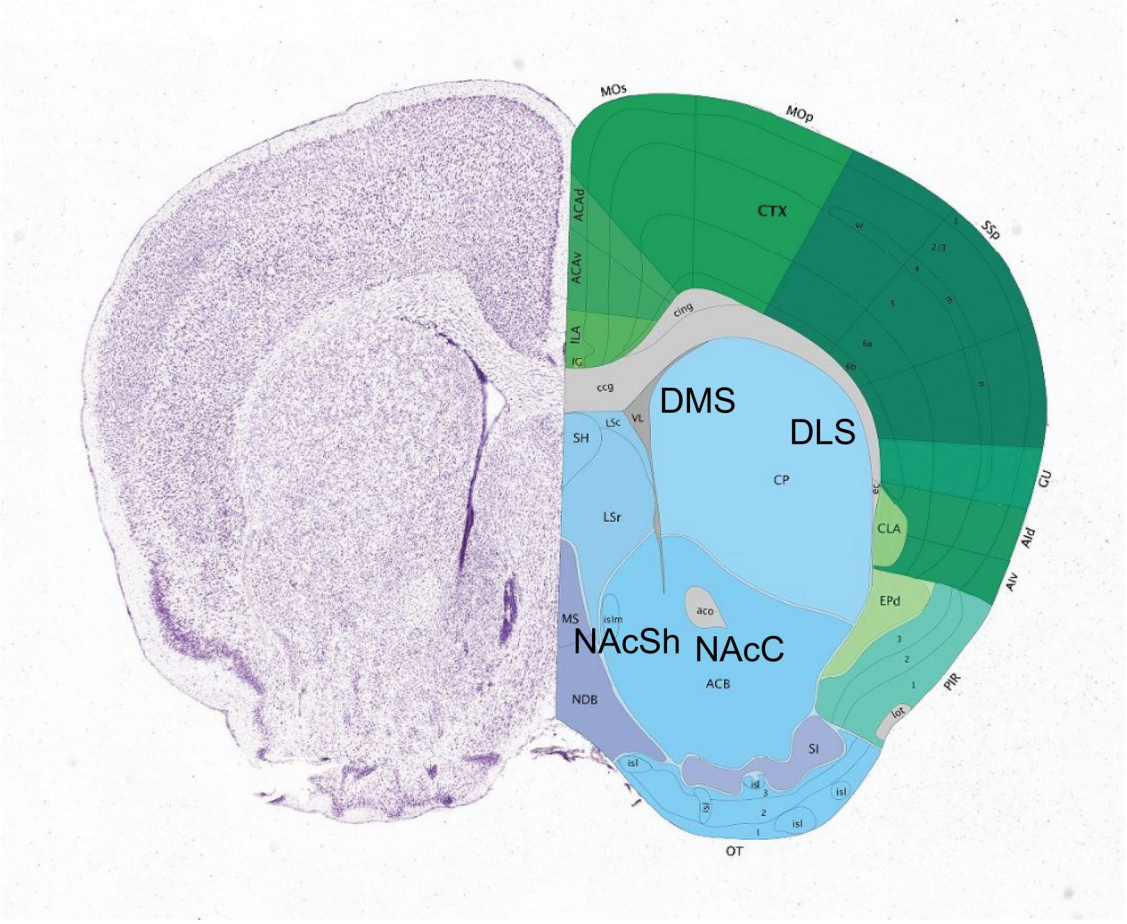

Figure 1.2. Coronal mouse brain section showing the striatum
Image showing a coronal mouse brain slice with Nissl-stain on the left hemisphere, and anatomical annotations on the right hemisphere. Dorsal striatum is labelled as caudate putamen (CP), and includes dorsolateral striatum (DLS) and dorsomedial striatum (DLS). Ventral striatum is labelled as the nucleus accumbens (ACB), and includes nucleus accumbens core (NAcC) and nucleus accumbens shell (NAcSh). Image taken from the Allen Mouse Brain Reference Atlas.

1.3. Mesostriatal DA system

The mesostriatal DA system encompasses the nigrostriatal and mesolimbic DAergic pathways (Molochnikov & Cohen, 2014), in which DA neurons originate in the SNc and VTA, and generally project to dorsal and ventral regions of the striatum, respectively, although some overlap exists (Björklund & Dunnett, 2007). Broadly, these nigrostriatal and mesolimbic DA neurons are implicated in action selection (Balleine & Ostlund, 2007; Howard et al., 2017)

and reward learning (Schultz et al., 1997), and dysfunction in these neurons is associated with PD (Kish et al., 1988) and substance-use disorders (Robinson & Berridge, 1993).

1.3.1. DA signalling in the mesostriatal system

Somatodendritic and axonal DA release in the mesostriatal system is dependent on DA neuron firing pattern (Patel et al., 1992; Rice et al., 1997; Cragg, 2003; Beckstead et al., 2007; Condon et al., 2019). DA neurons *in vivo* are thought to exhibit one of three activity states at any given time; inactive, a slow or single spike pattern, and a burst firing pattern (Grace & Bunney, 1983a; Grace et al., 2007). Slow, tonic firing rate in DA neurons is in the region of 1-10 Hz, whereas burst, or phasic, firing rate is on average 20-40 Hz, although occasionally frequencies of up to 100 Hz can be reached in the presence of salient stimuli (Grace & Bunney, 1984; Freeman et al., 1985; Hyland et al., 2002).

Mesostriatal DA signalling predominantly operates via volume transmission, whereby DA 'spills over' into extrasynaptic sites (Cragg & Rice, 2004; Rice & Cragg, 2008; Rice et al., 2011). Consistent with this, in the striatum, up to 70% of DA containing varicosities are asynaptic (Descarries et al., 1996), although a portion of these release sites are likely to be non-functional, because striatal DA axons possess silent DA-containing varicosities (Pereira et al., 2016). DA mediates its effects through DA receptors, which are predominantly located extrasynaptically (Hersch et al., 1995; Yung et al., 1995; Caillé et al., 1996). DA uptake is mediated by DATs, which tend to be located extrasynaptically in the striatum and cortex (Hersch et al., 1997; Nirenberg et al., 1997; Sesack et al., 1997), to limit the radius of extracellular DA (Cragg & Rice, 2004). Regulation of DA transmission by DATs is introduced in more detail in Section 1.4.

1.3.2. DA receptors

DA signals through two families of G protein-coupled receptors (GPCRs), D_1-like- (D_1 and D_5) and D_2-like-Rs (D_2, D_3, and D_4) (Kebabian, 1978; Spano et al., 1978; Kebabian & Calne, 1979; Beaulieu et al., 2015; Martel & Gatti McArthur, 2020). Members of each receptor family share a high level of homology (Beaulieu & Gainetdinov, 2011), so whilst pharmacological tools easily differentiate between D_1-like-Rs and D_2-like-Rs, they tend not to be selective for receptor subtypes within the same family (Vallone et al., 2000; Beaulieu & Gainetdinov, 2011). D_1-like-Rs have 10-100 fold reduced affinity for DA compared to D_2-like-Rs, therefore the balance of D_1-like/ D_2-like recruitment is dynamic, depending on extracellular DA levels (Martel & Gatti McArthur, 2020).

D_1-like-Rs exhibit 7 transmembrane domains (Vallone et al., 2000) and upon binding of a substrate, stimulate $G\alpha_{s/olf}$ proteins and subsequently adenylyl cyclase, which increases cyclic adenosine monophosphate (cAMP) (Beaulieu & Gainetdinov, 2011; Beaulieu et al., 2015). The genes encoding D_1-like-Rs (in humans, DRD1 and DRD5) are intronless (Gingrich & Caron, 1993; Beaulieu & Gainetdinov, 2011). D_1-like-Rs are found postsynaptically and are thought to be more abundant in the brain than D_2-like-Rs, with the D_1 subtype more commonly expressed than the D_5 subtype (Grandy et al., 1990; Vallone et al., 2000; Martel & Gatti McArthur, 2020). The D_1 subtype is expressed in areas such as the striatum, SNc, amygdala, hippocampus, cortex, and more, and the D_5 subtype is expressed in regions such as the SNc, cortex, hippocampus, hypothalamus, and dentate gyrus (Beaulieu & Gainetdinov, 2011; Vallone et al., 2000).

D_2-like-Rs, like D_1-like-Rs, have 7 transmembrane domains (Vallone et al., 2000). Upon binding of a substrate, D_2-like-Rs couple to $G\alpha_{i/o}$ proteins and inhibit cAMP production (Beaulieu & Gainetdinov, 2011; Beaulieu et al., 2015; Martel & Gatti McArthur, 2020). D_2-like-Rs are expressed both postsynaptically and presynaptically, where they can function as

autoreceptors (Beaulieu & Gainetdinov, 2011). The genes encoding D_2-like-Rs (in humans, DRD2, DRD3, and DRD4) have several introns, providing opportunity for splice variants (Gingrich & Caron, 1993; Beaulieu & Gainetdinov, 2011). In rodents, D_2 receptors have two splice variants, D_{2L} (long) and D_{2S} (short) (Giros et al., 1989; Monsma et al., 1989; Picetti et al., 1997; Beaulieu et al., 2015), which differ in their coupling to G proteins (Żuk et al., 2020). D_{2L} appears to be predominantly postsynaptic, whereas D_{2S} appears to be predominantly presynaptic (Beaulieu & Gainetdinov, 2011). Alternative splicing of the D_3 receptor has also been reported in rodents, for two shorter variants, in addition to the prototypical D_3 receptor (Giros et al., 1991). The existence of D_4 receptor polymorphic variants have been reported in humans (Van Tol et al., 1992). The D_2 subtype is more prominent in the brain than D_3 or D_4 subtypes, with the D_2 receptor being expressed in areas such as the striatum, SNc, VTA, olfactory tubercle, hypothalamus, cortex, and amygdala (Beaulieu & Gainetdinov, 2011; Vallone et al., 2000). D_3 receptors are expressed in areas such as the NAcSh, islands of Cajella, hypothalamus, and cerebellum, and D_4 receptors are expressed in regions such as the amygdala, frontal cortex, hippocampus, and SNr (Beaulieu & Gainetdinov, 2011; Vallone et al., 2000). Further, DA receptors can heterodimerise with other DA receptor subtypes (for example, D_1-D_2, D_1-D_3, and D_2-D_4 receptor heterodimers), and with other receptor subtypes (for example, with adenosine GPCRs, to generate D_1-A_1 and D_2-A_2 heterodimers, and with N-methyl-D-aspartate (NMDA) receptors, to generate D_1-NR1 and D_2-NR2B complexes) (Perreault et al., 2014; Beaulieu et al., 2015).

1.3.3. Local regulation of DA release in the striatum

Nigrostriatal, and to a lesser extent, mesolimbic, DA neurons form vast, unmyelinated, axonal arbours in the striatum (Matsuda et al., 2009; Aransay et al., 2015a). DA release in the striatum is not simply a product of DA firing and inputs at the level of the soma, but rather, modulation of DA release can occur at the level of striatal axons (Sulzer et al., 2016). D_2-like-

Rs function as autoreceptors on DA axons, but in *ex vivo* mouse striatum, do not impact initial release, only limiting re-release at stimulus intervals of >1 s (M. D. Condon et al., 2019). DA release is profoundly regulated by acetylcholine (ACh) acting at β2-subunit-containing nicotinic ACh receptors (nAChRs), whereby activity at nAChRs promotes single pulse-evoked DA release, and limits DA release in response to high frequency stimulation (Rice & Cragg, 2004; Zhang & Sulzer, 2004). Striatal ACh can initiate spontaneous subthreshold excitation and action potentials in DA axons, driving DA release (Threlfell et al., 2012; Kramer et al., 2022; Liu et al., 2022).

A growing collection of evidence now demonstrates that striatal DA release is regulated by intrinsic mechanisms on DA axons, such as DATs (Venton et al., 2006; Condon et al., 2019; Threlfell et al., 2021) and voltage-gated Ca^{2+} channels (VGCCs) (Brimblecombe et al., 2015, 2024), other neurotransmitter systems, such as GABA (Pitman et al., 2014; Brodnik et al., 2019; Lopes et al., 2019; Roberts et al., 2021a), and adenosine (Roberts et al., 2022a), and neuropeptides, such as substance P (Brimblecombe & Cragg, 2015), among others. Regulation of striatal DA signalling by GABA-Rs and DATs will be introduced in more detail in Section 1.4 (DATs) and Section 1.5 (GABA-Rs).

1.3.4. Behavioural roles of mesostriatal DA

The behavioural roles of DA in the mesostriatal system span from goal-directed action selection (Balleine & Ostlund, 2007; Howard et al., 2017) to locomotion and spontaneous movement (Dodson et al., 2016; Howe & Dombeck, 2016), to reward learning (Schultz et al., 1997; Schultz, 2013). Early studies exploring the role of DA was guided by the discovery that the brains of patients with PD exhibited loss of DAergic innervation (Ehringer & Hornykiewicz, 1960; Kish et al., 1988) and that administration of levodopa, the precursor to DA, improved patients' symptoms (Barbeau, 1969). Early experiments revealed that nigrostriatal neurons signal movement onset (Schultz et al., 1983), and recent experiments have furthered our

understanding of the nuanced role that DA neurons play in motor control (Dodson et al., 2016; Howe & Dombeck, 2016; Coddington & Dudman, 2019; Markowitz et al., 2023; Cai et al., 2024). Another notable role of mesostriatal DA is to signal reward (Mirenowicz & Schultz, 1996; Schultz, 2007, 2013). Nigrostriatal and mesolimbic DA neurons encode reward prediction errors, whereby an unpredicted reward elicits more DA neuron activity and DA release than a predicted award, and that when a reward is predicted but not delivered, DA neurons pause their firing (Schultz et al., 1997; Schultz, 1998, 2007, 2016). Mesolimbic DA signalling encodes the salience of cues, and supports an escalation in drug intake, which can become habitual, due to nigrostriatal DA signalling (Poisson et al., 2021). Taken together, mesostriatal DA neurons play key roles in fundamental behaviours.

1.4. DATs in the striatum

1.4.1. Structure and function of DATs

DATs are plasma membrane monoamine transporters, responsible for uptake of DA following exocytosis (Masson et al., 1999; Mortensen & Amara, 2003a). DATs are members of the neurotransmitter sodium symporter (NSS) family, requiring Na^+ and Cl^- to translocate DA, with a stoichiometry of one DA molecule being transported with two Na^+ ions and one Cl^- ion (Krueger, 1990; McElvain & Schenk, 1992; Gu et al., 1994). Like other Na^+/Cl^--dependent transporters, and a bacterial homologue, the leucine transporter (LeuT), DATs have 12 transmembrane helices (Yamashita et al., 2005; Penmatsa & Gouaux, 2014; Penmatsa et al., 2013; Grouleff et al., 2015; Nepal et al., 2023; Srivastava et al., 2024). High resolution structural investigations have been performed for *Drosophila melanogaster* DAT (dDAT) and human DAT (hDAT), and reveal that in both species, transmembrane helices 1-5 and 6-10 are related by a pseudosymmetrical two fold axis (Penmatsa et al., 2013; Srivastava et al., 2024).

In addition to binding sites for DA, Na^+ and Cl^-, DATs exhibit binding sites for a plethora of other ligands, placing DATs in a central position to regulate DA signalling from many angles. DATs exhibit binding sites for DAT inhibitors such as cocaine (Beuming et al., 2008; Xu & Chen, 2020), nortriptyline (Penmatsa et al., 2013) and modafinil (Schmitt & Reith, 2011), but also cholesterol (Penmatsa et al., 2013), Zn^{2+} (Srivastava et al., 2024), α-synuclein (Lee et al., 2001), Ca^{2+}/calmodulin-dependent protein kinase II (CaMKII) (Fog et al., 2006), and G proteins (Rojas et al., 2020), among others.

DATs are electrogenic transporters, generating currents greater than anticipated for a transporter with a fixed stoichiometry of 1 DA/2 Na^+/1 Cl^- (Sonders et al., 1997; Ingram et al., 2002). DATs have been shown to exhibit channel-like behaviour that can depolarise neurons (Carvelli et al., 2004) and increase neuronal excitability (Ingram et al., 2002). DA uptake is associated with a transport-coupled, depolarising inward current, in hDAT expressing *Xenopus laevis* oocytes (Sonders et al., 1997) and in rat midbrain cultured DA neurons (Ingram et al., 2002). Mutations to the DAT N-terminal triggers an increase in frequency of these currents, and is associated with pathological behaviour in *C. elegans* (Carvelli et al., 2008). DATs also generate transport-uncoupled currents, which may or may not be distinct from a leak current (Sonders et al., 1997; Ingram et al., 2002; Carvelli et al., 2004; Rodriguez-Menchaca et al., 2012). Surprisingly, DAT-mediated transport uncoupled currents regulate neuronal excitability and do so via Cl^-, which is paradoxically depolarising (Ingram et al., 2002; Sulzer & Galli, 2003). Cocaine inhibits, yet amphetamine promotes, transport-uncoupled currents (Ingram et al., 2002). Investigating the context in which these currents occur is therefore not only essential for understanding DAT function, but also understanding the roles of DATs in substance use disorders (Vaughan & Foster, 2013). DAT-mediated currents are modified not only by cocaine and amphetamine, but also substrates such as arachidonic acid and α-synuclein (Sonders et al., 1997; Ingram & Amara, 2000; Ingram et al., 2002; Erreger et al., 2008; Swant et al., 2011; Rodriguez-Menchaca et al., 2012).

1.4.2. Regulation of striatal DA transmission by DATs

In the striatum, DATs spatially and temporally restrict DA transmission (Cragg & Rice, 2004). The canonical role of DATs is to mediate DA uptake, but the roles of DATs are far more complex than simply regulating the extracellular lifetime of DA. Classic studies utilising knockout of the DAT gene (*Slc6a3*, or *DAT1*) in mice, triggers a hyperdopaminergic state and hyperlocomotion (Giros et al., 1996). DAT knockout (KO) mice do not exhibit heightened locomotor behaviour in response to cocaine or amphetamine, as wildtype mice do, nor do these substances induce an increase in extracellular DA in the striatum in DAT KO mice (Giros et al., 1996). Striatal DA lifetime is vastly prolonged in DAT KO mice, with estimates that loss of DATs prolongs clearance time by 100-300x, compared to wildtype mice (Giros et al., 1996; Gainetdinov et al., 1999). However, pharmacological DAT inhibition not only protracts the amount of time DA is in the extracellular space, but also results in an increase in initial DA release (Venton et al., 2006; John & Jones, 2007; Kile et al., 2010; Daberkow et al., 2013; Condon et al., 2019), indicating that the roles of DATs are more complex than simply mediating DA uptake.

DAT inhibition by cocaine increases striatal DA release via mobilisation of a synapsin-dependent vesicle reserve pool in dorsal striatum, in intact brain recordings in anaesthetised mice (Venton et al., 2006; Kile et al., 2010), and in *ex vivo* mouse brain slices (Kile et al., 2010). Global knockout of synapsin I, II, and III (synapsin TKO) in mice prevents an increase in striatal DA release upon application of cocaine (Venton et al., 2006; Kile et al., 2010). In wildtype mice, cocaine can increase striatal DA release despite near-depletion of the readily releasable vesicle pool, indicating that DAT inhibition by cocaine mobilises a vesicle reserve pool, rather than interacting with the readily releasable pool (Venton et al., 2006). Synapsin TKO mice exhibit higher striatal DA release compared to their wildtype counterparts and DAT function displays increased dependence on extracellular Ca^{2+} in the recording solution

($[Ca^{2+}]_o$) (Kile et al., 2010). The observation that DAT inhibitors increase striatal DA release has now been extended beyond cocaine, and in both dorsal and ventral striatal regions, to include ligands such as methylphenidate, the cocaine analog 2β-propanoyl-3β-(4-tolyl)-tropane (PTT), nomifensine, GBR 12909, and GBR 12935 (John & Jones, 2007; España et al., 2008; Condon et al., 2019; Threlfell et al., 2021). Together, these findings demonstrate that when DATs are active, DAT-mediated immobilisation of a vesicle reserve pool limits striatal DA release.

DATs not only limit initial striatal DA release, but also regulate short-term plasticity in striatal DA release (Condon et al., 2019). Striatal DA release exhibits intrinsic short-term biphasic plasticity, across both dorsal and ventral regions of the striatum (Cragg, 2003; Chadchankar & Yavich, 2011; Da Cunha et al., 2017; Condon et al., 2019). In mouse *ex vivo* striatal slices, when the influence of nAChRs are removed, DA release exhibits short-term facilitation (STF) at shorter inter-pulse intervals (IPIs) (10-25 ms, corresponding to 40-100 Hz firing frequency) and short-term depression (STD) at longer interval (25-200ms, corresponding to 5-40 Hz firing frequency) (Condon et al., 2019). Specifically, in DLS, STF occurs at IPIs of 10ms, and STD at IPIs of 25-200 ms, and in NAcC, STF occurs at IPIs of 10-25 ms, and STD occurs at 100-200 ms (M. D. Condon et al., 2019). Whilst canonical accounts of neurotransmitter re-release at classic fast central synapses report an inverse relationship with initial release probability (Thomson, 2000), striatal DA re-release only exhibits an inverse relationship with release probability only at the shortest IPIs, when STF occurs (Condon et al., 2019). STF is somewhat dependent on $[Ca^{2+}]_o$, especially in NAcC, indicating a dependence on initial release probability, but STD is release-independent (Condon et al., 2019). Rather, STD is dependent on concentrations of external K+ in the recording solution ($[K^+]_o$), and involves voltage-gated K^+ channel (VGKC) activation, particularly in DLS (Condon et al., 2019). Short-term plasticity at classical fast synapses is introduced in Section 1.6.2.

DAT inhibition with cocaine, methylphenidate, or nomifensine prevents STF in DLS and NAcC and relieves STD in DLS, indicating that DATs promote re-release at short IPIs, and limit re-release at longer IPIs (Condon et al., 2019). Under DAT inhibition, a dependence on $[Ca^{2+}]_o$ is revealed in DLS, yet short-term plasticity is no longer dependent on $[K^+]_o$ in DLS or NAcC (Condon et al., 2019). These findings demonstrate that DATs limit $[Ca^{2+}]_o$-dependence of short-term plasticity, and promote $[K^+]_o$-dependence (Condon et al., 2019). In DLS, Ca^{2+} imaging utilising the genetically-encoded Ca^{2+} indicator, GCaMP6f (Chen et al., 2013), reveals that when DATs are active, intracellular Ca^{2+} levels are higher at IPIs of 10ms compared to 40ms, consistent with increased re-release at IPIs of 10 ms (Condon et al., 2019). However, when DATs are inhibited, Ca^{2+} levels are increased at IPIs of 40ms, equivalent to those observed at IPIs of 10 ms (Condon et al., 2019). Although Ca^{2+} imaging is an indirect measure of axonal activation, taken with the observation that DATs support $[K^+]_o$-dependent STD, these findings indicate that DATs might limit axonal activation to limit re-release at longer IPIs (Condon et al., 2019). This, however, has not directly been tested.

Collectively, DATs mediate striatal DA uptake, but also limit initial DA release, and govern short-term plasticity in DA release. Evidence indicates that these roles of DATs are not necessarily interdependent, and can be dissociated. For example, although synapsin TKO prevents DAT-mediated changes to release probability, uptake is unchanged in these mice (Kile et al., 2010). In *ex vivo* recordings in striatal slices from mice overexpressing α-synuclein (*SNCA*-OVX model for PD; Janezic et al., 2013), it was found that some aspects of DAT function is potentiated in these mice (Threlfell et al., 2021). DATs limit initial DA release probability to a greater extent in *SNCA*-OVX mice than in control mice, and DA uptake rate is faster (Threlfell et al., 2021). However, only minor changes to STF in striatal DA release were observed in these mice, and no differences were found to STD (Threlfell et al., 2021). Furthermore, following an intermittent access cocaine self-administration paradigm, DA uptake rate was increased in rat *ex vivo* striatal slices, yet no changes were observed to initial

DA release (Alonso et al., 2022). These findings underpin the complexity of DAT regulation of DA transmission.

The extent to which DATs co-operate with other intrinsic mechanisms on striatal DA axons, to determine DA release, is largely unknown. The large number of regulatory sites expressed by DATs means that it is plausible that transporter function is modulated by several distinct mechanisms on DA axons. DATs share several parallel functions with GABA-Rs; limiting DA release probability yet supporting frequency-dependence, and electrogenic properties. Surprisingly, K^+-mediated changes to short-term plasticity in striatal DA release are dependent on activity at both DATs and GABA-Rs (Condon et al., 2019; unpublished data, Dr. E. Lopes, Cragg lab). These parallel functions led us to consider whether DATs and GABA-Rs could co-operate to determine striatal DA output.

1.5. GABA-Rs in the striatum

1.5.1. Structure and function of GABA-Rs

GABA-Rs comprise two distinct subtypes, ionotropic $GABA_A$-Rs and metabotropic, G protein-coupled, $GABA_B$-Rs (Chebib & Johnston, 1999; Watanabe et al., 2002; Bettler et al., 2004; Jembrek & Vlainic, 2015). Sometimes, GABA signals in a phasic manner, where a high concentration of GABA is released to act precisely and quickly, and other times, GABA signals in a tonic manner, where lower concentrations of GABA 'spill over' to activate extrasynaptic receptors (Farrant & Nusser, 2005).

$GABA_A$-Rs are heteropentameric ion channels (Macdonald & Olsen, 1994; Nayeem et al., 1994; Watanabe et al., 2002), made up of a combination of $\alpha_{1\text{-}6}$, $\beta_{1\text{-}3}$, $\gamma_{1\text{-}3}$, δ, ε, θ, π, and $\rho_{1\text{-}3}$ subunits in humans, rats and mice (Simon et al., 2004; Olsen & Sieghart, 2008; Ghit et al., 2021), with each subunit exhibiting 4 transmembrane domains (Ernst et al., 2005; Ghit et al., 2021). Upon binding of a substrate to $GABA_A$-Rs, the channel pore opens and, principally,

allows flow of Cl^- ions according to the electrochemical gradient (Watanabe et al., 2002). This typically involves Cl^- flux inward, hyperpolarising the neuron, however, in some cases GABA mediates depolarisation instead (Watanabe et al., 2002). In immature neurons, intracellular Cl^- concentration is higher than the extracellular concentration, therefore, opening of $GABA_A$-Rs results in outward Cl^- flux and membrane depolarisation (Ben-Ari et al., 1989; Peerboom & Wierenga, 2021). $GABA_A$-R pore opening is also thought to allow flow of HCO_3^- ions according to their electrochemical gradient, which is typically outward (Kaila et al., 1993; Kaila, 1994; Perkins & Wong, 1996). GABA-mediated depolarisations are not necessarily excitatory, however, as $GABA_A$-Rs can operate shunting inhibition and inactivation of Na^+ channels, reducing input resistance (Zhang & Jackson, 1995; Kramer et al., 2020; Kilb, 2021).

$GABA_B$-Rs are heterodimers, made up of $GABA_B$R1 and $GABA_B$R2 subunits (Jones et al., 1998; Kaupmann et al., 1998; White et al., 1998), each exhibiting 7 transmembrane domains (Pin & Bettler, 2016; Terunuma, 2018). The $GABA_B$R1 subunit has various splice variants, identified as $GABA_B$R1a, b, c, e, j, k, l, m, and n, in humans (Lee et al., 2010), though the $GABA_B$R1a and $GABA_B$R1b variants appear to be the only forms conserved across species, including rat and mouse (Bettler et al., 2004). Upon binding of a substrate to $GABA_B$-Rs, one of several scenarios occurs. $GABA_B$-Rs couple to $G\alpha_{i/o}$ and $G\beta\gamma$ G proteins, which then affect either VGCCs, GIRK channels, or adenylyl cyclase (Bettler et al., 2004; Terunuma, 2018). It is typically thought that presynaptic $GABA_B$-Rs couple to VGCCs, and that when $GABA_B$-Rs are activated, they inhibit N type or P/Q type VGCCs and thus limit neurotransmitter release (Amico et al., 1995; Cardozo & Bean, 1995; Bettler et al., 2004; Terunuma, 2018). On the other hand, postsynaptic $GABA_B$-Rs are thought to couple to GIRK channels, mediating a slow inhibitory postsynaptic current (IPSC) upon activation of $GABA_B$-Rs (Lüscher et al., 1997; Schuler et al., 2001; Bettler et al., 2004; Terunuma, 2018). The third scenario is that, upon binding of GABA, $GABA_B$-Rs trigger G-protein mediated inhibition of adenylyl cyclase, although mixed results exist regarding whether $GABA_B$-R activation always results in

inhibition of adenylyl cyclase, as some studies have observed $GABA_B$-R-mediated stimulation of adenylyl cyclase (Simonds, 1999; Bettler et al., 2004; Terunuma, 2018). Taken together, $GABA_A$-Rs and $GABA_B$-Rs operate via distinct mechanisms to limit neurotransmitter release.

1.5.2. Regulation of striatal DA transmission by GABA-Rs

GABAergic neurons comprise ~98% of striatal neurons, made up of ~95% MSNs, and ~2-3% GABAergic interneurons (Kemp, 1968; Tepper et al., 2007, 2010). Mesostriatal DA neurons send extensively arbourised axons to the striatum, with average innervation of the striatum per axon at ~2.7% in rodents (Matsuda et al., 2009). ~2.7% of the striatum contains ~75,000 GABA-containing striatal neurons. Therefore, a single DA axon may be under influence from ~75,000 GABAergic neurons, and on the other hand, a single DA axon can influence the activity of ~75,000 GABAergic neurons. Understanding the interaction between DA and GABA signalling is therefore paramount to understanding basal ganglia function.

In the striatum, DA release is under inhibition by $GABA_A$-Rs and $GABA_B$-Rs (Schmitz et al., 2002a; Pitman et al., 2014; Brodnik et al., 2019; Lopes et al., 2019; Roberts et al., 2020, 2021a). Application of GABA decreases electrically-evoked DA release in DLS, in a concentration-dependent manner in mouse *ex vivo* brain slices (Lopes et al., 2019). Pharmacological activation of $GABA_A$-Rs by muscimol, a $GABA_A$-R agonist, or diazepam, a $GABA_A$-R positive allosteric modulator, attenuates striatal DA release in NAcC in rat *ex vivo* brain slices and in DLS and DMS in mouse *ex vivo* brain slices (Brodnik et al., 2019; Lopes et al., 2019; Kramer et al., 2020). In rat NAcC, $GABA_A$-R-mediated decreases in DA release seem to require activation of $GABA_B$-Rs (Brodnik et al., 2019). Pharmacological activation of $GABA_B$-Rs by baclofen, a $GABA_B$-R agonist, attenuates striatal DA release in DLS and NAcC, in mouse *ex vivo* brain slices (Pitman et al., 2014; Lopes et al., 2019). Further, striatal DA axons are under tonic inhibition by GABA in both DLS and NAcC (Lopes et al., 2019; Roberts et al., 2020). This is demonstrated by an augmentation in optogenetically- or electrically-evoked DA

release, upon application of GABA-R antagonists (Lopes et al., 2019; Roberts et al., 2020). In DLS, ambient GABA tone is regulated by GABA transporters (GATs) on striatal astrocytes (Roberts et al., 2020). Striatal GABA-Rs not only limit initial DA release, but also support the frequency-dependence of striatal DA release (Lopes et al., 2019). In the presence of $GABA_A$- and $GABA_B$-R agonists, DA re-release is augmented when evoked by a stimulus train, compared to DA re-release in the absence of these agonists (Lopes et al., 2019). Together, these results indicate that whilst the primary action of GABA tone in the striatum is to limit DA release, activation of GABA-Rs also acts to promote DA re-release in response to high frequency stimulation.

Activation of $GABA_A$-Rs on mature striatal DA axons generates a depolarising current, and limits DA release via shunting inhibition and voltage-gated Na^+ channel (VGSC) inactivation (Kramer et al., 2020). Whole-cell patch clamp recordings of main axons of DMS-projecting DA neurons reveals that application of GABA to striatal *ex vivo* mouse brain slices produces subthreshold depolarisations via $GABA_A$-Rs, likely due to the observation that the GABA reversal potential is more depolarised than the hyperpolarised potential of the axon (Kramer et al., 2020). Application of GABA attenuates DA release by limiting action potential amplitude, through depolarisation-mediated VGSC inactivation, and enhancing membrane conductance to produce shunting inhibition (Kramer et al., 2020). Measurement of intracellular Ca^{2+} levels using GCaMP6f reveal that the $GABA_A$-R agonist, muscimol, attenuates Ca^{2+} levels in striatal DA axons, but only when the site of stimulation was distal to the recording site, indicating that $GABA_A$-Rs limit action potential propagation (Kramer et al., 2020). The benzodiazepine and $GABA_A$-R positive allosteric modulator, diazepam, decreases input resistance of striatal DA axons, demonstrating that positive allosteric modulation of $GABA_A$-Rs, in tandem with tonic GABA, supports shunting inhibition in DMS-projecting mouse DA axons (Kramer et al., 2020). This somewhat contrasts with the observation that diazepam

alone does not attenuate DA release in rat NAcC (Brodnik et al., 2019). Differences in GABA-R expression between striatal subregions, or between species, may be a contributing factor.

Historically, ultrastructural evidence regarding the localisation of GABA-Rs on striatal DAergic axons was lacking, but recent studies are beginning to pave the way. Immunocytochemical straining for $GABA_BR1$ subunits reveals that $GABA_BR1$ is located in unmyelinated axons and axons forming 'en passant' varicosities in the striatum, consistent with the structure of DA axons originating in the midbrain (Charara et al., 1999). Recent reports of staining against the $GABA_A$-R α_3 subunit revealed that these subunits co-localise with DA axons in both DLS and NAcC (J. C. Patel et al., 2024). Functional data for $GABA_A$- and $GABA_B$-R regulation of DA release (Pitman et al., 2014; Brodnik et al., 2019; Lopes et al., 2019; Roberts et al., 2020; Kramer et al., 2020; Roberts et al., 2021a), in addition to the demonstration that $GABA_A$-Rs are located on the main branch of striatal DA axons (Kramer et al., 2020), illustrate that it is highly likely GABA-Rs are located on DA axonal arbours in the striatum.

The ability of GABA-Rs, like DATs, to limit DA release, yet moderately support the frequency-dependence of DA release, indicates a paradoxical role for these receptors. Both DATs and $GABA_A$-Rs operate depolarising inward currents (Sonders et al., 1997; Kramer et al., 2020). Whether DATs and GABA-Rs co-operate to determine striatal DA release probability, or whether their effects are summative, or redundant, is not known. Mesostriatal DA axons are particularly well-placed to integrate information from several sources to determine DA output, due to their extensive axonal arbour and striatal innervation (Matsuda et al., 2009).

1.6. Mechanisms impacting neurotransmitter release

1.6.1. Synaptic release mechanisms and synapsins

Neurotransmitter release can predominantly be classified as synchronous exocytosis following an action potential, though release also occurs in asynchronous and spontaneous manners (Südhof, 2013; Kaeser & Regehr, 2014). The synaptic release mechanisms underlying each form of release may differ slightly, but generally overlap (Kaeser & Regehr, 2014). Synchronous neurotransmitter release is triggered following a sequence of events: arrival of an action potential, opening of VGCCs, Ca2+ influx, binding of intracellular Ca2+ to Ca2+ sensor(s), which triggers vesicle fusion with the intracellular plasma membrane, and results in exocytosis (Kaeser & Regehr, 2014). Vesicle fusion for fast synchronous release requires soluble N-ethylmaleimide-sensitive factor attachment protein receptor (SNARE) proteins and Sec1/Munc18-like (SM) proteins, which assemble together and adopt conformational changes to achieve fusion of the vesicle with the intracellular membrane, and open a pore through which neurotransmitters are expelled ((Südhof & Rothman, 2009; Südhof, 2013; Rizo, 2022). There are two types of SNARE proteins, vesicular v-SNAREs, and target membrane t-SNAREs, which zipper together to exert force and expel neurotransmitter into the extracellular space (Söllner et al., 1993; Südhof & Rothman, 2009; Sauvola & Littleton, 2021; Rizo, 2022). Vesicle fusion and therefore neurotransmitter release is dependent on vesicle availability, which is regulated at least in part by a family of phosphoproteins called synapsins (Kaeser & Regehr, 2014; Longhena et al., 2021).

The synapsin family is comprised of synapsin I (Ueda & Greengard, 1977), synapsin II (Forn & Greengard, 1978; Huang et al., 1982), and synapsin III (Kao et al., 1998). Synapsins are expressed in central and peripheral neurons, thought to be located on the cytoplasmic surface of neuronal synaptic vesicles (De Camilli et al., 1983; Huttner et al., 1983; Longhena et al., 2021). Synapsin I and II are the predominant forms expressed in adulthood, whereas

synapsin III expression peaks during early development, and tends to have a more localised expression pattern than synapsin I and II (Ferreira et al., 2000; Pieribone et al., 2002; Longhena et al., 2021). Synapsins regulate synaptic vesicle availability by modulating vesicle pool organisation, and therefore regulate neurotransmitter release (Longhena et al., 2021). Synapsins also play a role in neurogenesis and neural development (Longhena et al., 2021).

Synapsins maintain vesicles in a reserve pool, potentially by crosslinking synaptic vesicles, or by creating a liquid condensate to confine vesicles within a compartment (M. Zhang & Augustine, 2021). Phosphorylation of synapsin I has been suggested to disrupt synapsin binding to synaptic vesicles, and therefore liberate vesicles (Greengard et al., 1993; Hilfiker et al., 1999). Phosphorylation can occur at several sites on synapsins in response to kinases, phosphatases, and Ca2+ influx following membrane depolarisation (Cesca et al., 2010). Application of Ca2+ augments synapsin I phosphorylation in synaptosomal preparations (Huttner & Greengard, 1979). The presence of extracellular Ca2+ is required for veratridine or K+-induced changes to synapsin phosphorylation (Huttner & Greengard, 1979). Binding of adenosine triphosphate (ATP) to synapsin I requires Ca2+, but ATP can bind to synapsin II in the absence of Ca2+ (Hosaka & Südhof, 1998b). ATP binding to synapsin III is inhibited by Ca2+ (Hosaka & Südhof, 1998a). In some cases, Ca2+ influx is thought to activate Ca2+/calmodulin-dependent protein kinase I (CaMKI), which in turn phosphorylates synapsin I (Nairn & Greengard, 1987). STF in hippocampal slices is augmented in mice lacking synapsin I (Rosahl et al., 1993). In cultured hippocampal neurons, synapsin I acts as a Ca2+ buffer and therefore promotes recovery from synaptic depression, by supporting replenishment of the readily releasable vesicle pool (Moschetta et al., 2022). Synapsin II, like synapsin I, limits the size of the readily releasable pool, but unlike synapsin I, synapsin II also interacts with P/Q-type VGCCs in hippocampal neurons to regulate GABA signalling (Medrihan et al., 2013). Synapsin III regulates reserve pool size and supports development of

hippocampal axons (Feng et al., 2002), and promotes midbrain DA neuron development (Faustini et al., 2022).

In the striatum, DATs interact with synapsins to limit DA release probability (Venton et al., 2006; Kile et al., 2010). DATs immobilise a portion of the vesicle pool via a synapsin-dependent pathway (Venton et al., 2006; Kile et al., 2010). In wildtype mice, DAT inhibition relieves vesicle immobilisation and increases DA release probability, a phenomenon which is lost in synapsin TKO mice (Venton et al., 2006; Kile et al., 2010). Loss of synapsins renders striatal DA release more sensitive to changes in $[Ca^{2+}]_o$ (Kile et al., 2010), indicating that synapsins might act to buffer Ca2+ in DA neurons. It has been suggested that synapsin III mediates the interaction between striatal DATs and the vesicle pool (Kile et al., 2010), however, another study found that loss of synapsin III was not sufficient to prevent DAT-mediated interactions with the vesicle pool (M. D. Condon et al., 2019). Notably, DATs and synapsin III both bind α-synuclein in DA neurons (F. J. S. Lee et al., 2001; Zaltieri et al., 2015), which is a critical regulator of DA release (Abeliovich et al., 2000). Interactions between neurotransmitter transporters and members of the synapsin family are not well-understood. Loss of synapsins I, II, and III does not change 5-HT signalling in SNr, indicating that synapsins do not play a role in 5-HT release or uptake (Kile et al., 2010). Loss of synapsin I and II is associated with attenuated expression of vesicular transporters for glutamate and GABA (Bogen et al., 2006). Administration of valproate, an antiepilectic drug, reduces synapsin I expression and is associated with a increase in glutamate transporters EAAT1 and EAAT2, although it is unclear whether this involves a direct interaction between synapsin I and these transporters (Hassel et al., 2001).

In addition to synapsin-transporter interactions, relationships have been identified with transporters and other release-related mechanisms. Syntaxin-1A, a t-SNARE protein, binds and interacts with not only DATs (Carvelli et al., 2008), but also with GATs (Deken et al., 2000).

A syntaxin-1A homologue, UNC-64, associates with DATs and disrupts DAT-mediated currents in C. elegans (Carvelli et al., 2008). Syntaxin-1A binds to the N-terminus of GAT1, increases GAT1 expression yet attenuates GABA translocation rates through GAT1 transporters (Deken et al., 2000). Furthermore, syntaxin-1A inhibits L-type VGCC (LTCC) activity (Arien et al., 2003), and DATs can activate LTCCs (Cameron et al., 2015). Surprisingly, LTCC inhibition regulates striatal DA release only when DATs are active (Brimblecombe et al., 2024). These findings indicate a potential complex relationship between synaptic release mechanisms, transporters, Ca2+ handling, and neurotransmitter release. Neurotransmitter transporters are not well-studied with regard to regulation of neurotransmitter release and co-operation with synaptic release mechanisms, but precedent exists to indicate that release mechanisms and transporters might interact in complex ways not yet understood.

1.6.2. Neuronal integration

To understand how neurons function in a network, and what determines their signalling, it is imperative to decipher how these cells integrate information. For a neuron, their dendritic tree is a major source of information, receiving presynaptic input from the environment and performing computations to inform action potential generation (Stuart & Spruston, 2015). Dendritic morphology, ion channel expression, and the ability or inability to generate dendritic spikes, all give rise to the form of computations dendrites can perform (Takagi, 2000; Spruston, 2009; Spruston et al., 2016; Stuart & Spruston, 2015). The presence of dendritic spikes appears to not only amplify discrete synaptic inputs to inform integration, but dendritic spikes are also a product of integration, initially generated in separate dendritic compartments and then combined to shape neuronal output (Williams & Atkinson, 2008). From the dendrites, synaptic input is then converted to an action potential at the axon initial segment (AIS) (Coombs et al., 1957; Fuortes et al., 1957; Stuart & Häusser, 1994; Palmer & Stuart, 2006; Schmidt-Hieber et al., 2008).

Although an action potential is typically generated at the AIS, action potential amplitude and width can be shaped in axons, demonstrating that axons have a more complex role than simply action potential conduction (Debanne, 2004). Axons have been shown to transmit digital and analog signals, supporting propagation of subthreshold changes to membrane potential over long distances (Alle & Geiger, 2006; Clark & Häusser, 2006; Shu et al., 2006). Subthreshold depolarisations can potentiate subsequent action potential-generated neurotransmitter release from axons, indicating that integration occurs along the axon to shape output (Alle & Geiger, 2006; Clark & Häusser, 2006; Shu et al., 2006; Christie et al., 2011). In pyramidal neurons, subthreshold excitatory postsynaptic potentials (EPSPs) evoked in dendrites are subsequently augmented in axons via VGSCs (Stuart & Sakmann, 1995). Local input can modify or even generate axonal action potentials, for example, via axo-axonal interactions (Debanne, 2004). In the main axon of pyramidal neurons, DA, via D_1- and D_2-like-Rs, modulates VGKC activity and thus modifies the action potential waveform (Yang et al., 2013). In the striatum, cholinergic input to DA axons generates axonal excitatory postsynaptic potentials (EPSPs), which periodically produce spontaneous action potentials (Kramer et al., 2022; Liu et al., 2022). Recent evidence indicates that striatal DA axons perform signal integration. $GABA_A$-Rs on striatal DA axons limit subthreshold cholinergic input to DA axons in the DMS, in mouse *ex vivo* brain slices (Brill-Weil et al., 2024). Diazepam, a $GABA_A$-R positive allosteric modulator, attenuates subthreshold nAChR input to striatal DA axons, whilst gabazine, a $GABA_A$-R antagonist, augments nAChR-mediated Ca^{2+} influx (Brill-Weil et al., 2024). These findings indicate that like dendrites, axons can perform computations when faced with concurrent incoming signals (Brill-Weil et al., 2024). Striatal DA neuron morphology in particular may be well-suited for DA neurons to perform signal integration at the axonal level, due to the long range projections of these neurons and large numbers of branch points. If $GABA_A$-Rs modulate nAChR function on striatal DA axons (Brill-Weil et al., 2024), it is plausible that $GABA_A$-Rs could also modulate DAT function.

1.6.3. Presynaptic short-term plasticity

Presynaptic short-term plasticity, or use-dependent plasticity, is a process thought to bidirectionally change synaptic strength and regulate neurotransmitter release (Fioravante & Regehr, 2011; Regehr, 2012a). This form of plasticity lasts from tens of milliseconds to minutes and can be organised into three distinct categories; depression, facilitation, and augmentation or post-tetanic potentiation (Fioravante & Regehr, 2011; Regehr, 2012a). STD and STF operate on a timescale of milliseconds to seconds, whereas augmentation and post-tetanic potentiation operate on a timescale of seconds to minutes (Fioravante & Regehr, 2011; Regehr, 2012a). Some synapses exhibit a form of plasticity called short-term biphasic plasticity, in which a synapse undergoes facilitation, followed by depression (Markram et al., 1998; Barroso-Flores et al., 2015a, 2017). Striatal DA axons exhibit short-term biphasic plasticity (Condon et al., 2019). Canonical accounts of short-term plasticity at fast central synapses report an inverse relationship between initial release probability and neurotransmitter re-release; when release probability is low, synapses display facilitation, and when release probability is high, synapses display depression (Thomson, 2000). There are likely several distinct mechanisms which determine the form of plasticity a synapse undergoes.

STD can arise due to release-dependent processes such as depletion of the readily releasable vesicle pool, release site inactivation, attenuated Ca^{2+} entry, or activation of metabotropic receptors, or from release-independent processes, which are less understood (Thomson, 2000; Zucker & Regehr, 2002; Fioravante & Regehr, 2011; Regehr, 2012a). STF, on the other hand, is thought to arise due to release-dependent processes such as residual Ca^{2+} in the presynaptic neuron, Ca^{2+} buffer saturation (also known as pseudofacilitation), or augmented Ca^{2+} influx (Thomson, 2000; Zucker & Regehr, 2002; Blatow et al., 2003; Fioravante & Regehr, 2011; Regehr, 2012a). Augmentation and post-tetanic potentiation

occur following prolonged stimuli trains, following which augmentation can last 5-10 s, and post-tetanic potentiation can last from seconds to minutes (Zucker & Regehr, 2002; Fioravante & Regehr, 2011). These are thought to largely be release-dependent processes, similar to the mechanisms contributing to STF, involving slow removal of residual Ca^{2+}, saturation of Ca^{2+} buffers, an increase in Ca^{2+} sensitivity in the presynaptic neuron, or an increase of vesicles in the readily releasable pool (Zucker & Regehr, 2002; Fioravante & Regehr, 2011; Regehr, 2012a).

Functionally, short-term plasticity in neurotransmitter release adds an additional layer of capacity for neuronal encoding. STD in a presynaptic cell allows the receiving cell to detect novel inputs, because a previously silent presynaptic cell will generate a larger response than the ongoing activity of the initial presynaptic cell which underwent rapid STD (Thomson, 2000). Adaptation to incoming stimuli can be facilitated by STD (Anwar et al., 2017). In rat barrel cortex neurons, EPSPs exhibit rapid STD in response to repeated sensory stimulation, allowing for increased sensitivity to novel sensory inputs (Chung et al., 2002). STD therefore provides a low-pass filter whereas STF provides a high-pass filter, enhancing information transfer most efficiently when neurons fire at high frequencies (Anwar et al., 2017). Synapses which display both STD and STF act as band-pass filters (Anwar et al., 2017). On the other hand, STF is essential for encoding the firing rate, something which STD cannot reliably transmit (Thomson, 2000). The extent of STF is determined by the firing rate of the presynaptic cell, and thus the extent of STF informs the postsynaptic target of firing frequency (Thomson, 2000). STF supports reliable information transfer between synapses that are unreliable at low frequency, or single, spiking, such as those in the hippocampus, where STF likely promotes the encoding of memory-related information (Lisman, 1997).

In the striatum, three classes of GABAergic synapses are present; those that are depressing, facilitating, and biphasic (Barroso-Flores et al., 2015b). Following DA depletion by a 6-

hydroxydopamine (6-OHDA) lesion, short-term plasticity at synapses that exhibit facilitation, or biphasic activtity, is altered, though plasticity at synapses that display solely depression are unchanged (Barroso-Flores et al., 2015b). These results indicate that DA in the striatum plays a role in regulating plasticity at GABAergic synapses (Barroso-Flores et al., 2015b). Therefore, understanding the mechanisms which underlie DA signalling in the striatum is critical to our knowledge of basal ganglia function and dysfunction. DATs govern short-term plasticity in striatal DA release, but the precise mechanisms by which this occurs are not known. Furthermore, it is currently unclear whether DAT function and GABA-R function are independent, or whether they can co-operate.

1.7. Summary

DA transmission in the basal ganglia is critical for processes such as motor control and motivation. DA release in the striatum is regulated by a variety of local neuromodulators (e.g. GABA), in addition to mechanisms intrinsic to DA axons (e.g. DATs). Whether DA axons incorporate signalling from GABA-Rs and DATs to determine DA output, is not yet understood, but preliminary data from the Cragg laboratory indicates that these mechanisms may not be entirely independent (unpublished data, Dr. E. Lopes, Cragg lab). Furthermore, the roles that striatal DATs may play in modulating DA axonal activation, and how this may tally with DA re-release, has not been explored. In Chapter 3, I use fast-scan cyclic voltammetry to test if DATs and GABA-Rs co-operate in DLS and NAcC, and whether this occurs at the levels of axons, or instead recruits the wider striatal circuitry. In Chapter 4, I use fast-scan cyclic voltammetry and expand this line of enquiry to test whether activity at G protein gated inwardly rectifying K^+ (GIRK) channels support the control of DA release by DATs and GABA-Rs. In Chapter 5, I use fast-scan cyclic voltammetry and a newly developed genetically-encoded fluorescent voltage indicator, ASAP5 (Hao et al., 2024), to test whether DATs regulate DA axonal membrane potential and whether DAT-mediated currents are consistent

with the role of DATs in mediating short-term plasticity in DA release. Finally, I test whether GABA-Rs or GIRK channels play a role in modulating DA axonal membrane potential in the striatum.

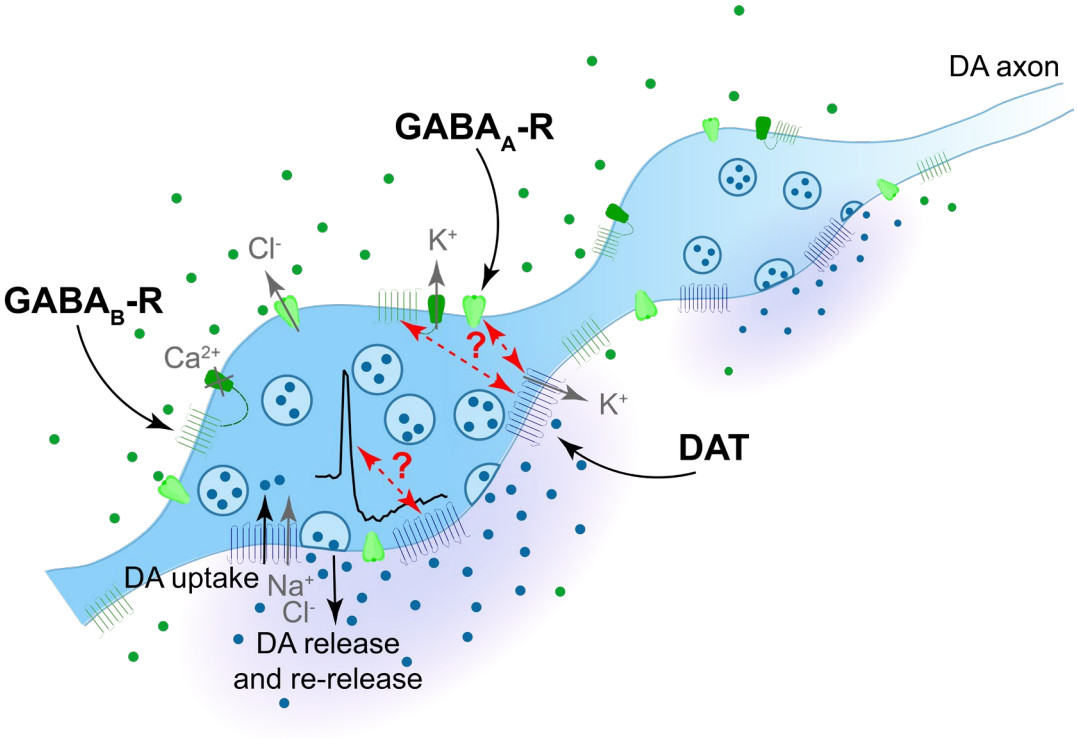

Figure 1.3. DATs are in a prime position to interact with GABA-Rs and axonal excitability
Simplified schematic of striatal DA axon, expressing DATs, $GABA_A$-Rs and $GABA_B$-Rs. DATs regulate DA release, re-release, and uptake. DATs translocate Na^+ and Cl^- with DA, and antiport K^+. $GABA_A$-Rs are depolarising in striatal DA axons and allow outward Cl^- flux. $GABA_B$-Rs may couple to VGCCs or GIRK channels. The overarching questions are whether DATs and GABA-Rs co-operate, and whether DATs modulate axonal membrane potential.

Chapter 2.

General methods

In this chapter, I will describe methodology applicable to Chapters 3, 4 and 5. Methods specific to a given chapter, including any variations on the below information, are described in the appropriate chapter. I will briefly discuss the use of mice as a model organism and the utility of recordings in acute brain slices, and subsequently describe in detail the experimental techniques used.

2.1. Studying mesostriatal DA signalling in mice as a model organism

2.1.1. Investigating DA signalling in mouse acute brain slices

Acute brain slices from mice were used in this thesis to investigate the regulation of striatal DA release by DATs and GABA-Rs. Mice were chosen as a model species due to several reasons, and in accordance with the 3Rs (Replacement, Reduction, Refinement) framework for performing humane animal research. Currently, there is no suitable replacement for animal brain tissue to study mechanisms of neurotransmission. To understand mammalian neurotransmission, with the eventual aim of translating knowledge to humans, it is imperative to use an experimental model which shares many conserved properties with humans, whilst balancing the ethical consideration of using least sentient animal model appropriate. Rodents share much conserved neural circuits with humans, and mice are the least sentient species, exhibiting several advantages for experimental use. Mice reach adulthood rapidly, facilitating the investigation of mature brain circuits. Mice are social creatures and small in size, meaning they can easily be group housed, benefitting mouse welfare but also lowering costs associated with research. It is possible to genetically manipulate mice, allowing for investigation of genetically defined circuits, for example. Lastly, mice are commonly used in the scientific field to study neurotransmission, therefore, results obtained in this thesis are readily comparable with a wide range of findings.

Acute coronal *ex vivo* brain slices were chosen due to the ability to preserve striatal connectivity, in particular the complex axonal arbour of DA neurons (Matsuda et al., 2009),

whilst isolating DA axons from somatodendritic influence to allow for exploration of axonal-only mechanisms. If parasagittal sections were used, preserving the mesostriatal pathway, bath application of drugs would yield confounded results, because it would not be clear whether the drug is acting at somatodendritic, or axonal, or both, regions. Furthermore, evoked DA release signals are small and inconsistent in parasagittal sections, and only one parasagittal section preserving DA neuron projections can be taken per hemisphere (Ammari et al., 2009). Acute slices allow for pharmacological and optogenetic dissection of striatal circuits. An *ex vivo* approach was chosen over an *in vivo* approach for several reasons. The potential for animal suffering is less in *ex vivo* experimentation, *ex vivo* experimentation allows for a more thorough dissection of mechanisms, and allow more experiments to be conducted per animal, reducing the total number of animals required. *Ex vivo* approaches, however, lack the ability to study intact brain circuits and behaviour, which *in vivo* approaches offer. In summary, acute coronal striatal slices from mice were chosen as the most appropriate experimental model for investigations into mesostriatal DA signalling.

Animals were group housed and provided with *ad libitum* access to food and water. Animals were maintained on a 12-hour light/dark cycle with environmental conditions between 20-24°C and 45-65% relative humidity. All procedures were performed in accordance with institutional guidelines and the U.K. Animals (Scientific Procedures) Act, 1986. All experimental datasets are mixed-sex, and typically contain equal numbers of male and female mice. The inclusion of female mice in all datasets is imperative because historically, research on female animals has been neglected (Beery & Zucker, 2011), despite evidence that female mice do not exhibit any more variance than males (Smarr & Kriegsfeld, 2022). The inclusion of both sexes in research ensures that results will be applicable to both sexes, and minimises animal wastage.

2.1.2. Wild-type mice

Male and female wild-type C57BL/6J mice (Charles River; 6-24 weeks of age) were used in the majority of experiments. The C57BL/6J strain was chosen as, unlike other strains, such as the C57BL/6JOlaHsd mouse (Harlan/Envigo/Inotiv; Specht & Schoepfer, 2001), C57BL/6J mice possess a wild-type gene for α-synuclein, which is important for DA release (Abeliovich et al., 2000). Furthermore, many genetically manipulated mice are generated on the C57BL/6J background.

2.1.3. DAT^{IREcre} mice

Locally generated male and female DAT^{IREcre} heterozygous mice (Jax strain #: 006660; 7-14 weeks of age) were used for experiments in which a genetically-encoded approach was required to target DA neurons. DAT^{IREcre} mice express Cre recombinase under a DAT promoter, therefore Cre recombinase is expressed in all DA neurons. The Cre-*loxP* system is widely used for targeting of genetically-defined cell types. Cre recombinase, from the P1 bacteriophage, interacts with two *loxP* DNA recognition sites, allowing for excision or inversion of DNS fragments (Nagy, 2000). In the case of DAT^{IREcre} mice, knock-in of Cre recombinase allows for the use of Cre-dependent tools specifically in DA neurons. DAT^{IREcre} heterozygous mice were also used for experiments requiring reduced DAT expression in DA neurons, because these mice exhibit lower DAT expression compared to wild-type mice (Bäckman et al., 2006).

2.1.4. Mice lacking GIRK2 channels in DA neurons

For a subset of experiments exploring the contribution of GIRK channels to striatal DA release, GIRK2$^{flox/flox}$ homozygous mice were obtained from the Wickman laboratory at the University of Minnesota, under a Material Transfer Agreement, and crossed with DAT^{IREScre}

mice to generate male and female mice which were then used in experimentation (5-11 weeks of age).

The generation of GIRK2$^{flox/flox}$ mice was described and these mice subsequently used in several publications from the Wickman laboratory (Kotecki et al., 2015; Victoria et al., 2016; McCall et al., 2017, 2019). Locally, DAT^{IREScre} mice were crossed with GIRK2$^{flox/flox}$ (DAT Cre$^{-/-}$:GIRK2 flox$^{+/+}$) mice to generate the following experimental genotypes: heterozygous for DAT^{IREScre} and heterozygous for GIRK2$^{flox/flox}$ (DAT Cre$^{+/-}$:GIRK2 flox$^{+/-}$; referred to subsequently as GIRK2 cKD), and heterozygous for DAT^{IREScre} and homozygous for GIRK2$^{flox/flox}$ (DAT Cre$^{+/-}$:GIRK2 flox$^{+/+}$; referred to subsequently as GIRK2 cKO). The generation of GIRK2 cKD mice was achieved by crossing DAT^{IREScre} homozygous mice with GIRK2$^{flox/flox}$ mice, from which all pups were the desired experimental genotype of GIRK2 cKD. The generation of GIRK2 cKO mice was achieved by initially crossing GIRK2$^{flox/flox}$ mice with GIRK2 cKD mice, from which a subset of pups were the desired genotype of GIRK2 cKO. To obtain experimental animals and establish a breeding strategy which minimised the generation of surplus animals, GIRK2$^{flox/flox}$ mice were crossed with GIRK2 cKO mice, from which pups were either the desired experimental genotype of GIRK2 cKO, or GIRK2$^{flox/flox}$ mice, which were required to maintain this transgenic mouse line. Experimental data obtained from GIRK2 cKD or GIRK2 cKO mice were collected alongside, and compared to, data obtained from age- and sex-matched mice heterozygous for DAT^{IREScre}.

2.1.5. Acute coronal brain slice preparation

Mice were culled by cervical dislocation and brains were extracted and submerged in ice-cold cutting solution, containing in mM: 194 sucrose, 30 NaCl, 4.5 KCl, 1 $MgCl_2$-$6H_2O$, 26 $NaHCO_3$, 1.2 NaH_2PO_4, 10 glucose, saturated with 95% O_2/5% CO_2. Brains were transferred to a vibratome (VT1200 S, Leica Biosystems) and 300 µm coronal slices containing the

striatum were prepared. Slices were immediately transferred to a holding chamber with recording solution (artificial cerebrospinal fluid; aCSF), containing in mM: 130 NaCl, 2.5 KCl, 2 $MgCl_2$-$6H_2O$, 26 $NaHCO_3$, 1.25 NaH_2PO_4, 10 glucose, 2.5 $CaCl_2$, saturated with 95% O_2/5% CO_2. The holding chamber was kept in a water bath at 34 °C for 15 minutes, then removed from the water bath and left to equilibrate at room temperature for a minimum of 45 minutes.

For experiments including manipulations to $[Ca^{2+}]_o$, the amount of $CaCl_2$ in aCSF was altered. To achieve 1.2 mM $[Ca^{2+}]_o$, 1.2 mL of 1 mM $CaCl_2$ solution was added to each litre of aCSF, compared to the typical 2.5 mL to achieve 2.5 mM $[Ca^{2+}]_o$. To achieve 4.0 mM $[Ca^{2+}]_o$, 4.0 mL of 1 mM $CaCl_2$ solution was added to each litre of aCSF. For experiments conducted in 1.2 mM $[Ca^{2+}]_o$, slices were held either in 1.2 mM or 2.5 mM $[Ca^{2+}]_o$ aCSF, and transferred to 1.2 mM $[Ca^{2+}]_o$ for a minimum of 30 minutes prior to commencing experimentation. For experiments conducted in 4.0 mM $[Ca^{2+}]_o$, slices were held 2.5 mM $[Ca^{2+}]_o$ aCSF, to prevent precipitation of Ca^{2+} out of solution, and transferred to 4.0 mM $[Ca^{2+}]_o$ for a minimum of 30 minutes prior to commencing experimentation.

2.2. Fast-scan cyclic voltammetry (FSCV) in *ex vivo* brain slices

2.2.1. Rationale for the use of FSCV

FSCV is a technique which allows for sub-second detection of DA, based on a reduction-oxidation (redox) reaction in response to applied voltages. FSCV in its current iteration was pioneered initially in the *in vivo* intact brain (Millar et al., 1985; Kuhr & Wightman, 1986; Stamford et al., 1986), but was soon determined suitable for *in vitro* approaches (Baur et al., 1988), and is now widely used in *ex vivo* (and *in vivo*) experiments to assess dopamine dynamics (e.g. Rice & Cragg, 2004; Threlfell et al., 2012; Calipari et al., 2017; Brimblecombe et al., 2019; Lopes et al., 2019; Brodnik et al., 2020; Brimblecombe et al., 2024). FSCV is utilised to record DA dynamics in human striatum during surgery for implantation of a deep brain stimulation (DBS) electrode (Kishida et al., 2011, 2016; Bang et al., 2020; Sands et al.,

2023). FSCV in rodent *ex vivo* coronal striatal slices allows for measurement of DA release and uptake dynamics in the extracellular space, whilst preserving striatal connectivity. Thus, we can determine to what extent DA signalling from the vastly arbourised striatal DA axons is governed by local mechanisms.

FSCV was chosen as a tool for monitoring striatal DA transmission for several reasons. FSCV has good temporal resolution, facilitating sub-second detection of extracellular DA levels, and the spatial resolution of FSCV permits measurement of DA released by a population of axons. DA collection methods such as microdialysis have lower temporal resolution, and must be coupled with an analytical technique, such as electrochemical detection, to identify the analyte. FSCV on the other hand, allows for concurrent detection and analysis of the electroactive species. FSCV is not only useful for determining DA levels, but can also be used to investigate release and uptake kinetics. Fluorescent DA indicators, such as dLight (Patriarchi et al., 2018) or $GRAB_{DA}$ (Sun et al., 2018) exhibit excellent on kinetics, but off kinetics tend to be slow. The use of fluorescent DA indicators also requires intracranial injections in mice, whereas FSCV can be conducted on mice with no procedures performed. FSCV is therefore an ideal experimental tool for refinement in animal experimentation. Fluorescent DA indicators are capable only of reporting relative changes in DA, whereas absolute DA concentrations can be obtained with FSCV. Constant-potential amperometry is a similar technique to FSCV, used to measure DA based on its redox reaction. Constant-potential amperometry exhibits superior temporal resolution to FSCV, but has little chemical resolution (Michael & Wightman, 1999). In complex environments such as brain slices, analyte identification is imperative, as several electroactive molecules besides DA are present (for example, 5HT and adenosine). FSCV is therefore the most useful tool at present for investigating striatal DA signalling in *ex vivo* approaches.

2.2.2. FSCV for the detection of DA

DA is an electroactive molecule, due to the presence of two hydroxyl groups which oxidise and reduce in response to applied voltages. The amplitude of these currents is directly proportional to the amount of DA present. Here, a triangular waveform (-0.7 to +1.3 V) was applied against a Ag/AgCl reference electrode, at a scan rate of 800 V/s (5 ms per scan). At 0.6 V, DA was oxidised to DA-o-quinone, and at -0.2 V, DA-o-quinone was reduced to DA. A voltammeter (Julian Millar, Barts and the London School of Medicine and Dentistry) was used to apply this triangular waveform, and sample the resultant current at a frequency of 8 Hz (every 125 ms). A background capacitive, or charging, current is present, though this background current is stable (Clark & España, 2023), and allows for background subtraction to reveal the faradaic current generated by the oxidation and reduction of DA. The background current was subtracted by the voltammeter, revealing current attributable to DA. Plotting the oxidation current over time generates a 'DA transient'.

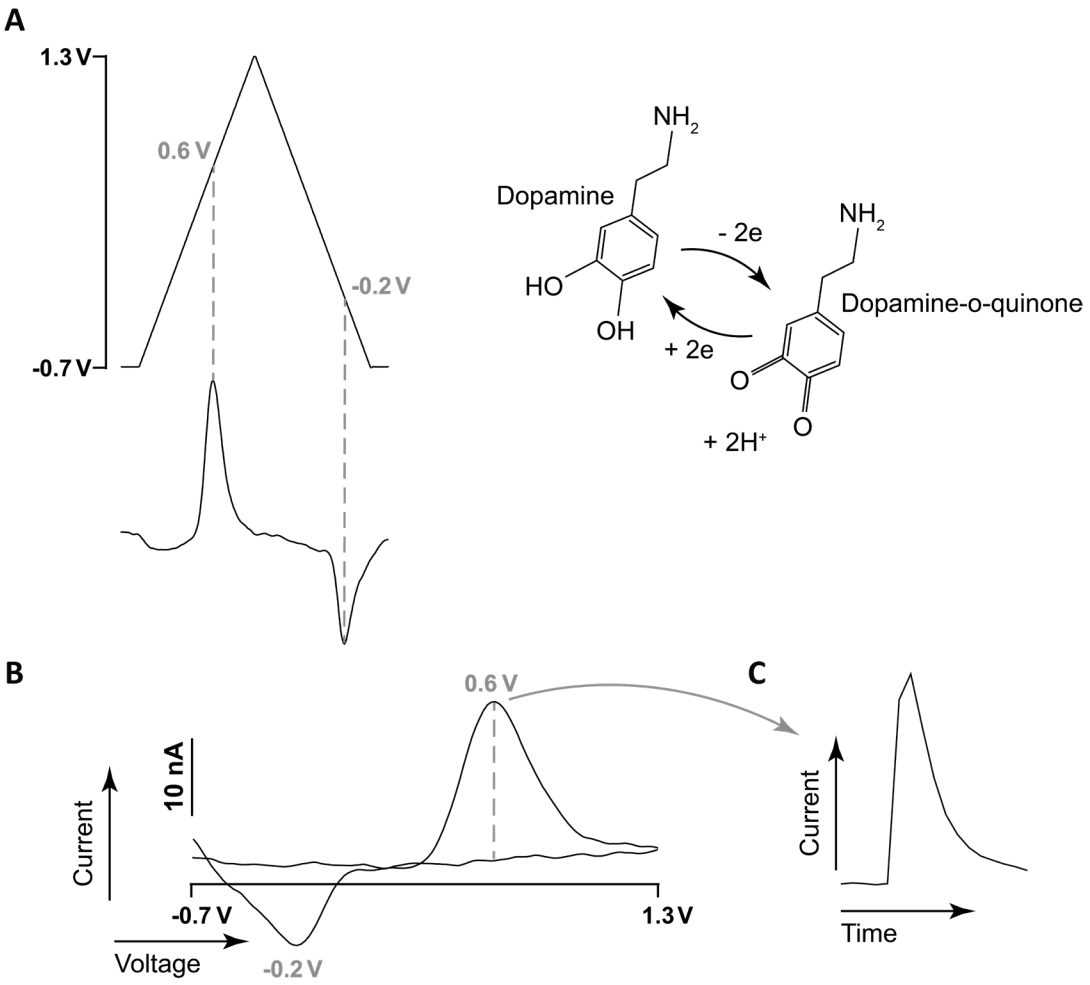

Figure 2.1. Fast-scan cyclic voltammetry for the detection of dopamine
(A) A triangular waveform is applied, ramping from -0.7 V, to +1.3 V and back to -0.7 V, vs Ag/AgCl. In the background-subtracted voltammogram, DA is oxidised at 0.6 V to DA-o-quinone, and reduced to DA at -0.2 V. (B) Current vs voltage plot showing background-subtracted cyclic voltammogram upon application of 2 μM DA. (C) Current vs time plot (at oxidation potential), showing how data is typically represented.

2.2.3. Carbon fibre microelectrode fabrication

All carbon fibre microelectrodes were fabricated in house and each electrode was used for one day of experimentation only. Epoxy free carbon fibre (7 μm diameter; Goodfellow Cambridge Ltd) was threaded into a borosilicate glass capillary tube (outer diameter 2.0 mm, inner diameter 1.6 mm; Multi Channel Systems, Harvard Bioscience Inc) filled with acetone. Following removal of acetone, the capillary tube containing the carbon fibre was placed into an upright electrode puller (PE-2, Narishige). The electrode puller ensured a tight seal between the capillary tube and carbon fibre. The seal was inspected under a microscope,

and if adequate, the carbon fibre protruding from the glass capillary was cut to a length of 50-150 µm. Insulated copper wire was partially stripped and coated in silver conductive paint (RS Components Ltd), then inserted at the opposite end of the capillary tube, until contact was made with the carbon fibre at the tip of the electrode. Finally, cyanoacrylate glue (Loctite) was applied to the opposite end of the electrode from the carbon fibre, to secure the wire in place.

Before use in an experiment, carbon fibre microelectrodes were connected to a headstage and Millar voltammeter, to assess the quality of the background charging current, and ensure that the amplification factor (full signal gain) was ~3-10 mV/nA, as values in between this range ensure an adequate signal-to-noise ratio for experiments. Electrodes ranged in sensitivity between ~4-23 nA/µM.

2.2.4. Electrical stimulation and experimental design

Electrical stimulation was utilised to evoke striatal DA release in coronal brain slices. Coronal slices containing the striatum do not contain DA cell bodies, therefore striatal DA axons are 'silent' and do not spontaneously fire. External stimulation is required to reliably evoke DA release, and allows for investigation of local modulation of DA release, without confounding influence from the somatodendritic region. However, electrical stimulation is non-specific and recruits cell types other than DA axons, which must be considered when interpreting data.

Electrical stimulation was delivered via a rounded concentric bipolar Pt/Ir stimulating electrode (outer pole diameter 125 µm, inner pole diameter 25 µm; FHC, Inc), placed on the tissue surface in either DLS or NAcC. DLS recordings were conducted in a region approximately ranging from A/P +1.6 to +0.1 from bregma, and dependent on A/P position, were conducted in a region which ranged approximately from M/L ±1.6 to ±2.8 and D/V -2.7 to

-3.2. NAcC recordings were conducted in a region approximately ranging from A/P +1.7 to +0.5 from bregma, and dependent on A/P position, were conducted in a region which ranged approximately from M/L ±0.9 to ±1.2 and D/V -4.2 to -5.0. The stimulating electrode was placed ~100 µm away from the carbon fibre microelectrode. Stimulation pulses (0.6 mA, 0.2 ms) were delivered as single pulses (1p), or as paired pulses, with varying IPIs (10-200 ms). Stimulations were delivered and evoked DA was recorded every 2.5 minutes. Stimulations were generated out-of-phase with the voltammeter scan rate, to minimise signal interference.

For single-pulse experiments, single electrical pulses were delivered every 2.5 minutes. Drug application was performed once signal stability was achieved: ≤ 10% variation across six consecutive recordings. Drugs were applied for a period of 8-16 recordings (20-40 minutes). For paired-pulse experiments, paired pulses with IPIs of 10-200 ms (corresponding to 5-100 Hz firing frequency) were delivered in a pseudorandom order, with each two instances of paired-pulse stimulation flanked by a single electrical pulse (e.g. 1p, 2p 40 ms, 2p 200ms, 1p, and so on). Each IPI was collected in triplicate. Drug application was performed once all data had been collected for each IPI in control conditions. Once the drug had reached its maximal effect on single pulse evoked $[DA]_o$ (~6 recordings), data was then collected for each IPI in the drug condition. Slow, tonic firing rate in DA neurons is in the region of 1-10 Hz, whereas burst, or phasic, firing rate is on average 20-40 Hz, although occasionally frequencies of up to 100 Hz can be reached in the presence of salient stimuli (Grace & Bunney, 1984; Freeman et al., 1985; Hyland et al., 2002).

2.2.5. Data acquisition and analysis

Coronal striatal slices were hemisected and transferred to a recording chamber, superfused with aCSF (~2 mL/min), saturated with 95% O_2/5% CO_2, and heated to 32±1 °C. Slices were secured with silver pins to prevent movement. A carbon fibre microelectrode was inserted

into striatal tissue, away from the recording site, while applying the triangular waveform, to equilibrate within tissue whilst minimising tissue damage at the recording site. After a minimum of 30 minutes equilibration, the carbon fibre microelectrode was inserted into tissue at the desired recording site (DLS or NAcC), so that the entire carbon fibre was within tissue, but a minimal amount of the glass capillary was in tissue. A concentric bipolar Pt/Ir stimulating electrode was then placed on the tissue surface, ~100 µm away from the carbon fibre microelectrode. Electrical stimulations were delivered every 2.5 minutes. DA was identified based on its oxidation at 0.6 V and reduction at -0.2 V. A triangular waveform was applied and sampled at 8 Hz by a Millar voltammeter. Data was digitised and acquired using a Digidata 1440A digitiser and Axoscope 10.7 software (Molecular Devices), with stimulation coordinated and generated via a Master-8 stimulator (A.M.P.I.) and a DS3 isolated current stimulator (Digitimer). At the end of each experimental day, carbon fibre microelectrodes were calibrated out of tissue with 2 µm DA, to obtain calibration factors which were subsequently used in analysis to convert voltage (current attributable to DA is recorded as voltage in our experimental preparation), into DA concentration.

Data were extracted using Axoscope 10.7 and locally-written Excel macros, or locally-written analysis code in Python. Here, data were converted to DA concentration. Data were subsequently analysed in Excel. Data are expressed as peak extracellular DA ($[DA]_o$), and are typically normalised to pre-drug conditions, to generate percentage values, or expressed as raw concentration values.

For single-pulse experiments assessing the impact of drug application on DA release, $[DA]_o$ from four recordings immediately preceding drug application were averaged, and compared to peak $[DA]_o$ from the last four recordings during drug wash-on. Whilst FSCV allows for sub-second detection of DA, the temporal kinetics are not fast enough to discern between DA attributable to the first or second pulse in paired-pulse experiments. For data from these

experiments, peak $[DA]_o$ from two flanking single pulses was averaged (P1), and subtracted from peak $[DA]_o$ from the sandwiched paired-pulse recordings (P1+P2), to obtain DA attributable to the second pulse only (P2). A paired-pulse ratio (PPR) was calculated by dividing P2 by P1 (P2/P1). This ratio informs us on how much DA was evoked by P2, compared to P1. Once PPR was calculated for each recording, PPR for each IPI was averaged to give a final overall PPR value. This average PPR before drug application was compared to an average PPR during drug application. For analysis of DA uptake rates, the fastest portion of the decay of a DA transient was isolated, and a mean decay constant, k (s^{-1}), was obtained by fitting a one-phase exponential decay to this portion of the transient. Decay constant rates were then compared between drug conditions or between genotypes. Data are expressed as mean ± standard error of the mean (SEM). Each n number typically comes from one slice and one animal only, such that each n number is slices from separate animals, unless otherwise stated.

2.3. Statistical testing

Statistical analysis was performed using GraphPad Prism 9 or 10. Statistical testing was applied to datasets containing $n \geq 4$. Pilot datasets containing $n < 4$ are included in this thesis but no statistical testing performed. Units of analysis are the number of brain slices.

In general, parametric statistical tests were used, the rationale being that evoked striatal DA release is a normally distributed variable. In our experience, the variation in DA release between slices and sites within a slice is equal. Nonparametric tests are used if the variance between experimental groups is visibly non-equal, or in the case of experiments using GIRK2 cKD and GIRK2 cKO animals, where there is insufficient data to confirm whether DA release from these animals is a normally distributed variable. An alternative approach is to perform testing of normality on each dataset, or to log-transform all data so that parametric testing

could be used throughout. The threshold for statistical significance was $p \leq 0.05$. Symbols to denote levels of significance are as follows: $*p \leq .05$, $**p \leq .01$, $**p \leq .001$, ns = non-significant. In the case of multiple comparisons, the absence of asterisks is taken to mean non-significant, unless otherwise stated that statistical comparisons were not performed (i.e. when datasets are $n < 4$).

2.4. Drugs

Drugs used are described in a table in each chapter. The nAChR antagonist, DHβE (1 μM), was present throughout unless otherwise stated, to exclude confounding effects of cholinergic regulation on striatal DA transmission.

Chapter 3.

Convergent regulation of striatal DA release by DATs and GABA-Rs

3.1. Introduction

3.1.1 DATs and GABA-Rs modulate striatal dopamine signalling

As outlined in Section 1.4.2., DATs are powerful regulators of DA output, governing DA uptake, but also DA release, and short-term plasticity of these release events. The striatum is largely a GABA-containing structure, with up to ~98% of neurons being identified as GABAergic (Kemp, 1968; Tepper et al., 2010). In mouse *ex vivo* brain slices, striatal DA axons are under tonic GABAergic inhibition at $GABA_A$- and $GABA_B$-Rs (Lopes et al., 2019). How axonal DATs and GABA-Rs may interact to influence striatal DA transmission is currently unknown.

DATs limit striatal DA release in rodent intact brain and *ex vivo* brain slices, as DAT inhibition leads to an increase in evoked DA release (Venton et al., 2006; Kile et al., 2010; Daberkow et al., 2013). $GABA_A$-Rs and $GABA_B$-Rs also limit striatal DA release in mouse *ex vivo* brain slices, as inhibition of $GABA_A$- and $GABA_B$-Rs lead to increases in evoked DA release (Lopes et al., 2019). $GABA_A$-Rs operate shunting inhibition and Na^+ channel inactivation to inhibit striatal DA release in mouse *ex vivo* brain slices (Kramer et al., 2020). Whilst DATs and GABA-Rs limit striatal DA release probability following a single stimulation, emulating a single action potential, both DATs and $GABA_A$-Rs have been shown to generate depolarising currents (Sonders et al., 1997; Carvelli et al., 2004; Kramer et al., 2020), and DATs and GABA-Rs support the frequency-dependence of DA release when multiple stimulations are applied (Pitman et al., 2014; Lopes et al., 2019; Condon et al., 2019). This demonstrates a complex relationship between release probability, membrane excitability, and short-term plasticity in release. If DATs and GABA-Rs similarly limit DA release probability, and support the frequency-dependence of DA release, it poses the question of whether DATs and GABA-Rs operate independently and have summative impacts on DA release, or whether they operate via overlapping mechanisms which may converge. To our knowledge, any interaction

between DAT- and GABA-R-mediated mechanisms on striatal DA axons has not yet been investigated.

3.1.2 Evidence for interaction between DATs and GABA-Rs

Unpublished preliminary findings from the Cragg laboratory indicate that striatal DA axons can integrate information from DATs and GABA-Rs to determine DA output. Inhibition of DATs with cocaine leads to an increase in DA release, via a mobilisation of a synapsin-dependent vesicle pool (Venton et al., 2006; Kile et al., 2010). We have observed that this cocaine-induced increase in extracellular DA ($[DA]_o$) is attenuated in DLS in the presence of a combination of $GABA_A$- and $GABA_B$-R antagonists, which reduce the level of tonic inhibition that DA axons are under (Fig. 3.1A, unpublished data, Dr. E. Lopes, Cragg lab). This indicates that, when GABA-Rs are active, GABA-Rs support cocaine-induced increases in $[DA]_o$. Furthermore, when GABA-Rs are active, DAT inhibition relieves short-term depression in DA release (Condon et al., 2019). Preliminary data indicates that in the presence of $GABA_A$- and $GABA_B$-R antagonists, DAT inhibition no longer relieves short-term depression (Fig. 3.1B, unpublished data, Dr. E. Lopes, Cragg lab). These preliminary observations demonstrate a potential co-dependence, whereby DAT function is dependent on activity at GABA-Rs. We will explore this co-dependence further in DLS, probe whether this convergence requires the wider striatal circuitry or whether DA axons might in fact integrate incoming signalling, and test whether the same relationship exists in the ventral striatal region of NAcC.

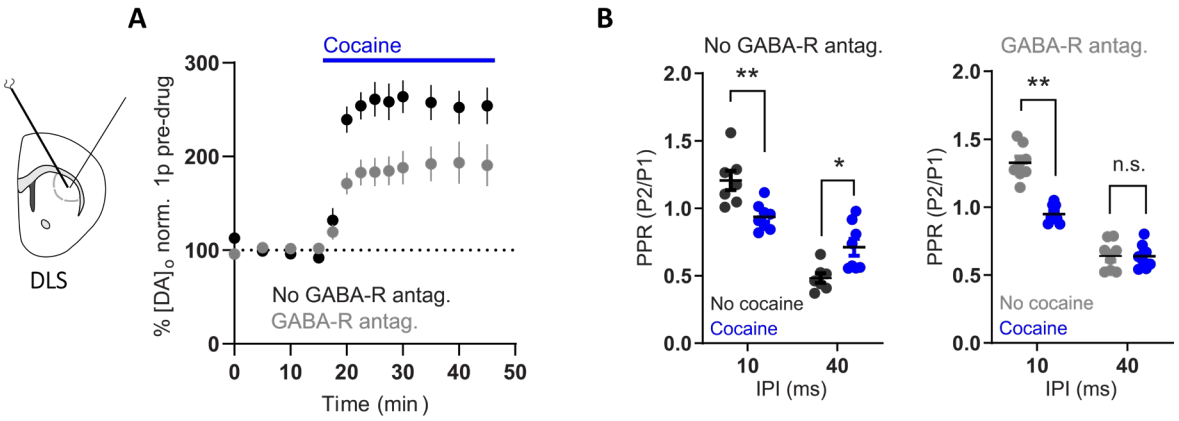

Figure 3.1. Convergent regulation of DA release by DATs and GABA-Rs in DLS
*(A) Peak $[DA]_o$ over time evoked by single pulses in DLS, before and during bath application of cocaine (5 µM). Data are normalised to pre-drug baseline. n = 8-9. (B) PPR in DLS before and during cocaine. n = 8-9. Data are mean ±SEM. 'No GABA-R antag.' is DHBE (1 µM), 'GABA-R antag.' is DHBE (1 µM), bicuculline (10 µM), and CGP 55845 (4 µM). *p ≤ .05, **p ≤ .01, ***p ≤ .001, ns = non-significant. Data collected by Dr. Emanuel Lopes.*

3.1.3 Involvement of Ca^{2+} handling

Ca^{2+} signalling in striatal DA axons is been implicated in DAT function (Kile et al., 2010; Brimblecombe et al., 2019). At low $[Ca^{2+}]_o$ concentrations, release probability is low, and only a subset of the vesicle pool is released (Neher & Sakaba, 2008). Decreasing release probability by using low $[Ca^{2+}]_o$ leads to higher cocaine-induced increases in striatal DA release in *ex vivo* mouse brain slices (Kile et al., 2010). On the other hand, increasing release probability by high $[Ca^{2+}]_o$ leads to an attenuated effect of cocaine on striatal DA release (Kile et al., 2010). Calbindin-D28k, a high affinity Ca^{2+} buffer, promotes cocaine-induced increases in $[DA]_o$ in *ex vivo* mouse brain slices (Brimblecombe et al., 2019). Knockdown of calbindin-D28k in NAcC DA neurons increases peak $[DA]_o$ and attenuates the effect of cocaine on $[DA]_o$ (Brimblecombe et al., 2019). These findings indicate that calbindin-D28k might support DAT-mediated modifications to the vesicle pool, at least in ventral striatum. Regional differences in calbindin-D28k expression are well documented in DA neurons; calbindin-D28k is highly expressed in DA neurons originating in the VTA which project to the NAcC, compared to those originating in the SNc and project to the DLS (Gerfen et al., 1985; Lavoie & Parent, 1991;

Chung et al., 2005; Poulin et al., 2014). Further, DATs co-operate with LTCCs; DAT-mediated membrane depolarisation activates LTCCs in HEK293T cells expressing hDAT (Cameron et al., 2015), and DAT function is required for the LTCC inhibitor, isradipine, to modify striatal DA release in DLS in *ex vivo* mouse brain slices (Brimblecombe et al., 2024). Lastly, inhibition of CaMKIIα blunts cocaine-induced increases in DA release in ventral striatum in intact mouse brain (Keighron et al., 2023). Together, these data indicate that DAT function is linked to Ca^{2+}-related mechanisms, and that Ca^{2+} handling varies with striatal region.

It is plausible that GABA-Rs regulate Ca^{2+} signalling in DA axons, because, consistent with an inhibition of DA release by GABA-Rs, application of a $GABA_A$-R agonist attenuates GCaMP6f Ca^{2+} signals in striatal DA axons, in *ex vivo* mouse brain slices, particularly when propagation distance from the stimulation site is larger (Kramer et al., 2020). $GABA_B$-Rs, which also modulate striatal dopamine release (Lopes et al., 2019), are known to couple with VGCCs, or GIRK channels, dependent on their location within the synapse (Bettler et al., 2004). The largely asynaptic nature of striatal DA axons (Descarries et al., 1996), and the paucity of data relating to the coupling nature of $GABA_B$-Rs on striatal DA axons, makes it plausible that $GABA_B$-Rs may be implicated in Ca^{2+} signalling, K^+ signalling, or both, in striatal DA axons. As part of our investigation into the convergent regulation of DA release by DATs and GABA-Rs, we therefore deemed it important to probe any implication of Ca^{2+} handling, and any regional differences that may exist between striatal subregions.

The experiments outlined in this chapter were aimed at exploring whether DA axons incorporate information from DATs and from GABA-Rs, and how this information may converge to shape striatal DA transmission.

3.2. Methods

Experiments detailed in this chapter were carried out in accordance with the general methods described in Chapter 2. Variations and further details are reported below.

3.2.1. Animals and slice preparation

Male and female wild-type C57BL/6J mice, or $DAT^{IREScre}$ heterozygous mice (Jax strain #: 006660) were culled by cervical dislocation and acute *ex vivo* brain slices were prepared as described in Section 2.1.5. All procedures were performed in accordance with institutional guidelines and the U.K. Animals (Scientific Procedures) Act, 1986.

3.2.2. Fast-scan cyclic voltammetry

Fast-scan cyclic voltammetry was used to measure changes in $[DA]_o$, as described in Section 2.2. Each experiment was performed at a single recording site in either the DLS or NAcC. DA was evoked every 2.5 minutes by single pulse electrical stimulation. Drug application was performed once signal stability was achieved: ≤ 10% variation across six consecutive recordings.

3.2.3. Drugs

Stock solutions were prepared at 1,000x – 20,000x the final concentration and stored at -20°C. Final drug concentrations were prepared in aCSF on the day of the experiment.

Drug	Supplier	Action	Concentration	Solvent	References
(+)-Bicuculline	Abcam	$GABA_A$-R antagonist	10 µM	Dimethyl sulfoxide (DMSO)	Roberts et al. (2020); Stedehouder et al. (2024)
CGP 55845 hydrochloride	Abcam	$GABA_B$-R antagonist	4 µM	Dimethyl sulfoxide (DMSO)	Roberts et al. (2020); Stedehouder et al. (2024)
Cocaine hydrochloride	Sigma-Aldrich	DAT inhibitor	5 µM	dH_2O	Condon et al. (2020); Threlfell et al. (2021)
Dihydro-β-erythroidine (DHβE) hydrobromide	Sigma-Aldrich	nAChR antagonist	1 µM	dH_2O	Threlfell et al. (2012); Roberts et al. (2020)
L-741,626	Abcam	D_2-like-R antagonist	1 µM	Dimethyl sulfoxide (DMSO)	Condon et al. (2019); Threlfell et al. (2021)
Nomifensine maleate	Sigma-Aldrich	DAT inhibitor	10 µM	Hydrochloric acid (HCl)	Condon et al. (2019); Threlfell et al. (2021)
SCH 39166 hydrobromide	Tocris	D_1-like-R antagonist	1 µM	Dimethyl sulfoxide (DMSO)	Zheng et al. (1999); Yang et al. (2020)

3.2.4. Data acquisition and analysis

Data were digitised and acquired using Axoscope 10.7, and extracted using locally written Excel macros or Python script. Statistical tests were performed in GraphPad Prism 9 or 10.

3.3. Results

3.3.1. GABA-R antagonists attenuate cocaine-induced increase in DA release independent of $D_{1/2}$-Rs, indicating axonal integration

It is plausible that the interaction between DATs and GABA-Rs, shown by the attenuation of cocaine-induced DA release in GABA-R antagonists, is either due to signal integration at the level of DA axons, or a circuit-mediated effect involving DA and GABA. In mouse *ex vivo* brain slices, striatal GABA tone dampens DA release (Lopes et al., 2019; Roberts et al., 2020). This GABA tone is regulated by GATs located on striatal astrocytes in DLS (Roberts et al., 2020). DAT inhibitors such as cocaine elicit a large increase in $[DA]_o$ and prolong the clearance rate (Venton et al., 2006; Verma, 2015), which could in turn impact striatal GABA transmission, via extrasynaptic activation of DAergic D_1- or D_2-like receptors, on GABA-containing neurons in the striatum. If GABA tone is altered, this could feedback onto DA axons and change DA release. In order to test whether our observation is due to striatal circuit-mediated feedback, we investigated whether an antagonist of D_1 or D_2-like DA receptors prevented an attenuation in the cocaine-induced increase in $[DA]_o$ by GABA-R antagonists.

If D_1-like-Rs were implicated, the cocaine-induced increase in $[DA]_o$ would activate D_1-Rs, which would in turn potentiate GABA release, and subsequently attenuate DA release through GABA-Rs on DA axons. The presence of GABA-R antagonists would therefore relieve this inhibition on DA release. If D_2-like-Rs were implicated, the cocaine-induced increase in $[DA]_o$ would activate D_2-Rs, which would in turn inhibit GABA release, and subsequently augment DA release through reduced activation of GABA-Rs on DA axons. The presence of GABA-R antagonists would therefore exert either no effect on DA release, or a slight augmentation. Though neither of these explanations easily fit with the observation that cocaine-induced increases in DA release are higher when GABA-Rs are active, and lower when GABA-Rs are inhibited (Fig. 3.1A), we explored the involvement of both D_1- and D_2-like-

Rs for completeness and for the possibility that any circuit-mediated effect involved a player we had not yet considered. We hypothesised that the GABA-R antagonist-mediated attenuation of cocaine-induced increases to DA release in DLS would prevail in the presence of D_1- and D_2-like-R antagonists.

Consistent with its role as a DAT inhibitor, cocaine (5 µM) increased single pulse-evoked $[DA]_o$ and widened transients in DLS, showing a slowed uptake rate. This occurred in the presence of the D_1-like-R antagonist, SCH39166 (1 µM), and in both the absence and presence of GABA-R antagonists (bicuculline, 10 µM and CGP55845, 4 µM) (Fig. 3.2A). In the presence of SCH39166, cocaine-induced increases in $[DA]_o$ differed between control and GABA-R antagonist conditions (Fig. 3.2B, two-way RM ANOVA, time x drug interaction, $F_{(19,95)} = 9.13$, $p = 0.0063$, n = 6). The magnitude of cocaine-induced increase in $[DA]_o$ was lower in GABA-R antagonists compared to control (Fig. 3.2C, unpaired t-test, $t_{(10)} = 6.06$, $p = 0.0001$, n = 6). These data indicate that the modulation of cocaine-induced increases in $[DA]_o$ by GABA-Rs do not require activation of D_1-like-Rs within the striatal circuitry.

In the presence of the D_2-like-R antagonist, L-741,626 (1 µM), cocaine increased single pulse-evoked $[DA]_o$ and widened transients in DLS, consistent with a slowed uptake rate, in both the absence and presence of GABA-R antagonists (Fig. 3.2D). In the presence of L-741,626, cocaine-induced increases in $[DA]_o$ differed between control and GABA-R antagonist conditions (Fig. 3.2E, two-way RM ANOVA, time x drug interaction, $F_{(19,95)} = 19.49$, $p < 0.0001$, n = 6). The magnitude of cocaine-induced increase in $[DA]_o$ was lower in GABA-R antagonists compared to control (Fig. 3.2F, unpaired t-test, $t_{(10)} = 3.86$, $p = 0.0031$, n = 6). These data indicate that the modulation of cocaine-induced increases in $[DA]_o$ by GABA-Rs do not require activation of D_2-like-Rs within the striatal circuitry, and is therefore likely a convergence of mechanisms on DA axons.

Together, these results demonstrate that DATs and GABA-Rs co-operate independently of DA receptor activation and therefore likely independently of the wider striatal circuitry. Rather, striatal DA axons integrate information from DATs and GABA-Rs, thus determining DA output.

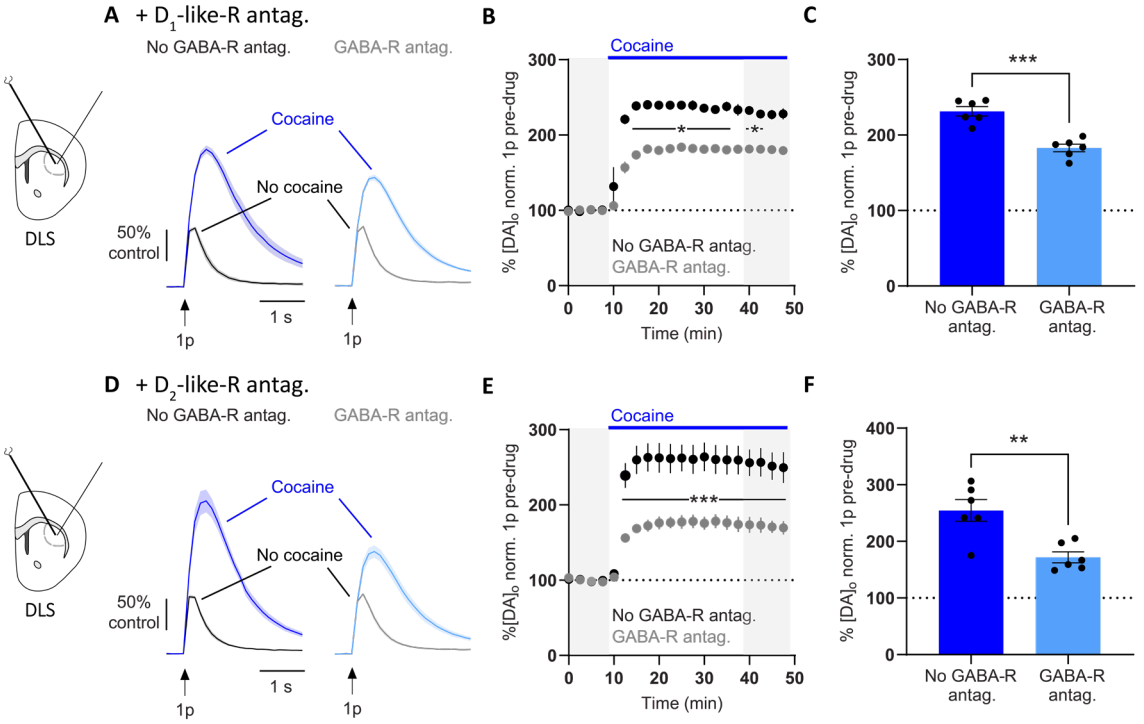

Figure 3.2. Convergent regulation of DA release by DATs and GABA-Rs is independent of D_1- or D_2-like receptors in DLS

*(A) $[DA]_o$ transients over time evoked by single pulses in DLS, before and during bath application of cocaine (5 μM). n = 6. (B) Peak $[DA]_o$ over time evoked by single pulses, before and during cocaine. n = 6. (C) Percentage increase of peak $[DA]_o$ following application of cocaine. n = 6. (D) $[DA]_o$ transients over time evoked by single pulses in DLS, before and during bath application of cocaine. n = 6. (E) Peak $[DA]_o$ over time evoked by single pulses, before and during cocaine. n = 6. (F) Percentage increase of peak $[DA]_o$ following application of cocaine. n = 6. Data are mean ±SEM and normalised to pre-drug baseline (grey shaded region). 'No GABA-R antag.' is DHBE (1 μM) and SCH 39166 (1 μM), 'GABA-R antag.' is DHBE (1 μM), SCH 39166 (1 μM), bicuculline (10 μM) and CGP 55845 (4 μM) (A, B, C). 'No GABA-R antag.' is DHBE (1 μM) and L-741,626 (1 μM), 'GABA-R antag.' is DHBE (1 μM), L-741,626 (1 μM), bicuculline (10 μM), and CGP 55845 (4 μM) (D, E, F). *p ≤ .05, **p ≤ .01, **p ≤ .001, ns = non-significant.*

3.3.2. GABA-R antagonists attenuate nomifensine-induced increase in DA release in DLS

To investigate whether the changes to cocaine-induced increases in DA release by the presence of GABA-R antagonists was generalisable to DAT inhibition, or specific to cocaine, we tested whether we could replicate the effects of cocaine with an alternative DAT inhibitor, nomifensine. Previous evidence in mouse *ex vivo* brain slices shows that nomifensine, similar to cocaine, increases peak $[DA]_o$ in the striatum (Condon et al., 2019; Threlfell et al., 2021), and reproduces the effect of cocaine on short-term plasticity in striatal DA release (M. D. Condon et al., 2019). We hypothesised that, like we observed for cocaine, that nomifensine-induced increases in $[DA]_o$ would be attenuated in the presence of GABA-R antagonists.

As expected, nomifensine (10 µM), like cocaine, increased single pulse-evoked $[DA]_o$ and widened transients in DLS, consistent with a slowed uptake rate, in both the absence and presence of GABA-R antagonists (Fig. 3.3A). Nomifensine-induced increases in $[DA]_o$ differed between control and GABA-R antagonist conditions (Fig. 3.3B, two-way RM ANOVA, time x drug interaction, $F_{(19,57)} = 2.40$, $p = 0.0057$, n = 4). However, a comparison of the magnitude of nomifensine-induced increase in $[DA]_o$ between conditions failed to reach significance (Fig. 3.3C, unpaired t-test with Welch's correction, $t_{(3)} = 1.74$, $p = 0.1705$, n = 4). It is likely that these experiments were underpowered, especially given the high variability in nomifensine-induced increase in $[DA]_o$ in control conditions. A post-hoc sample size calculation revealed that the sample size required to detect a minimum difference of 30% in cocaine-induced increases in $[DA]_o$ between groups, at a power of 80%, considering the large variability in the control condition, is n = 393.

Nevertheless, these pilot experiments indicate that the attenuation in DAT-mediated changes to $[DA]_o$ by GABA-R antagonists is observed with more than one DAT inhibitor and is therefore

unlikely to be via any off-target pharmacological effects of cocaine. Rather, we expect that this is a co-operation between DATs and GABA-Rs themselves.

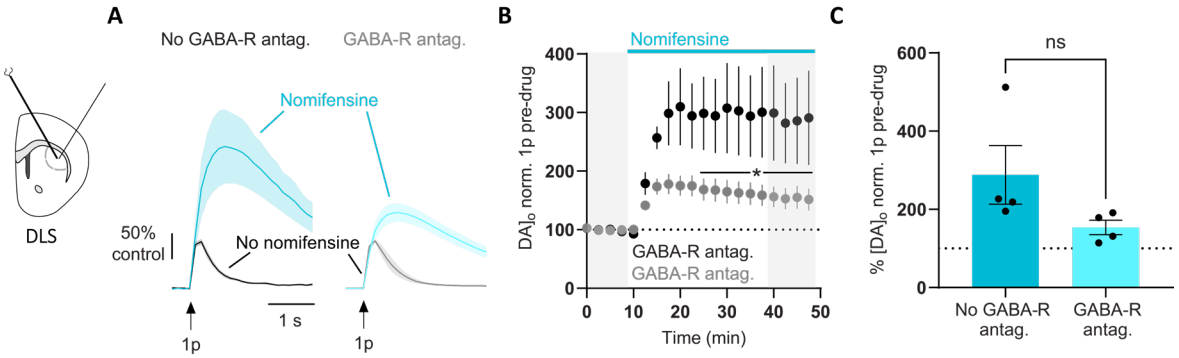

Figure 3.3. GABA-R antagonists attenuate the effect of nomifensine on DA release in DLS
*(A) $[DA]_o$ transients over time evoked by single pulses in DLS, before and during bath application of nomifensine (10 µM). n = 4. (B) Peak $[DA]_o$ over time evoked by single pulses, before and during nomifensine. n = 4. (C) Percentage increase of peak $[DA]_o$ following application of nomifensine. n = 4. Data are mean ±SEM and normalised to pre-drug baseline (grey shaded region). 'No GABA-R antag.' is DHBE (1 µM), 'GABA-R antag.' is DHBE (1 µM), bicuculline (10 µM) and CGP 55845 (4 µM). *p ≤ .05, **p ≤ .01, **p ≤ .001, ns = non-significant.*

3.3.3. GABA-R antagonists do not modulate DA uptake rate in DLS

Our data thus far indicate that activity at GABA-Rs supports DAT-mediated changes to striatal DA release. We therefore wondered whether GABA-Rs also affect other aspects of DAT function, particularly the role of DATs in mediating DA uptake. To do this, we pooled data from Fig. 3.2 and Fig. 3.3, prior to application of DAT inhibitors, and compared DA uptake rates in the absence and presence of GABA-R antagonists. We hypothesised that GABA-Rs promote DA uptake, therefore in the presence of GABA-R antagonists, we would see a slower uptake rate compared to the absence of GABA-R antagonists.

Contrary to our hypothesis, there were no significant differences between DA uptake rate in the absence or presence of GABA-R antagonists (Fig. 3.4A, unpaired t-test, $t_{(187)} = 1.40$, $p = 0.1623$, n = 94 transients in absence of GABA-R antagonists, 95 transients in presence of GABA-R antagonists). The mean decay constant, *k*, was obtained by fitting a one phase exponential decay to the decaying portion of DA transients. In the absence of GABA-R antagonists, *k* was 2.21 s^{-1}, and 2.06 s^{-1} in the presence of GABA-R antagonists.

The observation that activity at striatal GABA-Rs does not appear to affect DA uptake rate indicates that GABA-Rs specifically promote DAT-mediated changes to DA release, without exerting influence on DAT-mediated DA uptake, indicating that the roles of DATs can be dissociated.

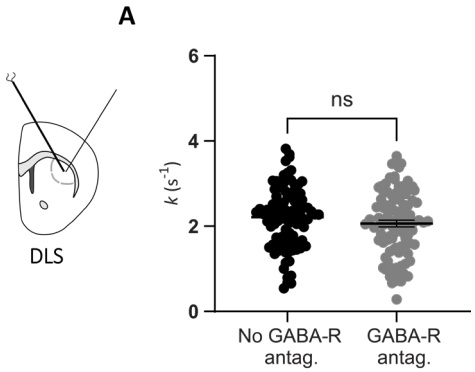

Figure 3.4. GABA-R antagonists do not affect DA uptake rate in DLS
*(A) Decay rates, k (s^{-1}), for $[DA]_o$ evoked by single pulses in DLS. n = 94-95 transients. Data are mean ±SEM. 'No GABA-R antag.' is DHBE (1 μM), 'GABA-R antag.' is DHBE (1 μM), bicuculline (10 μM) and CGP 55845 (4 μM). *p ≤ .05, **p ≤ .01, **p ≤ .001, ns = non-significant.*

3.3.4. GABA-Rs promote DAT-mediated changes to DA release across varying $[Ca^{2+}]_o$ concentrations (Sayon Choudhuri)

Given the relationship between Ca^{2+} signalling and DATs, the potential coupling of $GABA_B$-Rs to VGCCs, and the observation that $GABA_A$-R activation attenuates Ca^{2+} entry in striatal DA axons (Kramer et al., 2020), we explored whether the relationship between DATs and GABA-Rs was dependent on $[Ca^{2+}]_o$ in DLS. Varying $[Ca^{2+}]_o$ affects single pulse-evoked DA release in both DLS and NAcC, though this relationship is steeper in DLS (Brimblecombe et al., 2015; M. D. Condon et al., 2019), and regulates the extent to which DAT inhibition can increase DA release (Kile et al., 2010). To test this Ca^{2+}-dependence of the co-operation between DATs and GABA-Rs, we performed a cocaine wash-on in or out of GABA-R antagonists, in either low (1.2 mM) or high (4 mM) $[Ca^{2+}]_o$. $[Ca^{2+}]_o$ was varied by adding the corresponding volume of $CaCl_2$ to aCSF prior to the experiment (see Section 2.1.5). We hypothesised that cocaine-induced increases in $[DA]_o$ would be a function of $[Ca^{2+}]_o$, whereby low $[Ca^{2+}]_o$ would

potentiate cocaine-induced increases in $[DA]_o$, and high $[Ca^{2+}]_o$ would lead to lower cocaine-induced increases in $[DA]_o$. Furthermore, we hypothesised that the presence of GABA-R antagonists would attenuate cocaine-induced increases in $[DA]_o$ only in 1.2 mM $[Ca^{2+}]_o$, and not in 4 mM $[Ca^{2+}]_o$, as cocaine-induced increases in $[DA]_o$ at 4 mM $[Ca^{2+}]_o$ would already be low in the absence of GABA-R antagonists, therefore the addition of GABA-R antagonists would not result in attenuation of $[DA]_o$. These experiments were performed by Sayon Choudhuri, a FHS pre-clinical medicine student.

In 1.2 mM $[Ca^{2+}]_o$, cocaine (5 μM) increased single pulse-evoked $[DA]_o$ and widened transients in DLS, showing a slowed uptake rate, in both the absence and presence of GABA-R antagonists (Fig. 3.5A). There was a significant difference in cocaine-induced increase in peak $[DA]_o$ between drug conditions (Fig. 3.5B, two-way RM mixed effects model, time x drug interaction, $F_{(19,94)} = 15.36$, $p < 0.0001$, n = 6). As anticipated, the cocaine-induced increase in $[DA]_o$ was lower in the presence of GABA-R antagonists compared to the absence of GABA-R antagonists (Fig. 3.5C, unpaired t-test, $t_{(10)} = 4.83$, $p = 0.0007$, n = 6). Consistent with a potentiated cocaine-induced increase in DA release in low $[Ca^{2+}]_o$ (Kile et al., 2010), cocaine increased $[DA]_o$ by ~256% in 1.2 mM $[Ca^{2+}]_o$ (Fig. 3.4C), compared with ~157% in 2.4 mM $[Ca^{2+}]_o$ (Fig. 3.1A).

We observed that in both 1.2 mM $[Ca^{2+}]_o$ data shown here, and 2.4 mM $[Ca^{2+}]_o$ unpublished data collected previously (Fig. 3.1A), the magnitude of cocaine-induced increase in $[DA]_o$, in the presence of GABA-R antagonists, was similar (~98% and ~93%, respectively). Thus, we speculated that the magnitude of cocaine-induced increase in $[DA]_o$ in GABA-R antagonists was static, and not changing in response to varying $[Ca^{2+}]_o$. We hypothesised that if we increased $[Ca^{2+}]_o$, to decrease the effect of cocaine in the absence of GABA-R antagonists, to a similar level to that previously seen in the presence of GABA-R antagonists, then GABA-R antagonists may no longer modify the effect of cocaine.

In 4.0 mM $[Ca^{2+}]_o$, cocaine increased single pulse-evoked $[DA]_o$ and widened transients in DLS, showing a slowed uptake rate, in both the absence and presence of GABA-R antagonists (Fig. 3.4D). Contrary to our hypothesis, there was a significant difference in cocaine-induced increase in peak $[DA]_o$ between drug conditions (Fig. 3.5E, two-way RM mixed effects model, time x drug interaction, $F_{(19,83)} = 21.52$, $p < 0.0001$, n = 6). The cocaine-induced increase in $[DA]_o$ was lower in the presence of GABA-R antagonists compared to the absence of GABA-R antagonists (Fig. 3.5F, unpaired t-test, $t_{(10)} = 4.71$, $p = 0.0008$, n = 6). Again, consistent with a lower cocaine-induced increase in DA release in higher $[Ca^{2+}]_o$ (Kile et al., 2010), cocaine increased $[DA]_o$ by increased $[DA]_o$ by ~93% in 4.0 mM $[Ca^{2+}]_o$ (Fig. 3.5F), compared with ~157% in 2.4 mM $[Ca^{2+}]_o$ (Fig. 3.1A).

In agreement with previous observations (Kile et al., 2010), cocaine-induced increases in $[DA]_o$ in DLS are a function of $[Ca^{2+}]_o$ (Fig. 3.5G, two-way RM ANOVA, drug x $[Ca^{2+}]_o$ interaction, $F_{(2,35)} = 3.63$, $p = 0.0359$, n = 6 in 1.2 and 4.0 $[Ca^{2+}]_o$, n = 9 in 2.4 $[Ca^{2+}]_o$). At all $[Ca^{2+}]_o$ concentrations tested, GABA-R antagonists attenuate cocaine-induced increases in $[DA]_o$ (Fig. 3.5G, two-way RM mixed effects model, drug x $[Ca^{2+}]_o$ interaction, $F_{(2,3)} = 11.37$, $p = 0.0398$, n = 6-9 per condition).

These data show that, contrary to our expectations, the GABA-R antagonist condition is not static, and does in fact change in response to $[Ca^{2+}]_o$. Cocaine-induced increases in $[DA]_o$ were ~93% in the presence of GABA-R antagonists in 4.0 mM $[Ca^{2+}]_o$ (Fig. 3.5F), very similar to levels observed in the absence of GABA-R antagonists in 1.2 and 2.4 mM $[Ca^{2+}]_o$ (~98% and ~93%, respectively; Fig. 3.5C, Fig. 3.1A). Thus, lowering the cocaine-induced increase in $[DA]_o$ does not prevent regulation by GABA-R antagonists. Interestingly, whilst cocaine-induced increases in $[DA]_o$ in the absence of GABA-R antagonists show a strong inverse relationship with $[Ca^{2+}]_o$, with lower cocaine-induced increases in $[DA]_o$ at each increasing $[Ca^{2+}]_o$ concentration, cocaine-induced increases in $[DA]_o$ in the presence of GABA-R

antagonists does not show the same relationship. Cocaine-induced increases in $[DA]_o$ in the presence of GABA-R antagonists do not appear to differ from 1.2 to 2.4 mM $[Ca^{2+}]_o$.

One potential caveat in this interpretation is that data collected in 2.4 mM $[Ca^{2+}]_o$ used aCSF containing 5 mM $[K^+]_o$, whereas data collected in 1.2 and 4.0 mM $[Ca^{2+}]_o$ (and all other experiments in this thesis) used aCSF containing 2.5 mM $[K^+]_o$. Whilst we do not expect that this variation in $[K^+]_o$ concentration obscures our findings, due to the observation that changes in $[K^+]_o$ do not affect single pulse-evoked $[DA]_o$ in DLS or NAcC in mouse *ex vivo* brain slices (M. D. Condon et al., 2019), and the similarity of magnitudes of cocaine-induced increases in $[DA]_o$ between the dataset in 2.4 mM $[Ca^{2+}]_o$ and 5 mM $[K^+]_o$, and other datasets in 2.5 mM $[Ca^{2+}]_o$ and 2.5 mM $[K^+]_o$, it is imperative to keep this in mind as K^+ handling may affect the relationship between DATs and GABA-Rs.

Together, these data show that the attenuation of cocaine-induced increases in $[DA]_o$ by GABA-R antagonists is robust and occurs across all $[Ca^{2+}]_o$ concentrations tested (1.2, 2.4, and 4.0 mM). Regulation by GABA-R antagonists appears to be somewhat independent of the magnitude of cocaine-induced increases in $[DA]_o$ in control conditions, demonstrating that across all $[Ca^{2+}]_o$ concentrations tested, activity at GABA-Rs promotes the effect of cocaine on DA release.

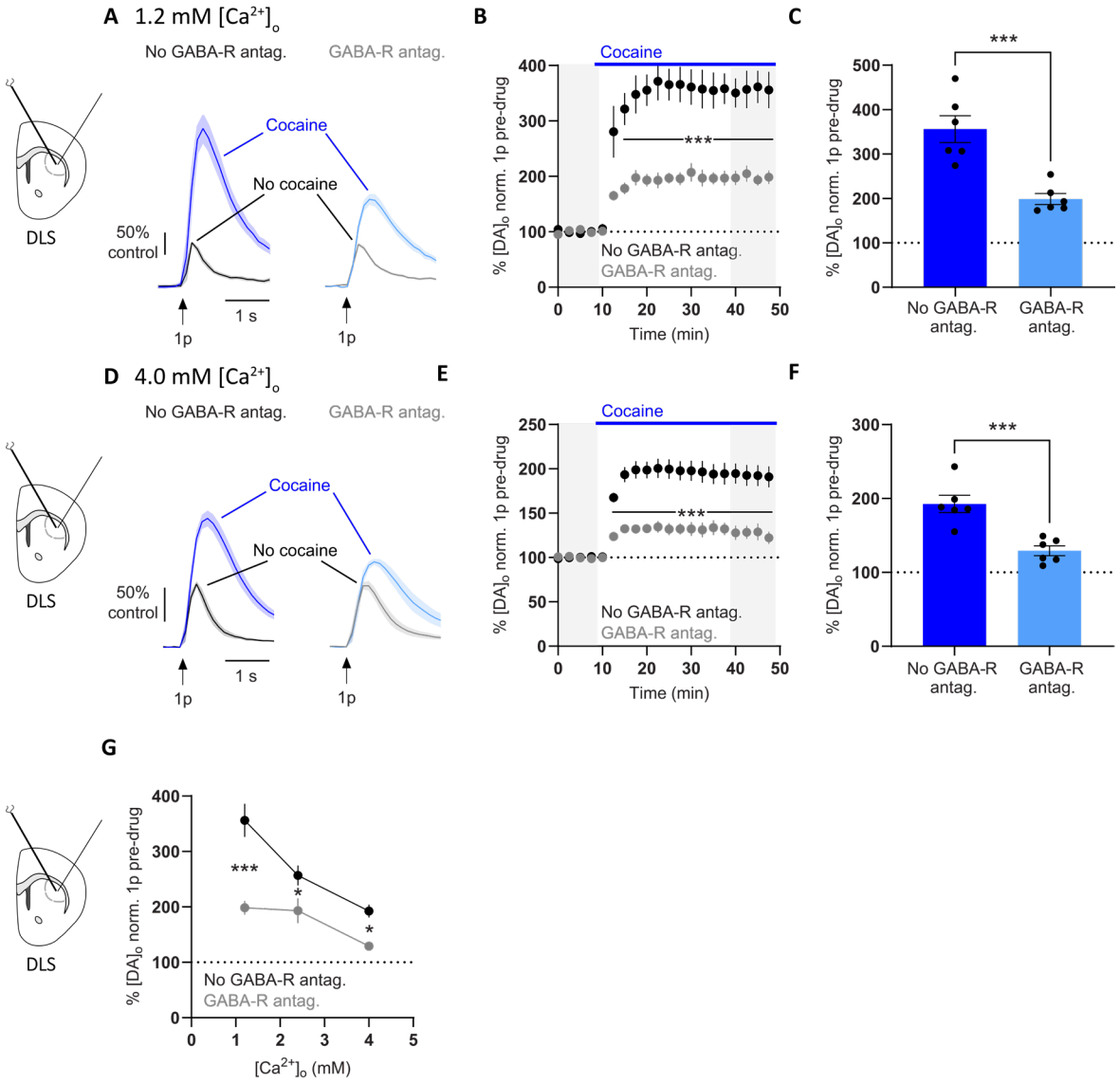

Figure 3.5. GABA-R antagonists attenuate cocaine-induced increase in DA release in varying $[Ca^{2+}]_o$ in DLS

*(A) $[DA]_o$ transients over time evoked by single pulses in DLS in 1.2 mM $[Ca^{2+}]_o$, before and during bath application of cocaine (5 µM). n = 6. (B) Peak $[DA]_o$ over time evoked by single pulses, before and during cocaine. n = 6. (C) Percentage increase of peak $[DA]_o$ following application of cocaine. n = 6. (D) $[DA]_o$ transients over time evoked by single pulses in DLS in 4.0 mM $[Ca^{2+}]_o$, before and during cocaine. n = 6. (E) Peak $[DA]_o$ over time evoked by single pulses, before and during cocaine. n = 6. (F) Percentage increase of peak $[DA]_o$ following application of cocaine. n = 6. (G) Percentage increase of peak $[DA]_o$ following application of cocaine in 1.2, 2.4, 4.0 mM $[Ca^{2+}]_o$. n = 6 in 1.2 and 4.0 mM $[Ca^{2+}]_o$, n = 8-9 in 2.4 mM $[Ca^{2+}]_o$. Data are mean ±SEM and normalised to pre-drug baseline (grey shaded region). 'No GABA-R antag.' is DHBE (1 µM), 'GABA-R antag.' is DHBE (1 µM), bicuculline (10 µM) and CGP 55845 (4 µM). *p ≤ .05, **p ≤ .01, **p ≤ .001, ns = non-significant.*

Data collected by Sayon Choudhuri (1.2 and 4.0 mM $[Ca^{2+}]_o$) and Dr. Emanuel Lopes (2.4 mM $[Ca^{2+}]_o$)

3.3.5. GABA-R antagonists do not modify cocaine-induced increase in DA release in NAcC

To explore whether there exists a convergence of mechanisms between DATs and GABA-Rs in NAcC, as observed in DLS, we investigated whether the presence of GABA-R antagonists modified the cocaine-induced increase in evoked DA release. In DLS and NAcC, DAT inhibition causes an increase in peak $[DA]_o$ in mouse *ex vivo* brain slices (e.g. Brimblecombe et al., 2019; Condon et al., 2019), though the extent to which DAT inhibition increases $[DA]_o$ can vary between striatal subregions, presumably in part due to differential DAT expression levels (Haber et al., 1995). Cocaine increases $[DA]_o$ to a lesser extent in NAcC than DLS (M. D. Condon et al., 2019). Application of GABA-R antagonists increases evoked $[DA]_o$ in NAcC in mouse *ex vivo* brain slices, indicating that NAcC DA axons are tonically inhibited by GABA, like they are in DLS (Roberts et al., 2020). Therefore, we expected to observe a similar relationship between DATs and GABA-Rs in NAcC, like has already been demonstrated in DLS. Specifically, we hypothesised that GABA-R antagonists would attenuate the cocaine-induced increase in $[DA]_o$ in NAcC.

As expected, application of cocaine (5 µM) increased single pulse-evoked $[DA]_o$ and widened transients in NAcC, consistent with a slowed uptake rate, in both the absence and presence of GABA-R antagonists (Fig. 3.6A). There was a significant interaction between conditions (Fig. 3.6B, two-way RM ANOVA, time x drug interaction, $F_{(19,95)} = 3.12$, $p = 0.0001$, n = 6), however, Šídák's multiple comparisons tests showed that drug conditions only differed at a singular timepoint. This was before the maximal effect of cocaine had been reached, and evoked $[DA]_o$ did not differ between conditions at any other timepoint. Consistent with this, the magnitude of cocaine-induced increase in $[DA]_o$ were not significantly different between conditions when the maximal effect of cocaine was reached (Fig. 3.6C, unpaired t-test, $t_{(10)} = 0.59$, $p = 0.5684$, n = 6).

These results show that, contrary to our hypothesis, the presence of GABA-R antagonists, do not have an impact on the extent to which cocaine increases $[DA]_o$ in NAcC.

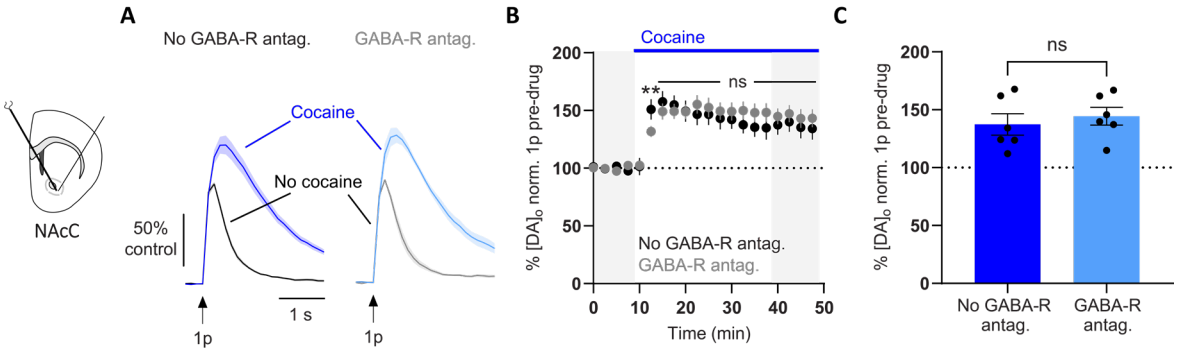

Figure 3.6. GABA-R antagonists do not modify effect of cocaine on DA release in NAcC
*(A) $[DA]_o$ transients over time evoked by single pulses in NAcC, before and during bath application of cocaine (5 μM). n = 6. (B) Peak $[DA]_o$ over time evoked by single pulses, before and during cocaine. n = 6. (C) Percentage increase of peak $[DA]_o$ following application of cocaine. n = 6. Data are mean ±SEM and normalised to pre-drug baseline (grey shaded region). 'No GABA-R antag.' is DHBE (1 μM), 'GABA-R antag.' is DHBE (1 μM), bicuculline (10 μM) and CGP 55845 (4 μM). *p ≤ .05, **p ≤ .01, **p ≤ .001, ns = non-significant.*

3.3.6. Low aCSF $[Ca^{2+}]_o$ concentration does not unveil relationship between DATs and GABA-Rs in NAcC

In 2.5 mM $[Ca^{2+}]_o$, the presence of GABA-R antagonists did not have an impact on the cocaine-induced increase in DA release in NAcC (Fig. 3.6). Due to the differential expression of calbindin-D28k between DLS and NAcC DA neurons (Gerfen et al., 1985; Lavoie & Parent, 1991; Chung et al., 2005; Poulin et al., 2014), we investigated whether, in fact, there is co-operativity between DATs and GABA-Rs in both DLS and NAcC, but Ca^{2+} buffering in NAcC is precluding or concealing a change in DA release.

In Section 3.3.4, consistent with previous literature, we observed that in DLS, cocaine-induced increases in $[DA]_o$ are a function of $[Ca^{2+}]_o$, where a lower aCSF $[Ca^{2+}]_o$ concentration (1.2 mM) will potentiate DA release more, compared to control (2.4 mM) or high $[Ca^{2+}]_o$ (4.0 mM). We speculated that in order to detect a potential attenuation of this cocaine-induced increase in $[DA]_o$ by GABA-R antagonists in NAcC, we would need to decrease $[Ca^{2+}]_o$,

therefore increasing the effect that cocaine has on $[DA]_o$. In DLS, the lowest cocaine-induced increase in $[DA]_o$ in control conditions was ~93% (in 4 mM $[Ca^{2+}]_o$). Although we saw a decrease in this magnitude in the presence of GABA-R antagonists in DLS, and speculate that GABA-R antagonists attenuate cocaine-induced increases in DA release regardless of $[Ca^{2+}]_o$ in DLS, it is possible that in NAcC, the relationship is not as apparent. In 2.5 mM $[Ca^{2+}]_o$, the magnitude of cocaine-induced increase in $[DA]_o$ in control conditions is ~37%; still far lower than the ~93% increase in DLS in 4 mM $[Ca^{2+}]_o$. We hypothesised that lowering $[Ca^{2+}]_o$, and therefore increasing the effect of cocaine on peak $[DA]_o$, we would observe modulation by GABA-R antagonists in NAcC.

In 1.2 mM $[Ca^{2+}]_o$, application of cocaine (5 µM) increased single pulse-evoked $[DA]_o$ and widened transients in NAcC, consistent with a slowed uptake rate, in both the absence and presence of GABA-R antagonists (Fig. 3.7A). We observed a non-significant trend towards an attenuation of the cocaine-induced increase in $[DA]_o$ with GABA-R antagonists (Fig. 3.7B, two-way RM ANOVA, time x drug interaction, $F_{(19,95)} = 1.50$, $p = 0.1045$, n = 6). The magnitude of cocaine-induced increase in $[DA]_o$ was not different between conditions (Fig. 3.7C, unpaired t-test, $t_{(10)} = 0.95$, $p = 0.3625$, n = 6). Fig. 3.7D shows within-subject data, demonstrating that in all animals bar one, GABA-R antagonists appeared to attenuate the cocaine-induced increase in $[DA]_o$. Nevertheless, the ROUT method did not identify any statistical outliers.

Consistent with previous observations regarding the Ca^{2+} dependence of DAT inhibitor induced increases in $[DA]_o$ (Kile et al., 2010), cocaine increased $[DA]_o$ to a greater extent in aCSF containing 1.2 mM $[Ca^{2+}]_o$ compared with 2.5 mM $[Ca^{2+}]_o$ (~95% and ~37%, respectively, Fig. 3.7E). However, it must be noted that in GABA-R antagonist conditions, cocaine-induced increases in $[DA]_o$ were also higher in 1.2 mM $[Ca^{2+}]_o$ compared with 2.5 mM $[Ca^{2+}]_o$ (~68% and ~44%, respectively, Fig. 3.7E). No statistically significant interaction was observed,

although a trend emerged (Fig. 3.7E, two-way RM ANOVA, $[Ca^{2+}]_o$ x drug interaction, $F_{(1,5)} = 6.00$, $p = 0.0580$, n = 6).

These data indicate that whilst low $[Ca^{2+}]_o$ concentration may appear to begin to shift the relationship between DATs and GABA-Rs, no significant convergence of mechanisms between DATs and GABA-Rs are apparent in NAcC.

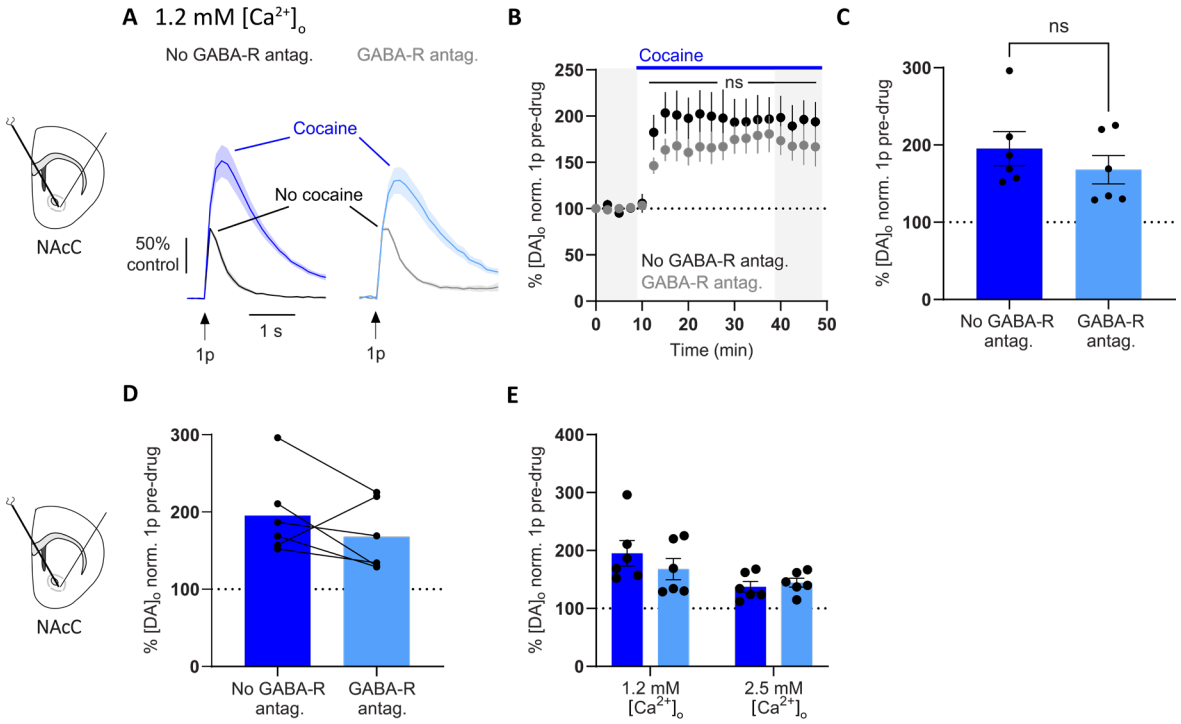

Figure 3.7. GABA-R antagonists do not impact cocaine-induced increase in DA release in NAcC in 1.2 mM *[Ca²⁺]ₒ*

*(A) $[DA]_o$ transients over time evoked by single pulses in NAcC in 1.2 mM $[Ca^{2+}]_o$, before and during bath application of cocaine (5 μM). n = 6. (B) Peak $[DA]_o$ over time evoked by single pulses, before and during cocaine. n = 6. (C) Percentage increase of peak $[DA]_o$ following application of cocaine. n = 6. (D) Percentage increase of peak $[DA]_o$ following application of cocaine, showing within-subject data. n = 6. (E) Percentage increase of peak $[DA]_o$ following application of cocaine, in 1.2 mM and 2.5 mM $[Ca^{2+}]_o$. n = 6. Data are mean ±SEM and normalised to pre-drug baseline (grey shaded region). 'No GABA-R antag.' is DHBE (1 μM), 'GABA-R antag.' is DHBE (1 μM), bicuculline (10 μM) and CGP 55845 (4 μM). *p ≤ .05, **p ≤ .01, **p ≤ .001, ns = non-significant.*

3.3.7 GABA-R antagonists attenuate cocaine-induced increase in DA release in DAT^{IREScre} mice

The apparent absence of a DAT-GABA relationship in NAcC led us to consider what some of the known differences are between DLS and NAcC DA neurons. DAT mRNA and gene expression levels are higher in DA neurons which project to the DLS, compared to those which project to NAcC (Haber et al., 1995; Poulin et al., 2014). Conversely, expression of calbindin-D28k is higher in DA neurons which project to the NAcC, compared to those which project to the DLS (Gerfen et al., 1985; Lavoie & Parent, 1991; Chung et al., 2005; Poulin et al., 2014). Presumably, DAT expression levels, at least in part, determine the extent to which DAT inhibition can increase $[DA]_o$, which is why DAT inhibitors produce a larger increase in $[DA]_o$ in DLS, than NAcC (~157% increase in DLS, Fig. 3.1A, unpublished data, Dr. E. Lopes, Cragg lab; ~37% increase in NAcC, Fig. 3.6C). In NAcC, lower DAT levels might mean that DAT function is not as susceptible to changes in GABA-R activity. If high DAT expression levels are required for the cocaine-induced increase in release to be modified by GABA-R antagonists, then we would expect this relationship to be weakened in mice with lower DAT expression in DLS.

DAT^{IREScre} homozygous mice exhibit a 47% decrease in DAT expression, and DAT^{IREScre} heterozygous mice exhibit a 17% decrease, compared to C57BL/6J wild-type controls (Bäckman et al., 2006). This reduction in DAT expression slows uptake rates in DLS and NAcC (Brimblecombe et al., 2019), and has also been reported in mice on a C57BL/6N background (Costa et al., 2021). Whilst DAT^{IREScre} mice are not intended as a model of DAT knockdown, we speculated that this reduction in DAT levels may help to disentangle the regional differences observed. Conducting experiments in DLS in DAT^{IREScre} mice may somewhat emulate the intrinsic lower DAT levels found in NAcC. Furthermore, in order to use genetically-encoded tools which require the expression of Cre recombinase, to investigate

this interaction between DATs and GABA-Rs, it was imperative to probe whether this convergence of mechanisms was intact in DAT^{IREScre} mice. We hypothesised that whilst GABA-R antagonists may still attenuate cocaine-induced increases in $[DA]_o$, that the regulation by GABA-R antagonists would be weakened because of lower cocaine induced increases in $[DA]_o$, caused by reduced striatal DAT expression.

As anticipated, application of cocaine (5 μM) increased single pulse-evoked $[DA]_o$ and widened transients in DLS in DAT^{IREScre} heterozygous mice, consistent with a slowed uptake rate, in both the absence and presence of GABA-R antagonists (Fig. 3.8A). Preliminary experiments indicate that, like in wildtype mice, GABA-R antagonists strongly attenuate the cocaine-induced increase in $[DA]_o$ in DLS (Fig 3.8B, C). These data were contrary to our initial hypothesis. Statistical comparisons were not performed due to low sample size (n = 2). As expected, due to reduced DAT levels in these mice, the effect of cocaine on evoked $[DA]_o$ in DLS was lower than in wildtype mice (~55% and ~157%, respectively; wildtype unpublished data collected by Dr. E. Lopes, Cragg lab).

This co-operation between DATs and GABA-Rs is consistent with all previous experiments in DLS, demonstrating that the co-operation is intact in DAT^{IREScre} heterozygous mice. We observed that although cocaine-induced increases in $[DA]_o$ in control conditions were now similar between DLS in DAT^{IREScre} mice (~55%) and NAcC in wildtype mice (~37%), this did not prevent GABA-R antagonists from attenuating cocaine-induced DA release in DLS. These preliminary findings indicate that DAT expression levels may not be responsible for the regional differences observed between DLS and NAcC.

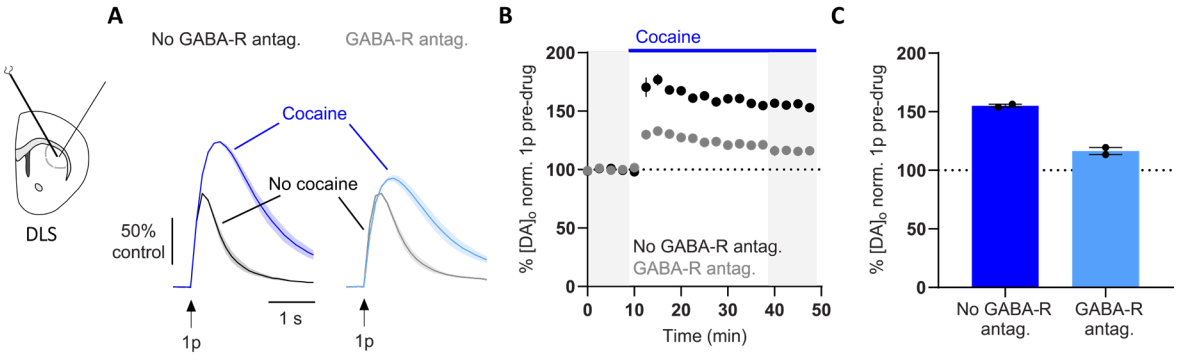

Figure 3.8. Preliminary: GABA receptor antagonists appear to attenuate effect of cocaine on DA release in DAT^{IREScre} mice

*(A) $[DA]_o$ transients over time evoked by single pulses in DLS in DAT^{IREScre} mice, before and during bath application of cocaine (5 μM). n = 2. (B) Peak $[DA]_o$ over time evoked by single pulses, before and during cocaine. n = 2. (C) Percentage increase of peak $[DA]_o$ following application of cocaine. n = 2. Data are mean ±SEM and normalised to pre-drug baseline (grey shaded region). 'No GABA-R antag.' is DHBE (1 μM), 'GABA-R antag.' is DHBE (1 μM), bicuculline (10 μM) and CGP 55845 (4 μM). *p ≤ .05, **p ≤ .01, **p ≤ .001, ns = non-significant.*

3.4. Discussion

I have shown that DA axons appear to integrate information from DATs and GABA-Rs, to determine striatal DA output. The convergent regulation of DA release by DATs and GABA-Rs did not require DA action at its receptors, indicating that these effects are not downstream of changes to DA action at its receptors, in response to the extended extracellular lifetime of DA in the presence of cocaine. The independence from DA receptors in turn indicates that the effects of DAT inhibition instead involve direct changes to DA axon function, and that there is axonal interaction or integration of activity arising through DATs and GABA-Rs, to affect the amplitude of DA release. This convergence persists across $[Ca^{2+}]_o$ concentrations and in mice with reduced DAT expression levels. There was also some regional variation in this convergence of mechanisms between DLS and NAcC.

3.4.1. Convergent regulation of DA release by DATs and GABA-Rs

Our results demonstrate that striatal DA release is modulated by a convergence of mechanisms involving DATs and GABA-Rs, demonstrating potential axonal integration. A related demonstration of axonal integration has recently been described in striatal DA axons, for co-operation between $GABA_A$-Rs and nAChRs, in mouse *ex vivo* brain slices. Diazepam, a $GABA_A$-R positive allosteric modulator, caused an attenuation of subthreshold nAChR input to striatal DA axons, whilst gabazine, a $GABA_A$-R antagonist, augmented nAChR mediated Ca^{2+} influx (Brill-Weil et al., 2024). These findings show that $GABA_A$-Rs limit cholinergic control of striatal DA signalling, and moreover, that DA axons make computations when faced with simultaneous incoming information, similar to that observed in dendrites (Brill-Weil et al., 2024). Whilst nAChR mediated changes to DA release are excluded in our results due to the presence of a nAChR antagonist throughout, it seems plausible that $GABA_A$-Rs govern not only nAChR mediated mechanisms, but also other receptor or transporter mediated signalling. Moreover, these findings not only demonstrate that DA axons

incorporate information from various sources, but also underpins the influence that GABA-Rs, and specifically $GABA_A$-Rs, exert over striatal DA axon excitability and output. Our data indicate that GABA-Rs govern DAT-mediated control of DA release. Potential mechanisms are discussed below.

Whilst future experiments could attempt to explore the separate contribution of $GABA_A$-Rs and $GABA_B$-Rs to this relationship, existing evidence in mouse *ex vivo* brain slices indicates that these receptors do not function independently on striatal DA axons. Whilst bicuculline, a $GABA_A$-R antagonist, increased DA release by ~10-15% and saclofen, a $GABA_B$-R antagonist, increased DA release by ~25%, co-application of both antagonists only increased DA release by ~25% (Lopes et al., 2019). This indicates some form of co-operation between $GABA_A$-Rs and $GABA_B$-Rs on striatal DA axons, and may complicate interpretations of experiments attempting to disentangle the contribution of each receptor. The observation that $GABA_A$- and $GABA_B$-Rs may co-operate on striatal DA axons (Lopes et al., 2019), supports the idea that these axons are performing signal integration.

Preliminary unpublished observations from the Cragg laboratory indicate that, in the presence of GABA-R agonists, the cocaine-induced increase in $[DA]_o$ is unchanged (unpublished data, Dr. E. Lopes, Cragg lab), indicating that the extent to which GABA-Rs can promote the cocaine-induced increase in DA release is at a maximum under basal conditions, in an *ex vivo* slice preparation. This observation is not simply due to a ceiling effect of DA release in GABA-R antagonists, as $[DA]_o$ in GABA-R antagonists starts at a higher baseline, as µM concentrations of $[DA]_o$ are higher in control conditions than GABA-R antagonists, following application of cocaine (unpublished data, Dr. E. Lopes, Cragg lab).

3.4.2. Potential mechanisms underlying co-operativity

It remains unclear what the substrate is for this co-operativity between DATs and GABA-Rs on striatal DA axons. A likely mechanism on which DATs and GABA-Rs could converge, especially relevant for DAT-mediated regulation of single pulse-evoked DA release, is a synapsin-dependent vesicle pool. Inhibition of DATs with cocaine leads to an increase in DA release, via a mobilisation of a synapsin-dependent reserve vesicle pool (Venton et al., 2006; Kile et al., 2010). This indicates that when DATs are active, they limit DA release by immobilisation of this pool. An explanation for our data is that DATs require activity at GABA-Rs, which may facilitate regulation of this synapsin-dependent vesicle pool. Phosphorylation of synapsins might regulate movement of vesicles between the reserve and readily releasable pools (Greengard et al., 1993). Hypothetically, if activity at GABA-Rs promotes phosphorylation of synapsins, this in turn could liberate vesicles and allow them to be readily released. A similar phenomenon has been suggested elsewhere (Greengard et al., 1993). Synapsin phosphorylation could therefore be a mechanism via which GABA-Rs support cocaine-induced increases to DA release. In the presence of GABA-R antagonists, synapsins could be dephosphorylated, making them unavailable for release. This could be an explanation as to why cocaine-induced increases in DA are lower in the presence of GABA-R antagonists, as DATs may not be able to liberate as many vesicles from the reserve pool, as when GABA-Rs are active. Another explanation, though less likely, is that the increase in DA release seen when GABA-R antagonists are applied (Lopes et al., 2019; Roberts et al., 2020), is due to mobilisation of a portion of this synapsin-dependent reserve pool, thus leaving less vesicles available for be liberated upon application of cocaine. Though it has been suggested that synapsin III is necessary for cocaine-induced increases in DA release (Kile et al., 2010), cocaine maintained the ability to augment DA release in mice lacking synapsin III in another investigation (Condon et al., 2019), suggesting the involvement of a compensatory mechanism. Future experiments aimed at exploring the involvement of synapsins in the

convergent regulation of DA release by DATs and GABA-Rs should be cautious and use triple synapsin knockout mice, to limit the possibility of compensation from other synapsins.

Evidence indicates that various proteins, including GPCRs, can regulate DAT trafficking and therefore DAT function (Gulley & Zahniser, 2003; Mortensen & Amara, 2003b; Eriksen et al., 2010; Schmitt & Reith, 2010). These GPCR-DAT interactions have particularly been studied for D_2-like-Rs. Application of a D_2-like-R antagonist reduces DA uptake rate in anaesthetised rats (Wu et al., 2002), however, this is not consistent with our observations. In our experiments, the presence of a D_2-like-R antagonist did not change uptake rate. It has ben found that DATs can form structural complexes with D_2-like-Rs, whereby D_2-like-R expression promotes uptake rate via increasing DAT surface expression (Lee et al., 2007). D_2-like-R activity specifically promotes DAT expression into PIP_2-containing nanodomains (Lycas et al., 2022). PIP_2 can bind to DATs and augments the effects of amphetamine (Hamilton et al., 2014; Khelashvili et al., 2015; Belovich et al., 2021), perhaps the same is true for cocaine. However, regulation of DAT trafficking by GPCRs is generally accompanied with a change in uptake rate. If transporter surface expression is increased, generally, so is uptake rate. In the case for a co-operation between GABA-Rs and DATs, it seems less likely that DAT trafficking is responsible. We found that GABA-Rs support DAT-mediated changes to striatal DA release. This could be consistent with higher DAT surface expression when GABA-Rs are active, and lower surface expression when GABA-Rs are inhibited. However, we did not observe any change to uptake rate in the presence of GABA-R antagonists. If GABA-Rs modulate DAT trafficking, then this would need to be accompanied with a change in uptake rate per transporter, to result in no net change in uptake rate. Whilst this seems unlikely, it is not impossible. Future experiments could test this by visualising DAT surface expression when GABA-Rs are active, or inactive, and comparing any differences. This could be accompanied by radiolabelled [^{3}H] DA, to visualise uptake rates per individual transporter.

DATs express binding sites for Gβγ G proteins (Rojas et al., 2020), and $GABA_B$-Rs can couple to Gβγ G proteins (Bettler et al., 2004). Gβγ binding to DATs results in reduced DA uptake and augments amphetamine-induced DA reverse transport through DATs (Garcia-Olivares et al., 2013; Mauna et al., 2019). In fact, activation of Gβγ proteins alone can induce DA reverse transport (Pino et al., 2021). Activation of Gβγ proteins augments amphetamine-induced hyperlocomotion, whereas Gβγ protein inhibition attenuates amphetamine-induced increases in locomotor behaviour and conditioned place preference (Mauna et al., 2019). However, cocaine-induced hyperlocomotion or conditioned place preference is not affected by activation or inhibition of Gβγ proteins (Mauna et al., 2019). These data indicate that whilst Gβγ proteins mediate the effects of amphetamine, they do not impact on the effects of cocaine. Nevertheless, future experiments could test whether Gβγ protein activation, using a cell-permeable activator such as mSIRK (Garcia-Olivares et al., 2013; Mauna et al., 2019), modulates DAT-mediated changes to DA release.

DATs belong to the NSS family, and require binding of two Na^+ ions and one Cl^- ion for translocation of DA (Masson et al., 1999). This ion flux through DATs is electrogenic, and typically depolarising (Carvelli et al., 2004). DAT-mediated inward currents are greater at more hyperpolarised potentials, at least in oocytes or HEK cells expressing hDAT (Sonders et al., 1997; Richardson et al., 2016a). Technical limitations mean that these currents have not yet been investigated in axons, but we speculate that, as striatal DA axons are more hyperpolarised than their soma (Kramer et al., 2020), and have high levels of DAT expression, especially in DLS DA neurons (Haber et al., 1995), these DAT-mediated currents are apparent and could contribute to striatal DA axon excitability. $GABA_A$-Rs allow flow of Cl^- ions upon binding of GABA (Scott & Aricescu, 2019), and in striatal DA axons, activation of these receptors is depolarising, as the $GABA_A$-R reversal potential is depolarised compared to the hyperpolarised potential of the axon (Kramer et al., 2020). It is important, however, to note that these axonal recordings (Kramer et al., 2020) were performed in the main branch of the

axon, which is unlikely to be the case in our fast-scan cyclic voltammetry recordings. As striatal DA axons are under tonic inhibition by GABA (Lopes et al., 2019), we might expect that the presence of GABA-R antagonists would slightly hyperpolarise the axonal membrane, and therefore favour DAT-mediated currents. We would not expect that $GABA_B$-Rs would depolarise the membrane; rather, $GABA_B$-Rs typically hyperpolarise the membrane by coupling to VGCCs, GIRK channels, or adenylyl cyclase, dependent on their location within the synapse (Bettler et al., 2004). If $GABA_B$-Rs hyperpolarise the DA axonal membrane, then in the absence of GABA-R antagonists, $GABA_B$-Rs may favour DAT-mediated currents. Conversely, in the presence of GABA-R antagonists, DAT function could be reduced, an explanation that is consistent with our data. Whilst these candidate mechanisms are unlikely to affect single pulse-evoked DA release, they may impact overall axonal excitability and short-term plasticity in striatal DA release, which will be explored later in this thesis

To our knowledge, there is no definitive evidence thus far on which $GABA_B$-R coupling mechanism(s) are present on striatal DA axons. $GABA_B$-Rs limit single-pulse evoked DA release, which could be consistent with a coupling to VGCCs, however, taking into account the role of these receptors in the frequency-dependence of DA release, GIRK channels appear to be a good candidate (Roberts et al., 2021b). It is of course plausible that more than one of these mechanisms is present, particularly due to the largely asynaptic and branched nature of striatal DA axons (Descarries et al., 1996; Matsuda et al., 2009; Aransay et al., 2015a). Interestingly, it was recently reported that DATs antiport K^+ (Schmidt et al., 2022), and DATs can localise with $K_V7.2/7.3$ channels (Bartolomé-Martín et al., 2019), therefore it is possible that changes in GIRK channel activity could affect DAT function through K^+ signalling. Maybe, DATs and $GABA_B$-Rs, when active, act in parallel to promote K^+ efflux. DA uptake rate is facilitated by antiporting K^+, therefore, it is possible that $GABA_B$-R mediated K^+ efflux through GIRK channels assists DAT regulation of DA release.

Future experiments are required to determine whether the substrate of the interaction between DATs and GABA-Rs is via Ca^{2+}, Cl^{-}, K^{+}, synapsins, Gβγ proteins, or another mechanism, such as post-translational modifications. Future investigations could also explore whether this co-operativity is specific to DATs and GABA-Rs, or whether DAT function or trafficking on striatal DA axons could be governed by other ionotropic or metabotropic receptors operating in similar ways to GABA-Rs.

3.4.3. Regional variation in co-operation between DATs and GABA-Rs

Our results indicate that the convergence of mechanisms involving DATs and GABA-Rs which is prominent in DLS, is either non-existent in NAcC, or obscured by another mechanism, possibly involving Ca^{2+} handling. Regional differences have been reported between DLS and NAcC regarding GABA transporter (GAT) -mediated changes to striatal DA release (Roberts et al., 2020). The broad spectrum GAT inhibitor, nipecotic acid (NPA), decreases DA release in DLS by ~40%, consistent with an increase in extracellular GABA and increased activity at $GABA_A$- and $GABA_B$-Rs (Roberts et al., 2020). However, in NAcC, NPA only slightly decreased DA release, and this was not significantly different from time-matched controls (Roberts et al., 2020). These data are puzzling considering the almost identical effect of GABA-R antagonists in increasing DA release between the two regions (Roberts et al., 2020). The inconsistency of these results appear to be somewhat explained by GAT expression levels; both GAT-1 and GAT-3 isoforms are expressed to higher levels in DLS than NAcC (Roberts et al., 2020).

The lack of an attenuation of cocaine-induced increase in DA release by GABA-R antagonists in NAcC, may be related to vulnerable versus resistant dopamine neuron populations regarding Parkinson's disease. It seems plausible that there are a variety of mechanisms, possibly involving Ca^{2+} buffering, in NAcC DA neurons which 'protect' them from strong regulation and thus dysregulation and degeneration. The strong modulation of DAT function,

and therefore DA axon function, by GABA-Rs in DLS may be a symptom of the vulnerability in these neurons. The potential disease relevance of these findings are discussed in Chapter 6.

Although our results do not strongly support a role for Ca^{2+} handling in the relationship between DATs and GABA-Rs in NAcC, this remains to be elucidated. There was no apparent difference between control and GABA-R antagonist conditions in 2.5 mM $[Ca^{2+}]_o$, but a trend appeared to be emerging in experiments conducted in 1.2 mM $[Ca^{2+}]_o$, with all replicates but one showing an attenuated effect of cocaine on DA release in NAcC (Fig. 3.7D), possibly due to subregional differences in calbindin-D28k expression patterns. Future experiments are required to disentangle any regional variation in co-operativity between DATs and GABA-Rs. It is possible that lowering $[Ca^{2+}]_o$ even further, such as to 0.5 mM, or testing a wider range of $[Ca^{2+}]_o$ concentrations, may reveal a modulation by GABA-R antagonists in NAcC in the future.

3.4.4. Summary

In summary, our data demonstrate that striatal DA release is regulated by DATs and GABA-Rs, which co-operate to determine DA output. DATs limit DA release, and when inhibited, elicit a large increase in DA release. This increase in DA release, and presumably DAT function, is supported by GABA-Rs, as when GABA-Rs are inhibited, the increase in DA release by DAT inhibitors is attenuated. However, activity at GABA-Rs does not influence DA uptake, indicating that GABA-Rs specifically promote DAT-mediated regulation of DA release, over other aspects of DAT function. This relationship is robust in DLS and occurs in the presence of DA-R antagonists, indicating integration at the level of DA axons themselves, and in various $[Ca^{2+}]_o$ concentrations, showing that this modulation by GABA-R antagonists occurs across different levels of DAT activity. A co-operation between DATs and GABA-Rs in NAcC requires further investigation. These findings may have implications for our understanding of the

integration of information that DA axons perform, and dysfunction in DAT and GABA signalling in Parkinson's disease.

Chapter 4.

GIRK channel contribution to the control of DA release by DATs and GABA-Rs

4.1. Introduction

4.1.1. GIRK channels in DA neurons

GIRK, or Kir3, channels are a subtype of inwardly rectifying K^+ channels, stimulated by $G_{i/o}$ proteins upon activation of specific GPCRs sensitive to GABA, DA, acetylcholine, 5-HT, and more (Lüscher & Slesinger, 2010). Above the reversal potential, GIRK channel activation typically results in hyperpolarisation, mediated by K^+ efflux through these channels (Lüscher & Slesinger, 2010; Luo et al., 2022). Four different GIRK channel subunits exist in mammals, GIRK1-4 (Lüscher & Slesinger, 2010; Luo et al., 2022), though GIRK4 expression is very low or undetectable in the brain (Karschin et al., 1996). Neuronal GIRK1 (Nelson et al., 1997; Steinecker et al., 2007) and GIRK2 (Lesage et al., 1994, 1995; Isomoto et al., 1996; Inanobe, Horio, et al., 1999; Lüscher & Slesinger, 2010) splice variants have been identified. The most common neuronal GIRK channel in rodents is composed of GIRK1/2 subunits (Liao et al., 1996; Luján et al., 2014), however, DA neurons are unusual regarding the GIRK channels they express, as they do not express GIRK1 subunits (Karschin et al., 1996).

SNc and VTA neurons are especially enriched with GIRK2, with only the hippocampus exhibiting higher expression in the rat brain (Karschin et al., 1996). VTA DA neurons express heterotetrametric channels composed of GIRK2a/3 subunits (Cruz et al., 2004; Labouèbe et al., 2007), and SNc DA neurons express homotetrameric channels composed of only GIRK2 (2a/2c) subunits (Inanobe, Yoshimoto, et al., 1999; del Burgo et al., 2008; Lüscher & Slesinger, 2010). GIRK2 homotetrameric channels tend to exhibit faster opening times compared to other GIRK channel subtypes (Lüscher & Slesinger, 2010). Regional differences in GIRK2 expression are well documented in DA neurons. SNc DA neurons, which project to DLS, have higher levels of GIRK2 mRNA and protein than VTA DA neurons, which project to NAcC (Schein et al., 1998; Chung et al., 2005; Poulin et al., 2014). It is currently unclear

whether these regional disparities in GIRK channel expression impact striatal DA transmission differently in DLS and NAcC.

4.1.2. GIRK channels and GABA-Rs

A functional relationship has been described for GIRK channels and $GABA_B$-Rs. $GABA_B$-Rs typically couple to VGCCs, GIRK channels, or adenylyl cyclase, dependent on their location within the synapse (Bettler et al., 2004; Terunuma, 2018). In *ex vivo* hippocampal slices from mice lacking the GIRK2 gene, only postsynaptic, and not presynaptic, $GABA_B$-R mediated outward currents were abolished (Lüscher et al., 1997). Therefore, postsynaptic, $GABA_B$-Rs are thought to couple to GIRK channels, to induce a slow inhibitory postsynaptic current (IPSC) (Lüscher et al., 1997; Schuler et al., 2001). This canonical view of $GABA_B$-R coupling has been challenged however, by reports of functional and anatomical $GABA_B$-R and GIRK channel colocalisation at presynaptic locations in cortical and hippocampal neurons (Ladera et al., 2008; Martín-Belmonte et al., 2022).

In rat SNc DA neurons, $GABA_B$-Rs recruit the same GIRK channel population as D_2-Rs (Lacey et al., 1988). In mouse SNc DA (and GABA) neurons, GIRK2 channel immunoreactivity was most prominent in dendritic compartments, and in close proximity to $GABA_{B(1)}$ immunoreactivity (Koyrakh et al., 2005). Regarding neuronal integration of these signals, in mouse *ex vivo* brain slices, SNc DA neurons integrate $GABA_B$-R and D_2-R activation to produce an outward K^+ current via GIRK channels which is larger than the sum of GIRK-mediated currents produced by either receptor alone (Condon et al., 2022). This might be specific to SNc DA neurons, as $GABA_B$-R and D_2-R GIRK currents in VTA DA neurons are differentially regulated by methamphetamine, demonstrating a dissociation between GIRK currents elicited by these receptors (Munoz et al., 2016). Though $GABA_B$-R coupling efficacy for GIRK channels in rat VTA DA neurons is thought to be low, compared to VTA GABA neurons, due to the unique GIRK subunit composition in DA neurons (Cruz et al., 2004), the

coupling efficacy in mouse VTA DA neurons has been shown to be dynamically regulated by RGS2, a member of the regulators of G protein signalling family (Labouèbe et al., 2007). This shows that the coupling efficacy of $GABA_B$-Rs and GIRK channels in DA neurons is not static (Labouèbe et al., 2007).

Coupling of $GABA_B$-Rs to GIRK channels has not yet been shown in striatal DA axons. Moreover, the largely asynaptic nature of these axons (Descarries et al., 1996) may mean that the typical scenario of $GABA_B$-R coupling being dependent on receptor location within the synapse may not apply. Though $GABA_B$-R and GIRK channel coupling is typically understood to be present only at postsynaptic sites (Lüscher et al., 1997; Schuler et al., 2001; Bettler et al., 2004; Terunuma, 2018), there have been observations, at least in the hippocampus, that $GABA_B$-Rs and GIRK channels could functionally couple at presynaptic sites (Thompson & Gähwiler, 1992). Nevertheless, functional data indicate that GIRK channels are a good candidate for $GABA_B$-R coupling in striatal DA axons (Roberts et al., 2021a). We aimed to test whether GIRK channels contribute to the control of striatal DA release by GABA-Rs.

4.1.3. GIRK channels and DATs

Numerous experiments have implicated GIRK channels in DAT-mediated, and often cocaine-mediated, behaviours. Knockout of sorting nexin 27 (SNX27), an endosomal sorting protein which directly regulates GIRK channel expression through a PDZ domain interaction (Balana et al., 2011), in DA neurons, causes a reduction in $GABA_B$-R mediated GIRK currents, and an enhancement of cocaine-induced locomotor activity, both of which were restored upon viral delivery of the SNX27-insensitive GIRK2a splice variant (Munoz & Slesinger, 2014). Loss of SNX27 in TH-positive neurons leads to a state of increased neuronal excitability in VTA and SNc, and these mice exhibit locomotor sensitisation to a subthreshold dose of cocaine, despite no change in total $GABA_B$-R or GIRK2 protein levels in these neurons (Rifkin et al., 2018). Mice with a conditional knockout of GIRK2 channels in DA neurons exhibit enhanced

cocaine-induced locomotor activity, and enhanced cocaine intake on a self-administration schedule (McCall et al., 2017), however, critically, this study did not control for the reduced DAT expression levels seen in $DAT^{IREScre}$ mice (Bäckman et al., 2006), which could confound results. However, when the expression of Cre in DAT-containing neurons is taken into account, overexpression of GIRK2c in VTA DA neurons reduces cocaine-induced locomotor activity, whereas overexpression of GIRK3 enhances cocaine-induced locomotor activity (McCall et al., 2019). Taken together, these findings demonstrate that GIRK channels mediate DAT-associated behaviours and pose the question of whether GIRK channels contribute to DAT-mediated changes in striatal DA transmission.

4.1.4. Pharmacologically targeting GIRK channels

Historically, the pharmacological toolbox available to target GIRK channels has been very limited, and existing ligands ligands have various off-target effects, or do not target non GIRK1-containing channels (Kozek et al., 2019; Jeremic et al., 2021; Zhao et al., 2021; Luo et al., 2022). SCH 23390, a drug widely used to inhibit DA D_1-like-Rs, inhibits GIRK channels in AtT-20 cells (Kuzhikandathil & Oxford, 2002). These AtT-20 cells express only GIRK1 and GIRK2 isoforms (Kuzhikandathil et al., 1998). At 10 μM, a concentration commonly used to inhibit DA D_1-like-Rs, SCH 23390 inhibits GIRK channel currents induced by DA D_3-R or somatostatin receptor activation (Kuzhikandathil & Oxford, 2002). Further, data from CHO cells expressing GIRK1 and/or GIRK2, without co-expression of any GPCR, show that SCH 23390 directly inhibits GIRK1/2 heterotetramers and GIRK2 homotetramers, identifying a halide atom responsible for GIRK channel inhibition (Kuzhikandathil & Oxford, 2002). In Section 3.3.1, we showed that D_1-like-Rs are not involved in regulation of DA release by DATs and GABA-Rs. Therefore, the affinity of SCH 23390 for GIRK2 channels (Kuzhikandathil & Oxford, 2002), and the lack of involvement of D_1-like-Rs in our mechanisms of interest,

means that SCH 23390 is an appropriate pharmacological ligand to explore GIRK channel function in striatal DA axons.

The experiments outlined in this chapter explored whether GIRK channels are involved in the control of striatal DA release by DATs and GABA-Rs.

4.2. Methods

Experiments detailed in this chapter were carried out in accordance with the general methods described in Chapter 2. Variations and further details are reported below.

4.2.1. Animals and slice preparation

Animals used for experiments in this chapter were male and female wild-type C57BL/6J mice, DAT^{IREScre} mice (Jax strain #: 006660), GIRK2 cKD (DAT Cre$^{+/-}$:GIRK2 flox$^{+/-}$) or GIRK2 cKO (DAT Cre$^{+/-}$:GIRK2 flox$^{+/+}$) mice.

GIRK2$^{flox/flox}$ mice were obtained from the Wickman laboratory at the University of Minnesota, under a Material Transfer Agreement. DAT^{IREScre} mice were crossed with GIRK2$^{flox/flox}$ (DAT Cre$^{-/-}$:GIRK2 flox$^{+/+}$) mice to generate the following genotypes: heterozygous for DAT^{IREScre} and heterozygous for GIRK2$^{flox/flox}$ (GIRK2 cKD), and heterozygous for DAT^{IREScre} and homozygous for GIRK2$^{flox/flox}$ (GIRK2 cKO). Data obtained from these mice were compared to data obtained from to age- and sex-matched mice heterozygous for DAT^{IREScre}.

Mice were culled by cervical dislocation and acute *ex vivo* brain slices were prepared as described in Section 2.1.5. All procedures were performed in accordance with institutional guidelines and the U.K. Animals (Scientific Procedures) Act, 1986.

4.2.2. Fast-scan cyclic voltammetry

Fast-scan cyclic voltammetry was used to measure changes in $[DA]_o$, as described in Section 2.2. Each experiment was performed at a single recording site in either the DLS or NAcC. DA was evoked every 2.5 minutes by single pulse electrical stimulation. Drug application was performed once signal stability was achieved: ≤ 10% variation across six consecutive recordings.

4.2.3. Drugs

Stock solutions were prepared at 1,000x – 20,000x the final concentration and stored at -20°C. Final drug concentrations were prepared in aCSF on the day of the experiment.

Drug	Supplier	Action	Concentration	Solvent	References
(+)-Bicuculline	Abcam	$GABA_A$-R antagonist	10 µM	Dimethyl sulfoxide (DMSO)	Roberts et al. (2020); Stedehouder et al. (2024)
CGP 55845 hydrochloride	Abcam	$GABA_B$-R antagonist	4 µM	Dimethyl sulfoxide (DMSO)	Roberts et al. (2020); Stedehouder et al. (2024)
Cocaine hydrochloride	Sigma-Aldrich	DAT inhibitor	5 µM	dH_2O	Condon et al. (2020); Threlfell et al. (2021)
Dihydro-β-erythroidine (DHβE) hydrobromide	Sigma-Aldrich	nAChR antagonist	1 µM	dH_2O	Threlfell et al. (2012); Roberts et al. (2020)
Nipecotic acid	Sigma-Aldrich	GAT inhibitor	1.5 mM	Hydrochloric acid (HCl)	Roberts et al. (2020)
SCH 23390 hydrochloride	Tocris	GIRK channel inhibitor	10 µM	dH_2O	Kuzhikandathil & Oxford (2002)
SCH 39166 hydrobromide	Tocris	D_1-like-R antagonist	1 µM	Dimethyl sulfoxide (DMSO)	Zheng et al. (1999); Yang et al. (2020)

4.2.4. Data acquisition and analysis

Data were digitised and acquired using Axoscope 10.7, and extracted using locally written Excel macros or Python script. Statistical tests were performed in GraphPad Prism 9 or 10.

4.3. Results

4.3.1. GIRK channel inhibition prevents modulation of DA release by GABA-R antagonists

Striatal DA release is under tonic inhibition by GABA at $GABA_A$- and $GABA_B$-Rs, demonstrated by an increase in single pulse-evoked DA release upon application of GABA-R antagonists (Lopes et al., 2019; Roberts et al., 2020). DA neurons express GIRK channels (Inanobe, Yoshimoto, et al., 1999; Cruz et al., 2004; Labouèbe et al., 2007; del Burgo et al., 2008; Lüscher & Slesinger, 2010), and $GABA_B$-Rs may couple to GIRK channels (Bettler et al., 2004; Terunuma, 2018). Therefore we explored whether GIRK channel inhibition impacted on modulation of striatal DA release by GABA-Rs. As discussed in Chapter 3, evidence indicates that $GABA_A$- and $GABA_B$-Rs co-operate in determining striatal DA release, because application of antagonists for each receptor do not result in a summative effect on single pulse-evoked DA release (Lopes et al., 2019). We therefore hypothesised that inhibition of GIRK channels, whilst most likely to particularly affect $GABA_B$-R modulation of striatal DA release, would attenuate the effect of combined $GABA_A$- and $GABA_B$-R antagonists on single pulse-evoked DA release. We hypothesised that inhibition of GIRK channels would attenuate the increase in DA release upon application of GABA-R antagonists in both DLS and NAcC, although with greater attenuation in DLS.

However, application of SCH 23390 (SCH; 10 µM) in DLS did not modify single pulse-evoked $[DA]_o$ (Fig. 4.1A, B). Comparison of $[DA]_o$ concentration before and during SCH 23390 application did not show any significant difference (Fig. 4.1C, paired t-test, $t_{(10)} = 0.59$, $p = 0.5686$, n = 11 from 7 animals). These data indicate that GIRK channel inhibition does not affect single pulse-evoked $[DA]_o$ in DLS.

Application of GABA-R antagonists (bicuculline, 10 μM and CGP 55845 4 μM) in the presence of SCH 23390 in DLS did not increase single pulse-evoked $[DA]_o$ (Fig. 4.1D, E). SCH 23390 is commonly used as a D_1-like-R antagonist, therefore, data are plotted against data obtained in the presence of an alternate D_1-like-R antagonist with no reported affinity for GIRK channels (SCH 39166, 1 μM), for comparison (Fig. 4.1 D-F only). SCH 39166 was absent during recordings exploring the effect of SCH 23390 on evoked $[DA]_o$. In the absence of the GIRK channel inhibitor, SCH 23390, GABA-R antagonists increase single pulse-evoked $[DA]_o$, but in the presence of SCH 23390, GABA-R antagonists no longer increase $[DA]_o$ (Fig 4.1D, E, two-way RM ANOVA, time x drug interaction, $F_{(11,55)} = 7.77$, $p < 0.0001$, n = 6). In the absence of SCH 23390, GABA-R antagonists increase evoked $[DA]_o$ concentration (Fig. 4.1F, paired t-test, $t_{(5)} = 3.51$, $p = 0.0170$, n = 6). On the contrary, in the presence of SCH 23390, GABA-R antagonists do not increase evoked $[DA]_o$ concentration (Fig. 4.1F, paired t-test, $t_{(5)} = 0.15$, $p = 0.8869$, n = 6). These data indicate that GIRK channel inhibition prevents GABA-R antagonists from increasing evoked $[DA]_o$ in DLS.

In NAcC, application of SCH 23390 (10 μM) appeared to slightly increase single pulse-evoked $[DA]_o$ (Fig. 4.1G, H). Comparison of $[DA]_o$ concentration before and during SCH 23390 application showed a significant increase in $[DA]_o$ in the presence of SCH 23390 (Fig. 4.1I, paired t-test, $t_{(11)} = 3.16$, $p = 0.0856$, n = 12 from 9 animals). These data indicate that GIRK channel inhibition increases single pulse-evoked $[DA]_o$ in NAcC. Application of GABA-R antagonists (bicuculline, 10 μM; CGP 55845 4 μM) in the presence of SCH 23390 in NAcC did not increase single pulse-evoked $[DA]_o$ (Fig. 4.1J,K, paired t-test, $t_{(6)} = 1.91$, $p = 0.1050$, n = 7). These data indicate that GIRK channel inhibition prevents the increase in evoked $[DA]_o$ with GABA-R antagonists in NAcC.

Fig. 4.1L shows the change in single pulse-evoked $[DA]_o$ in DLS and NAcC upon application of SCH 23390 (orange), and upon application of GABA-R antagonists following prior

application of SCH 23390 (green). Overall, SCH 23390 or GABA-R antagonists did not produce a net change in evoked $[DA]_o$, although variability exists, with some observations of an increase in $[DA]_o$ and some observations of a decrease in $[DA]_o$. Increases in $[DA]_o$ appear to be more common in NAcC. However, results in NAcC are interpreted with caution due to the tendency of evoked $[DA]_o$ in NAcC to marginally increase over time on occasion (unpublished observations, Cragg lab), and the observation that VTA neurons express fewer GIRK channels compared to SNc neurons (Schein et al., 1998; Chung et al., 2005; Poulin et al., 2014), and therefore we would not expect single pulse-evoked $[DA]_o$ in NAcC to be limited by GIRK channel activity.

Taken together, these data demonstrate that GIRK channels mediate GABA-R control of striatal DA release.

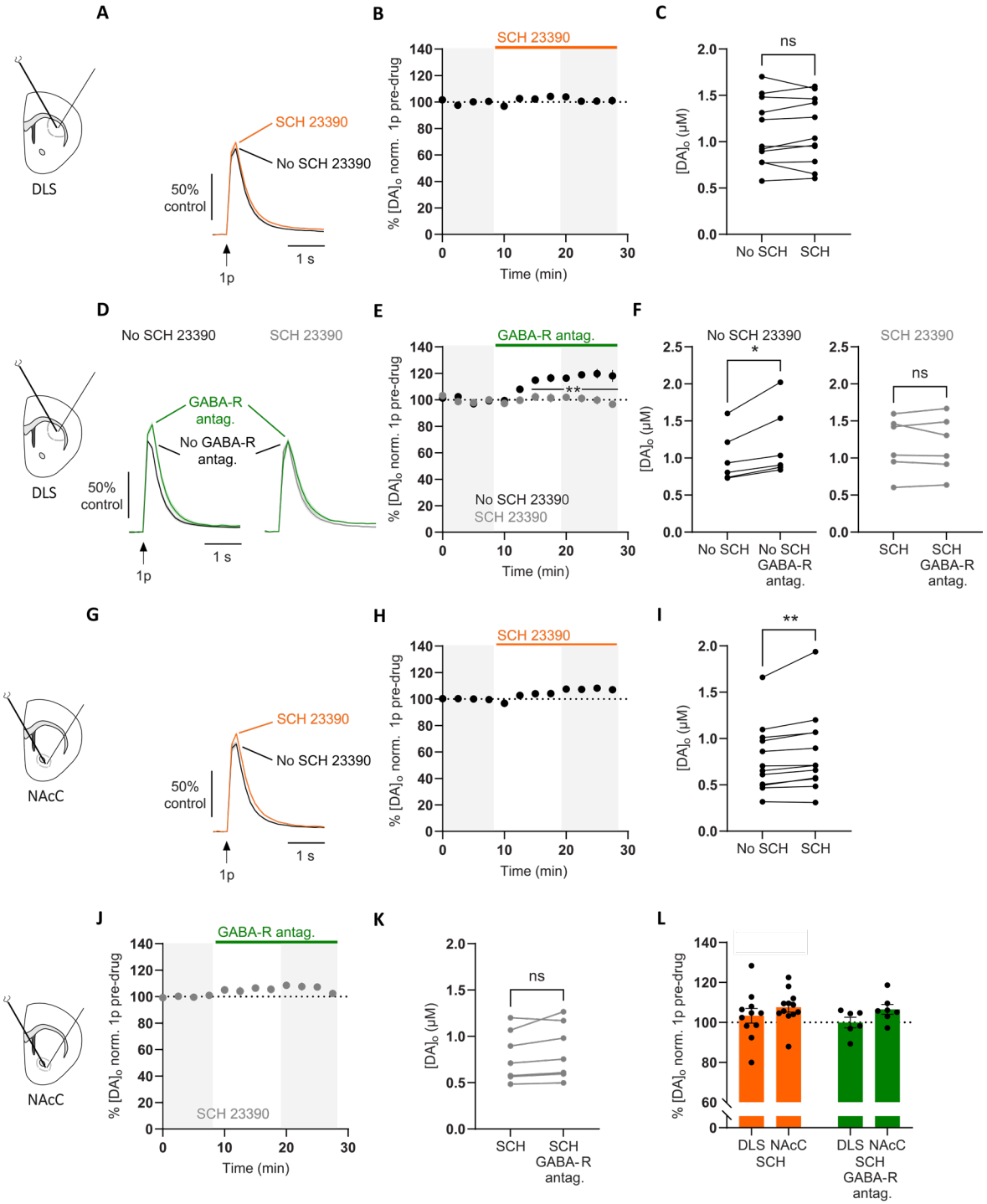

Figure 4.1. GIRK channel inhibition with SCH 23390 prevents increase in DA release by GABA-R antagonists in DLS and NAcC

(A) $[DA]_o$ transients over time evoked by single pulses in DLS, before and during bath application of SCH 23390 (SCH; 10 μM). n = 11. (B) Peak $[DA]_o$ over time evoked by single pulses, before and during SCH 23390. n = 11. (C) Peak $[DA]_o$ (μM) evoked by single pulses, before and during SCH 23390. n = 11. (D) $[DA]_o$ transients over time, evoked by single pulses in DLS, before and during bath application of GABA-R antagonists (bicuculline 10 μM and CGP 55845 4 μM). n = 6. (E) Peak $[DA]_o$ over time evoked by single pulses, before and during GABA-R antagonists. n = 6. (F) Peak $[DA]_o$ (μM) evoked by single pulses, before and GABA-R antagonists. n = 6. (G) $[DA]_o$ transients over time evoked by single pulses in NAcC, before and during SCH 23390. n = 12. (H) Peak $[DA]_o$ over time evoked by single pulses, before and during SCH 23390. n = 12. (I) Peak $[DA]_o$ (μM) evoked by single pulses, before and during SCH 23390. n

*= 12. (J) Peak [DA]$_o$ over time evoked by single pulses, before and during GABA-R antagonists. n = 7. (K) Peak [DA]$_o$ evoked by single pulses, before and during GABA-R antagonists. n = 7. (L) Percentage of peak [DA]$_o$ following application of SCH 23390 (orange) or GABA-R antagonists (green). Data are mean ±SEM and normalised to pre-drug baseline (grey shaded region) (A, B, D, E, G, H, J, L). 'No SCH 23390' is DHβE (1 μM) (and SCH 39166 (1 μM) in D, E, F only), 'SCH 23390' is DHβE (1 μM) and SCH 23390 (10 μM). *p ≤ .05, **p ≤ .01, **p ≤ .001, ns = non-significant.*

4.3.2. GIRK channel inhibition does not prevent GABA-R antagonist modulation of DA release by attenuating GABA tone

The observation that GABA-R antagonists do not increase DA release in the presence of the GIRK channel inhibitor, SCH 23390 (Section 4.3.1), led us to two alternative speculations. GIRK channel inhibition might either directly interact with GABA-R effector mechanisms on DA axons, or alternatively SCH 23390 might act on other striatal neurons to limit the source of ligand GABA that acts tonically at axonal GABA-Rs, constituting a form of disinhibition. Mixed evidence exists regarding whether striatal neurons express GIRK channels (Kobayashi et al., 1995; Shan et al., 2022). We explored whether GIRK channel inhibition reduces striatal GABA tone by disinhibition, to therefore prevent an increase in DA release upon application of GABA-R antagonists. To test this, we conducted a wash-on of GABA-R antagonists in the presence of SCH 23390 following application of NPA, a broad spectrum GAT inhibitor. GAT inhibition would prevent GABA uptake and therefore increase extracellular GABA. We hypothesised that, following GAT inhibition, GABA-R antagonists would increase DA release, even in the presence of SCH 23390.

Consistent with previous findings (Roberts et al., 2020), application of the GAT inhibitor, nipecotic acid (NPA; 1.5 mM) alone attenuated [DA]$_o$ in DLS (Fig. 4.2A, B). Comparison of [DA]$_o$ concentration before and during NPA application showed a significant decrease in NPA (Fig. 4.2C, paired t-test, $t_{(9)} = 4.77$, $p = 0.0010$, n = 10 from 6 animals). Application of SCH 23390 in the presence of NPA did not modify evoked [DA]$_o$ (Fig. 4.2D, E, F, , paired t-test, $t_{(4)} = 0.24$, $p = 0.8245$, n = 5). Following prior application of NPA, application of GABA-R antagonists in the absence of SCH 23390 increased single pulse-evoked [DA]$_o$, however, no

increase was observed in the presence of SCH 23390 (Fig. 4.2G, H, two-way RM ANOVA, time x drug interaction, $F_{(11,88)} = 12.23$, $p < 0.0001$, n = 5).

These data show that the presence of SCH 23390 prevents an increase in $[DA]_o$ upon application of GABA-R antagonists, even when extracellular GABA levels are augmented. This indicates that SCH 23390 does not prevent the effect of GABA-R antagonists on $[DA]_o$ by attenuating striatal GABA levels.

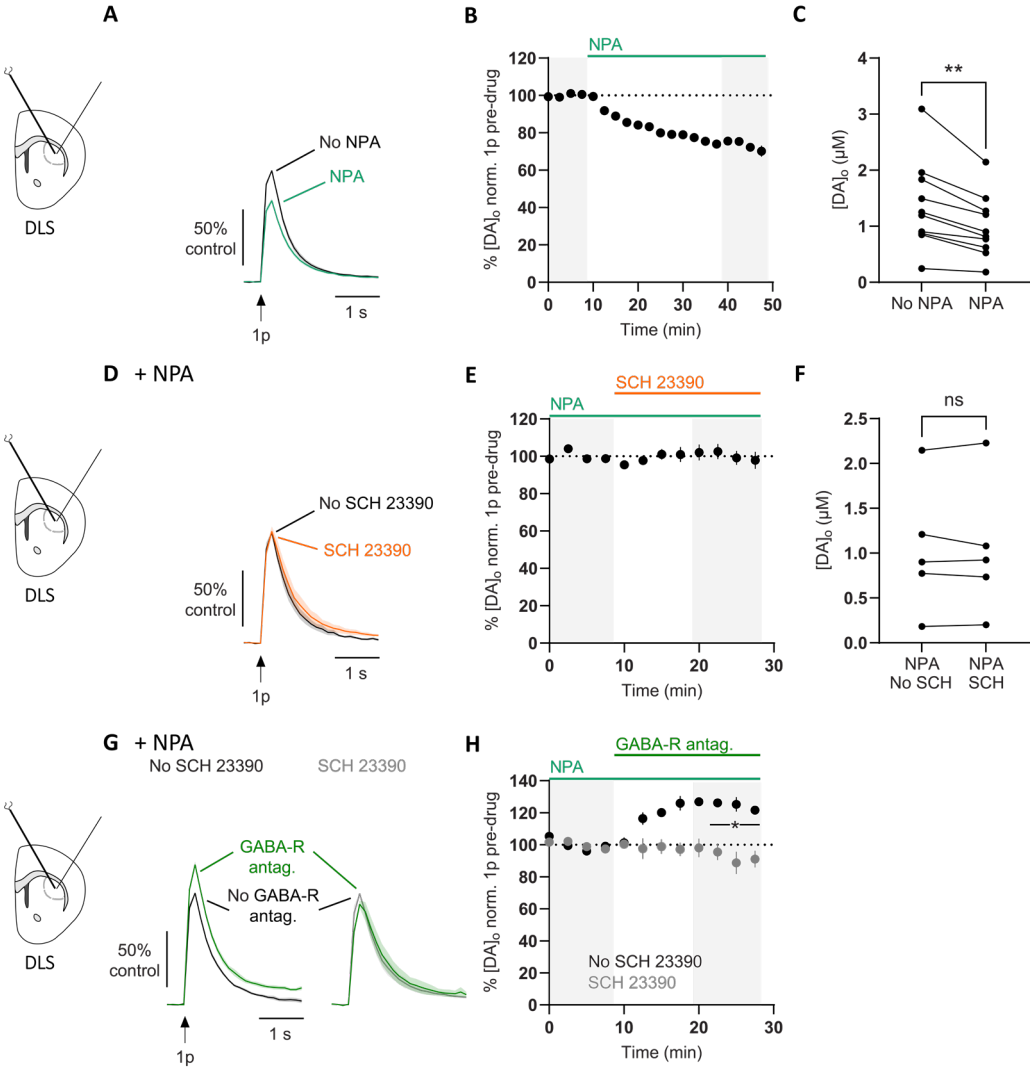

Figure 4.2. GIRK channel inhibition with SCH 23390 does not prevent GABA-R antagonist modulation of DA release by lowering striatal GABA tone

(A) $[DA]_o$ transients over time evoked by single pulses in DLS, before and during bath application of NPA (1.5 mM). n = 10. (B) Peak $[DA]_o$ over time evoked by single pulses, before and during NPA. n = 10. (C) Peak $[DA]_o$ (μM) evoked by single pulses, before and during NPA. n = 10. (D) $[DA]_o$ transients over time evoked by single pulses in DLS, before and during SCH 23390. n = 5. (E) Peak $[DA]_o$ over time evoked by single pulses, before and during SCH 23390. n = 5. (F) Peak $[DA]_o$ (μM) evoked by single pulses, before and during SCH 23390. n = 5. (G) $[DA]_o$ transients over time evoked by single pulses in DLS, before and

*during GABA-R antagonists (bicuculline, 10 μM and CGP 55845, 4 μM). n = 5. (H) Peak [DA]$_o$ (±SEM) over time evoked by single pulses, before and during GABA-R antagonists. n = 5. Data are mean ±SEM and normalised to pre-drug baseline (grey shaded region) (A, B, D, E, G, H). 'No SCH 23390' is DHβE (1 μM) and NPA (1.5 mM), 'SCH 23390' is DHβE (1 μM), NPA (1.5 mM) and SCH 23390 (10 μM). *p ≤ .05, **p ≤ .01, **p ≤ .001, ns = non-significant.*

4.3.3. Loss of GIRK2 channels in DA neurons does not affect modulation of DA release by GABA-R antagonists

Pharmacologically targeting GIRK channels is challenging, therefore, we utilised a previously described (Kotecki et al., 2015) genetically-modified mouse line to decrease GIRK2 channel expression in DA neurons. To generate mice with a conditional knockdown or knockout of GIRK2-containing channels in DA neurons, DAT^{IREScre} mice were crossed with GIRK2$^{flox/flox}$ mice to generate GIRK2 cKD and GIRK2 cKO mice. Data obtained from these mice were collected alongside data from to age- and sex-matched DAT^{IREScre} mice. We hypothesised that GABA-R antagonists would not increase single pulse-evoked DA release in DLS, in mice with conditional knockdown or knockout of GIRK2 channels in DA neurons. We hypothesised that whilst SCH 23390 would prevent the increase in DA release by GABA-R antagonists in DAT^{IREScre} mice, the absence or presence of SCH 23390 would not alter the effect of GABA-R antagonists on DA release in GIRK2 cKD and GIRK2 cKO mice.

Single pulse-evoked [DA]$_o$ did not differ between genotypes in DLS (Fig. 4.3A, Kruskal Wallis test, $H_{(2)} = 0.29$, $p = 0.8651$, n = 12) or NAcC (Fig. 4.3B, Kruskal Wallis test, $H_{(2)} = 3.65$, $p = 0.1670$, n = 6). Contrary to our hypothesis, application of GABA-R antagonists increased single pulse-evoked [DA]$_o$ to equivalent levels in all genotypes (Fig. 4.3C, D, two-way RM ANOVA, time x drug interaction, $F_{(3,13)} = 0.46$, $p = 0.6878$, n = 6). No significant differences were found between genotypes in DLS upon application of GABA-R antagonists in the presence of SCH 23390 (Fig. 4.3E, F, two-way RM ANOVA, time x drug interaction, $F_{(3,17)} = 1.82$, $p = 0.1788$, n = 6). These data indicate that either loss of GIRK2 channels in DA neurons

does not affect GABA-R antagonist modulation of DA release, or that some form of biological compensation has occurred in mice lacking GIRK2 channels in DA neurons.

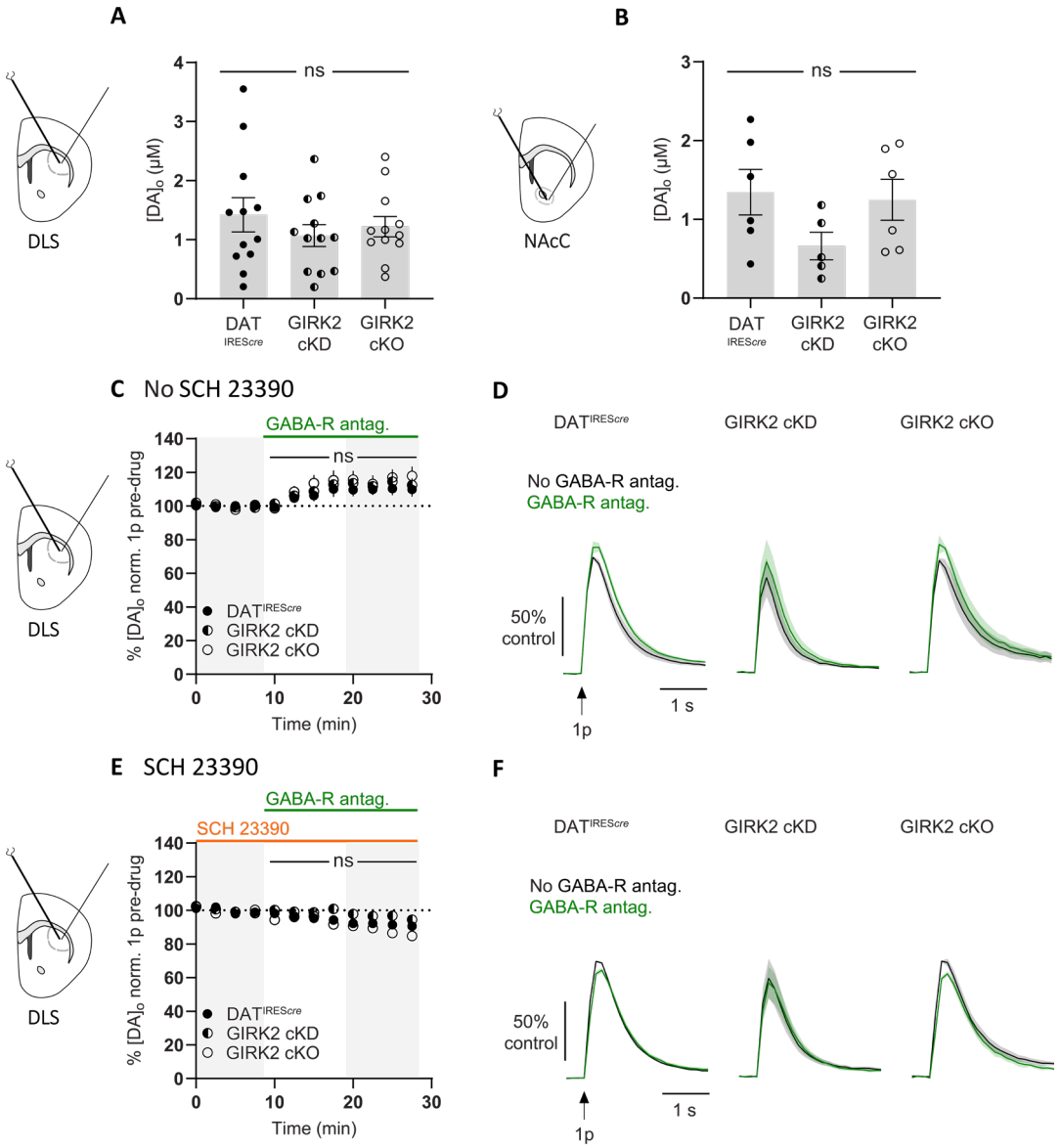

Figure 4.3. Loss of GIRK2 channels does not affect GABA-R antagonist modulation of DA release *(A) Peak $[DA]_o$ evoked by single pulses in DLS. n = 12. (B) Peak $[DA]_o$ evoked by single pulses in NAcC. n = 5-6. (C) Peak $[DA]_o$ over time evoked by single pulses in DLS, before and during bath application of GABA-R antagonists (bicuculline 10 μM and CGP 55845 4 μM). n = 6. (D) $[DA]_o$ transients over time evoked by single pulses in DLS, before and during GABA-R antagonists. n = 6. (E) Peak $[DA]_o$ over time evoked by single pulses in DLS, before and during GABA-R antagonists. n = 6. (F) $[DA]_o$ transients over time evoked by single pulses in DLS, before and during GABA-R antagonists. n = 6. Data are mean ±SEM and normalised to pre-drug baseline (grey shaded region) (C, D, E, F). 'No SCH 23390' is DHβE (1 μM), 'SCH 23390' is DHβE (1 μM) and SCH 23390 (10 μM). *p ≤ .05, **p ≤ .01, **p ≤ .001, ns = non-significant.*

4.3.4. GIRK channel inhibition attenuates cocaine-induced increases in DA release in DLS

In Chapter 3, we probed the attenuation of cocaine-induced increases in $[DA]_o$ by GABA-R antagonists in DLS. In Section 4.3.1, we showed that inhibition of GIRK channels lessens regulation of $[DA]_o$ by GABA-R antagonists. These findings prompted us to explore whether GIRK channels are involved in the convergent regulation of DA release by DATs and GABA-Rs in DLS. If SCH 23390 limits GABA-R function by inhibiting GIRK channels, and GABA-Rs support DAT function, then cocaine-induced increases in DA release will be attenuated in the presence of SCH 23390. We hypothesised that SCH 23390 would attenuate cocaine-induced increases in single pulse-evoked DA release in DLS. Furthermore, we hypothesised that, in the presence of SCH 23390, GABA-R antagonists would have no effect, or a reduced effect, on cocaine-induced increases in DA release.

In DLS, cocaine (5 µM) increased single pulse-evoked $[DA]_o$ and widened transients, showing a slowed uptake rate, in the presence of the GIRK channel inhibitor, SCH23390 (10 µM), and in both the absence and presence of GABA-R antagonists (Fig. 4.4A). In the presence of SCH 23390, cocaine-induced increases in $[DA]_o$ differed between control and GABA-R antagonist conditions (Fig. 4.4B, two-way RM mixed effects model, time x drug interaction, $F_{(19,91)} = 8.15$, $p < 0.0001$, n = 6). Cocaine-induced increases in $[DA]_o$ were lower in the presence of GABA-R antagonists compared to the absence of GABA-R antagonists (Fig. 4.4C, unpaired t-test, $t_{(10)} = 3.05$, $p = 0.0122$, n = 6). Whilst the presence of the GIRK inhibitor, SCH 23390, did not prevent modulation of cocaine-induced increases in $[DA]_o$ by GABA-R antagonists, we observed that cocaine-induced increases in $[DA]_o$ in the absence and presence of GABA-R antagonists were more similar to one another than in previous datasets (for example, Fig. 3.1). This prompted us to explore whether the presence of SCH 23390 modified cocaine-induced increases in

$[DA]_o$ when GABA-Rs are active, or inhibited. We plotted data obtained in SCH 23390 against data obtained in SCH 39166 (Fig. 4.4D, E), to control for any involvement of D_1-like-Rs.

In the absence of GABA-R antagonists, cocaine-induced increases in $[DA]_o$ differed between SCH 39166 and SCH 23390 conditions (Fig. 4.4D, two-way RM mixed effects model, time x drug interaction, $F_{(19,186)} = 7.48$, $p < 0.0001$, n = 6). In the presence of GABA-R antagonists, cocaine-induced increases in $[DA]_o$ also differed slightly between SCH 39166 and SCH 23390 conditions (Fig. 4.4E, two-way RM ANOVA, time x drug interaction, $F_{(19,190)} = 4.51$, $p < 0.0001$, n = 6). A comparison of the effect of GABA-R antagonists in SCH 39166 and SCH 23390 revealed that GIRK inhibition with SCH 23390 attenuates cocaine-induced increases in $[DA]_o$, either when GABA-Rs are active or inactive, although we observed that GIRK inhibition may preferentially affect the condition where GABA-Rs are active (Fig. 4.4F, two-way RM ANOVA, drug x drug interaction, $F_{(1,10)} = 15.62$, $p = 0.0027$, n = 6).

These data indicate that GIRK channels regulate cocaine-induced increases in $[DA]_o$, by interacting with DATs and GABA-Rs.

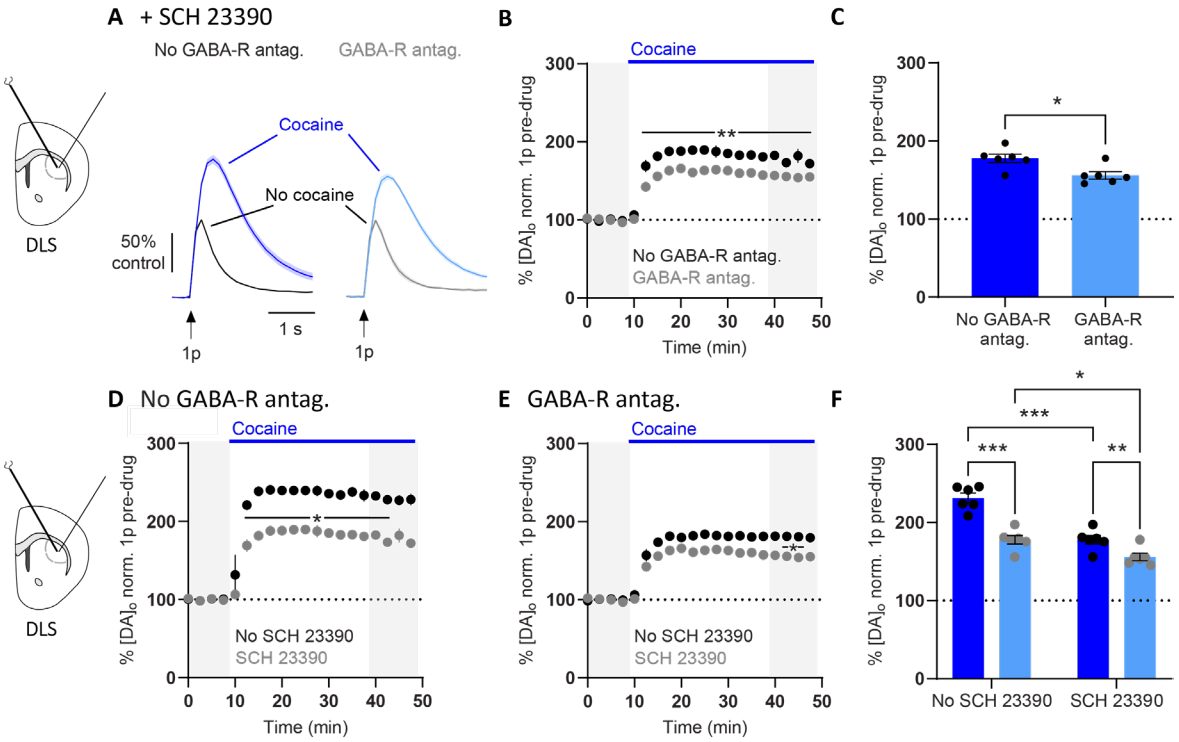

Figure 4.4. GIRK channel inhibition with SCH 23390 attenuates cocaine-induced increase in DA release in DLS

*(A) $[DA]_o$ transients over time evoked by single pulses in DLS, before and during bath application of cocaine (5 μM). n = 6. (B) Peak $[DA]_o$ over time evoked by single pulses, before and during cocaine. n = 6. (C) Percentage increase of peak $[DA]_o$ following application of cocaine. n = 6. (D) Peak $[DA]_o$ over time evoked by single pulse, before and during cocaine. n = 6. (E) Peak $[DA]_o$ over time evoked by single pulses, before and during cocaine. n = 6. (F) Percentage increase of peak $[DA]_o$ following application of cocaine. n = 6. Data are mean ±SEM and normalised to pre-drug baseline (grey shaded region). 'No GABA-R antag.' is DHβE (1 μM) and SCH 23390 (10 μM), 'GABA-R antag.' is DHβE (1 μM), bicuculline (10 μM), CGP 55845 (4 μM) and SCH 23390 (10 μM) (A, B, C). ''No SCH 23390' refers to the presence of DHβE (1 μM) and SCH 39166 (1 μM), 'SCH 23390' refers to the presence of DHβE (1 μM) and SCH 23390 (10 μM) (D, E, F). *p ≤ .05, **p ≤ .01, **p ≤ .001, ns = non-significant.*

4.3.5. GIRK channel inhibition hints at modulation of cocaine-induced increase in DA release by GABA-Rs in NAcC

We explored whether GIRK channels are involved in the control of striatal DA release by DATs in NAcC. In Chapter 3, we found that, unlike in DLS, the presence of GABA-R antagonists do not impact cocaine-induced increases in DA in NAcC. Due to this observation, and the finding that GIRK channel expression is lower in DA neurons which project to the NAcC, compared to those that project to the DLS (Schein et al., 1998; Chung et al., 2005; Poulin et

al., 2014), we hypothesised that GIRK channel inhibition would have no impact on the interaction between DATs and GABA-Rs in NAcC.

In the presence of the GIRK inhibitor, SCH 23390 (10 μM), cocaine (5 μM) increased single pulse-evoked $[DA]_o$ and widened transients in NAcC, consistent with a slowed uptake rate, in both the absence and presence of GABA-R antagonists (Fig. 4.5A). Analysis of cocaine-induced increases in $[DA]_o$ over time yielded a significant interaction between conditions (Fig. 4.5B, two-way RM mixed effects model, time x drug interaction, $F_{(19,75)} = 3.25$, $p = 0.0001$, n = 5-6), however, Šídák's multiple comparisons post-tests did not reveal any significant differences between conditions at any timepoint. The magnitude of cocaine-induced increase in $[DA]_o$ did not differ between conditions (Fig. 4.5C, unpaired t-test with Welch's correction, $t_{(4)} = 1.20$, $p = 0.2896$, n = 5 in absence of GABA-R antagonists, 6 in presence of GABA-R antagonists).

In agreement with data in Chapter 3, GABA-R antagonists do not modify cocaine-induced increases in $[DA]_o$. Similar to data shown in Fig. 3.7, where low $[Ca^{2+}]_o$ concentration appeared to begin to tease apart a modulation of cocaine-induced increases in $[DA]_o$ by GABA-R antagonists, here, inhibition of GIRK channels appears to slightly shift that relationship. Nevertheless, no statistically significant differences were observed.

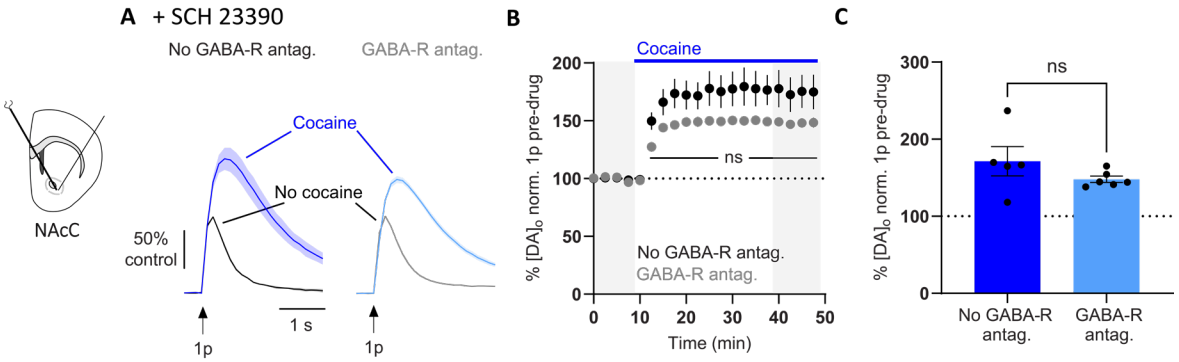

Figure 4.5. GIRK channel inhibition with SCH 23390 unveils modulation of cocaine-induced increase in DA release by GABA-Rs in NAcC

(A) $[DA]_o$ transients over time evoked by single pulses in NAcC, before and during bath application of cocaine (5 μM). n = 5-6. (B) Peak $[DA]_o$ over time evoked by single pulses, before and during cocaine. n = 5-6. (C) Percentage increase of peak $[DA]_o$ following application of cocaine. n = 5-6. Data are mean

*±SEM and normalised to pre-drug baseline (grey shaded region). 'No GABA-R antag.' is DHβE (1 μM) and SCH 23390 (10 μM), 'GABA-R antag.' is DHβE (1 μM), bicuculline (10 μM), CGP 55845 (4 μM) and SCH 23390 (10 μM). *p ≤ .05, **p ≤ .01, **p ≤ .001, ns = non-significant.*

4.3.6. Loss of GIRK2 channels in DA neurons does not affect modulation of DA release by DATs

In Section 4.3.3., we utilised mice lacking GIRK2-containing channels in DA neurons, to explore the involvement of GIRK channels in the control of striatal DA release by GABA-Rs. Here, we used mice lacking GIRK2 channels in DA neurons to explore the involvement of GIRK channels in DAT-mediated changes to striatal DA release. In Section 4.3.3., unexpectedly, loss of GIRK2 channels did not impact GABA-R antagonist-mediated changes to striatal DA release in DLS. Nevertheless, in Section 4.3.4., we observed an attenuation of cocaine-induced increases in DA release by the GIRK channel inhibitor, SCH 23390. We therefore hypothesised that cocaine-induced increases in DLS would be attenuated in GIRK2 cKD and GIRK2 cKO mice, compared to $DAT^{IREScre}$ mice. We hypothesised that no differences would be found between genotypes in NAcC.

In DLS, as expected, application of cocaine (5 μM) increased single pulse-evoked $[DA]_o$ in all genotypes, however, no significant differences were found between genotypes (Fig. 4.6A, B, two-way RM ANOVA, time x drug interaction, $F_{(2,11)} = 1.13$, $p = 0.3634$, n = 6). Consistent with this, no differences were found in the magnitude of cocaine-induced increase in $[DA]_o$ (Fig. 4.6C, Kruskal Wallis test, $H_{(2)} = 2.21$, $p = 0.3527$, n = 6). We observed that, specifically in GIRK2 cKD mice (half-filled circles), that there appeared to be a difference between younger and older mice in terms of the magnitude of cocaine-induced increases in $[DA]_o$. We therefore plotted data separately, into that obtained from mice younger than 60 days old (Fig 4.6D), and mice older than 60 days old (Fig. 4.6E). Whilst the cocaine-induced increase in $[DA]_o$ appeared to be attenuated in GIRK2 cKD mice < 60 days old, this was not statistically significant (Fig. 4.6D, two-way RM mixed effects model, time x drug interaction, $F_{(1,1)} = 1.92$, p

= 0.3414, n = 4 $DAT^{IREScre}$, 3 GIRK2 cKD, 2 GIRK2 cKO), and likely underpowered. No significant differences were detected in data obtained from mice > 60 days old (Fig. 4.6E, two-way RM mixed effects model, time x drug interaction, $F_{(1,2)} = 1.61$, $p = 0.3703$, n = 2 $DAT^{IREScre}$, 3 GIRK2 cKD, 4 GIRK2 cKO).

Application of cocaine increased single pulse-evoked $[DA]_o$ in NAcC in all genotypes, with no differences between genotypes (Fig. 4.6F, G, two-way RM ANOVA, time x drug interaction, $F_{(3,12)} = 1.14$, $p = 0.3660$, n = 5-6). No differences were found in the magnitude of cocaine-induced increase in $[DA]_o$ between genotypes (Fig. 4.6H, Kruskal Wallis test, $H_{(2)} = 0.58$, $p = 0.7624$, n = 5-6). In DLS, there were no significant differences in DA uptake rate between genotypes (Fig. 4.6I, Kruskal Wallis test, $H_{(2)} = 3.61$, $p = 0.1648$, n = 21-23 transients from 6 animals per genotype). The mean decay constant, *k*, was obtained by fitting a one phase exponential decay to the decaying portion of DA transients. *k* was 1.07 s^{-1} in $DAT^{IREScre}$ mice, 1.26 s^{-1} in GIRK2 cKD mice, and 0.88 s^{-1} in GIRK2 cKO mice.

In agreement with findings regarding GIRK channels and GABA-R antagonists in Section 4.3.3., loss of GIRK2 channels in DA neurons does not appear to have an impact on the control of striatal DA release by DATs. There is a tendency that, in GIRK2 cKD mice, below the age of 60 days, loss of GIRK2 channels attenuates cocaine-induced increases in DA in DLS. However, this comparison was likely underpowered and statistically non-significant. These data indicate that GIRK2 channels are not involved in DAT-mediated changes to striatal DA release. An alternative explanation is that some form of genetic compensation has occurred, which will be explored in the discussion.

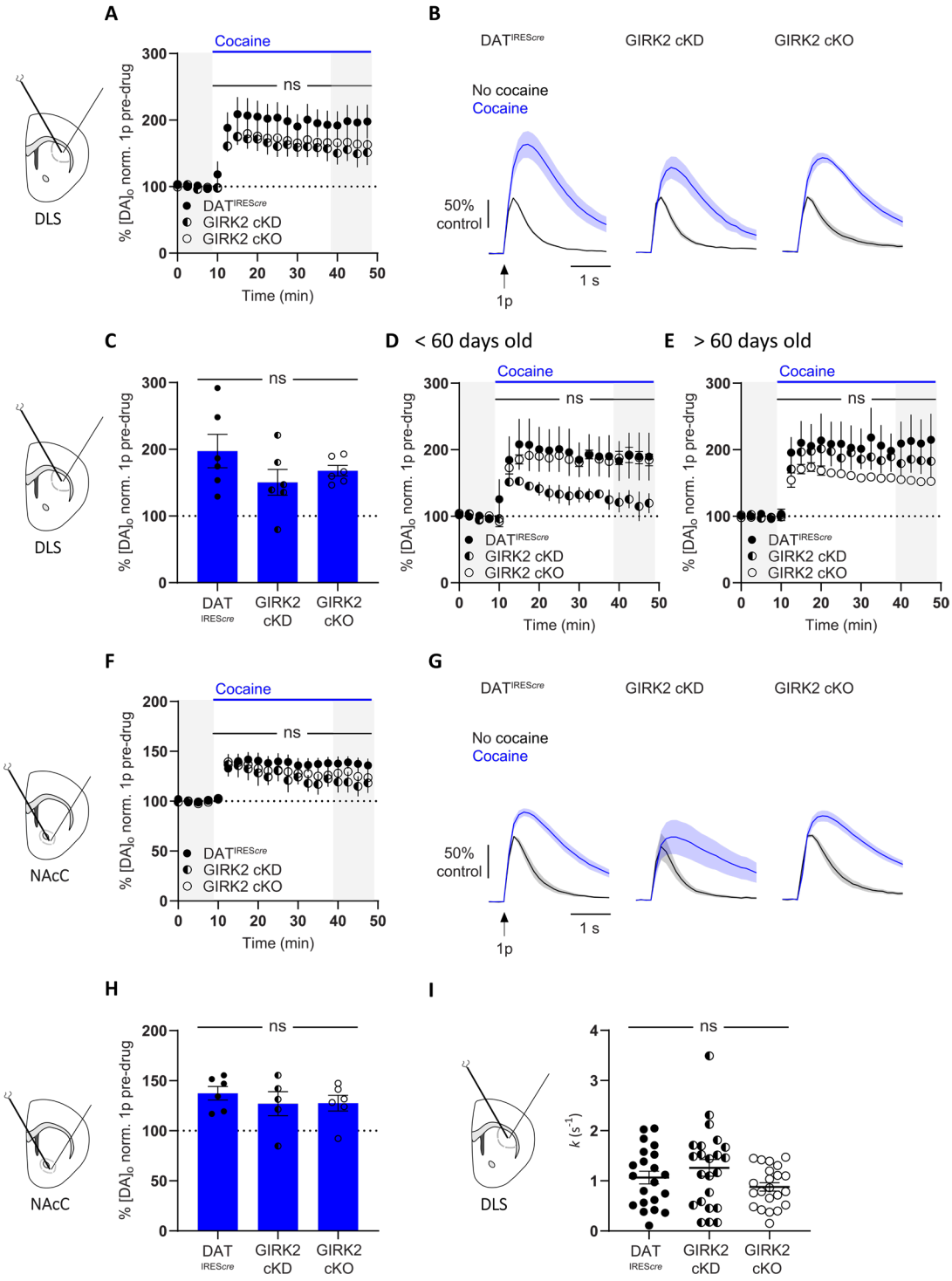

Figure 4.6. Loss of GIRK channels does not affect cocaine modulation of DA release
(A) Peak $[DA]_o$ over time evoked by single pulses in DLS, before and during bath application of cocaine (5 μM). n = 6. (B) $[DA]_o$ transients over time evoked by single pulses, before and during cocaine. n = 6. (C) Percentage increase of peak $[DA]_o$ following application of cocaine. n = 6. (D) Peak $[DA]_o$ over time evoked by single pulses in DLS, before and during cocaine, in animals <60 days old. n = 2-4. (E) Peak $[DA]_o$ over time evoked by single pulses in DLS, before and during cocaine, in animals >60 days old. n = 2-4. (F) Peak $[DA]_o$ over time evoked by single pulses in NAcC, before and during cocaine. n = 6. (G) $[DA]_o$ transients over time evoked by single pulses, before and during cocaine. n = 6. (H) Percentage increase of peak $[DA]_o$ following application of cocaine. n = 6. (I) Decay rates, k (s^{-1}) (±SEM), for $[DA]_o$

*evoked by single pulses in DLS. n = 21-23 transients. Data are mean ±SEM and normalised to pre-drug baseline (grey shaded region). *p ≤ .05, **p ≤ .01, **p ≤ .001, ns = non-significant.*

4.4. Discussion

I have shown that pharmacological inhibition of GIRK channels attenuated the impact of GABA-R antagonism and DAT inhibition on striatal DA release. These data indicate that activity at GIRK channels supports modulation of striatal DA release by GABA-Rs and DATs. GIRK channel inhibition alone caused no effect, or a minimal increase, to striatal DA release, but prevented antagonists of $GABA_A$- and $GABA_B$-Rs from increasing DA release. This did not appear to be caused by an indirect action involving changes to striatal GABA tone. Instead, it appears that GABA-R control of DA release is, at least somewhat, dependent on activity at GIRK channels. Further, GIRK channel inhibition attenuated the cocaine-induced increase in DA release in DLS. Surprisingly, knockdown or knockout of GIRK2-containing channels in DA neurons did not reproduce the pharmacological findings. Caveats will be discussed further.

4.4.1. Contributions of GIRK channels to control of DA release by GABA-Rs

The observation that SCH 23390 prevents GABA-R antagonists from increasing DA release indicates that inhibition of GIRK channels may act to also inhibit GABA-Rs. $GABA_B$-Rs are known to couple to GIRK channels (Bettler et al., 2004; Terunuma, 2018), therefore, inhibition of GIRK channels may limit $GABA_B$-R function. Activation of GIRK currents in DA neurons by the $GABA_B$-R agonist, baclofen, limits further activation of GIRK currents by D_2-R activation (Lacey et al., 1988). Whilst we are inhibiting, rather than activating, GIRK channels, a similar phenomenon might be at play. If the pool of GIRK channels are occupied by an inhibitor, there might not be any channels available for $GABA_B$-Rs to activate. It is less clear how GIRK inhibition could affect $GABA_A$-R function. However, $GABA_A$- and $GABA_B$-Rs might not function independently on striatal DA axons (Lopes et al., 2019).

In mouse *ex vivo* brain slices, $GABA_A$-R antagonism increases striatal DA release in DLS by ~10-15% and $GABA_B$-R antagonism increases DA release by ~25%, yet co-application of both

antagonists only increases DA release by ~25%, indicating some redundancy (Lopes et al., 2019). In fact, $GABA_B$-Rs may exert control over striatal DA release more reliably than $GABA_A$-Rs, since both agonism and antagonism of $GABA_B$-Rs affects the frequency-dependence of DA release, whilst only agonism of $GABA_A$-R significantly alters this frequency-dependence (Lopes et al., 2019). Furthermore, whilst antagonism of both $GABA_A$- and $GABA_B$-Rs appeared to increase single pulse-evoked DA release, this was statistically significant for only $GABA_B$-R antagonism (Lopes et al., 2019). In light of these findings, and our observation that GIRK channel inhibition prevents an increase in striatal DA release by GABA-R antagonists, it is plausible that $GABA_B$-Rs, rather than $GABA_A$-Rs, exert particular control over striatal DA transmission, at least in DLS.

Unpublished preliminary data in mouse *ex vivo* brain slices indicates that striatal DA release increases upon $GABA_B$-R antagonism, following prior $GABA_A$-R antagonism, but an increase in DA is less clear when a $GABA_A$-R antagonist is applied following prior $GABA_B$-R antagonism (unpublished data, Dr. E. Lopes, Cragg lab). These data, however, were collected using a recording solution containing 7.5 mM $[K^+]_o$ (data in this thesis was obtained in 2.5 mM $[K^+]_o$), and although changes in $[K^+]_o$ do not appear to change single pulse-evoked DA release (Condon et al., 2019), differing $[K^+]_o$ concentrations could impact driving forces in striatal DA axons. In rat *ex vivo* brain slices, activity at $GABA_B$-Rs is required for $GABA_A$-R control of DA release in NAcC (Brodnik et al., 2019). The authors speculate that this may be due to a circuit mechanism involving disinhibition of striatal GABA, or inhibition of a neuromodulator which typically increases striatal DA release (Brodnik et al., 2019). However, it is possible that activity at $GABA_B$-Rs is required for $GABA_A$-R control of DA release, because these receptors co-operate on striatal DA axons. Another possibility is that inhibition of GIRK channels alters membrane excitability and places striatal DA axons into a state of excitability in which DA release is less susceptible to changes in activity at GABA-Rs. In pyramidal neurons, loss of GIRK2 channels was associated with a depolarised resting membrane potential compared to

controls (Lüscher et al., 1997), which could plausibly affect membrane proteins with electrogenic properties, such as DATs (Carvelli et al., 2004; Sonders et al., 1997) or $GABA_A$-Rs (Kramer et al., 2020). Future experiments are required to delineate whether $GABA_A$- and $GABA_B$-Rs co-operate on striatal DA axons, and if GIRK channels mediate this interaction.

If GIRK channel inhibition leads to inhibition of $GABA_B$-Rs (and possibly also $GABA_A$-Rs), then a question remains as to why SCH 23390 does not reliably increase striatal DA release. Presumably, tonic GABAergic inhibition of DA release would have been operating prior to application of SCH 23390 (Lopes et al., 2019; Roberts et al., 2020). Therefore, if application of SCH 23390 inhibited GABA-R function, we would have observed an increase in DA release, similar to that seen upon application of GABA-R antagonists. In some cases, especially in NAcC, it did appear that SCH 23390 increased evoked DA, but as mentioned, these results must be treated with caution. Future experiments, and the development of selective pharmacological tools for GIRK2-containing GIRK channels, are necessary to explore GIRK channel control of striatal DA release. To explore the possibility that SCH 23390 renders $GABA_B$-Rs unable to modify striatal DA release, one should test whether changes to DA release are also prevented by a $GABA_B$-R agonist.

4.4.2. GIRK channels as mediators of DAT function

The observation that SCH 23390 attenuated the effect of cocaine on evoked DA release in DLS is consistent with the idea that SCH 23390 inhibited GABA-Rs. In Chapter 3, we showed that GABA-R antagonists attenuated cocaine-induced increases in striatal DA release. If, as speculated, GABA-Rs support DAT function, and if SCH 23390 limits GABA-R function, then SCH 23390 will also limit DAT function. This explanation is consistent with our data showing an attenuation in cocaine-induced increases in DA release in DLS, and consistent with the indication that striatal DA axons integrate signals coming via DATs and GABA-Rs.

It is unclear whether this also applies in NAcC. In Chapter 3, we showed that cocaine-induced increases in evoked DA in NAcC are not modified by the presence of GABA-R antagonists, at least not in our standard recording conditions. Whilst we cannot conduct a formal comparison, it seems possible that GIRK channel inhibition with SCH 23390 supports cocaine-induced increases in DA release in NAcC. In the absence of SCH 23390 (also in the absence of any alternate D_1-R antagonist), cocaine increased DA release by ~37% (Fig. 3.6), yet in the presence of SCH 23390, cocaine increased DA release by ~71% (Fig. 4.5). Though purely speculative at this stage, if GIRK channel inhibition does increase the effect of cocaine on DA release in NAcC, this could indicate a mechanism distinct from GABA-Rs, as GABA-R antagonism did not have any impact on cocaine-induced increases in DA release in NAcC (Fig. 3.6).

The vast majority of literature linking GIRK channels and DATs is behavioural, making it difficult to decipher the precise mechanisms via which GIRK channels contribute to DAT-mediated behaviour, and the brain region(s) in which these mechanisms are at play. In addition to the involvement of GIRK channels in cocaine-related behaviours, which was summarised in 4.1.3., GIRK channels also appear to be implicated in methamphetamine-related behaviours, supporting the hypothesis that GIRK channel activity may have functional implications for DAT signalling, and therefore behaviour. Self-administration of methamphetamine, a DAT substrate, attenuates D_2-R- and $GABA_B$-R-mediated GIRK channel current amplitudes in both SNc and VTA DA neurons (Sharpe et al., 2015). In VTA DA neurons, methamphetamine-induced changes to $GABA_B$-R mediated GIRK channel currents requires the GIRK3 subunit (Munoz et al., 2016). Switches in firing rate of VTA DA neurons regulate GIRK2/3 channel trafficking, demonstrating a plasticity in these currents based on neuronal activity (Lalive et al., 2014). To add another layer of complexity, in SNc DA neurons, GIRK channel function can be attenuated by Ca^{2+} release from internal stores, independent of G protein-coupled receptors (Kramer & Williams, 2016). These findings not only implicate GIRK

channels in DAT-mediated measures, but also underpin the importance of understanding the integration of information from DATs and GABA-Rs in DA neurons.

On occasion, in both DLS and NAcC, in GIRK2 cKD or GIRK2 cKO mice, cocaine did not increase single pulse-evoked DA, despite cocaine decreasing DA uptake rate. This was not observed in wildtype or $DAT^{IREScre}$ mice in any dataset, and points to a dissociation of the roles of DATs. In Chapter 3, we observed that although GABA-R antagonists modified DAT control of DA release, they did not affect DA uptake. Here, in a handful of cases, DAT inhibition did not affect DA release, but did decrease DA uptake rate. These limited observations support previous demonstrations that the roles of DATs in regulating DA release and uptake can be disconnected.

The *SNCA*-OVX mouse model of Parkinson's disease, which exhibits DA release deficits (Janezic et al., 2013b), exhibits augmented DAT function (Threlfell et al., 2021) and augmented GABAergic inhibition of DA axons (Roberts et al., 2020). Cocaine-induced increases in DLS DA release are augmented in *SNCA*-OVX mice, compared to control mice (Threlfell et al., 2021). Furthermore, GABA-R antagonists augment DLS DA release to a larger extent in *SNCA*-OVX mice, compared to control mice (Roberts et al., 2020). These dysfunctional mechanisms lead to increased DAT and GABA-R control of striatal DA release, and might contribute to cell stress and loss. SCH 23390 attenuates the effect of both cocaine and GABA-R antagonists on DA release, leading to the possibility that SCH 23390 might 'normalise' control of DA release by DATs and GABA-Rs. Future experiments should test the impact of SCH 23390 on DAT and GABA-R function in *SNCA*-OVX mice.

4.4.3. Potential confounding factors

Pharmacological tools which target GIRK channels, especially channel inhibitors, are extremely limited, and those that do exist have various off-target effects, or do not target non

GIRK1-containing channels (Kozek et al., 2019; Jeremic et al., 2021; Zhao et al., 2021; Luo et al., 2022). A commonly used ligand is tertiapin, or its derivative, tertiapin-Q, but these bind only to GIRK1 containing heterotetramers (Jin & Lu, 1998; Jin et al., 1999; Kanjhan et al., 2005). Another commonly used tool is the metal barium (Ba^{2+}), but Ba^{2+} acts as a channel blocker at a large number of K^+ channels, including inwardly rectifying K+ channels (both G protein-gated and non G protein-gated), K_v channels, and K_{Na} channels (British Pharmacological Society Guide to Pharmacology). Though the use of SCH 23390 as a GIRK channel inhibitor was most suitable for our application, we cannot entirely exclude the possibility that there are alternative explanations for our data obtained in SCH 23390, aside from the involvement of GIRK channels.

SCH 23390 is primarily used as a DAergic D_1-like-R antagonist (Bourne, 2001). Our data, however, indicates that D_1-like-Rs are not involved in the control of striatal DA release by DATs and GABA-Rs. In Chapter 3, we used SCH 39166, an alternate D_1-like-R antagonist, and demonstrated that cocaine-induced increases in striatal DA were unchanged, and the attenuation of the effect of cocaine by GABA-R antagonists was maintained (Fig. 3.2). Furthermore, unlike in the presence of SCH 23390, GABA-R antagonists increase evoked DA in the presence of SCH 39166 (Fig. 4.1). D_1-like-Rs recruit $G\alpha_{s/olf}$ proteins and are typically excitatory, stimulating cAMP production (Beaulieu & Gainetdinov, 2011). Therefore, if D_1-like-Rs are located on a GABAergic structure in the striatum, we would expect antagonism of D_1-like-Rs by SCH 23390 to either have no impact on GABA tone, as no DA tone is present in *ex vivo* striatal slices (Boumhaouad et al., 2025) and thus no tonic activation of D_1-like-Rs, or less likely, for SCH 23390 to decrease striatal GABA tone. Yet, increasing striatal GABA tone by application of the GAT inhibitor, NPA, did not change our observation that SCH 23390 precludes the effect of GABA-R antagonists on striatal DA release. For these reasons, it appears unlikely that the observations in SCH 23390 are due to antagonism of D_1-like-Rs.

SCH 23390 is also reported to be an agonist at 5-HT2c receptors (Briggs et al., 1991; Millan et al., 2001), formerly known as 5-HT1c receptors (Humphrey et al., 1993; Baxter et al., 1995). 5HT2c receptors are $G_{q/11}$ coupled and typically provide an excitatory influence on the target cell (Sharp & Barnes, 2020). In this scenario, if SCH 23390 activates 5HT2c receptors and increases striatal GABA tone, we would observe a larger increase in DA release upon application of GABA-R antagonists. However, in our experiments, SCH 23390 prevents an increase in DA release with GABA-R antagonists. It remains possible, however, that SCH 23390 is acting at a currently unidentified mediator of GABAergic regulation of striatal DA release.

Therefore, GIRK channels are still a promising candidate for our data obtained in the presence of SCH 23390. At the concentration used here, SCH 23390 inhibits GIRK-mediated currents through GIRK1/2 heterotetramers, and GIRK2 homotetramers (Kuzhikandathil & Oxford, 2002). The affinity for GIRK2 homotetramers is particularly important, as GIRK2 homotetrameric channels are believed to be the only GIRK channels expressed in SNc DA neurons (Inanobe, Yoshimoto, et al., 1999; del Burgo et al., 2008; Lüscher & Slesinger, 2010). It remains unclear whether SCH 23390 can inhibit GIRK2/3 heterotetramers, which are expressed in VTA DA neurons (Cruz et al., 2004; Labouèbe et al., 2007), though it seems likely, due to expression of the GIRK2 subunit.

Data obtained in mice lacking GIRK2 channels adds another layer of complication. Application of SCH 23390 to inhibit GIRK channels prevented GABA-R antagonists from increasing DA release, therefore, we hypothesised that if these channels are knocked down or knocked out in DA neurons, GABA-R antagonists would not increase striatal DA release. Contrary to our expectation, GABA-R antagonists did increase DA release in these mice (Fig. 4.3C). Either SCH 23390 does not act by inhibiting GIRK channels in DA neurons, as discussed above, or there has been some form of genetic compensation in GIRK2 cKD and

GIRK2 cKO mice, to make up for loss of the *KCNJ6* gene. Genetic compensation is a process by which levels of related proteins or genes can be upregulated, to compensate for loss of the target protein (El-Brolosy & Stainier, 2017). Upregulation of a non GIRK2-containing GIRK channel seems unlikely, as SNc DA neurons express only GIRK2 subunits (Inanobe, Yoshimoto, et al., 1999; del Burgo et al., 2008; Lüscher & Slesinger, 2010), and although VTA DA neurons express GIRK2/3 subunits (Cruz et al., 2004; Labouèbe et al., 2007), GIRK3 alone is unable to form functional channels (Ma et al., 2002). Perhaps another (non G protein-gated) inwardly rectifying K^+ channel subtype, or alternate K+ channel, has been upregulated, to maintain K^+ homeostasis in DA neurons. DATs can localise with K+ channels (Bartolomé-Martín et al., 2019) and antiport K^+ (Schmidt et al., 2022), making it plausible that any compensatory change in K^+ handling in DA axons could result in a no net change in DAT function, even if GIRK channels are ablated. We speculate that, at least in younger GIRK2 cKD, disruption in K^+ handling was evident in striatal DA axons, as spontaneous (non-stimulated) DA efflux was observed, an uncommon phenomenon that has also been observed upon application of K+ channel inhibitors (personal correspondence).

Alternatively, genetic compensation could be mediated by GABA-Rs, rather than K^+ channels. If loss of GIRK2 channels in DA neurons render $GABA_B$-Rs non-functional, it seems plausible that $GABA_A$-Rs may have been upregulated in striatal DA axons, to maintain a GABAergic influence over DA transmission. An upregulation of $GABA_A$-Rs may also explain the lack of a change in cocaine-induced increases in DA release in mice lacking GIRK channels, if $GABA_A$- and $GABA_B$-Rs can substitute for one another in promoting DAT function. Though $GIRK2^{flox/flox}$ mice were obtained externally and used in publications with no reports of compensatory mechanisms (Kotecki et al., 2015; McCall et al., 2017; Honda et al., 2018), the majority of experiments were behavioural, electrophysiological recordings were conducted exclusively at the soma of VTA DA neurons, and not all experiments adequately controlled for the use of $DAT^{IRESCre}$ mice. To explore these possibilities further, future experiments must employ a

quantification of protein levels, separate use of antagonists for $GABA_A$- and $GABA_B$-Rs, measurement of striatal GABA levels with iGABASnFR (Marvin et al., 2019), and ideally, more selective and potent pharmacological tools for targeting GIRK channels.

The generation of GIRK channel ligands appears to slowly be gaining traction. For example, to address the lack of pharmacological tools which target non GIRK1-containing channels, a characterisation of a GIRK channel activator, VU0529331, was published some years ago (Kozek et al., 2018). Unfortunately, VU0529331 does not exhibit adequate potency for *in* vivo or ex *vivo* experiments (Kozek et al., 2018). Thus, development of appropriate ligands for these channels is imperative for us to be able to explore the potential modulation of striatal DA release by GIRK channels.

4.4.4. Summary

In summary, our data indicate that GIRK channels contribute to the control of striatal DA release by DATs and GABA-Rs. GIRK channel inhibition precludes GABA-R antagonist-mediated changes to DA release in DLS and NAcC, and attenuate DAT inhibitor-mediated changes to DA release in DLS, possibly via GABA-Rs. The contribution of GIRK channels was independent of a circuit-mediated effect involving changes in striatal GABA, and rather appears that GIRK channels, at least in part, mediate axonal integration of information from GABA-Rs and DATs. However, data from mice lacking GIRK2 channels in DA neurons did not yield any significant changes to GABA-R- or DAT-mediated changes to striatal DA release. This raises the possibility that either an alternate mechanism to GIRK channels mediate the DAT-GABA interaction, or that in mice lacking GIRK2 channels, some form of biological compensation has occurred.

Chapter 5.

DATs shape plasticity in DA release and axonal membrane potential

5.1. Introduction

5.1.1. Striatal DA release exhibits short-term plasticity, governed by DATs

The canonical role for DATs is to mediate DA uptake, but DATs have far more complex roles in regulation of DA transmission than solely limiting the amount of time DA is in the extracellular space. Collectively, DATs are responsible for DA uptake, initial DA release, and short-term plasticity in DA release. Importantly, evidence indicates that these roles of DATs can be dissociated. DATs are prevented from immobilising a subset of the vesicle pool in synapsin TKO mice, yet DA uptake rates are unaffected (Kile et al., 2010). *SNCA*-OVX mice display increased DAT function, with DATs more efficiently limiting initial DA release and clearing DA from the extracellular space, yet plasticity in DA release in these mice is only marginally altered (Threlfell et al., 2021). DA uptake rate is potentiated following cocaine self-administration, yet no changes were observed to initial DA release (Alonso et al., 2022). Furthermore, in Chapter 3, I described that GABA-Rs promote DAT-mediated changes to initial DA release, without affecting uptake rate. Together, these data indicate that the roles of DATs are not interdependent, and are rather complex. In striatal DA axons, DATs act as a 'master regulator' of short-term plasticity (M. D. Condon et al., 2019).

DA release probability exhibits intrinsic short-term plasticity across dorsal and ventral striatum, with some regional variability (Cragg, 2003; Chadchankar & Yavich, 2011; Da Cunha et al., 2017; Condon et al., 2019). In mouse *ex vivo* slices, when the influence from nAChRs is removed, DA release exhibits STF at shorter inter-pulse intervals (IPIs) (10-25 ms, corresponding to 40-100 Hz firing frequency) and STD at longer interval (25-200ms, corresponding to 5-40 Hz firing frequency) (Condon et al., 2019). STF is somewhat dependent on initial release, but STD appears to be release-independent (Condon et al., 2019).

DATs govern short-term plasticity in release, because DAT inhibition prevents STF (Chadchankar & Yavich, 2011; Condon et al., 2019) and limits STD (Condon et al., 2019). DATs limit the Ca^{2+}-dependence of short-term plasticity, whilst supporting K^+-dependence (Condon et al., 2019). Whilst STF occurs at only the shortest timescales, STD prevails at a larger range of IPIs, and appears to be supported by factors governing axonal activation. Variations in $[K^+]_o$ can alter membrane excitability through Nernstian driving forces, and these changes in $[K^+]_o$ affect STD, particularly in DLS (Condon et al., 2019). Lowering $[K^+]_o$ can promote membrane repolarisation between pulses, and in line with this, low $[K^+]_o$ attenuates STD, increasing re-release at P2 (Condon et al., 2019). On the other hand, increasing $[K^+]_o$ promotes STD, decreasing re-release at P2 (Condon et al., 2019). Using a genetically-encoded fluorescent Ca^{2+} indicator, GCaMP6f, as a proxy of axonal activation in striatal axons, it was found that DAT inhibition augmented axonal Ca^{2+} levels at IPIs of 40 ms, indicating that DATs might limit underlying axonal re-activation and thus promote STD (Condon et al., 2019). However, changes in axonal Ca^{2+} are not directly indicative of changes in membrane potential, as Ca^{2+} influx can be manipulated downstream of axonal activation. The recent generation of ultrafast genetically-encoded fluorescent voltage indicators means that it is now possible to directly monitor changes in axonal membrane potential. The experiments outlined in this chapter will describe an approach taken to monitor changes in axonal membrane potential across a population of striatal DA axons, and test whether DATs regulate axonal membrane excitability. The hypothesis that DATs may regulate neuronal activation is supported by the electrogenic properties of DATs, which are summarised below.

5.1.2. Electrogenic properties of DATs

DA uptake through DATs generates a transport-coupled, depolarising inward current (Sonders et al., 1997; Carvelli et al., 2004). DA is transported with two Na^+ ions and one Cl^- ion (Krueger, 1990; Mcelvain & Schenk, 1992; Gu et al., 1994), however, DAT-mediated

currents are greater than expected for a transporter with this fixed stoichiometry, demonstrating that currents observed are not solely due to DA transport-associated ion flow (Sonders et al., 1997; Ingram et al., 2002), but rather that DATs exhibit channel-like behaviour that can depolarise neurons (Carvelli et al., 2004). An increase in frequency of these transport-coupled events was associated with swimming-induced paralysis in *C. elegans*, showing that modifications to these currents may contribute to pathology (Carvelli et al., 2008).

In addition to transport-coupled currents, DATs generate transport-uncoupled currents, which may or may not be distinct from a leak current (Sonders et al., 1997; Carvelli et al., 2004; Meinild et al., 2004; Rodriguez-Menchaca et al., 2012). Transport-uncoupled currents modulate DA neuron excitability (Ingram et al., 2002). The second Na^+ binding site in DAT controls the leak current via paradoxically depolarising Cl^- conductances (Ingram et al., 2002; Borre et al., 2014). Substrates such as cocaine, arachidonic acid or amphetamine can inhibit or induce these DAT-mediated currents (Sonders et al., 1997; Ingram & Amara, 2000; Ingram et al., 2002; Erreger et al., 2008; Rodriguez-Menchaca et al., 2012). DATs have also been found to antiport K^+, which facilitates the DA uptake rate, possibly by supporting the electrochemical driving force for DA transport, or by promoting an inward-facing confirmation to assist efficient turnover and unbinding of DA and Na^+ (Schmidt et al., 2022). Antiporting of K^+ by DATs is not required for DA uptake, but makes uptake more efficient (Schmidt et al., 2022). In fact, it has been suggested that the DAT Cl^- leak conductance also makes uptake more efficient, by lowering probability of Na^+ re-binding during inward-facing open conformations (Borre et al., 2014).

Together, these studies demonstrate that DATs are capable of generating several distinct electrical currents. We do not know, however, whether the electrogenic properties of DATs are observable in mouse striatal DA axons, and if so, whether they contribute to short-term

plasticity in DA release. DAT-mediated currents induced by methamphetamine have been observed at the soma in mouse *ex vivo* brain slices (Branch & Beckstead, 2012), but to our knowledge, currents generated by DATs have not been shown in axons. Condon et al. (2019) imaged axonal Ca^{2+} dynamics as a proxy of axonal activity and gained data to indicate that DATs limit axonal re-activation to, at least in part, promote STD in DA release. However, imaging Ca^{2+} dynamics in DA axons is not a direct measure of changes to electrical activation, and it is plausible that instead, DATs modulate Ca^{2+} signalling downstream of changes to membrane potential. DA, or amphetamine, binding to DATs activate LTCCs through DAT-mediated depolarisation (Cameron et al., 2015). Furthermore, the LTCC inhibitor, isradipine, modulates striatal DA release only when DATs are active (Brimblecombe et al., 2024). To explore whether DATs modulate axonal activation, we took advantage of a newly-developed genetically-encoded fluorescent voltage indicator, ASAP5 (Hao et al., 2024), to directly monitor changes in DA axon membrane potential. Experiments outlined in this chapter investigated whether DATs govern short-term plasticity in DA release in a mixed sex cohort, whether potentiation of DAT-mediated changes to DA uptake and release modulate short-term plasticity, and finally, whether DATs modulate striatal DA axonal membrane potential in a manner consistent with regulating STD in DA release.

5.2. Methods

Experiments detailed in this chapter were carried out in accordance with the general methods described in Chapter 2. Variations and further details are reported below.

5.2.1. Animals and slice preparation

Male and female wild-type C57BL/6J mice, or DAT^{IREScre} heterozygous mice (Jax strain #: 006660) were culled by cervical dislocation and acute *ex vivo* brain slices were prepared as described in Section 2.1.5. All procedures were performed in accordance with institutional guidelines and the U.K. Animals (Scientific Procedures) Act, 1986.

5.2.2. Stereotaxic intracranial injections

Stereotaxic intracranial injections were performed to achieve viral transfection of an adeno-associated virus (AAV) containing the ASAP5 genetically-encoded fluorescent voltage indicator (Fig. 5.1; Hao et al., 2024).

DAT^{IREScre} heterozygous mice (Jax strain #: 006660) were inspected to ensure good health, then anaesthetised with 4% isoflurane (IsoFlo, Zoetis) in 100% O_2, at a flow rate of ~1.5 L/min. Fur on the scalp was shaved, and mice were transferred to a stereotaxic frame (David Kopf Instruments). Isoflurane concentration was lowered to 1.5 – 2% for maintenance anaesthesia. Eye ointment was applied to protect the eyes. Pedal withdrawal reflex, breathing rate, and body temperature were monitored throughout the procedure to ensure appropriate anaesthetic depth. Following cleaning of the skin with isopropyl alcohol soaked wipes and chlorhexidine gluconate, bupivacaine hydrochloride (2 mg/kg, s.c.; Marcaine, Pfizer) was injected at the scalp. Meloxicam (5 mg/kg, s.c.; Metacam, Boehringer Ingelheim) and saline (0.9% w/v, s.c.; Irripod, CD Medical) were injected at left and right flanks. An incision was made along the scalp and stereotaxic coordinates were set relative to bregma,

for injection in SNc (A/P: -3, M/L: +/- 1.25, D/V: -4.25 to -4.2) or VTA (A/P: -3, M/L: +/- 1, D/V: -4.25 to -4.2). AAV9-EF1α-DIO-ASAP5-WPRE (1.92 x 10^{12} vg/mL) was infused bilaterally, with a Hamilton syringe and 32 gauge needle (Hamilton Company) at a rate of 200 nL/minute, for a total volume of 1000 nL per site. The needle was left *in situ* for 5 minutes post injection. The incision was closed using suture (Monocryl, Ethicon) and skin glue (Vetbond, 3M), and mice were transferred to a temperature-controlled cage to recover from anaesthesia. Mice were weighed and monitored daily for recovery for 7 days post-operatively, and subsequently every 7 days, until culling for an experiment. Mice were culled for experiments 3-4 weeks post-operatively.

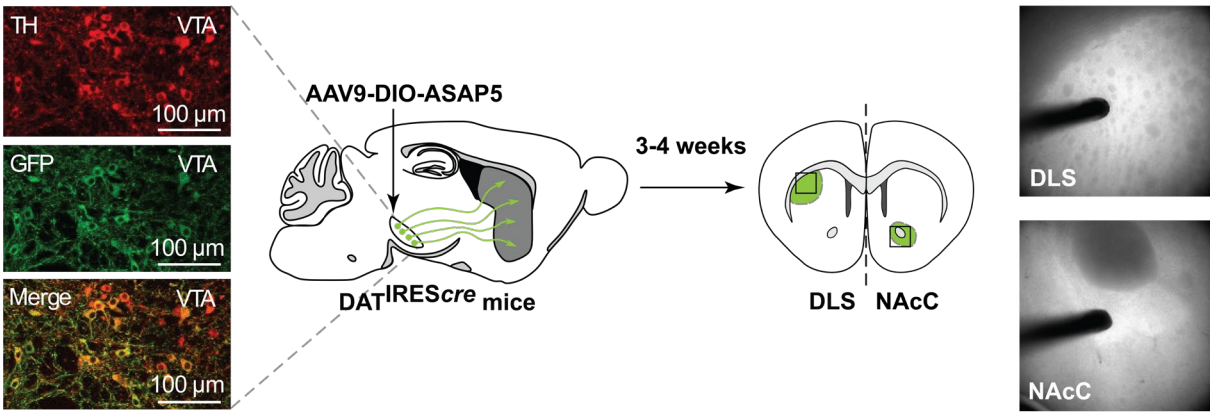

Figure 5.1. Schematic of procedure for ASAP5 expression in striatum
AAV-packaged ASAP5 sensors were injected into SNc (for experiments in DLS) or VTA (for experiments in NAcC) in DAT^{IREScre} mice. ASAP5 sensors express a GFP tag, and co-localisation with tyrosine hydroxylase (TH), a marker for DA neurons, was confirmed (images taken under 10x objective). Immunohistochemical staining and confocal images taken by Wenhui Wu. After 3-4 weeks, mice were culled and imaging experiments performed. Example images are shown from DLS and NAcC, showing ASAP5 expression, with a stimulating electrode placed (images taken under 10x objective).

5.2.3. Fast-scan cyclic voltammetry

Fast-scan cyclic voltammetry was used to measure changes in $[DA]_o$, as described in Sections 2.2.2. – 2.2.5. Each experiment was performed at a single recording site in either DLS or NAcC. DA was evoked every 2.5 minutes by single pulse or paired pulse electrical stimulation. For experiments assessing short-term plasticity in DA release, paired pulse electrical stimulations with IPIs of 10-200 ms were delivered, in a pseudorandom order and

distributed among single pulse electrical stimulations. Each paired pulse IPI was collected in triplicate. For drug wash-on experiments, drug application was performed once signal stability was achieved: ≤ 10% variation across six consecutive recordings. For short-term plasticity experiments, drug application was performed once all data had been collected for each IPI in control conditions. Once the drug had reached its maximal effect on single pulse evoked $[DA]_o$, data was then collected for each IPI in the drug condition. Data for each IPI (10-200 ms) was collected in one experiment.

5.2.4. Genetically-encoded fluorescent voltage indicator imaging

To monitor changes to membrane potential in a population of striatal DA axons, I used the recently developed ASAP5 genetically-encoded fluorescent voltage indicator (Hao et al., 2024). AAV9-EF1α-DIO-ASAP5-WPRE was injected in SNc or VTA in $DAT^{IREScre}$ heterozygous mice (Jax strain #: 006660), 3-4 weeks before an imaging experiment. The ASAP5 sensor is the newest publicly-available sensor in the Accelerated Sensor of Action Potentials (ASAP) sensor family, all of which were developed by inserting a circularly-permuted green fluorescent protein (cpGFP) into the extracellular loop of a voltage-sensing domain (VSD) from a *Gallus gallus* voltage-sensitive phosphatase (Figure 5.2; St-Pierre et al., 2014; Chamberland et al., 2017; Villette et al., 2019; Evans et al., 2023; Hao et al., 2024). ASAP5 is a negatively-correlated fluorescent indicator, such that GFP fluorescence decreases upon membrane depolarisation (Hao et al., 2024). ASAP5 is sensitive to single action potentials and subthreshold events (Hao et al., 2024).

Each experiment was performed at a single recording site in DLS or NAcC. Electrical stimulation was delivered every 1 minute and consisted of single pulse or paired pulse stimulation with IPIs of 10-200 ms. The order of paired pulse stimulations were alternated and each IPI was collected in triplicate. Drug application was performed once all data had

been collected in control conditions. Data for two IPIs (e.g. 10 ms and 40 ms) was collected in one experiment, and the selection of IPIs was pseudorandom for each experiment.

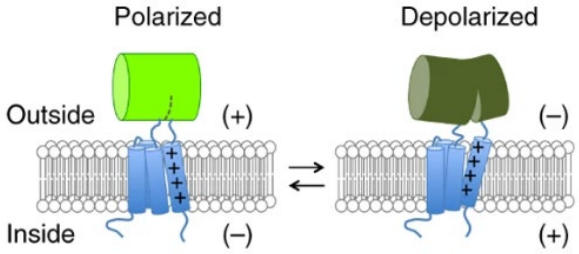

Figure 5.2. Depiction of ASAP sensor structure (from St-Pierre et al., 2014; Figure 1a)
ASAP5 sensor structure comprises a membrane-localised VSD and extracellular cpGFP. Upon membrane depolarisation, a conformational shift decreases cpGFP fluorescence.

5.2.5. Image acquisition for voltage indicator imaging

Brain slice preparation, recording solutions, flow rates, and temperature were adhered to as previously described in Chapter 2. ASAP5 expression in axons was visualised briefly with a 10x objective (plus a magnification changer at 1.25x to minimise vignetting) under blue light LED (λ = 470 nm, 10 mW; pE-300^{ultra}, CoolLED) using an iXon Ultra 888 Electron-Mutiplying Charge-Coupled Device (EMCCD) camera (Andor, Oxford Instruments). A concentric bipolar Pt/Ir stimulating electrode (FHC, Inc) was placed on the tissue surface in DLS or NAcC, ~100 µm from the edge of the field of view (FOV) and ~160 µm from the centre of the region of interest (ROI) (Fig. 5.3A). The FOV size was 148 x 496 pixels. Image acquisition was performed using Solis I software (Andor, Oxford Instruments), and time-locked electrical stimulation was achieved using MC Stimulus II software (Multi Channel Systems). Images were acquired with a 60x objective (plus 1.25x magnification changer; LED power ~ 3 mW), at a frame rate of 599.52 Hz (exposure time 1.59 ms; 4 x 4 pixel binning; exposure occurs every 1.67 ms to accommodate EMCCD readout time). Recordings lasted 3.5 s (2100 frames), with electrical stimulation delivered at 1.4 s into the recording (frame 839) (Fig. 5.3B). Images were acquired and electrical stimulation delivered at 1 minute intervals, with a typical experiment consisting of 34 acquisitions. Parameters used were selected as the optimal compromise

between temporal resolution and signal-to-noise ratio. Fluorescence was extracted using ImageJ software (National Institutes of Health) and subsequently analysed using locally written code for Matlab (Mathworks).

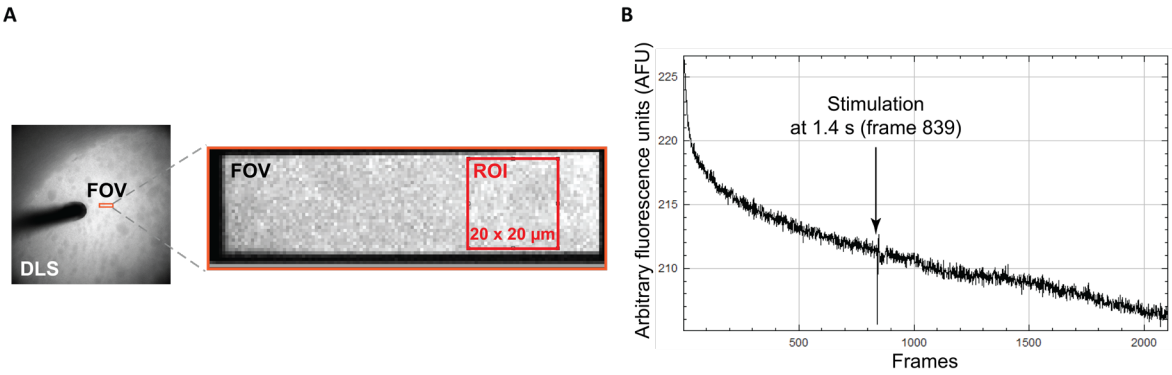

Figure 5.3. Schematic showing FOV, ROI, and ASAP5 raw signal
(A) Example image from DLS under 10x objective, showing approximate location of FOV, and image under 60x objective showing size and location of 20 x 20 µm ROI within the FOV. (B) ASAP5 raw signal over 2100 frames (3.5 s), and response to electrical stimulation at frame 839 (1.4 s).

5.2.6. Data processing for voltage indicator imaging

Arbitrary fluorescence units (F) over 2100 (3.5 s) frames were extracted from a 20 x 20 µm ROI within the FOV, using ImageJ software (National Institutes of Health). Subsequent analysis was undertaken using Matlab software (Mathworks) and locally written analysis code. Recordings without electrical stimulation indicated that following an initial exponential-like decay in fluorescence, signal decay was linear-like (Fig. 5.4A). Therefore, a linear fit function ($f(x) = a*x + b$; 'poly1' function in Matlab) was applied, based on frames 400-800, to obtain baseline fluorescence values (F_0), where a is the slope of the decay, and b is the intercept (Fig 5.4B). Average F between frames 400 to 800 was defined as the F_0 for each trace. Following slope correction, traces were inverted so that depolarisation is seen as an upward event. Data were converted to percentage values and are expressed as $-\Delta F/F_0$ (%) where ΔF is $F - F_0$ (Fig. 5.4C). Parameters for analysis are either taken from this initial longer trace (Fig. 5.4D), or a zoomed in spike trace, which is baselined for a second time for accuracy of parameters (Fig. 5.4E). No parameters for analysis are taken from beyond the point at which the linear fit function fails to accurately fit the raw traces.

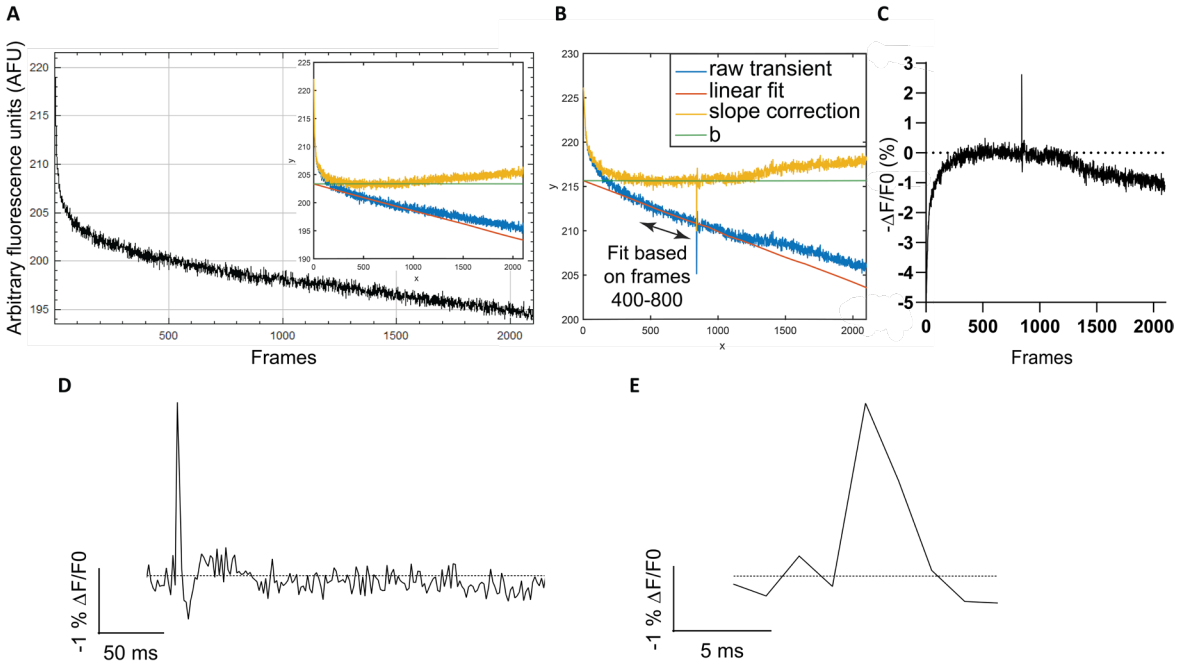

Figure 5.4. Schematic showing ASAP5 fluorescence decay, linear fit, and baselined traces
(A) ASAP5 raw signal over 2100 frames (3.5 s), with no electrical stimulation. Inset shows linear fit. (B) Depiction of linear fit function and subsequent slope correction. (C) ASAP5 trace following slope correction, baselining, conversion to percentage values, and inversion. (D) ASAP5 trace from C, zoomed in and with scale bars. (E) Re-baselined spike trace, zoomed in and with scale bars.

Parameters obtained from each trace were as follows, and are depicted in Fig. 5.5. Peak depolarisation was defined as the maximum depolarisation immediately following an electrical stimulation. For single-pulse experiments, and P1 in paired-pulse experiments, stimulation occurs at frame 839. Peak depolarisation was calculated by taking the maximum $\Delta F/F_0$ (%) between frames 839 and 843, from the initial longer trace after slope correction. For paired-pulse traces, a similar procedure was carried out later in the trace for P2. For example, when P2 occurs 40 ms after P1, stimulation occurs at frame 863 and peak depolarisation for P2 was calculated by taking the maximum $\Delta F/F_0$ (%) between frames 863 and 867. Afterhyperpolarisation (AHP) amplitude following single-pulse stimulation was calculated by taking the minimum $\Delta F/F_0$ (%) between frames 839 and 899 (100 ms duration following stimulation).

Spike height was calculated following the creation of a re-baselined trace comprising one spike only. Traces were re-baselined using the F_0 immediately preceding the spike. For single-

pulse experiments, and P1 in paired-pulse experiments, the 'spike F_0' was determined as the average fluorescence between frames 838 and 839. A re-baselined trace was subsequently created by subtracting this 'spike F_0' from fluorescence in frames 837-845. Spike height was calculated by taking the maximum $\Delta F/F_0$ (%) over this re-baselined trace. For paired-pulse traces, a similar procedure was carried out later in the trace for P2. For example, when P2 occurs 40 ms after P1, stimulation occurs at frame 863, and 'spike F_0' was determined as the average fluorescence between frames 862 and 863. A re-baselined trace was subsequently created by subtracting this 'spike F_0' from fluorescence in frames 861-869. Spike height was calculated by taking the maximum $\Delta F/F_0$ (%) over this re-baselined trace.

Spike area under the curve (spike AUC) was calculated, for single-pulse experiments, and P1 in paired-pulse experiments, using a trapezoidal method ('trapz' function in Matlab) to measure area above and below zero in the re-baselined spike trace. Spike AUC is therefore an integral, calculated to be an integrated measure of net deviation from zero, encompassing both positive and negative values (shaded regions in Fig 5.5). Spike AUC was calculated this way so as to be an unbiased measure. Area was calculated in $\Delta F/F_0$ (%) between frames 839 and 845. For paired-pulse traces, a similar procedure was carried out later in the trace for P2. For example, when P2 occurs 40 ms after P1, area was calculated $\Delta F/F_0$ (%) between frames 864 and 869. For paired-pulse experiments, a paired-pulse ratio (PPR; P2/P1) was calculated to compare peak depolarisation, spike height, or spike AUC.

Peak depolarisation for single-pulse traces, and P1 in paired-pulse traces are very similar to spike height for these spikes, and any differences in values are a result of baselining. Therefore, for single-pulse traces, the similarity between peak depolarisation and spike height was used as a quality control measure. Both values are shown in a time-matched control dataset below, but only spike height is reported in subsequent results. For paired-

pulse traces, both measures are reported, because peak depolarisation and spike height for P2 can differ.

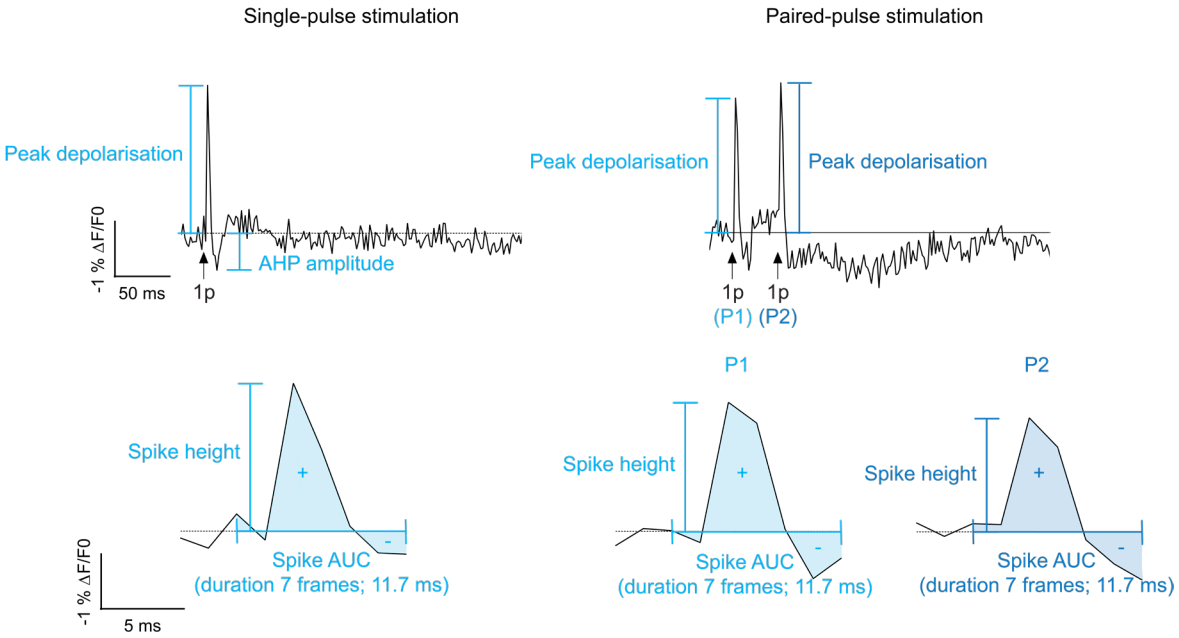

Figure 5.5. Cartoon outlining parameters used for analysis of ASAP5 data
Depiction of parameters obtained from ASAP5 traces for single-pulse and paired-pulse experiments. Parameters obtained are peak depolarisation, AHP amplitude, spike height, and spike AUC.

5.2.7. ASAP5 sensor characterisation in striatal DA axons

Following troubleshooting and optimisation, the ASAP5 genetically encoded fluorescent voltage indicator (Hao et al., 2024) reliably reported action potential-like spikes across a population of DA axons, following single-pulse electrical stimulation in DLS and NAcC (Fig. 5.6A, F). To confirm that signals were attributed to action potentials in DA axons, and to test stability over time, we performed some characterisation experiments.

ASAP5 fluorescent signals are consistent with the observation that midbrain DA neurons exhibit broad action potentials when measured with electrophysiology (Richards et al., 1997; Margolis et al., 2008; Blythe et al., 2009; Kramer et al., 2020, 2022). Recent reports of action potentials in the main axon of DA neurons indicate that action potentials take ~7-9 ms to return to baseline (Kramer et al., 2022), consistent with the timing of ASAP5 signals shown here (Fig. 5.6A, F). Surprisingly, following single-pulse stimulation and the resulting spike,

signals exhibited large, slow rebound depolarisation in DLS (Fig. 5.6A) and AHP in NAcC (Fig. 5.6F). This is likely due to the nature of the ASAP5 sensor. It is probable that the sensor is more sensitive to slower events, compared to fast events (personal correspondence with Lin lab, Stanford University). Signals in DLS exhibit a rebound depolarisation following a spike, whereas signals in NAcC do not exhibit a rebound depolarisation, and instead exhibit a prolonged AHP. It is not currently clear whether these differences reflect variation in biological mechanisms, or whether they are an experimental artefact, but these possibilities will be discussed in Section 5.4.3.

Signal shape in DLS is stable over time (Fig. 5.6A), and no significant differences were found between early and late in the experiment to peak depolarisation (Fig. 5.6B, paired t-test, $t_{(4)} = 0.53$, $p = 0.6214$, n = 5), spike height (Fig. 5.6C, paired t-test, $t_{(4)} = 1.03$, $p = 0.3633$, n = 5), spike AUC (Fig. 5.6D, paired t-test, $t_{(4)} = 0.79$, $p = 0.4730$, n = 5), or F_0 (Fig. 5.6E, paired t-test, $t_{(4)} = 1.95$, $p = 0.1237$, n = 5). Signal shape in NAcC is stable over time (Fig. 5.6F), and no significant differences were found between early and late in the experiment to peak depolarisation (Fig. 5.6G, paired t-test, $t_{(6)} = 2.13$, $p = 0.0768$, n = 7), spike height (Fig. 5.6H, paired t-test, $t_{(6)} = 2.00$, $p = 0.0925$, n = 7), spike AUC (Fig. 5.6I, paired t-test, $t_{(6)} = 0.12$, $p = 0.9074$, n = 7), or F_0 (Fig. 5.6J, paired t-test, $t_{(6)} = 2.02$, $p = 0.0905$, n = 7). In both regions, peak depolarisation and spike height yielded very similar measures, therefore, for the remainder of single-pulse traces, only spike height is reported.

Although signals are stable over time, to ensure accuracy and utilise independent measures, we compared the change in spike height, spike AUC, and F_0, in these time-matched control datasets, to the same parameters in experiments where drugs were applied. ‘Early’ is an average of recordings 11, 14, and 17. ‘Late’ is an average of recordings 28, 31, and 34. For drug wash-on experiments, single-pulse data before drug application were taken from ‘early’ timepoints (recordings 11, 14, and 17), and data during drug application were taken from

'late' timepoints (recordings 28, 31, and 34). Data shown in Fig. 5.6 are therefore used as time-matched control data. Subsequent single-pulse traces are corrected for slight signal decay over time, for visualisation only. Traces were corrected for ~8% decline in DLS, and ~2% decline in NAcC.

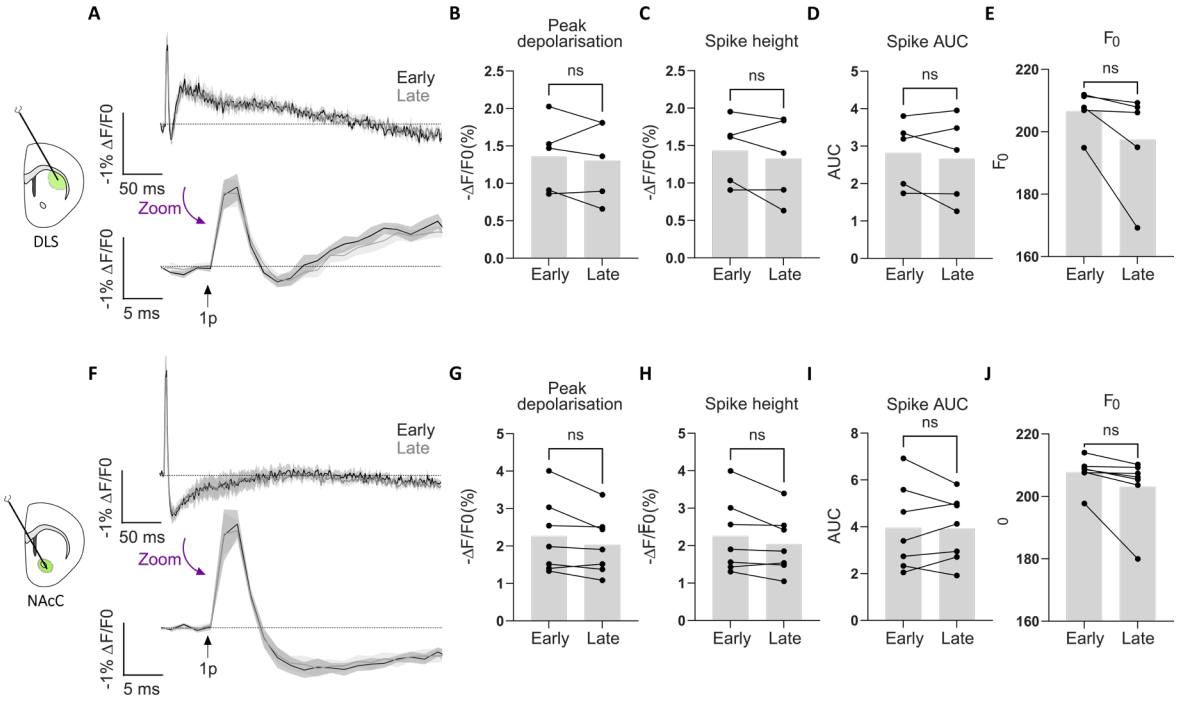

Figure 5.6. ASAP5 reliably reports changes in membrane potential in DA axons in DLS and NAcC *(A) ASAP5 traces in DLS from early and late periods in an experiment. n = 5. (B) Peak depolarisation in DLS. n = 5. (C) Spike height in DLS. n = 5. (D) Spike AUC in DLS. n = 5. (E) F_0 in DLS. n = 5. (F) ASAP5 traces in NAcC from early and late periods in an experiment. n = 7. (G) Peak depolarisation in NAcC. n = 7. (H) Spike height in NAcC. n = 7. (I) Spike AUC in NAcC. n =7. (J) F_0 in NAcC. n = 7. Data are mean ±SEM. 'Early' is an average of recordings 11, 14, and 17. 'Late' is an average of recordings 28, 31, and 34. DHβE (1 μM) is present throughout.*

ACh release from cholinergic interneurons in the striatum can trigger subthreshold events and action potentials in striatal DA axons, and subsequently, DA release (Threlfell et al., 2012; Kramer et al., 2022; Liu et al., 2022). In the absence of the β2-containing nAChR antagonist, DHβE, single-pulse stimulation triggers a multi-component event, comprised of the initial spike as shown in Fig. 5.6, but also a subsequent depolarisation in both DLS and NAcC (Fig. 5.7A, C). This observation again indicates that fluorescent signals are attributed to action potentials in striatal DA axons.

We tested whether, like action potentials, signals were dependent on VGSCs and VGKCs. Evoked signals were dependent on VGSCs, as tetrodotoxin (TTX) abolished all changes in fluorescence (Fig. 5.7A, C). Application of tetrodotoxin (TTX ;1 μM) rapidly abolished all stimulated changes in ASAP5 fluorescence, such that electrical stimulation no longer produced a response. Evoked signals were dependent on VGKCs, as signals widened upon application of the VGKC inhibitor 4-Aminopyridine (4-AP; 100 μM) (Fig. 5.7B, D).

Taken together, these data indicate that ASAP5 reliably reports action potentials across a population of striatal DA axons. Signals are stable over the duration of experiments, and are responsive to inhibition of VGSCs and VGKCs.

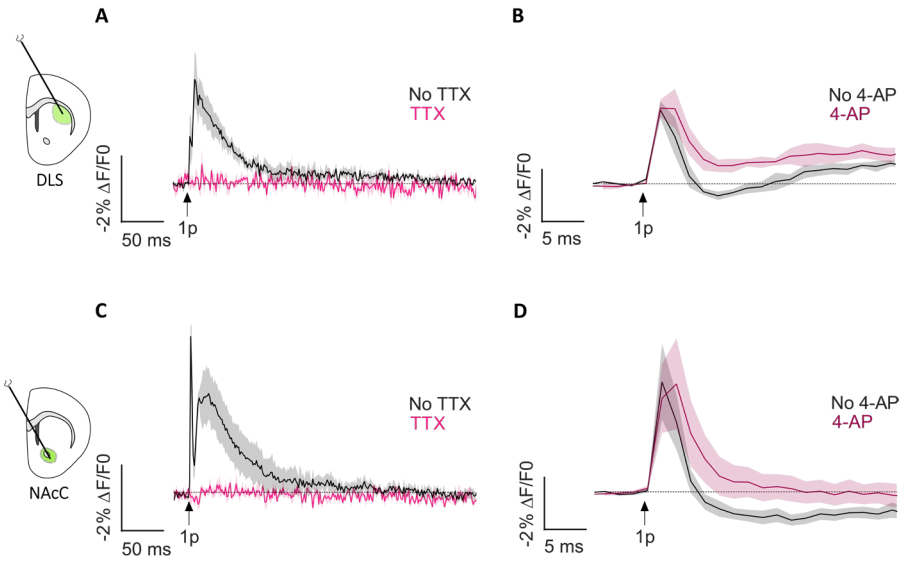

Figure 5.7. ASAP5 signals were TTX-sensitive and spike AUC increased in presence of 4-AP
(A) ASAP5 traces in DLS before and during TTX (1 μM). n = 3. (B) ASAP5 traces in DLS before and during 4-AP (100 μM). n = 3. (C) ASAP5 traces in NAcC before and during TTX (1 μM). n = 3. (D) ASAP5 traces in NAcC before and during 4-AP (100 μM). n = 5. Data are mean ±SEM. DHβE (1 μM) is absent in TTX experiments, and present in 4-AP experiments. Data collected in collaboration with Lucille Duquenoy.

5.2.8. Drugs

Stock solutions were prepared at 1,000x – 20,000x the final concentration and stored at -20°C. Final drug concentrations were prepared in aCSF on the day of the experiment.

Drug	Supplier	Action	Concentration	Solvent	References
4-Aminopyridine (4-AP)	Sigma-Aldrich	VGKC inhibitor	100 µM	Dimethyl sulfoxide (DMSO)	Condon et al. (2019)
(+)-Bicuculline	Abcam	$GABA_A$-R antagonist	10 µM	Dimethyl sulfoxide (DMSO)	Roberts et al. (2020); Stedehouder et al. (2024)
CGP 55845 hydrochloride	Abcam	$GABA_B$-R antagonist	4 µM	Dimethyl sulfoxide (DMSO)	Roberts et al. (2020); Stedehouder et al. (2024)
Cocaine hydrochloride	Sigma-Aldrich	DAT inhibitor	5 µM	dH_2O	Condon et al. (2020); Threlfell et al. (2021)
Dihydro-β-erythroidine (DHβE) hydrobromide	Sigma-Aldrich	nAChR antagonist	1 µM	dH_2O	Threlfell et al. (2012); Roberts et al. (2020)
L-741,626	Abcam	D_2-like-R antagonist	1 µM	Dimethyl sulfoxide (DMSO)	Condon et al. (2019); Threlfell et al. (2021)
Lidocaine	Tocris	VGSC inhibitor	5 µM	Dimethyl sulfoxide (DMSO)	Condon et al. (2019)
Methyl-β-cyclodextrin (MβCD)	Sigma-Aldrich	Vehicle for water-soluble cholesterol	1 mM	dH_2O	Threlfell et al. (2021)
Nomifensine maleate	Sigma-Aldrich	DAT inhibitor	10 µM	Hydrochloric acid (HCl)	Condon et al. (2019); Threlfell et al. (2021)
SCH 23390 hydrochloride	Tocris	GIRK channel inhibitor	10 µM	dH_2O	Kuzhikandathil & Oxford (2002)
Tetrodotoxin (TTX) citrate	Tocris	VGSC inhibitor	1 µM	dH_2O	Tritsch et al. (2012)
Water-soluble (ws) cholesterol	Sigma-Aldrich	Potentiates DAT function	50 µg/ml	dH_2O	Threlfell et al. (2021)

5.2.9. Data acquisition and analysis

Fast-scan cyclic voltammetry data were digitised and acquired using Axoscope 10.7, and extracted using locally written Excel macros or Python script. Voltage indicator imaging data were acquired with Andor Solis I and extracted using FIJI ImageJ software and locally written Matlab analysis code. Statistical tests were performed in GraphPad Prism 9 or 10.

5.3. Results

5.3.1. Short-term plasticity in DA release in male and female mice

Short-term plasticity in striatal DA release consists of STF and STD, and is governed by DATs (Condon et al., 2019). Past experiments in the Cragg laboratory investigating short-term plasticity in striatal DA release were completed using recording solutions containing 5 mM $[K^+]_o$, and in male mice only (Condon et al., 2019). To explore whether DATs modulate axonal excitability, it was imperative to begin by replicating these experiments in our updated recording solutions containing 2.5 mM $[K^+]_o$, and to test short-term plasticity in striatal DA release in both male and female mice. Previous literature examined the impact of variations in $[K^+]_o$ on short-term plasticity and found that lowering $[K^+]_o$ to 1.25 mM (compared to 5 mM) promotes STF and attenuates STD, overall increasing re-release (Condon et al., 2019). Therefore, we hypothesised that the use of 2.5 mM $[K^+]_o$ would only marginally affect short-term plasticity, and focused our efforts on evaluating whether there exists potential variation in short-term plasticity between male and female mice. We hypothesised that we would replicate previously published findings, where STF occurs at short IPIs, and STD at longer IPIs, and that DAT inhibition would attenuate STF and relieve STD.

Differences in DAT-mediated functionality have been reported between sexes. In general, female rodents display increased DAT function compared to males. For example, maximal DA uptake rate in the striatum is faster in female mice, compared to males, with no differences in DA release (Kuiper et al., 2024). In female mice, especially during the estrus phase of the female oestrous cycle, VTA DA neurons exhibit increased activity, which in turn drives posttranslational modifications to DATs, and augments cocaine potency at DATs (Calipari et al., 2017b). Sex differences are not consistently found in DAT-mediated measures, however, with several studies reporting no difference between males and females (e.g. Threlfell et al., 2021; Alonso et al., 2022). We investigated whether any subtle sex

differences might exist, by collecting datasets in male and female mice. We hypothesised that we would not find any substantial sex differences in short-term plasticity in striatal DA release, but, in line with increased DAT function in females, we hypothesised that both STF and STD would be marginally potentiated.

In male mice, STF occurs with IPIs of 10 ms, STD occurs with IPIs of 40-200ms in DLS (Fig. 5.8A). Application of cocaine modified short-term plasticity (Fig. 5.8A, two-way RM ANOVA, IPI x drug interaction, $F_{(2,8)} = 28.93$, $p = 0.0005$, n = 5). Cocaine prevented STF at 10 ms IPI. In female mice, STF occurs with IPIs of 10 ms, STD occurs with IPIs of 40-200ms in DLS (Fig. 5.8B). Application of cocaine modified short-term plasticity (Fig. 5.8B, two-way RM ANOVA, IPI x drug interaction, $F_{(2,8)} = 66.37$, $p < 0.0001$, n = 5). Cocaine prevented STF at 10 ms IPI and relieved STD at 200 ms IPI. A comparison of PPR separated by male and female mice do not show any significant differences between sexes at any timepoint in the absence (Fig. 5.8C, two-way RM ANOVA, IPI x sex, $F_{(4,16)} = 0.82$, $p = 0.5338$, n = 5 for each sex) or presence (Fig. 5.8D, two-way RM ANOVA, IPI x sex, $F_{(4,16)} = 1.42$, $p = 0.2726$, n = 5 for each sex) of cocaine. The change in PPR in DLS was calculated (cocaine – control) for male and female mice and again, this did not significantly differ between sexes at any timepoint (Fig. 5.8E, two-way RM ANOVA, IPI x sex, $F_{(4,16)} = 0.98$, $p = 0.4483$, n = 5 for each sex). As hypothesised, updated recording solutions containing 2.5 mM $[K^+]_o$ did not dramatically change PPR. However, contrary to our hypothesis regarding short-term plasticity in female mice, neither STF nor STD was potentiated.

The use of PPR as a measure of short-term plasticity means that $[DA]_o$ attributed to P2 is normalised to that attributed from P1. Thus, PPR alone does not assess any differences in single pulse evoked $[DA]_o$ between sexes, or the magnitude of cocaine-induced increase in $[DA]_o$ between sexes. Evoked $[DA]_o$ concentrations in DLS did not significantly differ between male and female mice in control conditions (Fig. 5.8F, unpaired t-test, $t_{(8)} = 1.36$, $p = 0.2112$, n

= 5 for each sex). Furthermore, evoked $[DA]_o$ concentrations in DLS did not significantly differ between sexes following application of cocaine (Fig. 5.8G, two-way RM ANOVA, drug x sex, $F_{(1,4)} = 0.02$, $p = 0.9013$, n = 5 for each sex). The magnitude of cocaine-induced increase in $[DA]_o$ in DLS did not differ between sexes (Fig. 5.8H, unpaired t-test, $t_{(8)} = 1.36$, $p = 0.2105$, n = 5 for each sex). Whilst no statistically significant differences were found between sexes, these comparisons may be underpowered. A possible trend for lower initial DA release, and higher effects of cocaine on DA release, were observed in female mice. A post-hoc sample size calculation revealed that the sample size required to detect a minimum difference of 30% in cocaine-induced increases in $[DA]_o$ between sexes, at a power of 80%, is n = 54. Lower initial release and larger cocaine-induced increases in release are consistent with increased DAT function. Our results in DLS do not indicate any overt differences between DA transmission in male and female mice, but still pose a question of whether some subtle sex differences could exist, under the right experimental conditions.

In NAcC, in male mice, STF occurs with IPIs of 10-25 ms, and STD occurs with IPIs of 100-200 ms (Fig. 5.8I). Application of cocaine modified short-term plasticity (Fig. 5.8I, two-way RM ANOVA, IPI x drug interaction, $F_{(4,12)} = 11.79$, $p = 0.0004$, n = 4). Cocaine prevented STF at 10-25 ms IPI and prompted STD at 40 ms IPI. In female mice, STF occurs with IPIs of 10-25 ms, and STD occurs with IPIs of 100-200 ms in NAcC (Fig. 5.8J). Application of cocaine modified short-term plasticity (Fig. 5.8J, two-way RM ANOVA, IPI x drug interaction, $F_{(4,16)} = 27.41$, $p < 0.0001$, n = 5). Cocaine prevented STF at 10-25 ms IPI and prompted STD at 40 ms IPI. PPR separated by male and female mice do not show any significant differences between sexes at any timepoint in the absence (Fig. 5.8K, mixed-effects model, IPI x sex, $F_{(4,11)} = 0.19$, $p = 0.9412$, n = 4 male, 5 female) or presence (Fig. 5.8L, mixed-effects model, IPI x sex, $F_{(4,11)} = 0.78$, $p = 0.5638$, n = 4 male, 5 female) of cocaine. The change in PPR in NAcC was calculated (cocaine – control) for male and female mice (Fig. 5.8M, mixed-effects model, IPI x sex, $F_{(4,35)}$

= 0.41, p = 0.8023, n = 4 male, 5 female), and again, this did not significantly differ between sexes at any timepoint.

Evoked $[DA]_o$ concentrations in NAcC did not significantly differ between male and female mice in control conditions (Fig. 5.8N, unpaired t-test, $t_{(7)}$ = 0.01, p = 0.9962, n = 4 male, 5 female). Furthermore, evoked $[DA]_o$ concentrations in NAcC did not significantly differ between sexes following application of cocaine (Fig. 5.8O, mixed-effects model, drug x sex, $F_{(1,2)}$ = 1.49, p = 0.3467, n = 4 male, 5 female). The magnitude of cocaine-induced increase in $[DA]_o$ in NAcC did not differ between sexes (Fig. 5.8P, unpaired t-test, $t_{(7)}$ = 1.78, p = 0.1179, n = 4 male, 5 female). These comparisons might be underpowered, because in both DLS and NAcC, there was a non-significant trend towards higher cocaine-induced increases in DA release in female mice. Nevertheless, taken together, our data do not support any significant differences in short-term plasticity in striatal DA release or striatal DAT function between sexes.

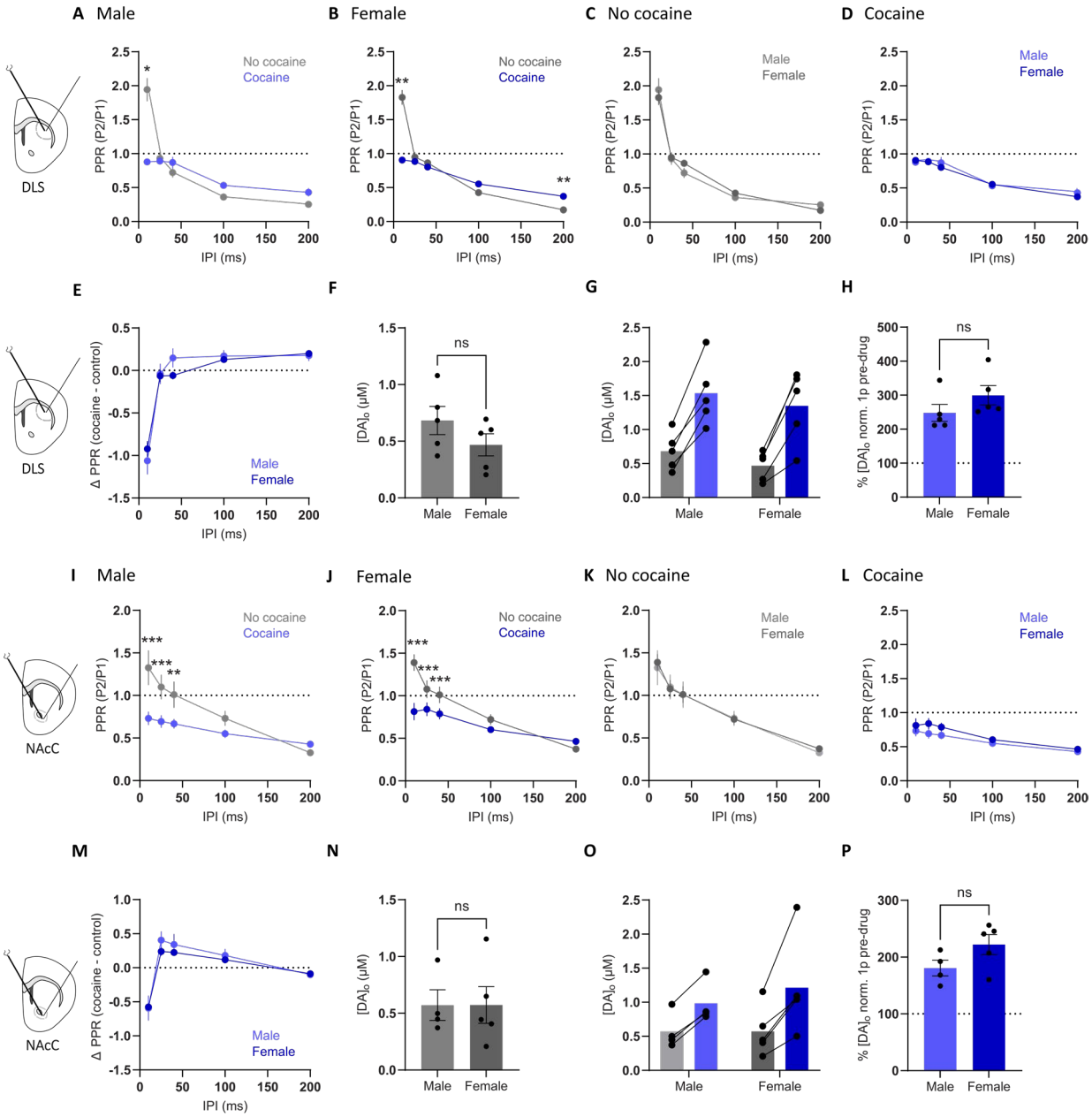

Figure 5.8. Examination of short-term plasticity between male and female mice

*(A) PPR in DLS in males. n = 5. (B) PPR in DLS in females. n = 5. (C) PPR in DLS in absence of cocaine in males and females. n = 5. (D) PPR in DLS in cocaine in males and females. n = 5. (E) Change in PPR in DLS upon application of cocaine in males and females. n = 5. (F) Peak $[DA]_o$ evoked by single pulses in DLS. n = 5. (G) Peak $[DA]_o$ evoked by single pulses in DLS before and during application of cocaine. n = 5. (H) % peak $[DA]_o$ in DLS following application of cocaine. n = 5. (I) PPR in NAcC in males. n = 4-5. (J) PPR in NAcC in females. n = 4-5. (K) PPR in NAcC in absence of cocaine in males and females. n = 4-5. (L) PPR in NAcC in cocaine in males and females. n = 4-5. (M) Change in PPR in NAcC upon application of cocaine in males and females. n = 4-5. (N) Peak $[DA]_o$ evoked by single pulses in NAcC. n = 4-5. (O) Peak $[DA]_o$ evoked by single pulses in NAcC before and during application of cocaine. n = 4-5. (P) % peak $[DA]_o$ in NAcC following application of cocaine. n = 4-5. Data are mean ±SEM. 'No cocaine' is DHβE (1 μM), 'Cocaine' is DHβE (1 μM) and cocaine (5 μM). *p ≤ .05, **p ≤ .01, ***p ≤ .001, ns = non-significant.*

5.3.2. Short-term plasticity in striatal DA release is governed by DATs in mixed sex cohort

Due to the absence of differences between male and female mice in short-term plasticity in striatal DA release, we pooled data and created a mixed-sex cohort.

In DLS, it was previously reported that, in male mice, in 5 mM $[K^+]_o$, STF (PPR > 1) occurs with IPIs of 10 ms, and STD (PPR < 1) occurs with IPIs of 25-200 ms (Condon et al., 2019). Consistent with the finding that PPR is dependent on $[K^+]_o$ concentration (Condon et al., 2019), we found that, in 2.5 mM $[K^+]_o$, and in a mixed-sex cohort, STF occurs with IPIs of 10 ms, STD occurs with IPIs of 40-200ms (Fig. 5.9A). Application of cocaine modified short-term plasticity (Fig. 5.9A, two-way RM ANOVA, IPI x drug interaction, $F_{(2,18)} = 72.61$, $p < 0.0001$, n = 10). Cocaine prevented STF at 10 ms IPI, and relieved STD at 100-200 ms IPIs.

In NAcC, it was previously found that, in male mice, in 5 mM $[K^+]_o$, STF occurs with IPIs of 10-25 ms, and STD occurs with IPIs of 100-200 ms (Condon et al., 2019). In agreement with this, we found that, in 2.5 mM $[K^+]_o$, and in a mixed-sex cohort, STF occurs with IPIs of 10-25 ms, and STD occurs with IPIs of 100-200 ms (Fig. 5.9C). Application of cocaine modified short-term plasticity (Fig. 5.9C, two-way RM ANOVA, IPI x drug interaction, $F_{(2,18)} = 35.72$, $p < 0.0001$, n = 9). Cocaine prevented STF at 10-25ms IPIs, prompted STD at 40 ms IPIs, and relieved STD at 200 ms IPI.

These results support previous literature (Condon et al., 2019) detailing short-term plasticity in striatal DA release, replicating the observation that STF occurs in both DLS and NAcC at short IPIs, and STD at longer IPIs. Our data indicate that, in updated recording solutions, and a mixed-sex cohort, DATs support STF at short IPIs, and promote STD at longer intervals, with some regional variation.

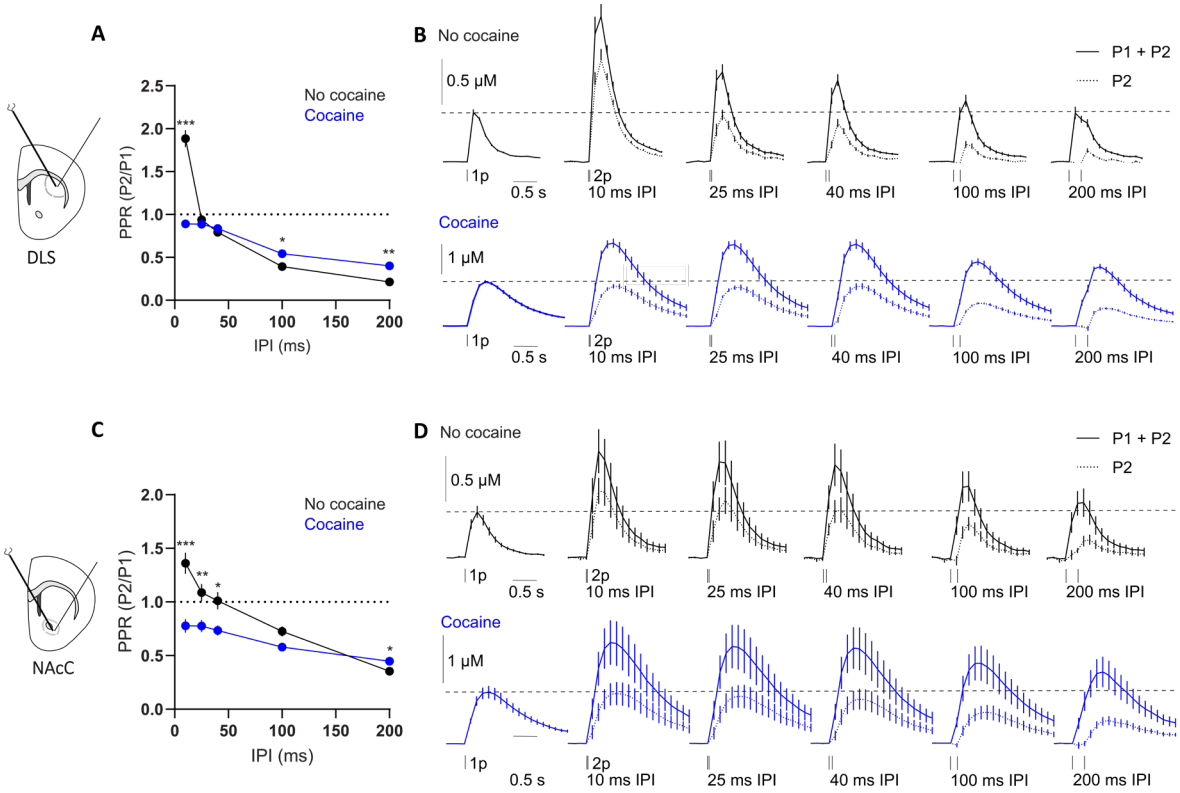

Figure 5.9. Short-term plasticity in striatal DA release is governed by DATs in mixed sex cohort
*(A) PPR in DLS. n = 10. (B) $[DA]_o$ transients over time evoked by single or paired pulses in DLS. (C) PPR in NAcC. n = 9. (D) $[DA]_o$ transients over time evoked by single or paired pulses in NAcC. Data are mean ±SEM. 'No cocaine' is DHβE (1 µM), 'Cocaine' is DHβE (1 µM) and cocaine (5 µM). *p ≤ .05, **p ≤ .01, ***p ≤ .001, ns = non-significant.*

5.3.3. Potentiation of DAT function by cholesterol does not impact plasticity

DATs govern short-term plasticity in striatal DA release (Condon et al., 2019; Sections 5.3.1 and 5.3.2). I assessed whether STF or STD could be potentiated, by potentiating striatal DAT function in DLS. Literature indicates a complex relationship between DATs and cholesterol, depending on the experimental preparation and form of cholesterol used. DATs express binding sites for cholesterol (Penmatsa et al., 2013). Cholesterol has been reported to promote DATs to an outward-facing conformation and to increase binding of cocaine analogues (Hong & Amara, 2010; Morissette et al., 2018). In another report, binding of the cocaine analogue [^{3}H]CFT is not altered following cholesterol incubation, but cholesterol does facilitate a faster DA uptake rate (Jones et al., 2012). In mouse striatal slices *ex vivo*, incubation in cholesterol decreases single pulse-evoked $[DA]_o$, increases DA clearance rate,

and augments cocaine-induced increases in $[DA]_o$ (Threlfell et al., 2021). Together, these studies are consistent with cholesterol promoting DAT function. We hypothesised that potentiation of striatal DAT function with cholesterol would increase the extent of both STF and STD, leading to a steeper PPR curve than in vehicle.

To assess whether potentiation of DAT function alters short-term plasticity in striatal DA release, we first confirmed that incubation in ws-cholesterol (50 µg/ml) enhanced DAT function, relative to vehicle (MβCD, 1 mM). As shown previously (Threlfell et al., 2021), cholesterol strongly decreased single pulse-evoked $[DA]_o$ by ~75% (Fig. 5.10A), increased DA uptake rate (Fig. 5.10B, unpaired t-test, $t_{(22)} = 4.46$, $p = 0.0002$, n = 12 DA transients from 2 mice), and augmented cocaine-induced increases in single pulse evoked $[DA]_o$ (Fig. 5.10C). Cocaine-induced increases in $[DA]_o$ following MβCD incubation were ~67%, whereas incubation in cholesterol boosted cocaine-induced increases in $[DA]_o$ to ~230%. Statistical comparisons were not performed for Fig. 5.10A or 5.10C due to low sample size (n = 2).

Consistent with previous observations in DLS (Condon et al., 2019), and our data in Sections 5.3.1 and 5.3.2, we found that STF operates at the shortest timescales, and STD occurs with longer IPIs. Contrary to our hypothesis, we found that incubation in cholesterol did not modify either STF or STD in control conditions (Fig. 5.10D, two-way RM ANOVA, IPI x drug interaction, $F_{(4,16)} = 0.72$, $p = 0.5913$, n = 5) or cocaine (Fig. 5.10E, IPI x drug interaction, $F_{(4,16)} = 0.52$, $p = 0.7194$, n = 5), relative to vehicle.

These data indicate that although incubation in cholesterol promoted DAT-mediated changes to striatal DA release and DA uptake, cholesterol did not impact short-term plasticity in striatal DA release. The lack of a change in short-term plasticity following cholesterol incubation could indicate that striatal DATs are supporting short-term plasticity in DA release to a maximal extent in our *ex vivo* slice preparations. Alternatively, the data might point towards a dissociation of the roles of DATs, in that promoting DAT-mediated changes to initial

release, and the rate of DA uptake, does not necessarily translate to a potentiation in DAT-regulated short-term plasticity in DA release.

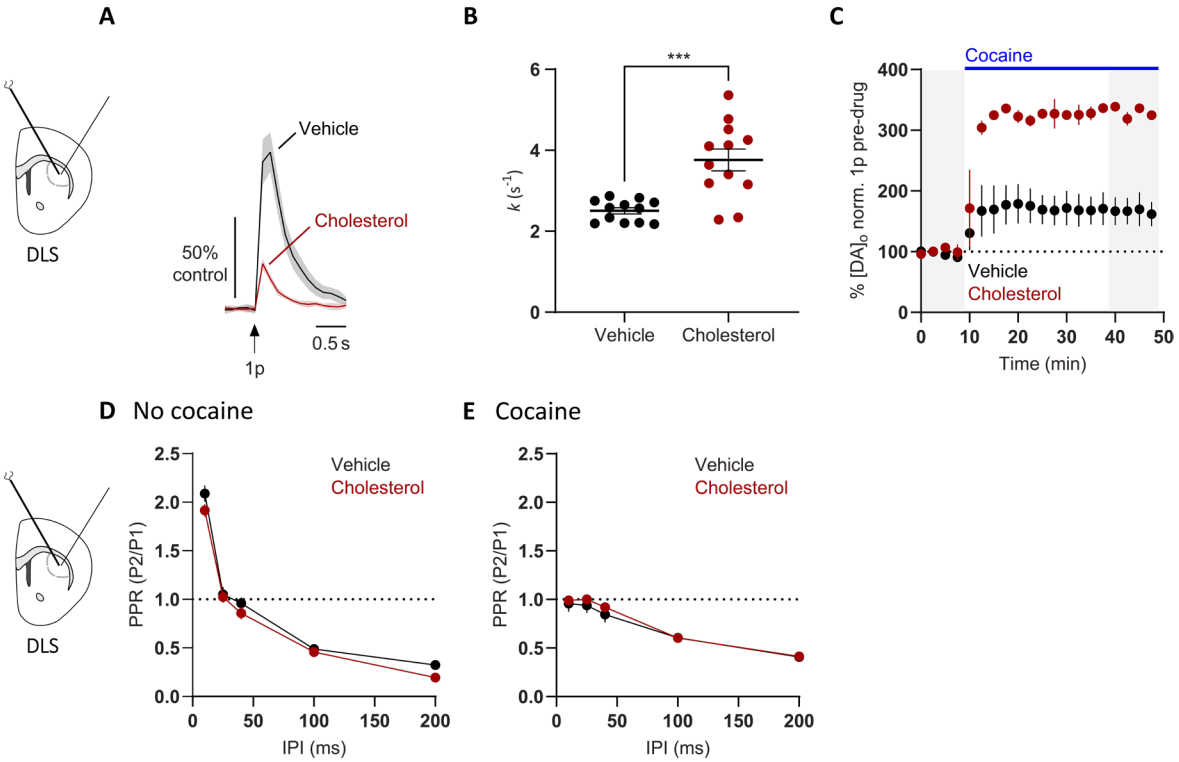

Figure 5.10. Potentiation of DAT function does not impact short-term plasticity in DA release
*(A) $[DA]_o$ transients over time evoked by single pulses in DLS, following vehicle or cholesterol incubation. Data normalised to vehicle. n = 2. (B) Decay rates for $[DA]_o$ evoked by single pulses in DLS following vehicle or cholesterol incubation. n = 12 transients. (C) Peak $[DA]_o$ over time evoked by single pulses in DLS, before and during bath application of cocaine. Data normalised to the first four data points. n = 2. (D) PPR in DLS in control following vehicle or cholesterol incubation. n = 5. (E) PPR in DLS in cocaine following vehicle or cholesterol incubation. n = 5. Data are mean ±SEM. 'Vehicle' is MβCD (1 mM), 'Cholesterol' is ws-cholesterol (50 µg/ml). 'No cocaine' is DHβE (1 µM), 'Cocaine' is DHβE (1 µM) and cocaine (5 µM). *p ≤ .05, **p ≤ .01, ***p ≤ .001, ns = non-significant.*

5.3.4. DATs promote DA axon repolarisation after hyperpolarisation, following single pulse stimulation

Due to the electrogenic nature of DATs (e.g. Sonders et al., 1997; Carvelli et al., 2004), and the potential for DATs to modify DA axonal activation in the striatum to govern short-term plasticity (Condon et al., 2019), we assessed whether striatal DATs modify DA axonal membrane potential using the newly developed, genetically-encoded fluorescent voltage indicator, ASAP5 (Hao et al., 2024).

We hypothesised that DAT inhibition would have a minimal impact on the initial spike, as DATs are likely to have little impact on membrane potential before DA uptake begins. DAT-mediated changes to single pulse evoked $[DA]_o$ are downstream of axonal excitability and instead rely on mobilisation of a synapsin-dependent vesicle pool (Venton et al., 2006). Furthermore, changes in $[K^+]_o$ do not affect single pulse evoked $[DA]_o$ (Condon et al., 2019). We hypothesised that, instead, DAT inhibition would limit DAT-mediated depolarisation on a slower timescale, following the initial spike, on a timeframe where DATs are expected to mediate DA uptake. DAT inhibition greatly slows uptake, and therefore will limit DAT-mediated depolarising transport-associated currents. Fig. 5.11 depicts when we would expect DATs to be most active and have the greatest impact on axonal membrane potential.

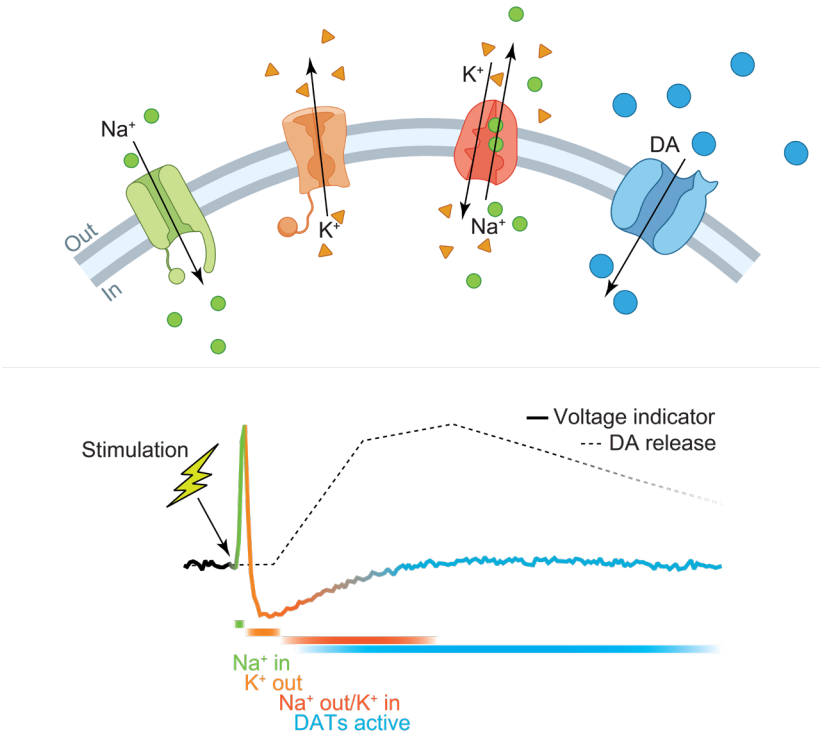

Figure 5.11. Simplified cartoon with timescale of DAT-mediated changes to membrane potential
Cartoon depicting hypothesised timescale of DAT-mediated changes to axonal membrane potential. Na^+ flows inward on the action potential upstroke, and K^+ flows outward on the downstroke. The Na^+/K^+ pump restores resting membrane potential. Upon DA release, DATs are rapidly activated and translocate DA inward, generating depolarising currents. Image partially created in BioRender under an Academic License.

In DLS, application of cocaine (5 µM) caused axonal membrane potential to be hyperpolarised following single pulse stimulation, compared to membrane potential in the absence of cocaine (Fig. 5.12A). Traces are corrected for the slight signal decay over time in DLS, as outlined in Section 5.2.7. Compared to a time-matched control dataset (Fig. 5.6), spike height was unchanged in the presence of cocaine, (Fig 5.12B, unpaired t-test, $t_{(13)} = 1.95$, $p = 0.0729$, n = 5 time-matched control, 10 cocaine), as was spike AUC (Fig 5.12C, unpaired t-test, $t_{(13)} = 0.81$, $p = 0.4327$, n = 5 time-matched control, 10 cocaine). Application of cocaine appeared to slightly increase the F_0 in DLS (Fig 5.12D, unpaired t-test, $t_{(13)} = 2.32$, $p = 0.0374$, n = 5 time-matched control, 10 cocaine).

Following the initial spike, axonal membrane potential was significantly hyperpolarised in the presence of cocaine (Fig. 5.12E, two-way RM ANOVA, time x drug interaction, $F_{(5,45)} = 21.19$, p

< 0.0001, n = 10). Prior to the application of cocaine, the maximum AHP amplitude in DLS occurred on average ~9 ms following stimulation (range ~8-11 ms), whereas following cocaine, the timing of the peak AHP amplitude was noticeably scattered, occurring on average ~52 ms following stimulation (range ~16-93 ms) (Fig. 5.12F). Cocaine significantly increased the AHP amplitude, leading to a deeper AHP (Fig. 5.12G, paired t-test, $t_{(9)} = 16.23$, p < 0.0001, n = 10).

In NAcC, application of cocaine caused axonal membrane potential to be hyperpolarised following single pulse stimulation, compared to membrane potential in the absence of cocaine (Fig. 5.12H). Traces are corrected for the slight signal decay over time in NAcC, as outlined in Section 5.2.7. Compared to a time-matched control dataset (Fig. 5.6), cocaine did not affect spike height (Fig 5.12I, unpaired t-test, $t_{(15)} = 0.73$, $p = 0.4770$, n = 7 time-matched control, 10 cocaine). Spike AUC trended towards being lower in cocaine (Fig 5.12J, unpaired t-test, $t_{(15)} = 2.13$, $p = 0.0501$, n = 7 time-matched control, 10 cocaine). F_0 in NAcC was not affected by the presence of cocaine (Fig 5.12K, unpaired t-test, $t_{(15)} = 1.94$, $p = 0.0712$, n = 7 time-matched control, 10 cocaine).

Following the initial spike, axonal membrane potential was significantly hyperpolarised in the presence of cocaine (Fig. 5.12L, two-way RM ANOVA, time x drug interaction, $F_{(5,45)} = 10.47$, p < 0.0001, n = 10). Pre-cocaine, the peak AHP amplitude in NAcC occurred on average ~26 ms following stimulation (range ~13-53 ms), whereas following cocaine, the peak AHP amplitude occurred on average ~50 ms following stimulation (range ~14-98 ms) (Fig. 5.12M). Unlike DLS, there was not a clear separation of the timing of peak AHP amplitude. Cocaine did not change the AHP amplitude (Fig. 5.12N, paired t-test, $t_{(9)} = 1.68$, $p = 0.1267$, n = 10).

Consistent with our hypothesis, the main impact of DAT inhibition on axonal membrane potential was following the initial spike, in both DLS and NAcC. These data, in combination with previous literature, indicate that when striatal DATs are active, DATs generate

depolarising currents to assist the return to resting membrane potential following a single stimulation.

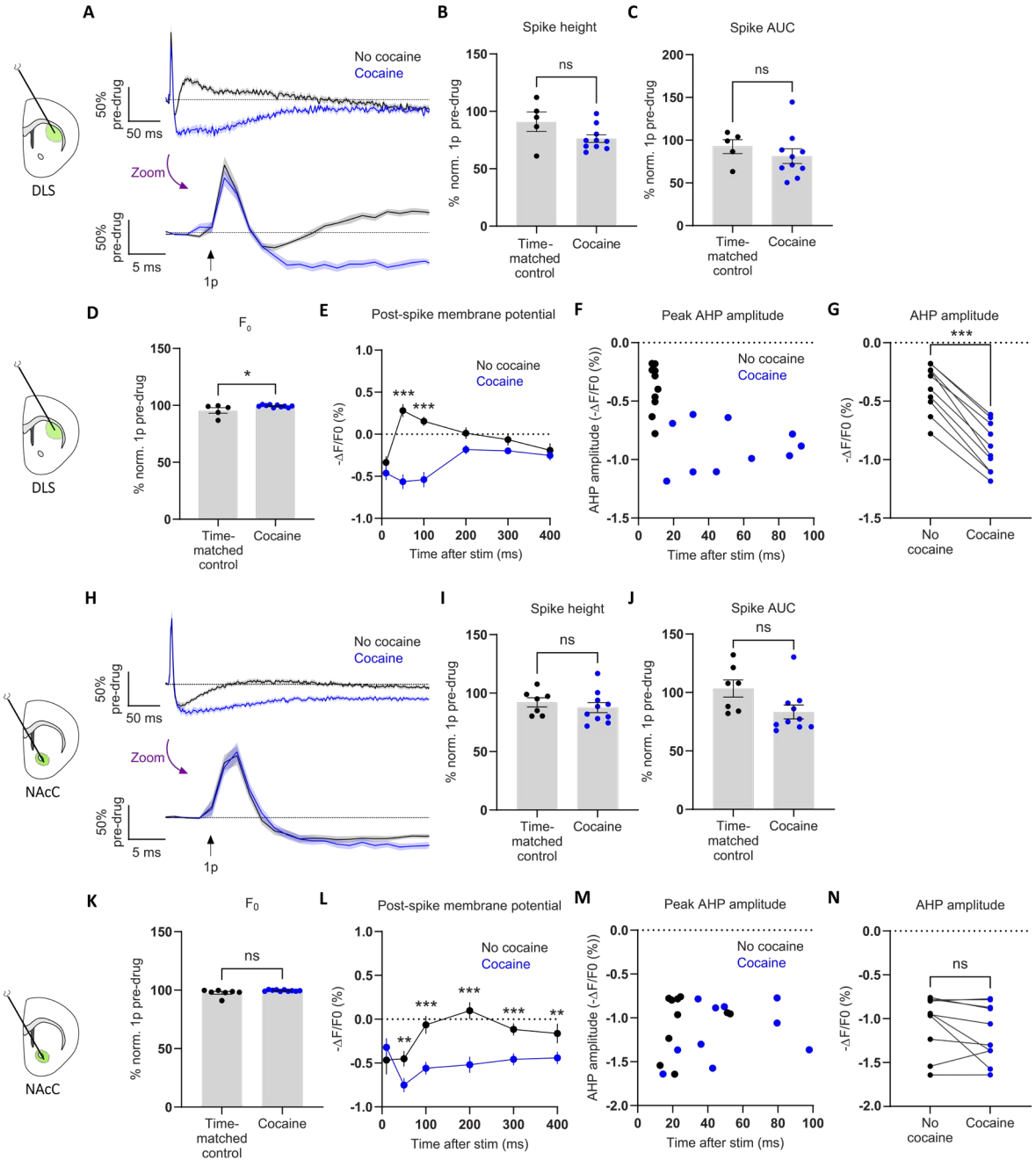

Figure 5.12. DATs promote axonal membrane repolarisation to resting potential following single pulse stimulation

(A) Changes in membrane potential over time in DLS before or during cocaine. n = 10. (B) Spike height (%) in DLS. n = 5/10. (C) Spike AUC (%) in DLS. n = 5/10. (D) F_0 (%) in DLS. n = 5/10. (E) Membrane potential following initial spike in DLS. n = 10. (F) Peak AHP amplitude in DLS. n = 10. (G) Change in AHP amplitude in DLS. n = 10. (H) Changes in membrane potential over time in NAcC before or during cocaine. n = 10. (I) Spike height (%) in NAcC. n = 7/10. (J) Spike AUC (%) in NAcC. n = 7/10. (K) F_0 (%) in NAcC. n = 7/10. (L) Membrane potential following initial spike in NAcC. n = 10. (M) Peak AHP amplitude

*in NAcC. n = 10. (N) Change in AHP amplitude in NAcC. n = 10. Data are mean ±SEM. 'No cocaine' is DHβE (1 μM), 'Cocaine' is DHβE (1 μM) and cocaine (5 μM). Traces are corrected for signal decay over time using a time-matched control (A, I). Data are normalised to pre-drug for cocaine, and equivalent recordings for time-matched control (B, C, D, I, J, K). *p ≤ .05, **p ≤ .01, ***p ≤ .001, ns = non-significant.*

5.3.5. Testing whether impact of cocaine on membrane repolarisation is due to VGSC inhibition

In some cases, cocaine acts as a VGSC inhibitor (O'Leary & Chahine, 2002), and Na^+ currents through VGSCs are known to be essential for AP initiation and propagation (Hodgkin & Huxley, 1952a, 1952b; Armstrong & Bezanilla, 1973; Agnew, 1984; reviewed in Catterall, 2000; Debanne, 2004; Catterall, 2012; Rama et al., 2018). Cocaine does not inhibit VGSCs on DA neurons at concentrations < 20 μM (Acevedo-Rodriguez et al., 2014), and the concentration of cocaine in our experiments is 5 μM. Nevertheless, due to the strong impact of cocaine on DA axonal activation in Fig. 5.12, we conducted experiments to exclude the possibility that cocaine was acting via a local anaesthetic action at VGSCs.

Lidocaine decreases single pulse-evoked DA release by ~30% in DLS (Condon et al., 2019). However, the modification of short-term plasticity by cocaine is not due to action at VGSCs, as lidocaine, a VGSC inhibitor which is thought to target the same subset of VGSCs as cocaine, does not replicate the effect of cocaine short-term plasticity in striatal DA release (Condon et al., 2019). Therefore, we hypothesised that lidocaine would slightly decrease spike size, but would not replicate the effects of cocaine on striatal DA axonal activation following single pulse electrical stimulation.

Surprisingly, in DLS, application of lidocaine (5 μM) did not appear to change the ASAP5 signal obtained during single pulse electrical stimulation (Fig. 5.13A). Traces are corrected for the slight signal decay over time in DLS, as outlined in Section 5.2.7. No changes were observed to spike height (Fig. 5.13B, unpaired t-test, $t_{(7)} = 0.49$, $p = 0.6417$), spike AUC (Fig. 5.13C, unpaired t-test, $t_{(7)} = 1.26$, $p = 0.2471$), or F_0 (Fig. 5.13D, unpaired t-test, $t_{(7)} = 0.14$, $p =$

0.8952). Lidocaine did not affect post-spike membrane polarisation (Fig. 5.13E, two-way RM ANOVA, time x drug interaction, $F_{(5,15)} = 1.11$, $p = 0.3962$, n = 4). AHP amplitude did not differ with lidocaine (Fig. 5.13F, paired t-test, $t_{(3)} = 0.77$, $p = 0.4963$). To confirm that lidocaine attenuated DA release, we collected a pilot dataset using FSCV. Lidocaine decreased single pulse-evoked $[DA]_o$ by ~18% (Fig. 5.13G). Statistical comparisons were not performed for the DA release dataset due to low sample size (n = 3).

In NAcC, application of lidocaine did not appear to change the ASAP5 signal obtained during single pulse electrical stimulation (Fig. 5.13H). Traces are corrected for the slight signal decay over time in NAcC, as outlined in Section 5.2.7. No changes were observed to spike height, spike AUC, or F_0 (Fig. 5.13I, J, K). Lidocaine did not appear to affect post-spike membrane polarisation, or AHP amplitude (Fig. 5.13L, M). Statistical comparisons were not performed due to low sample size (n = 2-3).

Consistent with our hypothesis, lidocaine did not replicate the effects on axonal activation seen with cocaine, consistent with the report that cocaine does not act at VGSCs at the concentration used in this study (Acevedo-Rodriguez et al., 2014), and that VGSC inhibition is not involved in DAT-mediated changes to short-term plasticity in striatal DA release (Condon et al., 2019). It was surprising, however, given that lidocaine is a VGSC inhibitor, that lidocaine did not have any impact on membrane potential in striatal DA axons. The concentration of lidocaine used here (5 µM), was a like-for-like concentration with cocaine, and chosen based on published data showing that this concentration of lidocaine attenuates striatal DA release (Condon et al., 2019). In our pilot dataset, lidocaine also attenuated DA release, the magnitude of which is slightly lower than published data, but this discrepancy could be due to the use of aCSF with different ionic compositions. The observation that lidocaine does not impact DA axon membrane potential may be explained by VGSC expression patterns. Cocaine, and lidocaine, are thought to affect only a subset of VGSCs

(Na_V 1.4 and 1.5; Wright et al., 1997; O'Leary & Chahine, 2002), and it is not known whether these subtypes exist on striatal DA axons. It is expected that at least one of these VGSC subtypes exist in the striatum, due to the attenuation in striatal DA release, but this phenomenon could via another striatal cell type.

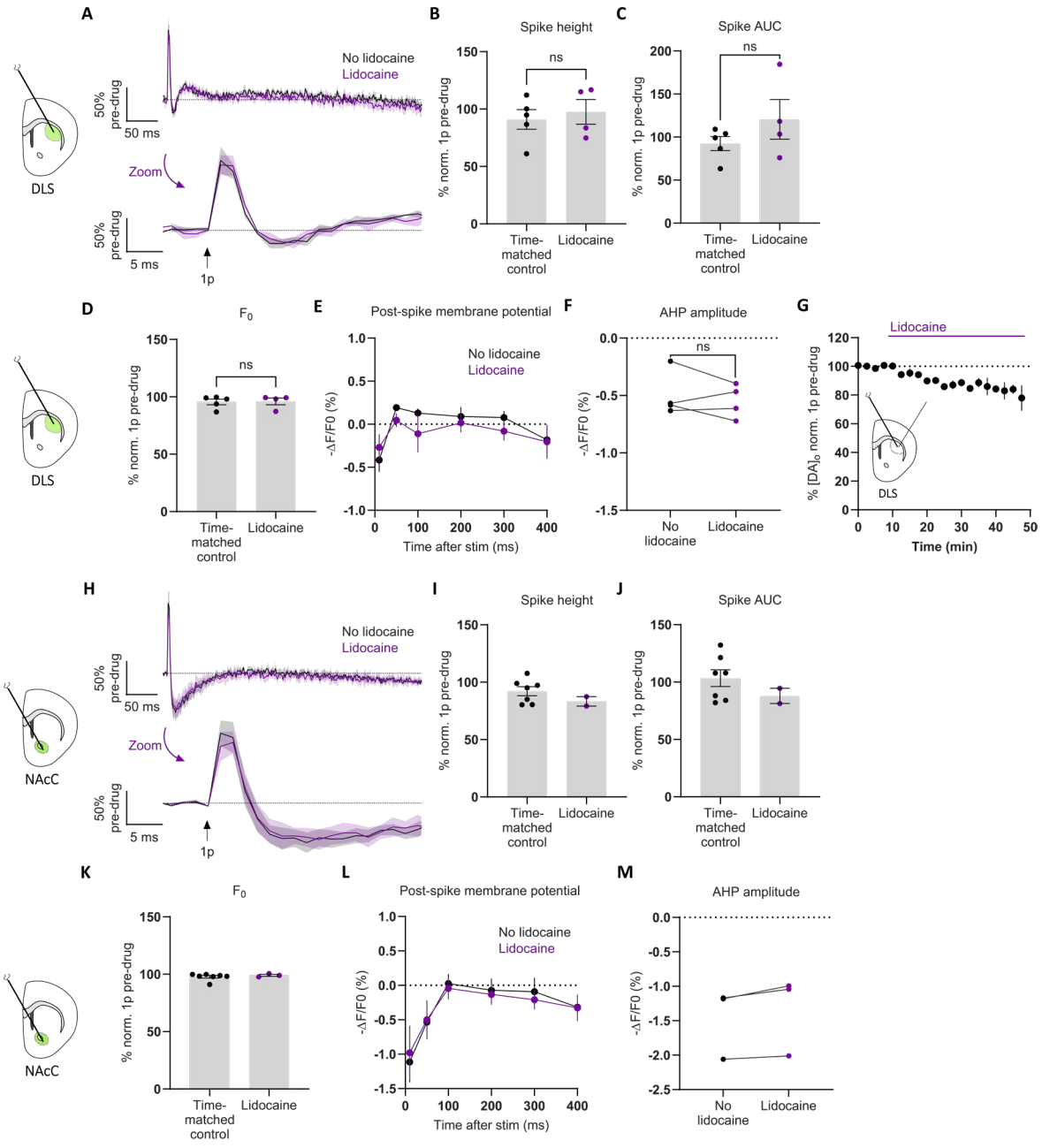

Figure 5.13. Preliminary: Lidocaine does not replicate effects of cocaine on DA axonal activation
(A Changes in membrane potential over time in DLS before or during lidocaine. n = 4. (B) Spike height (%) in DLS. n = 5/4. (C) Spike AUC (%) in DLS. n = 5/4. (D) F_0 (%) in DLS. n = 5/4. (E) Membrane potential following initial spike in DLS. n = 4. (F) Change in AHP amplitude in DLS. n = 4. (G) Peak $[DA]_o$ over time evoked by single pulses in DLS, before and during bath application of cocaine. Data normalised to the

*first four data points. n = 3. (H) Changes in membrane potential over time in NAcC before or during lidocaine. n = 3. (I) Spike height (%) in NAcC. n = 7/3. (J) Spike AUC (%) in NAcC. n = 7/3. (K) F_0 (%) in NAcC. n = 7/3. (L)) Membrane potential following initial spike in NAcC. n = 3. (M) Change in AHP amplitude in NAcC. n = 3. Data are mean ±SEM. 'No lidocaine' is DHβE (1 μM), 'Lidocaine' is DHβE (1 μM) and lidocaine (5 μM). Traces are corrected for signal decay over time using a time-matched control (A, H). Data are normalised to pre-drug for lidocaine, and equivalent recordings for time-matched control (B, C, D, I, J, K). *p ≤ .05, **p ≤ .01, ***p ≤ .001, ns = non-significant.*

5.3.6. Alternate DAT inhibitor, nomifensine, replicates effects of cocaine on membrane repolarisation following single pulse stimulation

To assess whether results obtained with cocaine were due to the action of cocaine at DATs, or VGSCs, we tested whether the VGSC inhibitor, lidocaine, replicated the effects of cocaine on membrane potential. Lidocaine did not replicate the effects of cocaine, indicating that the changes to axonal activation with cocaine are not due to cocaine acting at VGSCs. However, it was surprising that lidocaine did not have any impact on membrane potential. We therefore tested whether the effects on membrane potential with cocaine (prolonged time to repolarisation after hyperpolarisation in DLS and NAcC, and deeper AHP amplitude in DLS), were specific to cocaine only. To do this, we used an alternative DAT inhibitor, nomifensine, which has not been reported to act at VGSCs, to explore whether the effects on membrane polarisation in cocaine could be replicated, and therefore generalisable to other DAT inhibitors. We hypothesised that, like cocaine, nomifensine would lead to a hyperpolarised state following a single pulse stimulation, and prolong time to membrane repolarisation.

In DLS, preliminary data indicate that application of nomifensine (10 μM) caused the membrane to be hyperpolarised following single pulse stimulation, compared to the no nomifensine condition (Fig. 5.14A). Traces are corrected for the slight signal decay over time in DLS, as outlined in Section 5.2.7. Comparisons of spike height, spike AUC, and F_0 against time-matched controls indicate that nomifensine does not influence any of these measures (Fig. 5.14B, C, D). Following the spike, membrane potential was hyperpolarised in the

presence of nomifensine (Fig. 5.14E), and the AHP amplitude was deeper (Fig. 5.14F). Statistical comparisons were not performed due to low sample size (n = 2).

In NAcC, preliminary data indicate that application of nomifensine caused the membrane to be hyperpolarised following single pulse stimulation, compared to the no nomifensine condition (Fig. 5.14G). Traces are corrected for the slight signal decay over time in NAcC, as outlined in Section 5.2.7. Comparisons of spike height, spike AUC, and F_0 against time-matched controls indicate that nomifensine does not influence any of these measures (Fig. 5.14H, I, J). Following the spike, membrane potential appeared to be hyperpolarised in the presence of nomifensine (Fig. 5.14K), though the small sample size and large variability make this difficult to confirm. The AHP amplitude appeared deeper in nomifensine (Fig. 5.14L). Statistical comparisons were not performed due to low sample size (n = 2).

These preliminary datasets indicate that nomifensine-induced changes to membrane polarisation are similar to the cocaine-induced changes, therefore it is likely that DATs are responsible for promoting membrane repolarisation following hyperpolarisation.

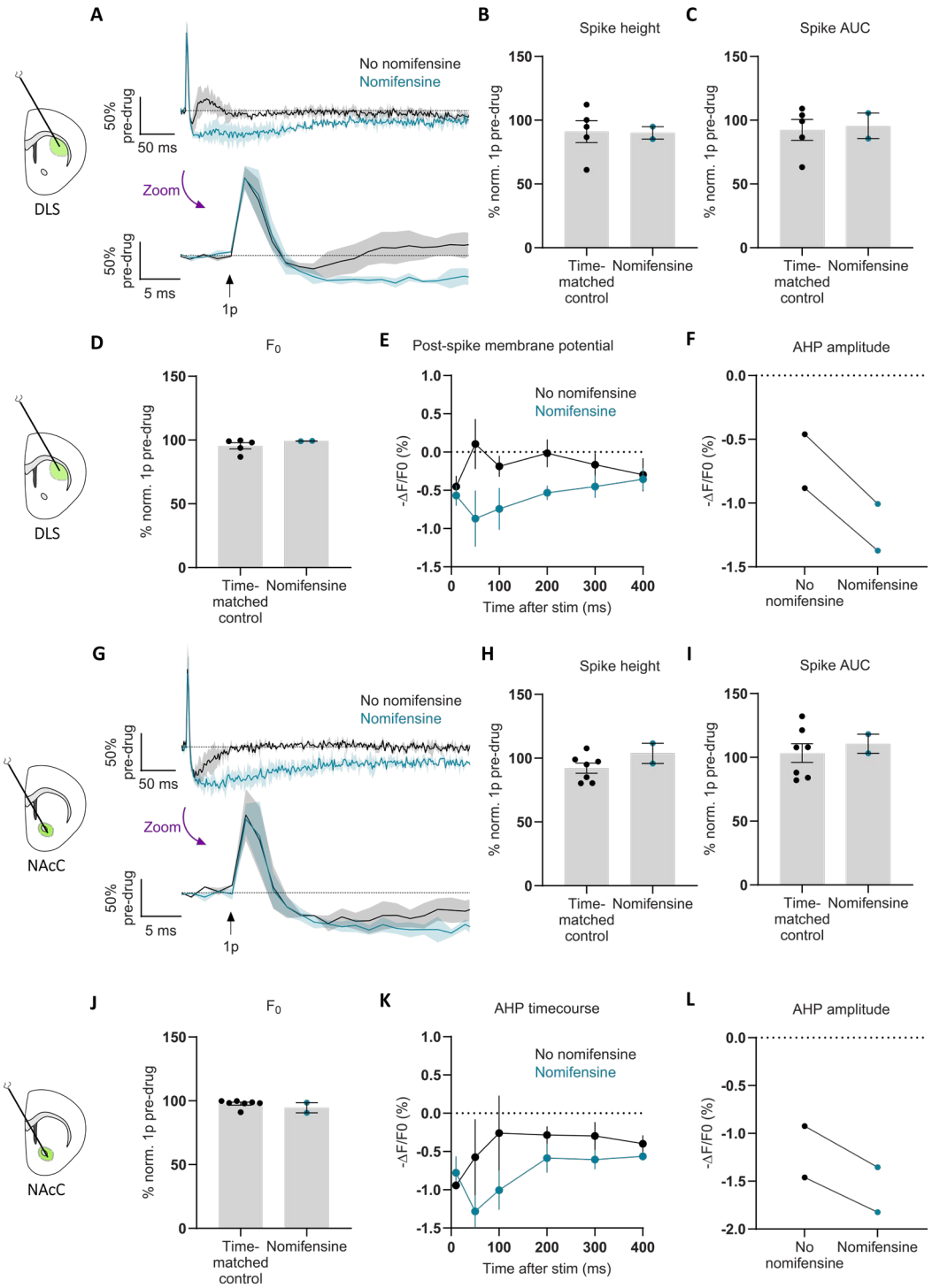

Figure 5.14. Preliminary: effects of cocaine on axonal membrane potential replicated with nomifensine

(A) Changes in membrane potential over time in DLS before or during nomifensine. n = 2. (B) Spike height (%) in DLS. n = 5/2. (C) Spike AUC (%) in DLS. n = 5/2. (D) F_0 (%) in DLS. n = 5/2. (E) Membrane potential following initial spike in DLS. n = 2. (F) Change in AHP amplitude in DLS. n = 2. (G) Changes in membrane potential over time in NAcC before or during nomifensine. n = 2. (H) Spike height (%) in NAcC. n = 7/2. (I) Spike AUC (%) in NAcC. n = 7/2. (J) F_0 (%) in NAcC. n = 7/2. (K) Membrane potential following initial spike in NAcC. n = 2. (L) Change in AHP amplitude in NAcC. n = 2. Data are mean ±SEM. 'No nomifensine' is DHβE (1 μM), 'Nomifensine' is DHβE (1 μM) and nomifensine (10 μM). Traces are corrected for signal decay over time using a time-matched control (A, G). Data are normalised to pre-

*drug for lidocaine, and equivalent recordings for time-matched control (B, C, D, H, I, J). *p ≤ .05, **p ≤ .01, ***p ≤ .001, ns = non-significant.*

5.3.7. DATs promote membrane repolarisation to resting potential, which modifies subsequent spike size

DATs are electrogenic (e.g. Sonders et al., 1997; Carvelli et al., 2004), and govern short-term plasticity in striatal DA release (Condon et al., 2019). Previous speculation was that DATs might limit axonal re-activation to promote release-independent STD, but techniques used could not directly measure of axonal activation (Condon et al., 2019). We have demonstrated that DATs promote membrane repolarisation following a spike and hyperpolarisation, because DAT inhibition prolongs time to repolarisation (Fig. 5.12 & 5.14). We therefore explored whether DAT-mediated changes to axonal excitability might be involved short-term plasticity in DA release.

STF at the shortest IPIs is somewhat release-dependent, and involves Ca^{2+}-mediated gating (supported by DATs) (Condon et al., 2019). On the other hand, STD is release- and Ca^{2+}-independent, and instead relies on factors that may govern axonal excitability, such as K^{+}-mediated gating, and DATs (Condon et al., 2019). We therefore hypothesised that DAT-mediated changes to membrane potential would mirror results obtained for DA release at IPIs where STD occurs, rather than STF.

DAT-mediated changes to axonal membrane potential likely impact on VGSC availability. VGSCs activate upon membrane depolarisation, and then typically inactivate rapidly in a few milliseconds (Yu & Catterall, 2003), although several timescales of slower inactivation have been described, from tens of milliseconds to seconds, and even minutes in some cases (e.g. Goldin, 2003; Silva, 2014; Chen et al., 2024). Recovery from inactivation depends on the duration of depolarisation, and can be a prolonged process (Toib et al., 1998; Ellerkmann et al., 2001). Therefore, the availability of VGSCs for subsequent spike generation is dynamic.

For short IPIs, subsequent spikes could occur during the refractory phase, alternatively if the refractory phase is short and VGSCs have not yet inactivated, subsequent action potentials could be larger than the first. For longer IPIs, VGSCs may not have recovered from inactivation, therefore action potential generation is limited by VGSC availability. Recovery from VGSC inactivation appears to play an important role in short-term presynaptic plasticity, alongside axon morphology and arbourisation (Debanne, 2004). If the membrane is more depolarised, less VGSCs are available (e.g. Vandael et al., 2015), yet membrane potential is closer to threshold for action potential generation. On the other hand, more VGSCs may be available when the membrane is more hyperpolarised. Hyperpolarisation-induced facilitation has been described, where a brief hyperpolarisation prior to generation of the action potential, results in larger action potential amplitude (Rama et al., 2015). Taken together, VGSC availability, and therefore action potential size, will depend on membrane potential and intrinsic factors to the neuron of interest.

DAT inhibition with cocaine produces membrane hyperpolarisation which lasts for hundreds of milliseconds (Fig. 5.12). We hypothesised that, consistent with augmented DA release in the presence of DAT inhibitors at subsequent stimulations (Condon et al., 2019; Fig. 5.8 & 5.9), the hyperpolarised state of the membrane in cocaine would give rise to larger subsequent spikes, akin to hyperpolarisation-induced facilitation. We hypothesised that, at longer IPIs, when DATs are active, the membrane repolarisation following a single pulse stimulation would promote STD and therefore, the size of the second spike would be smaller than the first spike. Further, when DATs are inhibited, the hyperpolarised state following the first spike, would promote a larger second spike than in conditions where DATs are active.

In DLS, for IPIs of 10-200 ms, application of cocaine (5 μM) caused a marked hyperpolarisation following the initial spike, compared to the no condition (Fig. 5.15A, B, C, D, E). Paired-pulse traces are normalised for visualisation, so that the first spike (P1) is the

same height in both conditions. Insets showing a comparison of P2 for each IPI shows that P2 appears larger in the presence of cocaine, at IPIs of 25 ms, 40 ms and 100 ms. In the absence of cocaine, PPR (P2/P1) of spike height (Fig. 5.15F), and spike AUC (Fig. 5.15G), revealed a strikingly similar relationship between PPR and IPI to that observed for DA release (Condon et al., 2019; Fig. 5.8 & 5.9) with STF (PPR > 1) at 10 ms IPI, and STD at IPIs of 25-200 ms. The similarity of data indicates that short-term plasticity in striatal DA release may, at least in part, be determined by axonal activation.

DAT inhibition with cocaine significantly increased PPR of spike height at 40 ms IPI (Fig. 5.15F, two-way RM ANOVA, IPI x drug interaction, $F_{(4,20)} = 3.21$, $p = 0.0346$, n = 6 for each IPI), and increased PPR of spike AUC at IPIs of 25-200 ms (Fig. 5.15G, two-way RM ANOVA, IPI x drug interaction, $F_{(4,20)} = 10.76$, $p < 0.0001$, n = 6 for each IPI). PPR of peak depolarisation differs between conditions, in that PPR is lower in the presence of cocaine, at IPIs of 25 ms (Fig. 5.15H, two-way RM ANOVA, IPI x drug interaction, $F_{(4,20)} = 2.97$, $p = 0.0445$, n = 6 for each IPI). This is not surprising, as we observe membrane hyperpolarisation in the presence of cocaine, which leads to a smaller peak depolarisation across IPIs, as seen in the traces (Fig. 5.15A, B, C, D, E). This indicates that peak depolarisation may not be the optimal measure in this scenario, as it does not mirror observations in striatal DA release.

Whilst we cannot measure absolute changes in membrane potential using a fluorescent indicator, the measure of peak depolarisation is a similar readout. The impact of absolute, versus relative, changes in membrane potential is an important consideration. Published findings in the main axon of DA neurons, and unpublished data from the Cragg laboratory, corroborates the indication that, for DA axons, relative changes in membrane potential may be more impactful in determining DA release. Whole-cell patch clamp electrophysiology on the main axon of DA neurons reveals that local application of GABA is depolarising, and reduces action potential amplitude (Kramer et al., 2020). The combination of GABA-

mediated depolarisation and reduction in action potential amplitude results in equivalent absolute depolarisation between control conditions and in the presence of GABA, but a smaller relative change in membrane potential in the presence of GABA (Kramer et al., 2020). The relevance of relative changes in membrane potential are also supported by data from the Cragg laboratory. When nAChRs are active, the amount of DA released by subsequent stimulations is minimal, yet when nAChRs are inhibited, DA released from subsequent pulses is far greater (Rice & Cragg, 2004). When nAChRs are active, peak depolarisation is larger than when nAChRs are inhibited, yet the relative change in membrane potential for each subsequent spike is far greater when nAChRs are inhibited (unpublished data, L. Duquenoy, Cragg lab). Subsequent spike amplitude is minimal when nAChRs are active (unpublished data, L. Duquenoy, Cragg lab). Therefore, relative changes in membrane potential may determine striatal DA release more reliably than absolute changes.

Plotting PPR of spike height and spike AUC against the point at which the second spike (P2) sits (the baseline just preceding P2), indicates that for both measures of spike height and spike AUC, the relationship between membrane polarisation and PPR is such that a more depolarised baseline (i.e. when DATs are active) lends itself to a smaller PPR, and a more hyperpolarised baseline (i.e. when DATs are inactive) lends itself to a larger PPR (Fig. 5.15I, J). To test whether the relationship between membrane polarisation and PPR was similar for conditions in which DATs are active, or inhibited, and along the same continuum, I performed a simple linear regression. For spike height, the slopes were not significantly different (Fig. 5.15I, $F_{(1,52)} = 0.14$, $p = 0.7078$, n = 28; simple linear regression and slope significantly non-zero, no cocaine $R^2 = 0.18$, $p = 0.0265$, cocaine $R^2 = 0.04$, $p = 0.3402$). For spike AUC, the slopes were also not significantly different (Fig. 5.15J, $F_{(1,52)} = 0.74$, $p = 0.3946$, n = 28; simple linear regression and slope significantly non-zero, no cocaine $R^2 = 0.52$, $p < 0.0001$, cocaine $R^2 = 0.37$, $p = 0.0006$).

These data indicate that the relationship between membrane polarisation and spike size are similar in the absence and presence of cocaine, and that they are along the same continuum. DATs generate depolarising currents and promote membrane repolarisation following hyperpolarisation. On the other hand, DAT inhibition with cocaine causes the membrane to be more hyperpolarised following the initial spike (due to lack of DAT-mediated currents), and promotes a larger second spike.

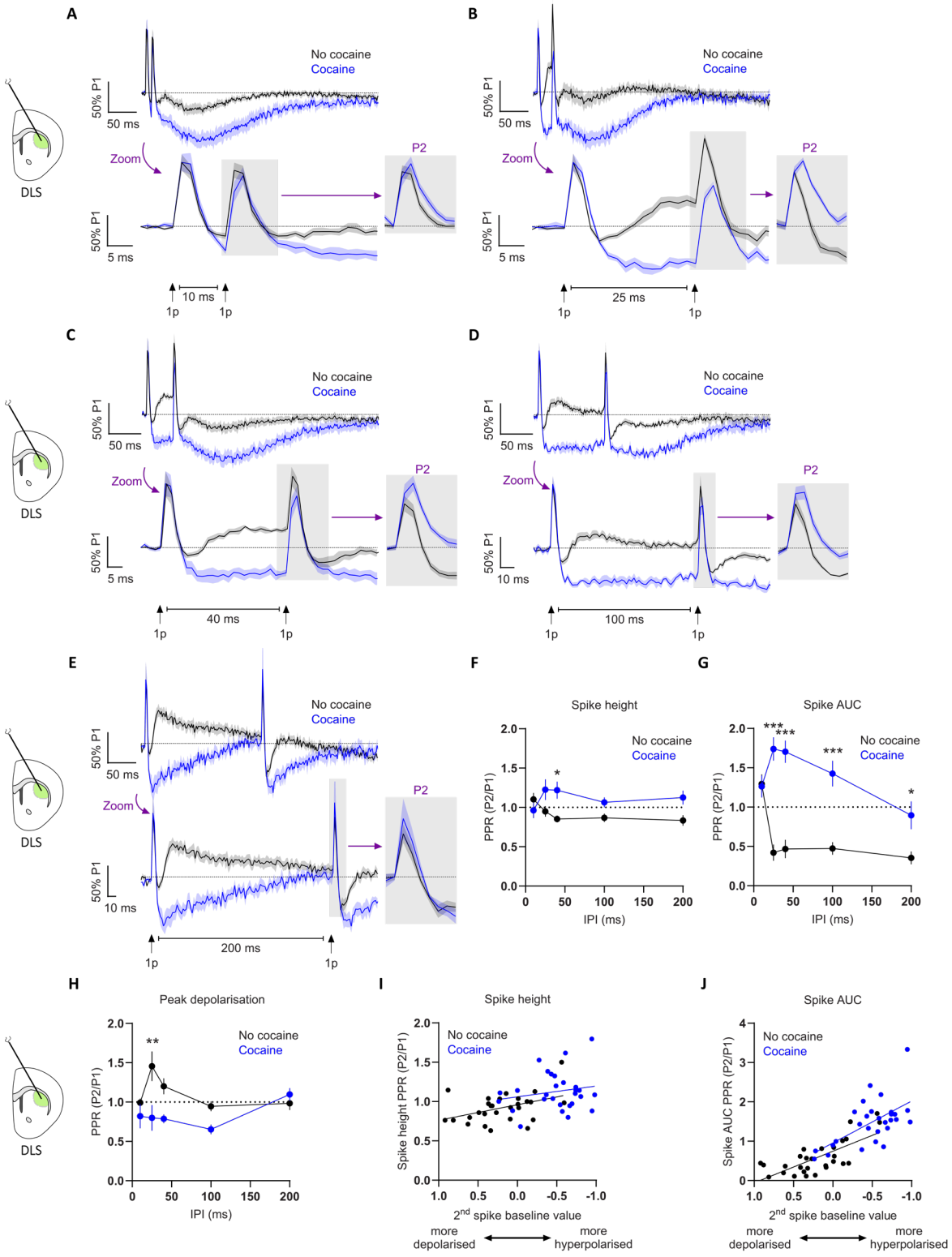

Figure 5.15. DAT inhibition with cocaine relieves short-term depression in spike height and AUC in DLS

*(A-E) Changes in membrane potential over time in DLS before or during cocaine. n = 6. (F) PPR of spike height in DLS. n = 6. (G) PPR of spike AUC in DLS. n = 6. (H) PPR of peak depolarisation in DLS. n = 6. (I) Relationship between PPR of spike height and 2nd spike baseline in DLS. n = 6. (J) Relationship between PPR of spike AUC and 2nd spike baseline in DLS. n = 6. Data are mean ±SEM. 'No cocaine' is DHβE (1 μM), 'Cocaine' is DHβE (1 μM) and cocaine (5 μM). Traces are normalised to pre-drug for visualisation (A, B, C, D, E). *p ≤ .05, **p ≤ .01, ***p ≤ .001, ns = non-significant.*

In NAcC, for IPIs of 10-200 ms, application of cocaine caused membrane potential to be hyperpolarised following the initial spike (Fig. 5.16A, B, C, D, E). Paired-pulse traces are normalised for visualisation, so that the first spike (P1) is the same height in both conditions. Insets showing a comparison of P2 for each IPI shows that P2 appears slightly larger in the presence of cocaine, at IPIs of 40 ms and 100 ms. Like in DLS, in the absence of cocaine, PPR (P2/P1) of spike height (Fig. 5.16F), and spike AUC (Fig. 5.16G), revealed a similar relationship between PPR and IPI to that observed for DA release (Condon et al., 2019; Fig. 5.8 & 5.9) with STF (PPR > 1) at IPIs of 10-40 ms, and STD at IPIs of 100-200 ms.

DAT inhibition with cocaine did not modify PPR of spike height (Fig. 5.16F, two-way RM ANOVA, IPI x drug interaction, $F_{(4,20)} = 2.10$, $p = 0.1193$, n = 6 for each IPI). However, PPR of spike AUC did differ between conditions at IPIs of 100 ms (Fig. 5.16G, two-way RM ANOVA, IPI x drug interaction, $F_{(3,13)} = 6.29$, $p = 0.0095$, n = 6 for each IPI). PPR of peak depolarisation did not significantly differ between conditions (Fig. 5.16H, two-way RM ANOVA, IPI x drug interaction, $F_{(4,20)} = 1.79$, $p = 0.1707$, n = 6 for each IPI).

To test whether the relationship between membrane polarisation and PPR was similar for conditions in which DATs are active, or inhibited, and along the same continuum, I performed a simple linear regression. For spike height, the slopes were not significantly different (Fig. 5.16I, $F_{(1,32)} = 3.21$, $p = 0.0828$, n = 18; simple linear regression and slope significantly non-zero, no cocaine $R^2 = 0.12$, $p = 0.1546$, cocaine $R^2 = 0.39$, $p = 0.0055$). For spike AUC, the slopes were also not significantly different (Fig. 5.16J, $F_{(1,32)} = 0.96$, $p = 0.7593$, n = 18; simple linear regression and slope significantly non-zero, no cocaine $R^2 = 0.43$, $p = 0.0034$, cocaine $R^2 = 0.19$, $p = 0.0704$). These data indicate that the relationship between membrane polarisation and spike size are similar in the absence and presence of cocaine.

Together, these results indicate that in both DLS and NAcC, when DATs are active, DATs promote repolarisation of the axonal membrane, which in turn leads to a smaller P2,

consistent with STD. A lower PPR, and therefore STD, is associated with a more depolarised axonal membrane potential, consistent with the ability of DATs to carry depolarising currents (e.g. Sonders et al., 1997; Carvelli et al., 2004). On the contrary, when DATs are inhibited, these depolarising currents are prevented, leading to a more hyperpolarised membrane and larger P2, and thus relief of STD. As expected, DAT-mediated changes to axonal excitability did not impact PPR at the shortest IPIs, consistent with STF in striatal DA release being downstream of axonal activation.

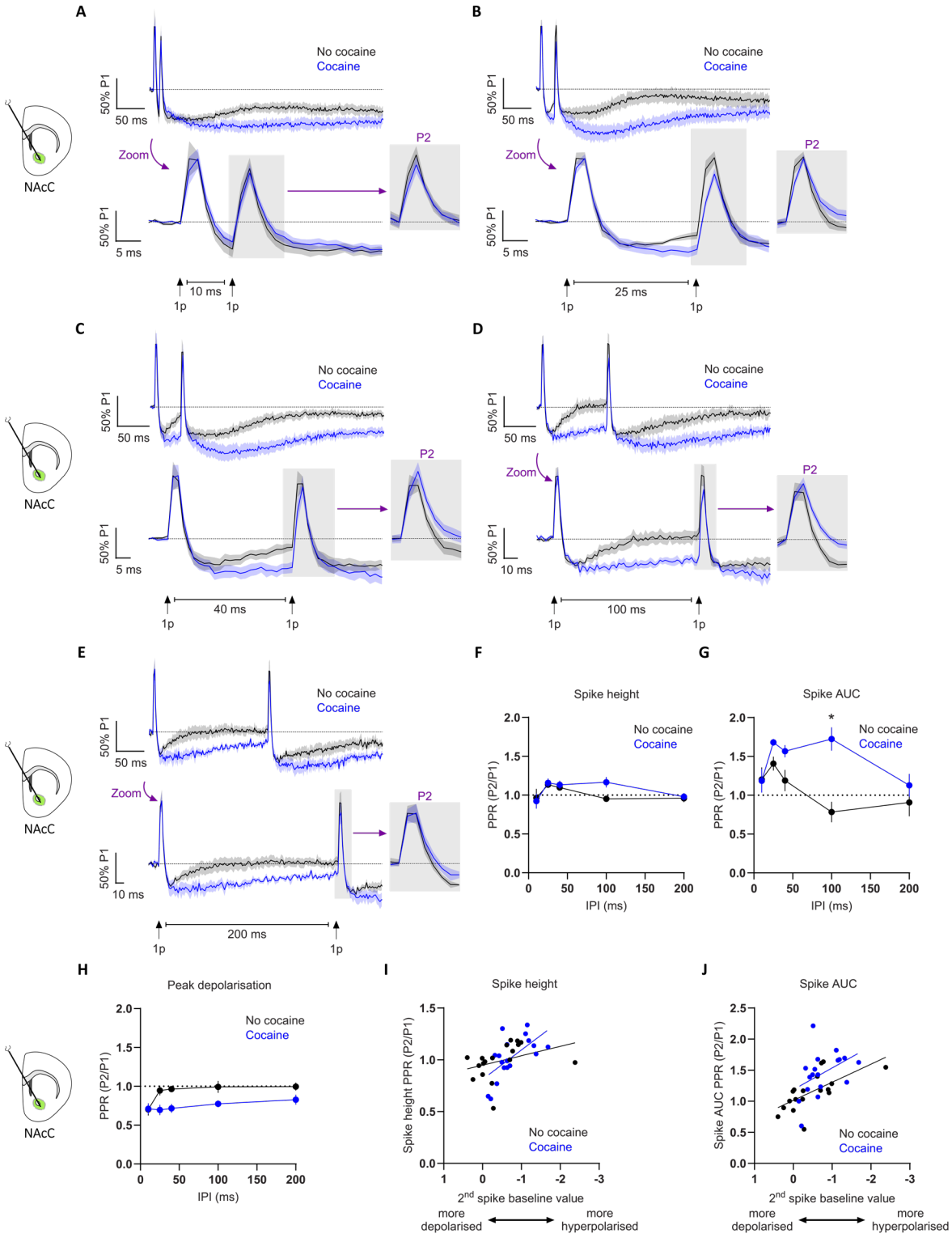

Figure 5.16. DAT inhibition with cocaine relieves short-term depression in spike height and AUC in NAcC

*(A-E) Changes in membrane potential over time in NAcC before or during cocaine. n = 6. (F) PPR of spike height in NAcC. n = 6. (G) PPR of spike AUC in NAcC. n = 6. (H) PPR of peak depolarisation in NAcC. n = 6. (I) Relationship between PPR of spike height and 2nd spike baseline in NAcC. n = 6. (J) Relationship between PPR of spike AUC and 2nd spike baseline in NAcC. n = 6. Data are mean ±SEM. 'No cocaine' is DHβE (1 μM), 'Cocaine' is DHβE (1 μM) and cocaine (5 μM). Traces are normalised to pre-drug for visualisation (A, B, C, D, E). *p ≤ .05, **p ≤ .01, ***p ≤ .001, ns = non-significant.*

5.3.8. Alternate DAT inhibitor, nomifensine, mirrors effects of cocaine by relieving STD in membrane potential

We assessed whether the alternative DAT inhibitor, nomifensine, mirrored the effects of cocaine on membrane repolarisation and subsequent spike size, in paired-pulse experiments. We have described a preliminary observation in which nomifensine replicates the effects of cocaine in increasing AHP amplitude and time to membrane repolarisation after hyperpolarisation (Fig. 5.14). In light of these data, and the observation that nomifensine replicates the effects of cocaine on short-term plasticity in DA release (Condon et al., 2019), we hypothesised that nomifensine, like cocaine, would cause axonal membranes to be hyperpolarised following the initial spike, and increase subsequent spike size.

In DLS, preliminary experiments in nomifensine revealed a similar trend to that with cocaine (Fig. 5.17A, B). Paired-pulse traces are normalised for visualisation, so that the initial spike (P1) is the same height in both conditions. Nomifensine prolongs time to repolarisation following hyperpolarisation, and at IPIs of 40 ms, there is a trend towards an increased spike AUC PPR (Fig. 5.17E, F). These pilot data indicate that nomifensine, like cocaine, relieves a limitation on subsequent spike size. Statistical comparisons were not performed due to low sample size (n = 2).

In NAcC, preliminary experiments in nomifensine also revealed a similar trend to that observed previously with cocaine (Fig. 5.17C, D). Nomifensine prolongs time to repolarisation following hyperpolarisation, and at IPIs of 40 ms, there is a trend towards an increased spike AUC PPR (Fig. 5.17G, H). Statistical comparisons were not performed due to low sample size (n = 2).

As hypothesised, these data indicate that nomifensine mirrors the effects of cocaine on membrane potential, thus the ability to promote membrane repolarisation and limit subsequent spike size is likely a feature generalisable to DATs, and not specific to cocaine.

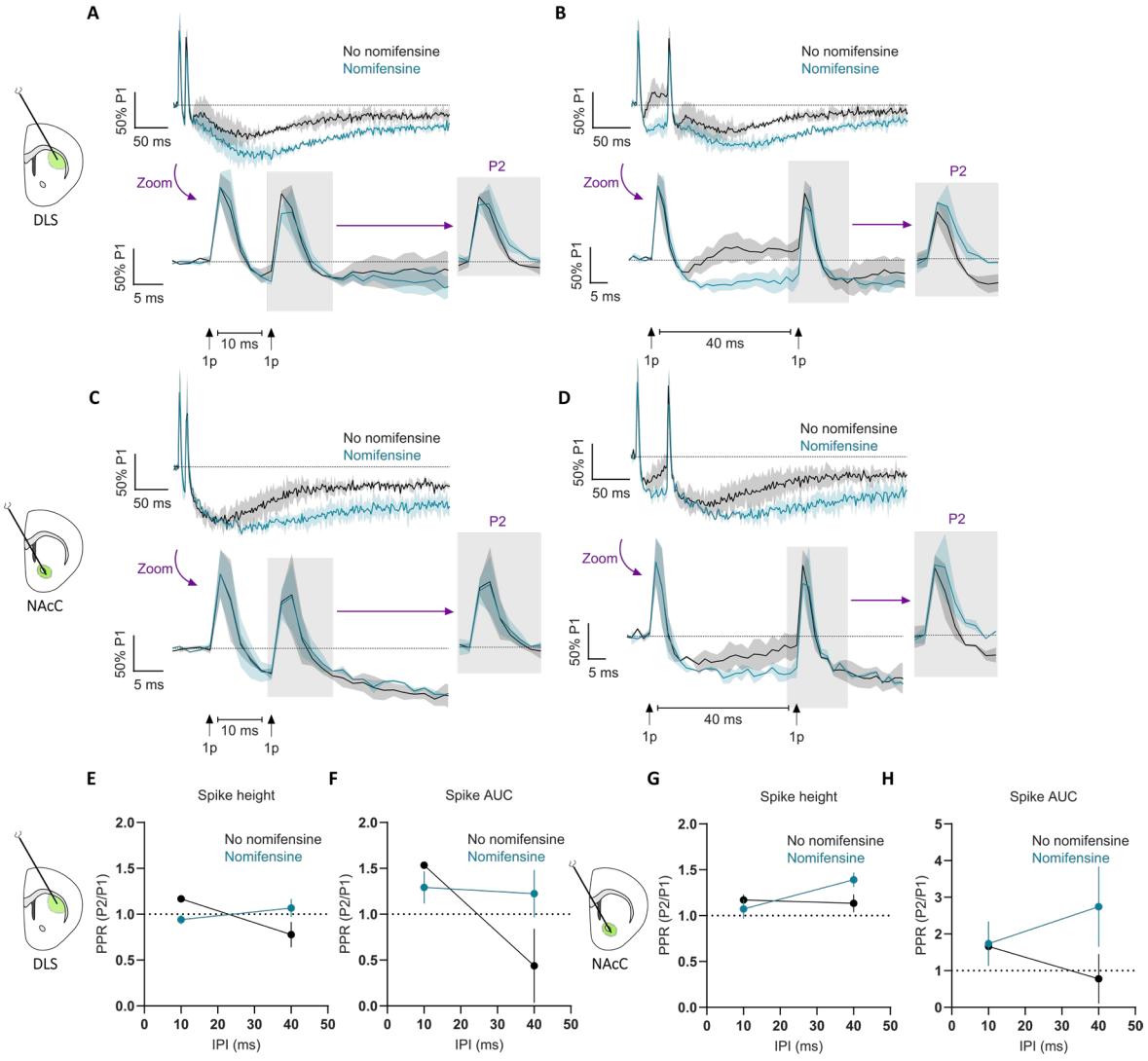

Figure 5.17. Preliminary: DAT inhibition with nomifensine relieves short-term depression in spike AUC

*(A, B) Changes in membrane potential over time in DLS before or during nomifensine. n = 2. (C, D) Changes in membrane potential over time in NAcC before or during nomifensine. n = 2. (E) PPR of spike height in DLS. n = 2. (F) PPR of spike AUC in DLS. n = 2. (G) PPR of spike height in NAcC. n = 2. (H) PPR of spike AUC in NAcC. n = 2. Data are mean ±SEM. 'No nomifensine' is DHβE (1 μM), 'Nomifensine' is DHβE (1 μM) and nomifensine (10 μM). Traces are normalised to pre-drug for visualisation (A, B, C, D). *p ≤ .05, **p ≤ .01, ***p ≤ .001, ns = non-significant.*

5.3.9. DATs do not require D_2-R activation to promote membrane repolarisation to resting potential

DAT inhibition induces an inhibitory, hyperpolarising current following electrical stimulation, and large amounts of DA are released under DAT inhibition. We therefore explored whether there was any involvement of DA D_2-like-Rs in the results observed with cocaine. D_2-like-Rs mediate a slow inhibitory influence on DA neurons, operating on a timescale of hundreds of milliseconds, to several seconds (Benoit-Marand et al., 2001; Phillips et al., 2002; Schmitz et al., 2002b; Patel et al., 2024). D_2-like-Rs do not contribute to DAT-mediated changes to short-term plasticity in striatal DA release, as short-term plasticity is unaffected by antagonism of D_2-Rs up to intervals of 200 ms (Cragg, 2003; Condon et al., 2019). Rather, D_2-like-Rs promote STD at intervals of 1-2 s (Condon et al., 2019). Nevertheless, due to the large amounts of extracellular DA in the presence of DAT inhibitors, we tested whether D_2-like-Rs could be contributing to our data obtained in the presence of cocaine. We hypothesised that the presence of a D_2-like-R antagonist would not modify the impact of cocaine on membrane polarisation. Specifically, we hypothesised that DAT inhibition with cocaine would prolong time to membrane repolarisation after hyperpolarisation, even in the presence of a D_2-like-R antagonist.

In DLS, application of cocaine (5 µM), in the presence of a D_2-like-R antagonist (L-741,626, 1 µM) caused the axonal membrane to be hyperpolarised following single pulse stimulation, compared to the no cocaine condition (Fig. 5.18A). Traces are corrected for the slight signal decay over time in DLS, as outlined in Section 5.2.7. No statistically significant changes were observed to spike height (Fig. 5.18B, unpaired t-test, $t_{(8)} = 1.71$, $p = 0.1265$), spike AUC (Fig. 5.18C, unpaired t-test, $t_{(8)} = 2.10$, $p = 0.0694$), or F_0 (Fig. 5.18D, unpaired t-test, $t_{(8)} = 0.07$, $p = 0.9456$). Following the spike, membrane potential was significantly hyperpolarised in the presence of cocaine (Fig. 5.18E, two-way RM ANOVA, time x drug interaction, $F_{(5,20)} = 5.31$, $p =$

0.0029, n = 5). Surprisingly, in contrast with data obtained in the absence of a D_2-like-R antagonist, the peak AHP amplitude occurred at a similar time in both conditions (Fig. 5.18F). In agreement with data obtained in the absence of a D_2-like-R antagonist, the AHP amplitude was deeper following application of cocaine (Fig. 5.18G, paired t-test, $t_{(4)} = 4.99$, $p = 0.0075$).

In NAcC, application of cocaine, in the presence of a D_2-like-R antagonist caused the membrane to be hyperpolarised following single pulse stimulation (Fig. 5.18H). Traces are corrected for the slight signal decay over time in DLS, as outlined in Section 5.2.7. No statistically significant changes were observed to spike height (Fig. 5.18I, unpaired t-test, $t_{(9)} = 0.38$, $p = 0.7130$), spike AUC (Fig. 5.18J, unpaired t-test, $t_{(9)} = 1.29$, $p = 0.2282$), or F_0 (Fig. 5.18K, unpaired t-test, $t_{(9)} = 1.38$, $p = 0.1996$). Post-spike membrane potential was significantly hyperpolarised in the presence of cocaine (Fig. 5.18L, two-way RM ANOVA, time x drug interaction, $F_{(5,15)} = 5.46$, $p = 0.0046$, n = 4). Peak AHP amplitude appeared to occur at a similar time in both conditions, though the cocaine condition was more scattered, and this comparison is likely underpowered (Fig. 5.18M). In agreement with data obtained in the absence of a D_2-like-R antagonist in NAcC, the AHP amplitude unchanged following application of cocaine (Fig. 5.18N, paired t-test, $t_{(3)} = 1.44$, $p = 0.2451$).

Taken together, these results indicate that cocaine-mediated changes to axonal activation do not require activation of D_2-like-Rs, because even in the presence of a D_2-R antagonist, DAT inhibition with cocaine prolongs time to membrane repolarisation following hyperpolarisation.

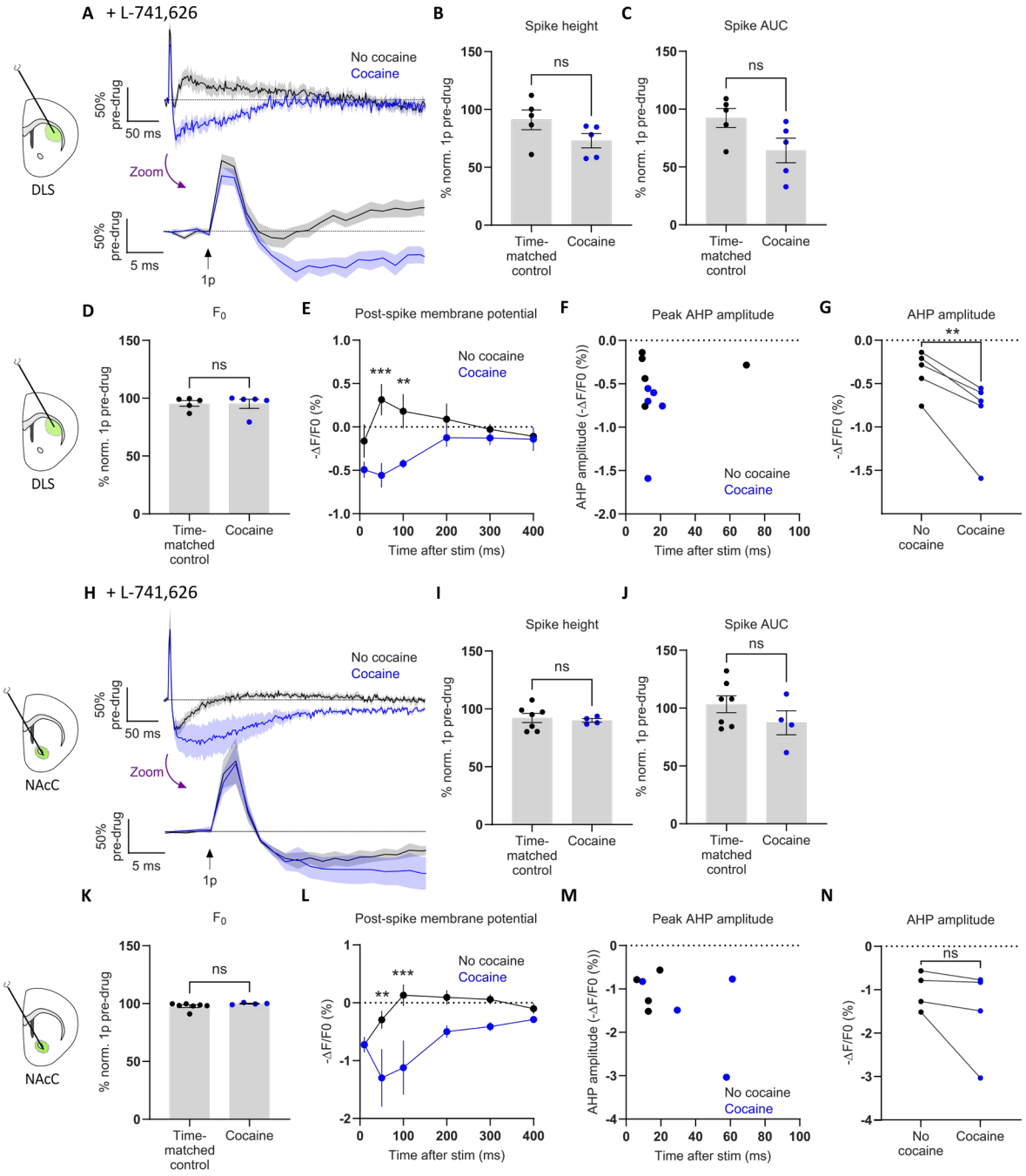

Figure 5.18. DAT-mediated regulation of membrane potential does not require activity at D_2-like-Rs

*(A) Changes in membrane potential over time in DLS before or during cocaine. n = 5. (B) Spike height (%) in DLS. n = 5. (C) Spike AUC (%) in DLS. n = 5. (D) F_0 (%) in DLS. n = 5. (E) Membrane potential following initial spike in DLS. n = 5. (F) Peak AHP amplitude in DLS. n = 5. (G) Change in AHP amplitude in DLS. n = 5. (H) Changes in membrane potential over time in NAcC before or during cocaine. n = 4. (I) Spike height (%) in NAcC. n = 7/4. (J) Spike AUC (%) in NAcC. n = 7/4. (K) F_0 (%) in NAcC. n = 7/4. (L) Membrane potential following initial spike in NAcC. n = 4. (M) Peak AHP amplitude in NAcC. n = 4. (N) Change in AHP amplitude in NAcC. n = 4. Data are mean ±SEM. 'No cocaine' is DHβE (1 μM), 'Cocaine' is DHβE (1 μM) and cocaine (5 μM). Traces are corrected for signal decay over time using a time-matched control (A, H). Data are normalised to pre-drug for cocaine, and equivalent recordings for time-matched control (B, C, D, I, J, K). *p ≤ .05, **p ≤ .01, ***p ≤ .001, ns = non-significant.*

5.3.10. DATs do not require D_2-R activation to limit subsequent spike size

Cocaine-mediated changes to repolarisation following single-pulse stimulation do not involve activation of D_2-like-Rs (Fig. 5.18). We subsequently assessed whether the impact of cocaine on subsequent spike size was also independent of D_2-like-Rs. D_2-like-Rs are implicated in STD only at intervals >1 s (Condon et al., 2019), therefore we hypothesised that the presence of a D_2-like-R antagonist would not affect DAT-mediated changes to axonal activation.

In DLS, preliminary experiments indicate that the presence of a D_2-like-R antagonist does not affect membrane potential dynamics, either in the absence or presence of cocaine (Fig. 5.19A, B). Paired-pulse traces are normalised for visualisation, so that the initial spike (P1) is the same height in both conditions. Cocaine prolongs time to repolarisation following hyperpolarisation, and at IPIs of 40 ms, there is a trend towards an increased spike height PPR and spike AUC PPR (Fig. 5.19E, F). Statistical comparisons were not performed due to low sample size (n = 3).

In NAcC, large variation in signals make data difficult to interpret as of yet. Preliminary observations indicate that the presence of a D_2-like-R antagonist does not affect membrane potential dynamics, either in the absence or presence of cocaine (Fig. 5.19C, D), but the sample size needs to be increased. Cocaine does not appear to modify spike height PPR or spike AUC at IPIs of 10 or 40 ms, consistent with the observation that NAcC DA release exhibits release-dependent STF at these timescales (Condon et al., 2019), and that cocaine only modifies spike height or AUC at longer IPIs (Fig. 5.16). Statistical comparisons were not performed due to low sample size (n = 2).

These pilot datasets indicate that regulation of axonal membrane potential does not require activity at D_2-like-Rs, at least in DLS.

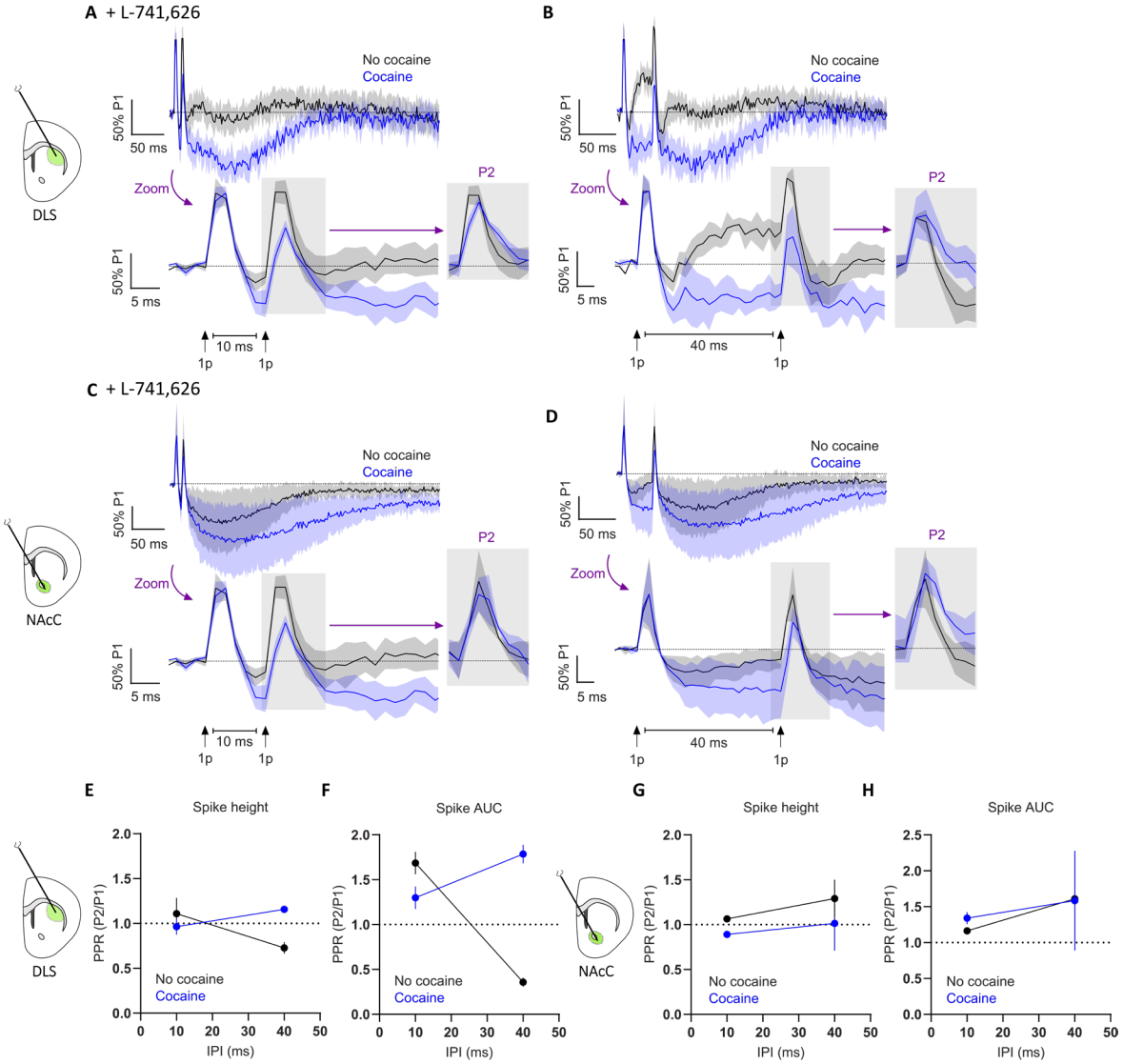

Figure 5.19. Preliminary: DAT-mediated regulation of membrane potential does not require activity at D_2-like-Rs

*(A, B) Changes in membrane potential over time in DLS before or during cocaine. n = 3. (C, D) Changes in membrane potential over time in NAcC before or during cocaine. n = 2. (E) PPR of spike height in DLS. n = 3. (F) PPR of spike AUC in DLS. n = 3. (G) PPR of spike height in NAcC. n = 2. (H) PPR of spike AUC in NAcC. n = 2. Data are mean ±SEM. 'No cocaine' is DHβE (1 μM), 'Cocaine' is DHβE (1 μM) and cocaine (5 μM). Traces are normalised to pre-drug for visualisation (A, B, C, D). *p ≤ .05, **p ≤ .01, ***p ≤ .001, ns = non-significant.*

5.3.11. Zero $[Ca^{2+}]_o$ aCSF prevents DAT-mediated changes to membrane potential

DATs exhibit transport-coupled and transport-uncoupled currents (e.g. Sonders et al., 1997). We observed robust changes to axonal membrane potential when DATs are inhibited, indicating that when DATs are active, they contribute to axonal excitability. Our observations of DAT-mediated changes to axonal membrane potential are the most prominent shortly following the spike, when DA would be released, indicating that these might be transport-associated currents. To assess whether these currents are transport-coupled or -uncoupled, we used recording solutions lacking $[Ca^{2+}]_o$. $[Ca^{2+}]_o$ is required for striatal DA release (Brimblecombe et al., 2015), therefore, in aCSF with 0 mM $[Ca^{2+}]_o$, DA release should be prevented, and DATs prevented from translocating DA. We hypothesised that in the absence of $[Ca^{2+}]_o$, the repolarisation following hyperpolarisation would be prolonged, like data obtained in the presence of DAT inhibitors. Further, we hypothesised that in the absence of $[Ca^{2+}]_o$, application of cocaine would not affect axonal activation.

Strikingly, the ASAP5 signal obtained in 0 mM $[Ca^{2+}]_o$ did not exhibit rebound depolarisation in DLS, or the deep AHP in NAcC (Fig. 5.20A, F). Traces are corrected for the slight signal decay over time, as outlined in Section 5.2.7. In DLS, following the spike, membrane polarisation only differed between no cocaine and cocaine immediately (10ms) following the stimulation (Fig. 5.20B, two-way RM ANOVA, time x drug interaction, $F_{(5,20)} = 3.62$, $p = 0.0170$, n = 5). This contrasts with the finding that, in 2.5 mM $[Ca^{2+}]_o$, membrane polarisation significantly differed between conditions 50-100 ms following the stimulation (Fig. 5.12E). In contrast to previous findings in 2.5 mM $[Ca^{2+}]_o$, the AHP was shallower following application of cocaine (Fig. 5.20C, paired t-test, $t_{(4)} = 3.68$, $p = 0.0212$, n = 5).

A comparison of the post-spike membrane potential between $[Ca^{2+}]_o$ concentrations did not reveal any significant differences between in the absence of cocaine (Fig 5.20D, mixed

effects model, time x drug interaction, $F_{(5,15)} = 1.87$, $p = 0.1597$, n = 10 in 2.5 mM $[Ca^{2+}]_o$, n = 5 in 0 mM $[Ca^{2+}]_o$). However, in the presence of cocaine, membrane polarisation differed at 10-100 ms between $[Ca^{2+}]_o$ concentrations (Fig 5.20E, mixed effects model, time x drug interaction, $F_{(5,15)} = 8.15$, $p = 0.0007$, n = 10 in 2.5 mM $[Ca^{2+}]_o$, n = 5 in 0 mM $[Ca^{2+}]_o$). Time-matched controls were not performed in the absence of $[Ca^{2+}]_o$, therefore we did not make comparisons for F_0, maximum absolute depolarisation, spike height, or spike AUC.

In NAcC, following the spike, membrane potential did not appear to differ between conditions (Fig. 5.20G). This contrasts with the finding that, in 2.5 mM $[Ca^{2+}]_o$, membrane potential significantly differed between no cocaine and cocaine 50-400 ms following the stimulation (Fig. 5.12L). AHP amplitude did not appear to be changed following application of cocaine (Fig. 5.20H), though without a larger sample size, a conclusion cannot be drawn. Statistical comparisons were not performed due to low sample size (n = 3). Time-matched controls were not performed in the absence of $[Ca^{2+}]_o$, therefore we did not make comparisons for F_0, maximum absolute depolarisation, spike height, or spike AUC.

Contrary to our initial hypothesis, the absence of $[Ca^{2+}]_o$ did not reflect data obtained in the presence of a DAT inhibitor, and prolong a hyperpolarised state following the spike. Rather, the absence of $[Ca^{2+}]_o$ prevented rebound depolarisation in DLS and a deep AHP in NAcC. Surprisingly, the absence of $[Ca^{2+}]_o$ also prevented cocaine-mediated changes to membrane potential. The absence of cocaine-mediated changes in 0 mM $[Ca^{2+}]_o$ indicate that the activity state of DATs does not impact on membrane potential. Whilst non-straightforward to interpret, these data do not exclude the possibility that DAT-inhibitor-mediated changes to membrane repolarisation are via transport-coupled DAT currents. Interpretations and future directions will be discussed later in this chapter, and in Chapter 6.

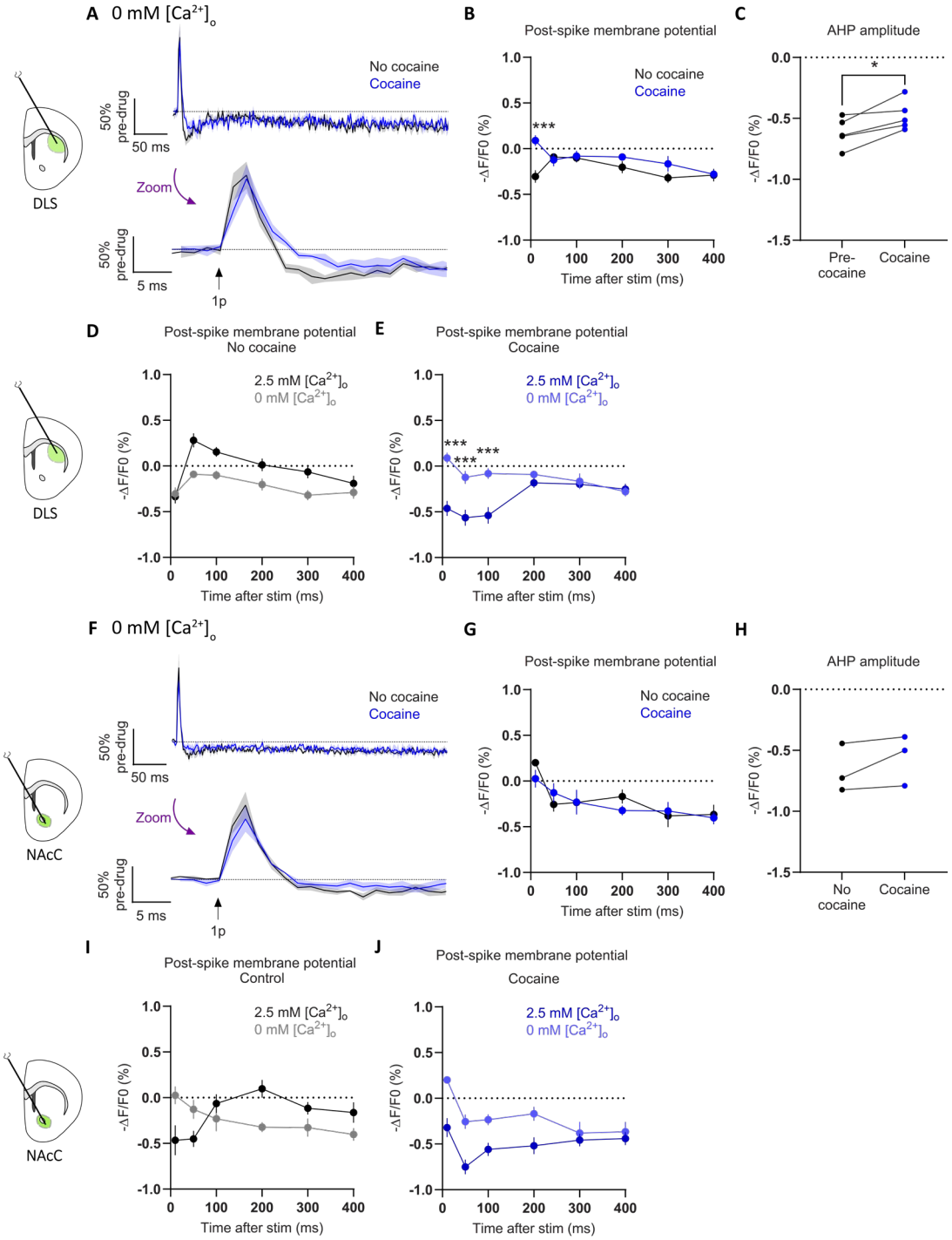

Figure 5.20. DAT inhibition does not modify axonal membrane potential in 0 mM $[Ca^{2+}]_o$ aCSF
*(A) Changes in membrane potential over time in DLS before or during cocaine. n = 5. (B) Membrane potential following initial spike in DLS. n = 5. (C) Peak AHP amplitude in DLS. n = 5. (D) Membrane potential following initial spike in DLS in no cocaine. n = 5. (E) Membrane potential following initial spike in DLS in cocaine. n = 5. (F) Changes in membrane potential over time in NAcC before or during cocaine. n = 3. (G) Membrane potential following initial spike in NAcC. n = 3. (H) Peak AHP amplitude in NAcC. n = 3. (I) Membrane potential following initial spike in NAcC in no cocaine. n = 3. (J) Membrane potential following initial spike in NAcC in cocaine. n = 3. Data are mean ±SEM. 'No cocaine' is DHβE (1 μM), 'Cocaine' is DHβE (1 μM) and cocaine (5 μM). Traces are corrected for signal decay over time using a time-matched control (A, F). *p ≤ .05, **p ≤ .01, ***p ≤ .001, ns = non-significant.*

5.3.12. Zero $[Ca^{2+}]_o$ aCSF prevents DAT-mediated changes to subsequent spike size

We have shown that DAT-mediated changes to membrane repolarisation after hyperpolarisation is prevented in recording solutions lacking $[Ca^{2+}]_o$ (Fig. 5.20). We assessed whether DAT-mediated changes to subsequent spike size are also prevented in the absence of $[Ca^{2+}]_o$. We hypothesised that the application of cocaine would not modify subsequent spike size.

In DLS, membrane potential dynamics were altered in the absence of $[Ca^{2+}]_o$, compared to the presence of 2.5 mM $[Ca^{2+}]_o$. ASAP5 traces did not appear drastically different to those obtained in 2.5 mM $[Ca^{2+}]_o$ at IPIs of 10 ms in the absence of cocaine (Fig 5.21A). However, at 40 ms, as in Fig. 5.20, there was a noticeable lack of rebound depolarisation following the initial spike, meaning that the subsequent spike did not occur on top of the rebound depolarisation (Fig. 5.21B). In 2.5 mM $[Ca^{2+}]_o$, the second spike at IPIs of 40 ms typically occurs on top of the rebound depolarisation (Fig. 5.15B). The relationship between PPR and IPI was altered in 0 mM $[Ca^{2+}]_o$, because at IPIs of both 10 ms and 40 ms, in the absence of cocaine, spike height and spike AUC PPR was ≥1. In 2.5 mM $[Ca^{2+}]_o$, spike height and AUC PPR is >1 at 10ms, and <1 at 40 ms (Fig. 5.15F, G). In 0 mM $[Ca^{2+}]_o$, cocaine did not significantly alter spike height PPR (Fig. 5.21E, two-way RM ANOVA, IPI x drug interaction, $F_{(1,4)} = 0.36$, $p = 0.5830$, n = 5 for each IPI), or spike AUC PPR (Fig. 5.21F, two-way RM ANOVA, IPI x drug interaction, $F_{(1,4)} = 2.07$, $p = 0.2232$, n = 5 for each IPI).

In NAcC, membrane potential dynamics were also altered in the absence of $[Ca^{2+}]_o$, compared to the presence of 2.5 mM $[Ca^{2+}]_o$ (Fig. 5.21C, D). Notably, there was a distinct lack of the deep AHP that is typically observed in NAcC at 2.5 mM $[Ca^{2+}]_o$ (e.g. Fig. 5.16). In 0 mM $[Ca^{2+}]_o$, cocaine did not significantly alter spike height PPR or spike AUC PPR. Statistical comparisons were not performed due to low sample size (n = 3).

These data indicate that DAT-mediated changes to membrane potential observed in this thesis require $[Ca^{2+}]_o$, possibly because the DAT-mediated changes are transport-coupled currents. Data obtained in the absence of $[Ca^{2+}]_o$ is difficult to interpret, however, and is likely confounded. Possibilities for future investigations into the nature of DAT-mediated currents are discussed later.

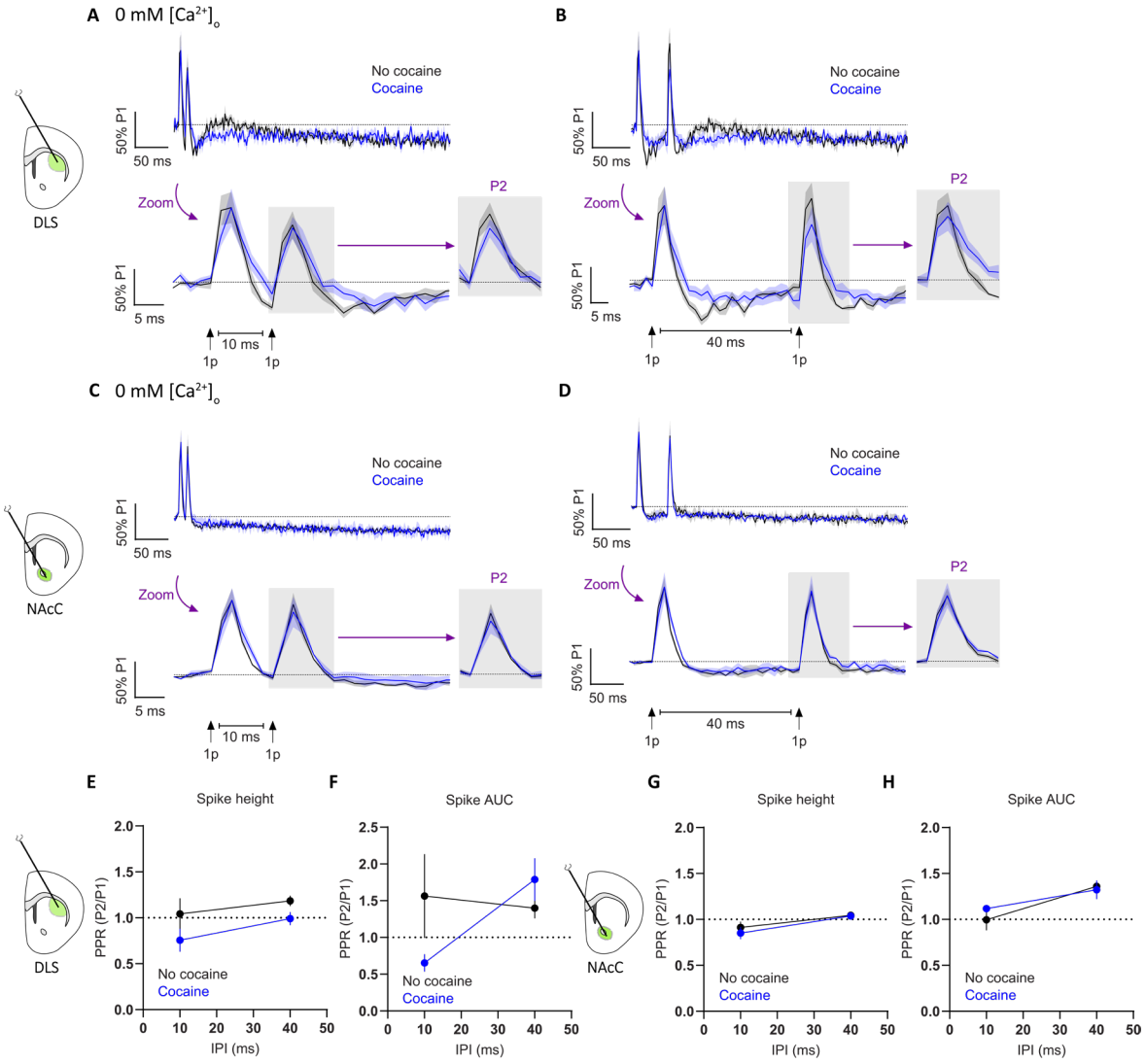

Figure 5.21. DAT inhibition does not modify axonal membrane potential in 0 $[Ca^{2+}]_o$ aCSF
*(A, B) Changes in membrane potential over time in DLS before or during cocaine. n = 5. (C, D) Changes in membrane potential over time in NAcC before or during cocaine. n = 3. (E) PPR of spike height in DLS. n = 5. (F) PPR of spike AUC in DLS. n = 5. (G) PPR of spike height in NAcC. n = 3. (H) PPR of spike AUC in NAcC. n = 3. Data are mean ±SEM. 'No cocaine' is DHβE (1 μM), 'Cocaine' is DHβE (1 μM) and cocaine (5 μM). Traces are normalised to pre-drug for visualisation (A, B, C, D). *p ≤ .05, **p ≤ .01, ***p ≤ .001, ns = non-significant.*

5.3.13. GABA-Rs modify axonal membrane potential following single pulse stimulation

The strong impact of DATs on axonal membrane potential led us to consider which other mechanisms locally on striatal DA axons contribute to axonal activation, and whether we could observe these using the genetically-encoded fluorescent voltage indicator, ASAP5 (Hao et al., 2024). $GABA_A$-Rs on DA axons are paradoxically depolarising, operating via shunting inhibition and VGSC inactivation to limit DA release (Kramer et al., 2020). Striatal DA axons are under tonic inhibition by GABA acting at $GABA_A$- and $GABA_B$-Rs (Lopes et al., 2019). To assess the contribution of GABA-Rs to DA axon membrane potential, we tested the impact of pharmacologically inhibiting these receptors. Activity at $GABA_A$-Rs limits action potential amplitude when measured by whole-cell patch-clamp electrophysiology (Kramer et al., 2020). We therefore hypothesised that GABA-R antagonists would relieve a small limitation on spike size. Though $GABA_A$-R activation on DA axons mediates a depolarising current (Kramer et al., 2020), we did not expect to see acute hyperpolarisation upon $GABA_A$-R antagonism, due to the use of bath application of drugs, rather than local pressure ejection. $GABA_B$-Rs on DA axons are also tonically active (Lopes et al., 2019), therefore, we hypothesised that $GABA_B$-R antagonism would cause a subtle change in membrane potential following the spike. Specifically, we hypothesised that the repolarisation following hyperpolarisation would be augmented in the presence of a $GABA_B$-R antagonist. Together, we expected that co-application of $GABA_A$-R and $GABA_B$-R antagonists would result in larger spike size, and a more depolarised membrane potential during rebound depolarisation and return to resting membrane potential.

In DLS, co-application of $GABA_A$-R and $GABA_B$-R antagonists (bicuculline, 10 µM & CGP 55845 4 µM) appeared to phase-shift the rebound depolarisation following single pulse stimulation and the initial spike (Fig. 5.22A). Traces are corrected for the slight signal decay

over time in DLS, as outlined in Section 5.2.7. Compared to a time-matched control dataset (Fig. 5.6), spike height was unchanged in the presence of GABA-R antagonists, (Fig 5.22B, unpaired t-test, $t_{(11)} = 0.25$, $p = 0.8105$, n = 5 time-matched control, 8 GABA-R antagonists), as was spike AUC (Fig 5.22C, unpaired t-test, $t_{(11)} = 0.87$, $p = 0.4030$, n = 5 time-matched control, 8 GABA-R antagonists). This was in contrast to our hypothesis, because we expected spike size to be larger in the presence of GABA-R antagonists. It is possible that there is a trend towards higher spike AUC in the presence of GABA-R antagonists, but large variability in this dataset makes it unclear. Application of GABA-R antagonists appeared to slightly increase the F_0 in DLS (Fig 5.22D, unpaired t-test, $t_{(11)} = 2.56$, $p = 0.0266$, n = 5 time-matched control, 8 GABA-R antagonists). Following the initial spike, no statistically significant changes to membrane potential were found (Fig. 5.22E, two-way RM ANOVA, time x drug interaction, $F_{(5,35)} = 2.05$, $p = 0.0955$, n = 8), although, surprisingly, membrane potential did appear to be shifted to a slightly more hyperpolarised state. GABA-R antagonists significantly changed the AHP amplitude, leading to a deeper AHP (Fig. 5.22F, paired t-test, $t_{(7)} = 3.55$, $p = 0.0093$, n = 8).

Next, we tested whether the effects observed to axonal membrane potential were attributed to $GABA_A$-Rs or $GABA_B$-Rs. $GABA_A$-Rs are ionotropic receptors which open to allow flow of Cl^- ions according to the electrochemical gradient (Watanabe et al., 2002). In mature striatal DA axons, $GABA_A$-Rs are depolarising and inhibit DA release by VGSC inactivation and shunting inhibition (Kramer et al., 2020). Therefore, antagonism of $GABA_A$-Rs, which are tonically active on striatal DA neurons, was expected to result in hyperpolarisation, combined with larger spike size. $GABA_B$-Rs are metabotropic receptors which typically operate on a slower timescale and inhibit neurotransmitter release by coupling to GIRK channels to promote K^+ efflux, or inhibit VGCCs (Bettler et al., 2004). Therefore, antagonism of $GABA_B$-Rs, which are tonically active on striatal DA neurons, was expected to either have no effect on such short timescales following electrical stimulation, or to result in slight depolarisation. Due to the

observation that membrane potential was hyperpolarised, rather than depolarised, in the presence of GABA-R antagonists, we anticipated that this was via $GABA_A$-Rs.

Application of the $GABA_A$-R antagonist bicuculline (10 µM) in DLS appeared to hyperpolarise axonal membrane potential ~50 ms following the spike, but large variability makes this unclear (Fig. 5.22G). Traces are corrected for the slight signal decay over time in DLS, as outlined in Section 5.2.7. In contrast to our hypothesis, compared to a time-matched control dataset (Fig. 5.6), spike height was unchanged in the presence of bicuculline, (Fig 5.22H, unpaired t-test, $t_{(7)} = 0.77$, $p = 0.4641$, n = 5 time-matched control, 4 bicuculline), as was spike AUC (Fig 5.22I, unpaired t-test, $t_{(7)} = 0.30$, $p = 0.7755$, n = 5 time-matched control, 4 bicuculline). Post-spike membrane potential did not significantly differ at any timepoint in the presence of bicuculline, compared to no bicuculline (Fig. 5.22J, two-way RM ANOVA, time x drug interaction, $F_{(5,15)} = 0.69$, $p = 0.6393$, n = 4), although this comparison is likely underpowered.

Surprisingly, application of the $GABA_B$-R antagonist CGP 55845 (4 µM) in DLS appeared to hyperpolarise axonal membrane potential immediately following the spike, with no impact later in the trace (Fig. 5.22K). Traces are corrected for the slight signal decay over time in DLS, as outlined in Section 5.2.7. Compared to a time-matched control dataset (Fig. 5.6), spike height was unchanged in the presence of CGP5 55845, (Fig 5.22L, unpaired t-test, $t_{(8)} = 0.92$, $p = 0.3865$, n = 5 time-matched control, 5 CGP 55845), as was spike AUC (Fig 5.22M, unpaired t-test, $t_{(8)} = 0.69$, $p = 0.5086$, n = 5 time-matched control, 5 CGP 55845). Post-spike membrane potential did not differ at any timepoint (Fig. 5.22N, two-way RM ANOVA, time x drug interaction, $F_{(5,20)} = 1.15$, $p = 0.3681$, n = 5).

Taken together, these data indicate that in DLS, $GABA_A$-Rs and $GABA_B$-Rs both subtly modify axonal action potential. Surprisingly, we did not find an increase in spike size upon application of GABA-R antagonists. Pilot datasets aimed at separating the contribution of

$GABA_A$-Rs and $GABA_B$-Rs appear to indicate that $GABA_B$-Rs limit AHP amplitude immediately following a spike, and $GABA_A$-Rs contribute to membrane depolarisation on a slower timecourse. Future experiments and larger datasets will assist in testing the validity of these interpretations, and test whether $GABA_A$-Rs and $GABA_B$-Rs are interdependent, rather than having separate, summative impacts on membrane excitability.

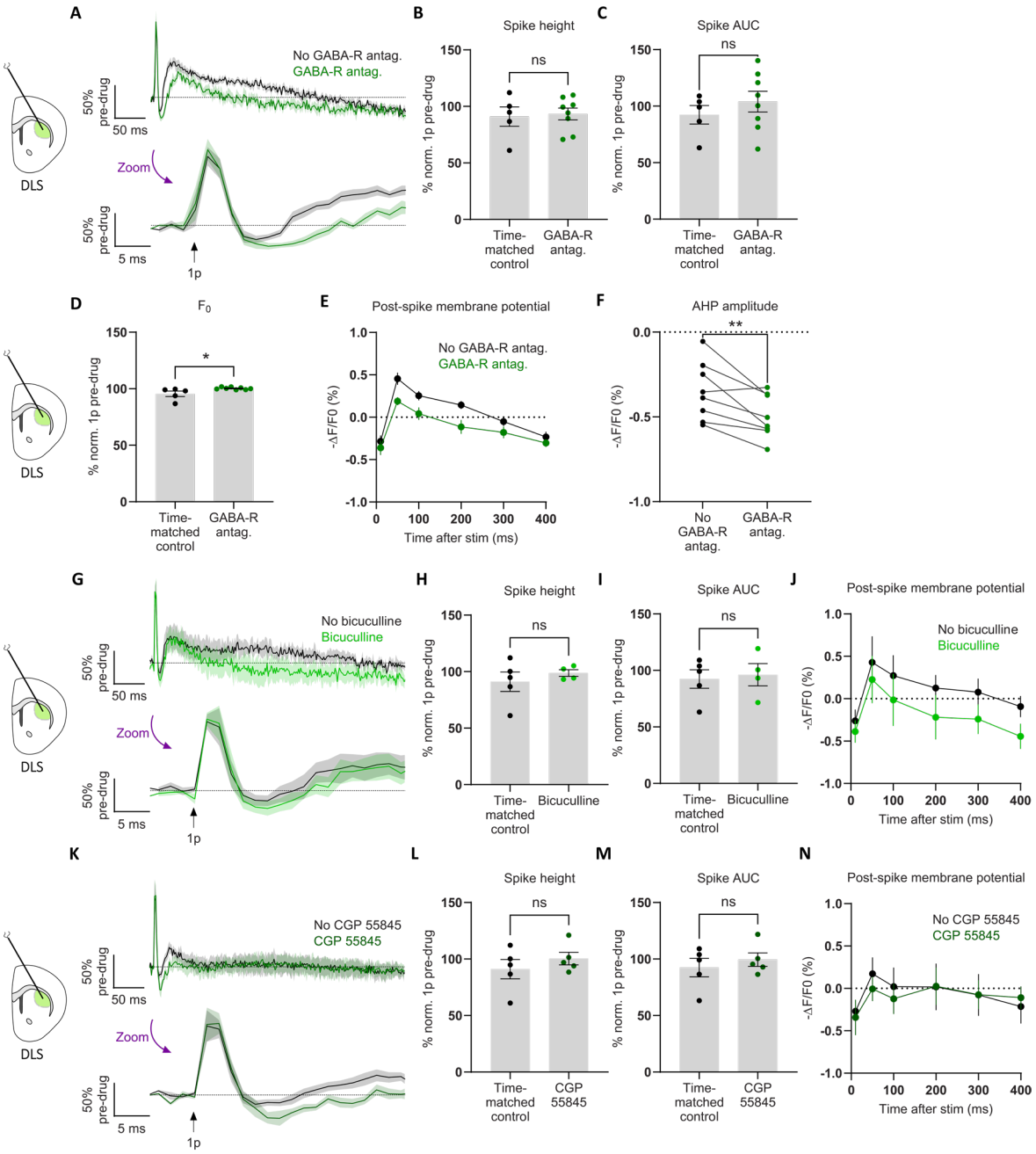

Figure 5.22. GABA-Rs modify AHP amplitude and post-spike membrane potential in DLS
*(A) Changes in membrane potential over time in DLS before or during GABA-R antagonists. n = 8. (B) Spike height (%) in DLS. n = 5/8. (C) Spike AUC (%) in DLS. n = 5/8. (D) F_0 (%) in DLS. n = 5/8. (E) Membrane potential following initial spike in DLS. n = 8. (F) Change in AHP amplitude in DLS. n = 8. (G) ASAP5 traces in DLS before or during bicuculline. n = 4. (H) Spike height (%) in DLS. n = 5/4. (I) Spike AUC (%) in DLS. n = 5/4. (J) Membrane potential following initial spike in DLS. n = 4. (K) Changes in membrane potential over time in DLS before or during CGP 55845. n = 5. (L) Spike height (%) in DLS. n = 5/5. (M) Spike AUC (%) in DLS. n = 5/5. (N) Membrane potential following initial spike in DLS. n = 5. Data are mean ±SEM. 'No GABA-R antag.' is DHβE (1 μM), 'GABA-R antag.' is DHβE (1 μM), bicuculline (10 μM) and CGP 55845 (4 μM). Traces are corrected for signal decay over time using a time-matched control (A, G, K). Data are normalised to pre-drug, and equivalent recordings for time-matched control (B, C, D, H, I, L, M). *p ≤ .05, **p ≤ .01, ***p ≤ .001, ns = non-significant.*

In NAcC, co-application of $GABA_A$-R and $GABA_B$-R antagonists appeared to prolong hyperpolarisation following the initial spike and AHP (Fig. 5.23A). Traces are corrected for the slight signal decay over time in NAcC, as outlined in Section 5.2.7. Compared to a time-matched control dataset (Fig. 5.6), spike height was unchanged in the presence of GABA-R antagonists, (Fig 5.23B, unpaired t-test, $t_{(10)} = 0.60$, $p = 0.5600$, n = 7 time-matched control, 5 GABA-R antagonists), as was spike AUC (Fig 5.23C, unpaired t-test, $t_{(10)} = 0.07$, $p = 0.9439$, n = 7 time-matched control, 5 GABA-R antagonists). As seen in DLS in Fig. 5.22, in contrast to our hypothesis, antagonism of GABA-Rs does not appear to change spike size. Application of GABA-R antagonists did not affect F_0 (Fig 5.23D, unpaired t-test, $t_{(10)} = 1.09$, $p = 0.3107$, n = 7 time-matched control, 5 GABA-R antagonists). Following the initial spike, membrane potential was significantly hyperpolarised in GABA-R antagonists (Fig. 5.23E, two-way RM ANOVA, time x drug interaction, $F_{(5,20)} = 3.40$, $p = 0.0219$, n = 5). GABA-R antagonists did not affect the AHP (Fig. 5.23F, paired t-test, $t_{(4)} = 1.65$, $p = 0.1747$, n = 5).

Next, we tested whether the effects observed to axonal membrane potential were attributed to $GABA_A$-Rs or $GABA_B$-Rs. Application of the $GABA_A$-R antagonist bicuculline in NAcC had a similar effect on membrane potential as co-application of both antagonists, leading to a slightly more hyperpolarised state following the AHP (Fig. 5.23G). Traces are corrected for the slight signal decay over time in NAcC, as outlined in Section 5.2.7. Compared to a time-matched control dataset (Fig. 5.6), spike height was unchanged in the presence of bicuculline, (Fig 5.23H, unpaired t-test, $t_{(9)} = 2.12$, $p = 0.0628$, n = 7 time-matched control, 4 bicuculline), although there was a trend for decreased spike height. Spike AUC was also unchanged (Fig 5.23I, unpaired t-test, $t_{(9)} = 1.41$, $p = 0.1922$, n = 7 time-matched control, 4 bicuculline). Post-spike membrane potential did not significantly differ at any timepoint in the presence of bicuculline, compared to no bicuculline (Fig. 5.23J, two-way RM ANOVA, time x drug interaction, $F_{(5,15)} = 1.87$, $p = 0.1599$, n = 4), although these statistics are likely underpowered due to the small sample size.

Application of the $GABA_B$-R antagonist CGP 55845 in NAcC did not appear to impact axonal membrane potential (Fig. 5.23K). Traces are corrected for the slight signal decay over time in NAcC, as outlined in Section 5.2.7. Compared to a time-matched control dataset (Fig. 5.6), spike height appeared unchanged in the presence of CGP5 55845, as did spike AUC. Post-spike membrane potential did not appear to be changed. Statistical comparisons were not performed due to low sample size (n = 2).

Taken together, these data indicate that in NAcC, $GABA_A$-Rs are the predominant mechanism which impacts DA axonal action potential, and the effects are subtle. Surprisingly, we did not find an increase in spike size upon application of GABA-R antagonists. Future experiments and larger datasets will assist in testing the validity of these interpretations, and test whether regional differences exist regarding $GABA_A$- and $GABA_B$-R function on striatal DA axons.

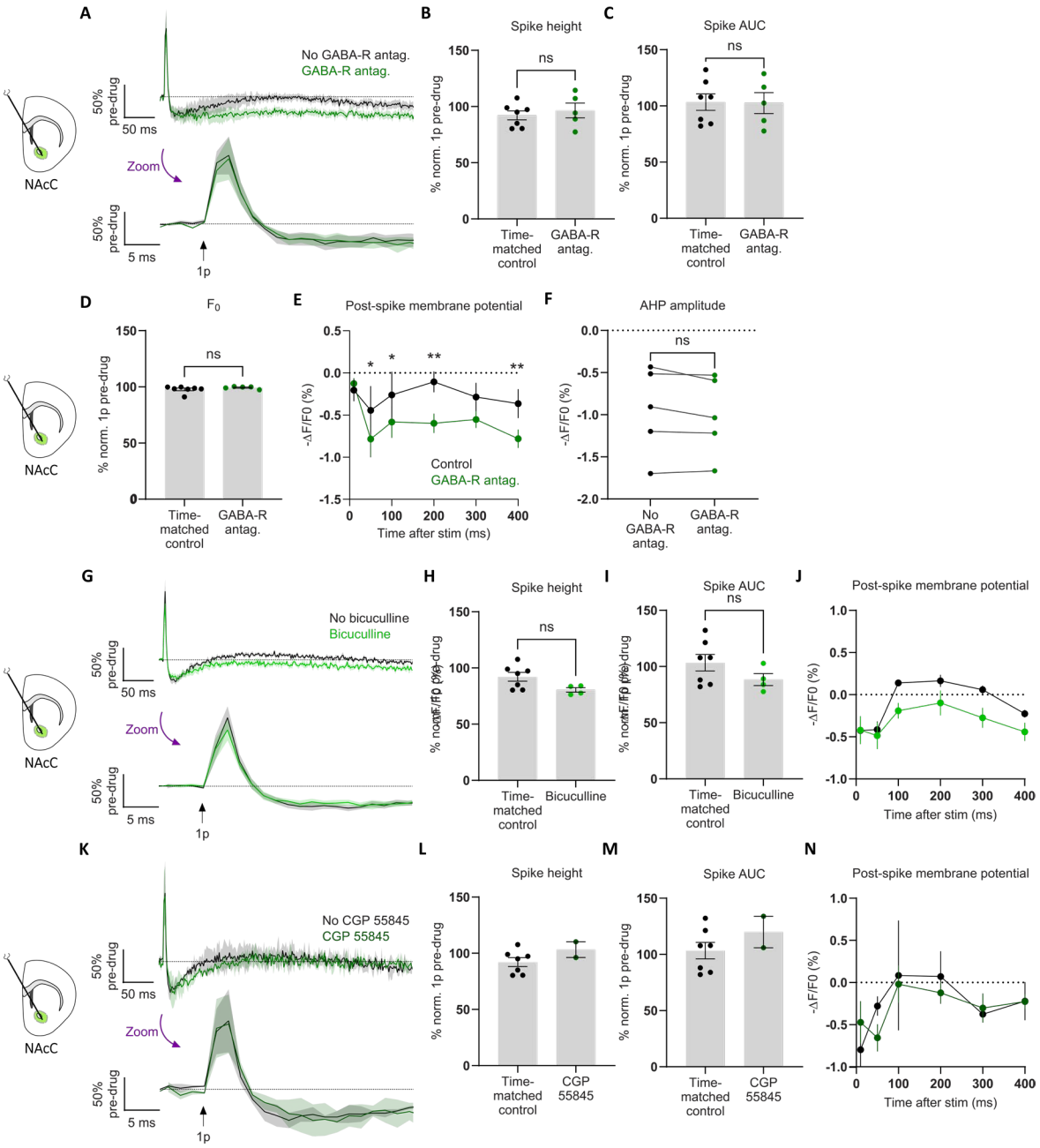

Figure 5.23. GABA-Rs modify post-spike membrane potential in NAcC

*(A) Changes in membrane potential over time in NAcC before or during GABA-R antagonists. n = 5. (B) Spike height (%) in NAcC. n = 5/5. (C) Spike AUC (%) in NAcC. n = 5/5. (D) F_0 (%) in NAcC. n = 5/5. (E) Membrane potential following initial spike in NAcC. n = 5. (F) Change in AHP amplitude in NAcC. n = 5. (G) Changes in membrane potential over time in NAcC before or during bicuculline. n = 4. (H) Spike height (%) in NAcC. n = 7/4. (I) Spike AUC (%) in NAcC. n = 7/4. (J) Membrane potential following initial spike in NAcC. n = 4. (K) Changes in membrane potential over time in NAcC before or during CGP 55845. n = 2. (L) Spike height (%) in NAcC. n = 5/2. (M) Spike AUC (%) in NAcC. n = 5/2. (N) Membrane potential following initial spike in NAcC. n = 2. Data are mean ±SEM. 'No GABA-R antag.' is DHβE (1 μM), 'GABA-R antag.' is DHβE (1 μM), bicuculline (10 μM) and CGP 55845 (4 μM). Traces are corrected for signal decay over time using a time-matched control (A, G, K). Data are normalised to pre-drug, and equivalent recordings for time-matched control (B, C, D, H, I, L, M). *p ≤ .05, **p ≤ .01, ***p ≤ .001, ns = non-significant.*

5.3.14. Activity at GABA-Rs is depolarising following paired-pulse stimulation

Next, we explored the impact of $GABA_A$- and $GABA_B$-Rs on axonal membrane potential during and following paired-pulse stimulation. Following single pulse stimulation, GABA-R antagonism slightly hyperpolarises membrane potential during the return to resting membrane potential (Fig. 5.22 & 5.23). In DLS, activation of $GABA_A$- and $GABA_B$-Rs on striatal DA axons promotes frequency-dependence of DA release, but effects of GABA on frequency-dependence following paired-pulse stimulation are subtle, and generally require longer stimulation trains (Lopes et al., 2019; Roberts et al., 2020). We hypothesised that application of GABA-R antagonists would slightly attenuate second spike height at IPIs of 10 ms, and that membrane potential would be hyperpolarised following stimulation, similar to that observed in Fig. 5.22 and 5.23.

In DLS, application of GABA-R antagonists resulted in membrane hyperpolarisation following the spike and AHP at IPIs of 10 ms and 40 ms (Fig. 5.24A, B). Paired-pulse traces are normalised for visualisation, so that the initial spike (P1) is the same height in both conditions. The presence of GABA-R antagonists did not significantly change spike height PPR (Fig. 5.24E, two-way RM ANOVA, time x drug interaction, $F_{(1,4)} = 5.86$, $p = 0.0727$, n = 5). Statistical testing revealed a significant interaction for spike AUC PPR (Fig. 5.24F, two-way RM ANOVA, time x drug interaction, $F_{(1,4)} = 9.07$, $p = 0.0397$, n = 5), however, Šídák's multiple comparisons tests did not reveal any significant differences between conditions at either IPI. These data indicate that, in DLS, GABA-Rs might subtly promote both STF and STD, but not to a large extent, or perhaps our comparisons are underpowered in this case.

In NAcC, application of GABA-R antagonists resulted in membrane hyperpolarisation following the spike and AHP at IPIs of 10 ms and 40 ms (Fig. 5.24C, D). Paired-pulse traces are normalised for visualisation, so that the initial spike (P1) is the same height in both conditions. The presence of GABA-R antagonists did not change spike height PPR (Fig. 5.24G,

two-way RM ANOVA, time x drug interaction, $F_{(1,4)} = 0.21$, $p = 0.6690$, n = 5) or spike AUC PPR (Fig. 5.24H, two-way RM ANOVA, time x drug interaction, $F_{(1,4)} = 0.001$, $p = 0.9790$, n = 5).

Together, these data indicate that activity at GABA-Rs is depolarising following stimulation, and promotes repolarisation after hyperpolarisation. Activity at GABA-Rs might have subtle effects on subsequent spike size in DLS, but not in NAcC.

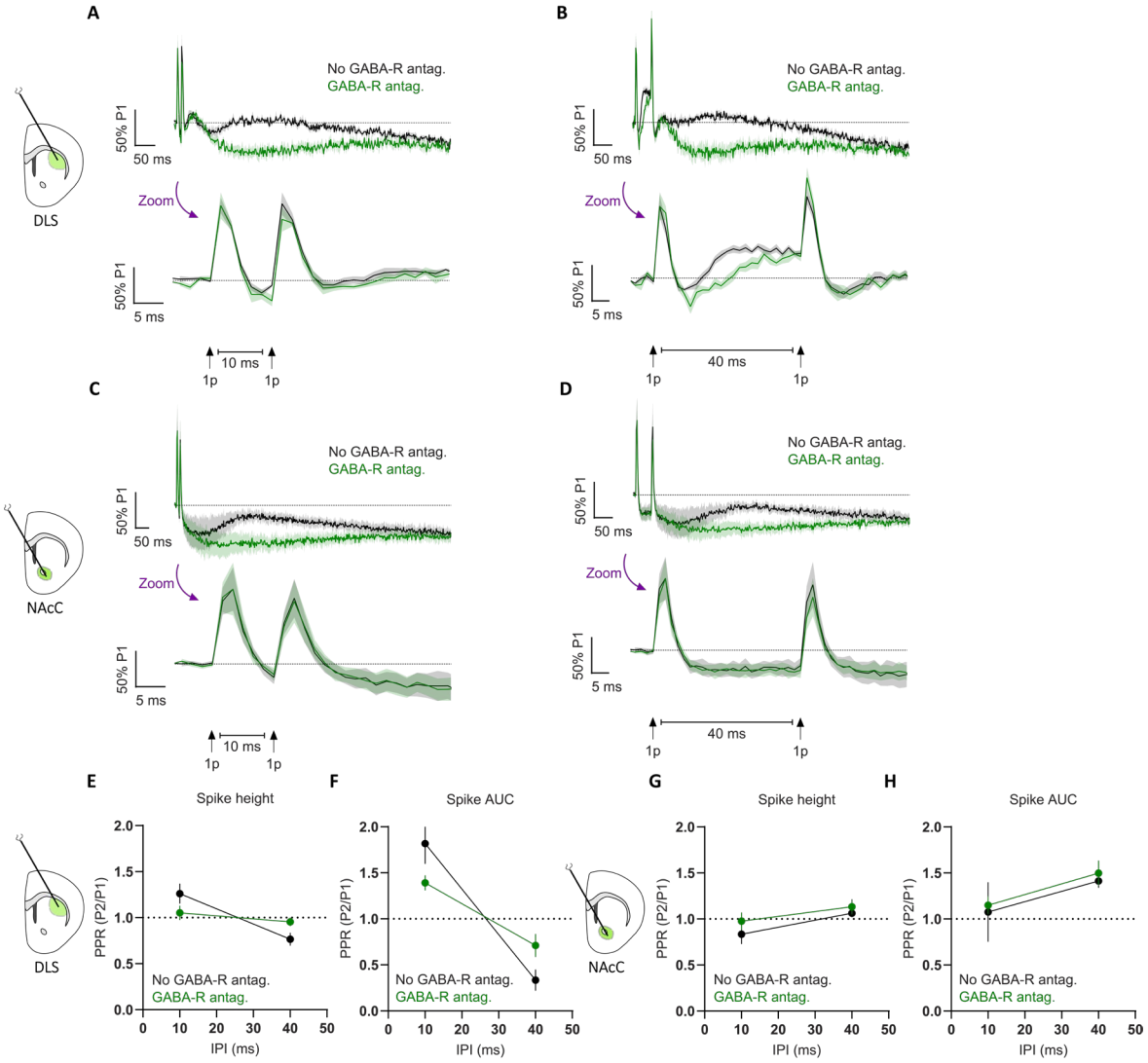

Figure 5.24. Activity at GABA-Rs promotes membrane repolarisation following the AHP
*(A, B) Changes in membrane potential over time in DLS before or during GABA-R antagonists. n = 5. (C, D) Changes in membrane potential over time in NAcC before or during GABA-R antagonists. n = 5. (E) PPR of spike height in DLS. n = 5. (F) PPR of spike AUC in DLS. n = 5. (G) PPR of spike height in NAcC. n = 5. (H) PPR of spike AUC in NAcC. n = 5. Data are mean ±SEM. 'No GABA-R antag. is DHβE (1 μM), 'GABA-R antag.' is DHβE (1 μM), bicuculline (10 μM) and CGP 55845 (4 μM). Traces are normalised to pre-drug for visualisation (A, B, C, D). *p ≤ .05, **p ≤ .01, ***p ≤ .001, ns = non-significant.*

5.3.15. GIRK channels do not impact axonal membrane potential following single or paired pulse stimulation

We explored whether activity at GIRK channels impacts on DA axon excitability. Inhibition of GIRK channels with SCH 23390 prevents an increase in DA release upon application of GABA-R antagonists (Fig. 4.1). We therefore hypothesised that, tonic activity at $GABA_B$-Rs (Lopes et al., 2019) on striatal DA axons involves activation of GIRK channels, and therefore GIRK channels are expected to be tonically active. Inhibition of $GABA_B$-Rs had very subtle, if any, impact on axonal membrane potential in DLS. We hypothesised that GIRK channel inhibition would not impact axonal membrane potential.

In DLS, application of SCH 23390 (10 µM) did not affect axonal membrane potential, as hypothesised (Fig. 5.25A). Traces are corrected for the slight signal decay over time in DLS, as outlined in Section 5.2.7. Compared to a time-matched control dataset (Fig. 5.6), spike height was unchanged in the presence of SCH 23390 (Fig 5.25B, unpaired t-test, $t_{(7)} = 1.57$, $p = 0.1601$, n = 5 time-matched control, 4 SCH 23390). Spike AUC was unchanged (Fig 5.25C, unpaired t-test, $t_{(7)} = 0.94$, $p = 0.3795$, n = 5 time-matched control, 4 SCH 23390). F_0 did not change in the presence of SCH 23390 (Fig 5.25D, unpaired t-test, $t_{(7)} = 0.19$, $p = 0.8571$, n = 5 time-matched control, 4 SCH 23390). Following the initial spike, no statistically significant changes to membrane potential were found (Fig. 5.25E, two-way RM ANOVA, time x drug interaction, $F_{(1,4)} = 2.34$, $p = 0.2024$, n = 4). The presence of SCH 23390 did not change AHP amplitude (Fig. 5.25F, paired t-test, $t_{(3)} = 1.00$, $p = 0.3909$, n = 4).

In NAcC, as expected, application of SCH 23390 (10 µM) did not affect axonal membrane potential (Fig. 5.25G). Traces are corrected for the slight signal decay over time in DLS, as outlined in Section 5.2.7. Compared to a time-matched control dataset (Fig. 5.6), spike height was smaller in the presence of SCH 23390 (Fig 5.25H, unpaired t-test, $t_{(10)} = 2.49$, $p = 0.0320$, n = 7 time-matched control, 5 SCH 23390). Spike AUC was also attenuated (Fig 5.25I,

unpaired t-test, $t_{(10)} = 2.50$, $p = 0.0313$, n = 7 time-matched control, 5 SCH 23390). F_0 did not change in the presence of SCH 23390 (Fig 5.25J, unpaired t-test, $t_{(10)} = 0.44$, $p = 0.6709$, n = 7 time-matched control, 5 SCH 23390). Post-spike membrane potential did not differ between the absence and presence of SCH 23390 (Fig. 5.25K, two-way RM ANOVA, time x drug interaction, $F_{(5,20)} = 0.28$, $p = 0.9212$, n = 5), neither did AHP amplitude (Fig. 5.25L, paired t-test, $t_{(4)} = 1.64$, $p = 0.1768$, n = 5).

Together, these data indicate that inhibition of GIRK channels does not modulate membrane potential in striatal DA axons following single-pulse stimulation.

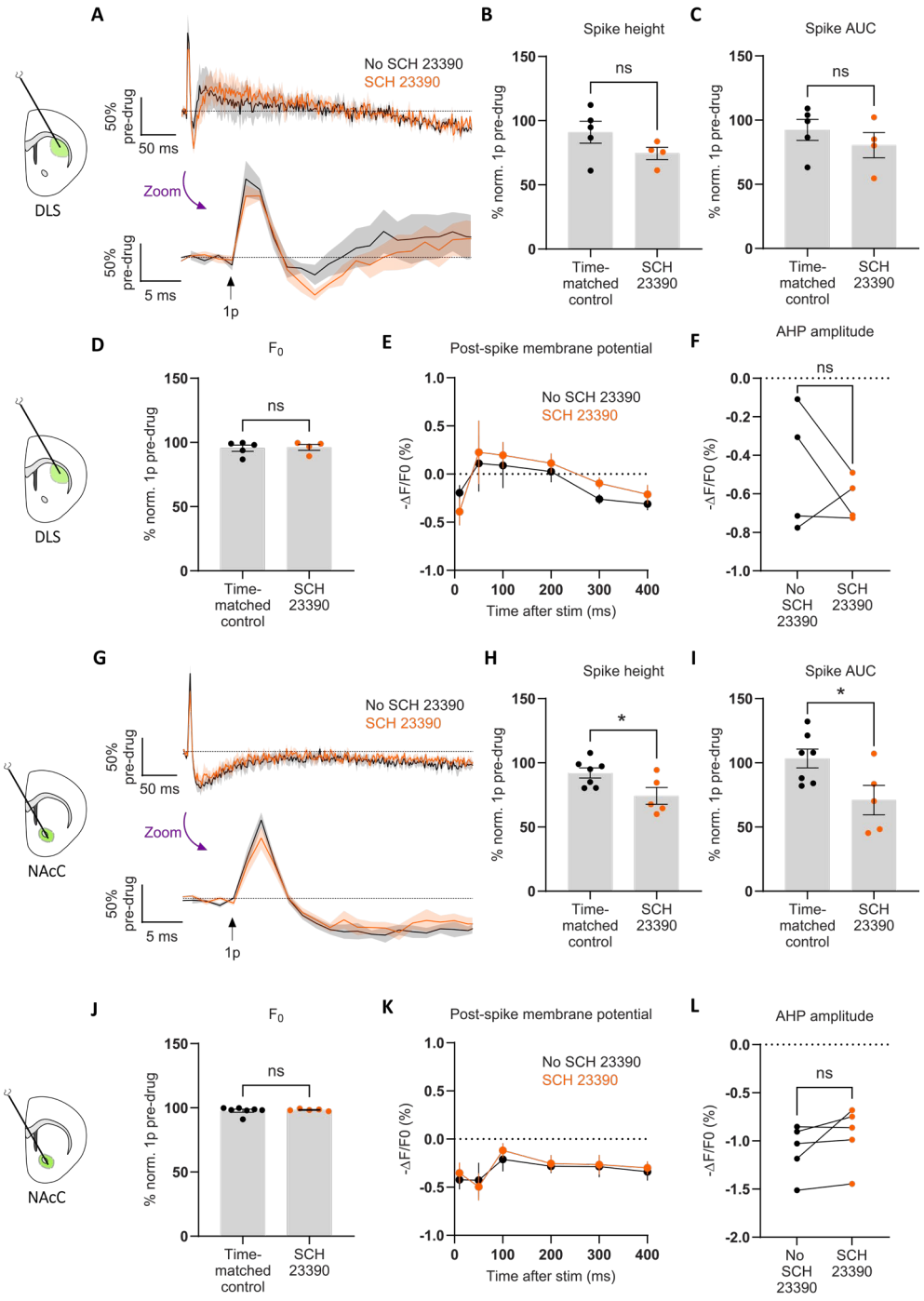

Figure 5.25. GIRK channels do not modulate axonal membrane potential following single-pulse stimulation

*(A) Changes in membrane potential over time in DLS before or during SCH 23390 (10 µM). n = 4. (B) Spike height (%) in DLS. n = 5/4. (C) Spike AUC (%) in DLS. n = 5/4. (D) F_0 (%) in DLS. n = 5/4. (E) Membrane potential following initial spike in DLS. n = 4. (F) Change in AHP amplitude in DLS. n = 4. (G) Changes in membrane potential over time in NAcC before or during SCH 23390. n = 5. (H) Spike height (%) in NAcC. n = 7/5. (I) Spike AUC (%) in NAcC. n = 7/5. (J) F_0 (%) in NAcC. n = 7/5. (K) Membrane potential following initial spike in NAcC. n = 5. (L) Change in AHP amplitude in NAcC. n = 5. Data are mean ±SEM. 'No SCH 23390.' is DHβE (1 µM), 'SCH 23390.' is DHβE (1 µM) and SCH 23390 (10 µM). Traces are corrected for signal decay over time using a time-matched control (A, G). Data are normalised to pre-drug, and equivalent recordings for time-matched control (B, C, D, H, I, J). *p ≤ .05, **p ≤ .01, ***p ≤ .001, ns = non-significant.*

We tested whether inhibition of GIRK channels affected axonal membrane potential following paired-pulse stimulation in DLS. The impact of GIRK channels on axonal excitability under basal levels may be minimal, and therefore difficult to observe following single pulse stimulation. Therefore, we tested whether we could observe an impact of GIRK channel inhibition on axonal membrane potential following paired-pulse stimulation. We hypothesised that GIRK channel inhibition would not affect membrane potential.

In DLS, application of SCH 23390 resulted in only minimal changes in membrane potential following stimulation (Fig. 5.26A, B). Paired-pulse traces are normalised for visualisation, so that the initial spike (P1) is the same height in both conditions. It appeared as though, shortly following the AHP, membrane potential was slightly more depolarised in the presence of the GIRK channel inhibitor, however, large variability, small sample size, and small effect size makes this difficult to interpret. The presence of SCH 23390 did not significantly change spike height PPR (Fig. 5.26C, two-way RM ANOVA, time x drug interaction, $F_{(1,3)} = 3.23$, $p = 0.1702$, n = 4) or spike AUC PPR (Fig. 5.26D, two-way RM ANOVA, time x drug interaction, $F_{(1,3)} = 0.26$, $p = 0.6434$, n = 4).

These data indicate that, in DLS, GIRK channels do not significantly contribute to axonal membrane potential following single-pulse or paired-pulse stimulation.

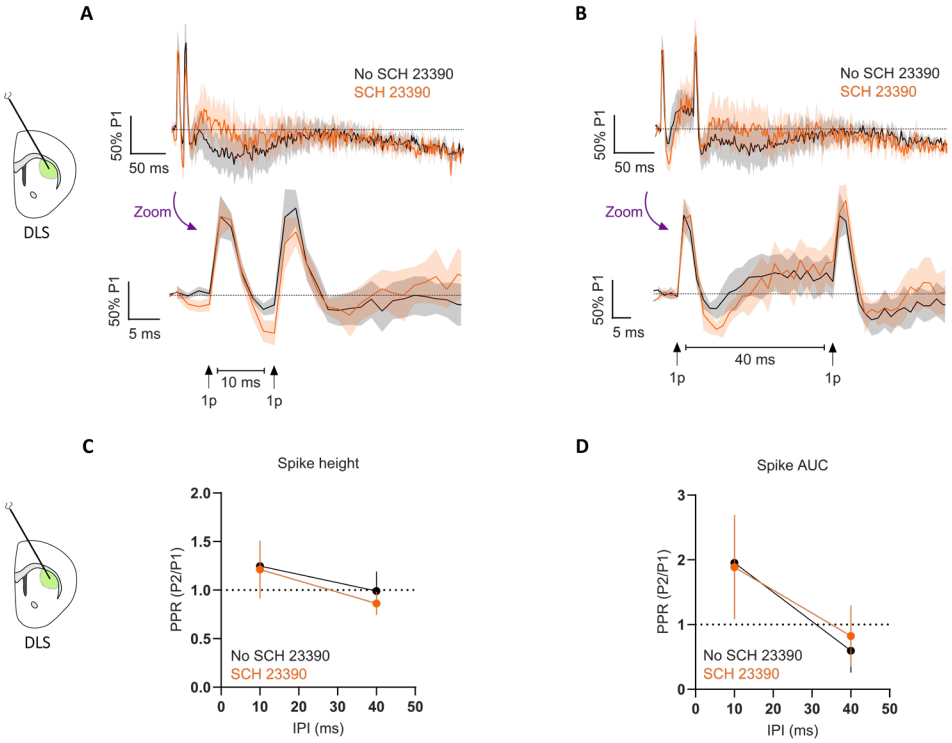

Figure 5.26. GIRK channels do not modulate axonal membrane potential following paired-pulse stimulation

*(A, B) Changes in membrane potential over time in DLS before or during SCH 23390 (10 μM). n = 4. (C) PPR of spike height in DLS. n = 4. (D) PPR of spike AUC in DLS. n = 4. Data are mean ±SEM. 'No SCH 23390' is DHβE (1 μM), 'SCH 23390' is DHβE (1 μM) and SCH 23390 (10 μM). Traces are normalised to pre-drug for visualisation (A, B). *p ≤ .05, **p ≤ .01, ***p ≤ .001, ns = non-significant.*

5.3.16. GABA-Rs do not modulate DAT-mediated currents, but might operate in parallel

Finally, we tested whether GABA-Rs support the electrogenic properties of DATs in DLS. In Chapter 3, we found that GABA-Rs support DAT-mediated changes to DA release, but did not affect uptake. The roles of DATs can be dissociated, and it was unclear whether GABA-Rs on striatal DA axons affect DAT-mediated changes to axonal membrane potential. Antagonism of GABA-Rs on striatal DA axons was expected to impact on Cl^- conductances via $GABA_A$-Rs, and likely K^+ conductances via $GABA_B$-Rs. $GABA_A$-Rs typically depolarise DA axons and presumably allow Cl^- to flow out of the cell, therefore, when inhibited, the intracellular Cl^- concentration will be higher and the axon more hyperpolarised. DAT-mediated currents are greater at more hyperpolarised potentials (Sonders et al., 1997; Richardson et al., 2016b). On

the other hand, if $GABA_B$-Rs couple to GIRK channels (which we speculate but has not been confirmed), and upon $GABA_B$-R activation, K^+ flows outward, then inhibiting $GABA_B$-Rs will result in higher intracellular K^+. High intracellular K^+ may promote DA uptake (Schmidt et al., 2022), however, DA uptake is not affected in the presence of GABA-R antagonists (Fig. 3.4). We therefore hypothesised that any change in ion gradients attributable to inhibition of GABA-Rs, would be too subtle to have an effect on DAT-mediated currents.

In DLS, application of cocaine (5 µM), in the presence of GABA-R antagonists (bicuculline, 10 µM & CGP 55845 4 µM), increased AHP amplitude and prolonged time to membrane repolarisation following hyperpolarisation (Fig. 5.27A). Traces are corrected for the slight signal decay over time in DLS, as outlined in Section 5.2.7. Post-spike membrane potential was more hyperpolarised at 50 and 100 ms following the stimulation, compared to membrane potential prior to application of cocaine (Fig. 5.27B, two-way RM ANOVA, time x drug interaction, $F_{(5,30)} = 20.90$, $p < 0.0001$, n = 7). Cocaine produced a deeper AHP (Fig. 5.27C, paired t-test, $t_{(6)} = 7.10$, $p = 0.0004$, n = 7). The observation that DAT inhibition hyperpolarises the membrane potential, and increases AHP amplitude in the presence of GABA-R antagonists, is consistent with the impact of DAT inhibition in the absence of GABA-R antagonists (Fig. 5.12). To investigate whether DAT-mediated currents were altered in the presence of cocaine, we therefore plotted traces from separate experiments together (Fig. 5.27D). Comparing post-spike membrane potential between cocaine alone, and GABA-R antagonists and cocaine, did not yield any significant differences (Fig. 5.27E, mixed effects analysis, time x drug interaction, $F_{(5,27)} = 2.21$, $p = 0.0824$, n = 10 cocaine, 7 GABA-R antagonists and cocaine). These data indicate that GABA-Rs do not affect DAT-mediated currents following single-pulse stimulation, although subtle changes may be present.

Due to the strong modulation of axonal membrane potential following paired-pulse stimulation by DATs (Fig. 5.15) and GABA-Rs (Fig. 5.24), we tested whether the presence of

GABA-R antagonists affects DAT-mediated currents during these stimulation paradigms. Between stimulations, DAT-mediated effects on axonal membrane potential were consistent to that previously observed (Fig. 5.15), however, strikingly, cocaine barely changed membrane potential following P2 (Fig. 5.27F, G). No significant changes were observed to spike height PPR (Fig. 5.27H, two-way RM ANOVA, time x drug interaction, $F_{(1,4)} = 0.79$, $p = 0.4249$, n = 7) or spike AUC PPR (Fig. 5.27I, two-way RM ANOVA, time x drug interaction, $F_{(1,4)} = 2.03$, $p = 0.2275$, n = 7).

Together, these data indicate that whilst GABA-Rs appear not to alter DAT-mediated currents, GABA-Rs and DATs might be working via parallel mechanisms to promote repolarisation following hyperpolarisation, particularly following multiple stimulations. Future experiments are required to determine whether $GABA_A$-Rs, or $GABA_B$-Rs, contribute to these depolarising currents, that appear similar to DAT-mediated currents. Thus far, we have determined that GABA-Rs support DAT-mediated changes to DA release, but maybe an interdependence exists, wherein DATs promote GABA-R-mediated changes to axonal excitability. Future experiments are necessary to fully unravel the interactions between DATs, GABA-Rs, DA release, and axonal excitability.

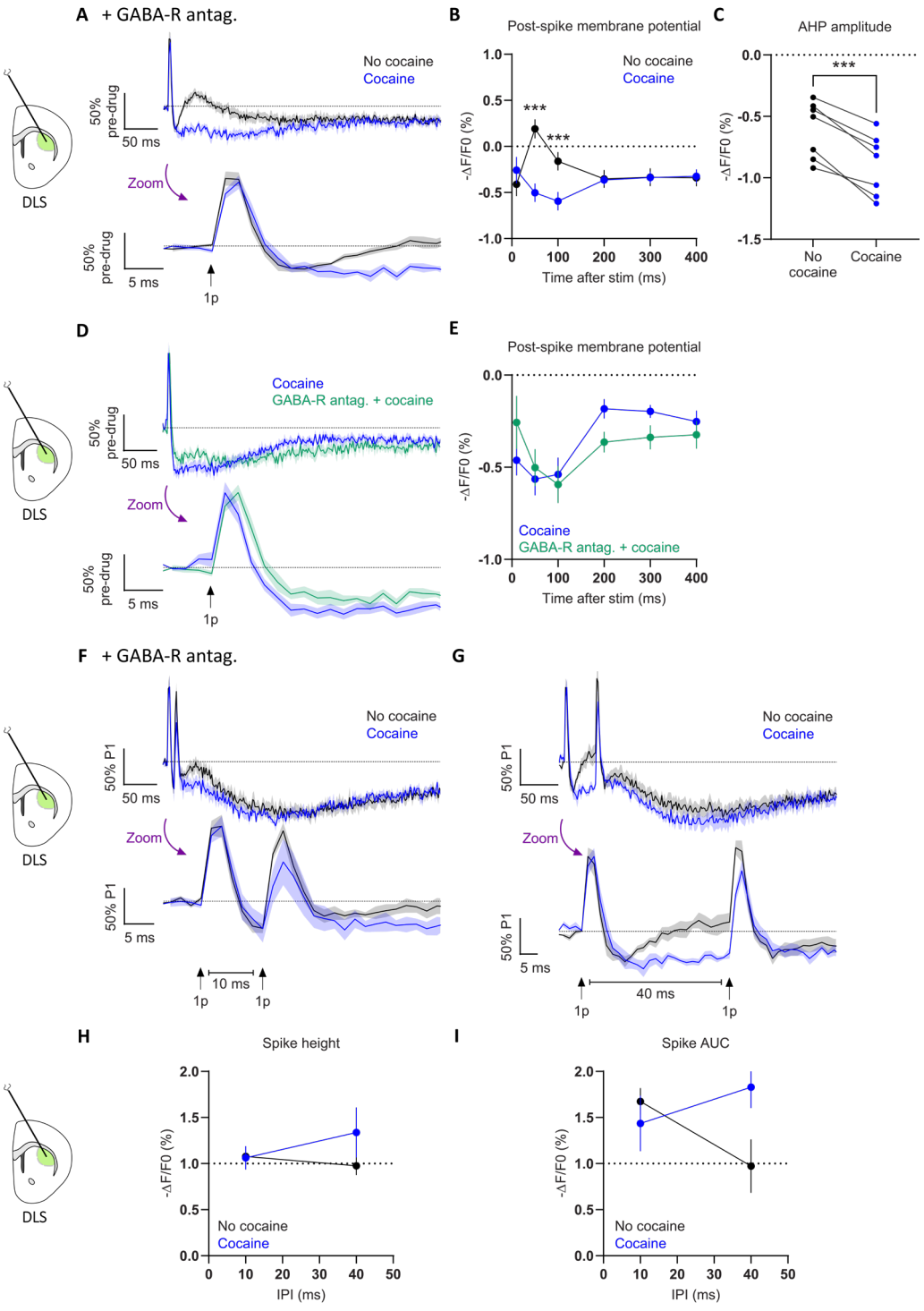

Figure 5.27. GABA-Rs do not modify DAT-mediated currents, but operate in parallel
*(A) Changes in membrane potential over time in DLS before or during cocaine (5 μM). n = 7. (B) Membrane potential following initial spike in DLS. n = 7. (C) Change in AHP amplitude in DLS. n = 7. (D) ASAP5 traces in DLS in cocaine, or GABA-R antagonists and cocaine. n = 10/7. (E) Membrane potential following initial spike in DLS. n = 10/7. (F, G) Changes in membrane potential over time in DLS before or during cocaine. n = 7. (H) PPR of spike height in DLS. n = 7. (I) PPR of spike AUC in DLS. n = 7. Data are mean ±SEM. 'No cocaine' is DHβE (1 μM), bicuculline (10 μM) and CGP 55845 (4 μM). 'Cocaine' is DHβE (1 μM), bicuculline (10 μM), CGP 55845 (4 μM), and cocaine (5 μM). Traces are corrected for signal decay over time using a time-matched control (A), or normalised to pre-drug for visualisation (D, F, G). *p ≤ .05, **p ≤ .01, ***p ≤ .001, ns = non-significant.*

5.4. Discussion

I have shown that DATs support short-term plasticity in striatal DA release in male and female mice. Potentiating DAT-mediated changes to DA release and uptake with cholesterol does not affect short-term plasticity. Using a newly-developed, genetically-encoded fluorescent voltage indicator to image fast dynamics at the level of axons, I have shown that DATs modulate membrane potential in mouse striatal DA axons. DATs limit AHP amplitude and promote membrane repolarisation following hyperpolarisation. DATs modulate axonal membrane potential in a manner consistent with DATs limiting axonal activation to promote STD. Furthermore, GABA-Rs contribute to axonal excitability, mostly mediated via $GABA_A$-Rs.

5.4.1. Short-term plasticity in striatal DA axons

Consistent with previously published findings, we found that striatal DA release exhibits short-term plasticity, which is governed by DATs (Condon et al., 2019). Canonical accounts of neurotransmitter re-release at classic central synapses (e.g. glutamate, GABA) report an inverse relationship with initial release probability; when release probability is low, synapses display facilitation, and when release probability is high, synapses display depression (Thomson, 2000). However, in the case of striatal DA axons, re-release displays an inverse relationship with release probability only at the shortest IPIs (Condon et al., 2019). At these short IPIs, STF is often reported to be due to residual Ca^{2+} (Katz & Miledi, 1968), or saturation of high-affinity Ca^{2+} buffers (also known as pseudofacilitation) (Blatow et al., 2003; Regehr, 2012b). However, knockdown of the high-affinity Ca^{2+} buffer, calbindin-D28k, in NAcC DA neurons, does not appear to have a large impact on STF (Brimblecombe et al., 2019). This indicates that saturation of calbindin-D28k is not solely responsible for STF in striatal DA axons, at least in NAcC. Surprisingly, DAT inhibition no longer modifies PPR in NAcC when calbindin-D28k is knocked down, indicating either a direct interaction between DATs and calbindin-D28k, or a convergence of DATs and calbindin-D28k on the vesicle pool

(Brimblecombe et al., 2019). Recent evidence indicates that, rather than calbindin-D28k, the Ca^{2+} sensor synaptotagmin-7 may permit STF in DLS DA axons (Lebowitz et al., 2024). The reliance of STF on Ca^{2+} dependent mechanisms, permitted by DATs (Condon et al., 2019), is consistent with our data, because we did not find a strong role for DATs in mediating axonal activation at the shortest IPIs in DLS or NAcC. DATs robustly attenuate STF when measuring DA release, which indicates that DATs are supporting a Ca^{2+}-mediated mechanism downstream of membrane potential. It should be noted, however, that in both DLS and NAcC (10 ms IPI in DLS; 10-40 ms IPIs in NAcC), when measuring axonal activation with ASAP5, PPR of spike height and spike AUC are all >1, indicating that the second spike (P2) is larger than the first (P1), and therefore that STF in DA release may not be entirely independent of changes in membrane potential at these IPIs. Either the second spike size is directly contributing to STF, or the second spike size is reflective of a mechanism determining membrane potential. The complex relationships between ion homeostasis, membrane potential, and Ca^{2+} signalling, in determining striatal DA release, requires a holistic approach including manipulations to these measures. Synaptotagmin-7 also appears to be implicated in DA re-release at longer IPIs, when STD occurs, as global synaptotagmin-7 knockout augments STD (Lebowitz et al., 2024). At these longer IPIs, when factors governing axonal activation come into play, DA re-release is no longer inversely proportional to initial release probability (Condon et al., 2019). Instead, DATs appear to limit axonal Ca^{2+} influx, leading to attenuated re-release (Condon et al., 2019). We speculate, based on experiments described herein, that axonal Ca^{2+} influx is attenuated by DATs at longer IPIs, due to DAT-mediated depolarisations (and therefore fast repolarisation of the membrane following an action potential), which attenuates the impact of subsequent action potentials.

Using a newly-developed genetically encoded fluorescent voltage indicator, ASAP5 (Hao et al., 2024), we observed that in DLS, DAT inhibition significantly increased PPR of axonal spike height at IPIs of 40 ms, and PPR of axonal spike AUC at IPIs of 25-200 ms. In NAcC, DAT

inhibition significantly increased PPR of axonal spike AUC at IPIs of 100 ms. These results indicate that when DATs are active, they promote repolarisation of the axonal membrane following P1, which subsequently leads to a smaller P2. These findings are consistent with the hypothesis that DAT-mediated changes to membrane potential promote release-independent STD in DA release. Future experiments utilising manipulations of membrane potential are necessary to directly test whether this is the mechanism underlying DAT regulation of STD.

Elsewhere in the brain, release-independent STD has been reported in cultured glutamatergic hippocampal neurons (Brody & Yue, 2000). The authors suggest that the STD observed was consistent with failure of AP propagation at axonal branch points, though technical limitations precluded examination of AP propagation along the axons (Brody & Yue, 2000). Though VGSC activity is critical for AP propagation (Rama et al., 2018), an examination of the contribution of VGSC channel inactivation to STD in cultured hippocampal neurons demonstrates that VGSC channel inactivation only minimally contributes to STD in these cells (He et al., 2002). Whether the mechanisms responsible for STD in glutamatergic hippocampal neurons are similar to those in striatal DA axons is unclear, though the speculation that AP propagation failure may be responsible, is a plausible explanation. Striatal DA axons are highly branched and consist of vast, unmyelinated, axonal arbours (Matsuda et al., 2009; Aransay et al., 2015b), requiring extensive energy for AP propagation (Pissadaki & Bolam, 2013). These vast axonal arbours may give rise to a high rate of axonal AP branch point failure, as has been reported in other neuron types (Krnjević & Miledi, 1959; Debanne et al., 1997; Deschênes & Landry, 1980; Debanne, 2004; Ofer et al., 2017). A computational model indicates that STD may be a result of neurons regulating energetic demand, and this can occur without compromising information transfer across the synapse (Salmasi et al., 2019). Thus, STD in striatal DA axons could, at least in part, be a function of

their morphology and resulting AP propagation failure. If so, DATs may limit AP propagation, a mechanism which has been reported for $GABA_A$-Rs in striatal DA axons (Kramer et al., 2020).

Though STD in striatal DA axons is predominantly a result of mechanisms intrinsic to DA axons, demonstrated by the expression of Ca^{2+}-independent STD during optical activation of DA axons (Condon et al., 2019), it is possible that other striatal mechanisms contribute to the excitability of DA axons. For example, recent evidence indicates that inwardly-rectifying Kir4.1 channels on astrocytes control $[K^+]_o$ homeostasis, which in turn affects plasticity in glutamate release in hippocampal glutamatergic axons (Tyurikova et al., 2025). If a similar mechanism is present in the striatum, striatal astrocytes could mediate extracellular K^+ concentrations and contribute to the regulation of DA axon excitability. DATs can colocalise with $K_V2.1$ and $K_V7.2/7.3$ channels (Bartolomé-Martín et al., 2019; Lebowitz et al., 2019), therefore DATs are likely sensitive to changes in K^+ gradient. Activation of $K_V7.2/7.3$ channels, when clustered with DATs, mildly augments DA uptake (Bartolomé-Martín et al., 2019), yet activation of $K_V2.1$ attenuates uptake rate and transport-coupled currents (Lebowitz et al., 2019).

We propose that striatal DATs, through DAT-mediated depolarisation, limit the AHP amplitude immediately following a spike in DLS, and then, in both DLS and NAcC, promote membrane repolarisation following the AHP. This return to, or above, resting membrane potential, subsequently limits subsequent spike size (amplitude and/or width), and thus limits axonal Ca^{2+} influx. Though we expect that DAT-mediated depolarisations using Na^+ will primarily be responsible for membrane repolarisation following AHP, it is plausible that DAT-mediated K^+ antiport (Schmidt et al., 2022) also supports the return to resting membrane potential. DAT inhibition prevents K^+ efflux through DATs (Schmidt et al., 2022), which could contribute to reduced rate of return to resting membrane potential. Thus far, our data obtained from imaging changes to axonal membrane potential are consistent with DA release data.

However, to directly test whether STD in DA release is determined by membrane repolarisation following an initial spike, future experiments must include manipulations to membrane potential. Ideally, membrane potential would be manipulated in between the first and second stimulation in a recording. To achieve membrane potential manipulation, future experiments could include patch-clamp electrophysiology on single DA axons. However, this technique is technically challenging, and is only possible at present on the main branch of DA axons, rather than the thin axonal arbour. An optical approach could be taken to excite (e.g. Channelrhodopsin-2 or ChrimsonR), or inhibit (e.g. GtACR2, Halorhodopsin-2, or Archaerhodopsin-3) striatal DA axons. Caution must be taken however, when using a dual optical approach, as dual-opsin experiments often report interference. Signal sizes with ASAP5 tend to be small in the presence of DHβE (on average, 1-2 % $\Delta F/F_0$), so it is particularly important to consider any impact of crossover.

5.4.2. DAT-mediated currents

DATs are electrogenic and generate transport-coupled and transport-uncoupled depolarising inward currents (Sonders et al., 1997; Carvelli et al., 2004; Meinild et al., 2004; Rodriguez-Menchaca et al., 2012). We have demonstrated that the electrogenic activity of DATs is present in mouse striatal DA axons. A question remains whether the DAT-mediated currents observed herein are transport-coupled or -uncoupled currents. It seems most plausible that the depolarising currents we observe in striatal DA axons are transport-coupled, due to the fact that they are observed following electrical stimulation and a spike in membrane potential, where DA is released. Additionally, DAT-mediated currents are not observed when recording solutions do not include $[Ca^{2+}]_o$. However, particularly in DLS, DAT inhibition has a very rapid effect on membrane potential following the spike, and it is not clear whether uptake via DATs would have begun yet. Furthermore, the changes to membrane potential in the presence of DAT inhibitors observed in our experiments cease before we would expect DA

to be cleared from the extracellular space. Using FSCV, we can estimate that single pulse-evoked increases in $[DA]_o$ are not cleared from the extracellular space before 500 ms following stimulation. On the other hand, DAT-mediated changes to membrane potential following a single pulse stimulation appear to last ~200 ms. It is important to note that FSCV likely reports DA clearance rate with a slight delay. Constant-potential amperometry has superior temporal resolution to FSCV and could be used in future experiments to investigate the time course of DA uptake and DAT-mediated axonal currents.

It is plausible that DAT-mediated currents are transport-associated, and only observable during the fastest rates of DA uptake. During the fastest rates of uptake immediately following DA release, DATs may undergo conformational shifts faster, or maybe a larger pool of DATs is recruited, compared to the latter stages of DA uptake. If so, we would expect that the length of DAT-mediated currents would vary with rate of uptake. To test this, we could use several approaches. Following a single pulse stimulation in our preparation, uptake rate is not at its maximal (V_{max}), but driving more DA release with stimulation trains would achieve elevated release and V_{max}. At V_{max}, we would expect larger DAT-mediated currents, either due to faster conformational shifts, or recruitment of a larger pool of DATs. ASAP5 signals will also report depolarisations resulting from stimulation, therefore these data could be challenging to interpret. Alternatively, we could use an approach to manipulate DA uptake rate, such as cholesterol, and test whether these manipulations alter the time course of DAT-mediated currents. To confirm whether currents are attributable to DA transport, future experiments could use a viral approach to deliver tetanus toxin light chain conditionally to DA neurons, preventing exocytosis. If DAT-mediated currents are abolished following tetanus toxin light chain, it is highly likely that DAT-mediated currents are transport-coupled. If DAT-mediated currents remain following tetanus toxin light chain administration, it is likely that DAT-mediated currents are transport-uncoupled.

In addition to DAT electrogenic activity, we found that GABA-Rs modulate axonal excitability in DLS and NAcC, most prominently following paired-pulses. Data indicated that, as expected, these changes, at least following single-pulse stimulation, were mainly via $GABA_A$-Rs. Whilst GABA-R antagonism did not strongly modify PPR of spike height or spike AUC at IPIs of 10 and 40 ms, we speculate that, following paired-pulse stimulation, if another stimulation was delivered ~200-300 ms following P2, the hyperpolarised membrane potential in the presence of GABA-R antagonists could have a large impact on spike size. The hyperpolarisation observed in the presence of GABA-R antagonists could give rise to a large spike ~200-300 ms following P2. We speculate that, in the presence of cocaine, this would also be the case. If a third stimulation was delivered ~50-100 ms following P2 (at IPIs of 10 or 40 ms), the hyperpolarised membrane potential may give rise to a large third spike. If we compare GABA-R inhibition against when both DATs and GABA-Rs are inhibited, however, a third stimulation might not result in different spike sizes. When GABA-Rs were inhibited, then we subsequently inhibited DATs, no change was observed to the hyperpolarised state late in the ASAP5 traces. This could indicate that DATs and GABA-Rs work through parallel mechanisms. Perhaps, striatal GABA tone contributes to STD in striatal DA release. Future experiments could test these speculations by using updated stimulation paradigms, which could mimic more regular firing rates, as seen *in vivo*.

5.4.3. Interactions between region, DATs, and Ca^{2+} in DA axon excitability

To explore whether DAT-mediated currents in striatal DA axons were transport-coupled or -uncoupled, we conducted experiments in recording solutions lacking $[Ca^{2+}]_o$, to prevent DA release and subsequent uptake. However, results obtained from these experiments were not straightforward to interpret. Importantly, DAT function is not equivalent in the presence of cocaine, and 0 mM $[Ca^{2+}]_o$. In the presence of cocaine, a DAT inhibitor, DA uptake is slowed, but not entirely abolished. Therefore, in the presence of cocaine, DATs still undergo

conformational shifts to translocate DA. In 0 mM $[Ca^{2+}]_o$, we expect that all DA transport is inhibited, though whether this impacts on DAT-mediated transport-uncoupled currents is unknown. Cocaine inhibits the DAT leak conductance and transport-associated conductance (Sonders et al., 1997), so we cannot extrapolate from cocaine data, which current(s) is present in DA axons. Cocaine evokes outward currents via DATs, likely due to the blockade of the leak current (Sonders et al., 1997). The surprising results obtained in the absence of $[Ca^{2+}]_o$ are likely due to the involvement of Ca^{2+}, VGCCs, or other channels activated by Ca^{2+} on membrane excitability, but also interactions between DATs and Ca^{2+}. Ca^{2+} handling and VGCC function, particularly LTCC function, varies by striatal subregion.

DAT function, at least regarding regulation of DA release probability, is dependent on $[Ca^{2+}]_o$ (Kile et al., 2010). Decreasing release probability with low $[Ca^{2+}]_o$ results in larger cocaine-induced increases in striatal DA release, and vice versa (Kile et al., 2010). Calbindin-D28k promotes cocaine-induced increases in DA release, indicating that calbindin-D28k supports DAT-mediated modifications to the vesicle pool (Brimblecombe et al., 2019). The interaction between DATs and Ca^{2+} signalling extends to the electrogenic properties of DATs, too. DA uptake through DATs activates LTCCs, as does amphetamine (Cameron et al., 2015). In fact, DATs can activate LTCCs in the absence of any substrate, indicating that both transport-associated and transport-independent DAT currents are adequate for LTCC activation (Cameron et al., 2015). It is therefore very plausible that DATs activate LTCCs in striatal DA axons. Perhaps DAT activity is even required for LTCC function, because LTCC inhibition modulates striatal DA release only when DATs are active (Brimblecombe et al., 2024).

Our data indicate that, prior to drug application, DLS and NAcC exhibit different dynamics. DLS signals typically, although not 100% of the time, exhibit a rebound depolarisation immediately following the AHP. On the other hand, NAcC signals, in our experience, never exhibit a rebound depolarisation. NAcC DA axons typically have a pronounced and prolonged

AHP, before returning to resting membrane potential. Whilst we cannot confirm whether these observations are due to underlying biology, or a technical confound, the idea that these neurons differ in their action potential waveform is supported by literature regarding recordings in DA neuron somas, even if not directly tested. SNc, calbindin-D28k-negative, DA neurons exhibit rebound depolarisation (or afterdepolarisation) at the soma that is more prominent when neurons are more hyperpolarised (Evans et al., 2017; Beaver & Evans, 2025). Striatal DA axons are typically more hyperpolarised than the somatodendritic region (Kramer et al., 2020). This rebound depolarisation is mediated in part by muscarinic ACh receptors, and T-type VGCCs (Beaver & Evans, 2025). SNc DA neuron pacemaking traces appear to have a steeper slope following the AHP, than VTA DA neurons (Guzman et al., 2010). VTA DA neurons exhibit a rounded, longer AHP (Guzman et al., 2010). Unfortunately, most published data focuses on either SNc or VTA DA neurons, rather than both, or do not report action potential waveforms, making it difficult to compare data, but we speculate that regional differences in our signals may be due to underlying biology. Regional differences could point to an involvement of DATs. DATs are expressed at greater levels in SNc DA neurons than VTA neurons (Haber et al., 1995; Poulin et al., 2014), therefore DAT-mediated depolarisations are likely to affect SNc DA neurons to a greater extent. Rebound depolarisation in DLS, or the ability to return to resting membrane potential quicker, could be supported by DAT-mediated currents. NAcC axons express less DATs, and do not repolarise following the AHP as quickly. In DLS, application of cocaine entirely abolishes the rebound depolarisation (Fig. 5.12). To attempt to titrate the rebound depolarisation, future experiments could be conducted in $DAT^{IREScre}$ homozygous mice, which have lower DAT expression that the heterozygous mice used here (Bäckman et al., 2006).

LTCC function, differs between DLS and NAcC DA axons, in a sex-dependent manner (Brimblecombe et al., 2015, 2024). The key determinant of whether LTCCs can support DA release, however, is the activity status of DATs; if DATs are inhibited, LTCC no longer support

DA release (Brimblecombe et al., 2024). The involvement of LTCCs in modulating single-pulse evoked DA release points to transport-uncoupled DAT currents, rather than transport-associated currents. In *ex vivo* preparations, we would anticipate that transport-coupled currents are only present following electrical stimulation, whereas transport-uncoupled currents could be ongoing at basal levels. To test for the involvement of LTCCs in DAT-mediated currents, future experiments should conduct voltage indicator imaging in the presence of a LTCC inhibitor.

5.4.4. Voltage dependence of DAT function

Mesostriatal DA neurons, and particularly striatal DA axons, are very hyperpolarised (Kramer et al., 2020). What impact could this hyperpolarised state have on DAT function, and DAT-mediated currents? The voltage dependence of DAT function appears to vary with experimental preparation. hDATs expressed in oocytes exhibit voltage dependent uptake, where uptake rate was 85% faster when oocytes were held at -120 mV, compared to those held at -30 mV (Sonders et al., 1997). Transport-associated currents, which are greater than predicted for a transporter with fixed stoichiometry, also vary with membrane polarisation, with larger transport-associated currents at more hyperpolarised potentials (Sonders et al., 1997). In rat midbrain cultured neurons, DA uptake rate was unaffected by pharmacological hyperpolarisation (Prasad & Amara, 2001). However, amphetamine-induced DA efflux is voltage dependent in EM4 cells expressing hDAT (Khoshbouei et al., 2003). Interestingly, changes to membrane potential alter DAT trafficking, with membrane depolarisation triggering trafficking of DATs into early endosomes in Human Embryonic Kidney (HEK) cells expressing hDAT, and depolarisation-mediated DAT trafficking in mouse midbrain cultures (Richardson et al., 2016). In agreement with Sonders et al. (1997), DAT-mediated currents were greater at more hyperpolarised potentials (Richardson et al., 2016). $GABA_A$-R-mediated

depolarising currents are also greater at more hyperpolarised potentials (Kramer et al., 2020).

The voltage dependence of uptake via DATs may be a product of intracellular K^+ handling, as voltage-dependent transporters (DATs, NETs) are less likely to antiport K^+ than other voltage-independent transporters (SERTs) in HEK cells expressing hDAT, hNET and hSERT (Bhat et al., 2021). Differences in intracellular K^+ handling appears to account for all functional disparities between these monoamine transporters (Bhat et al., 2021). Though DATs are reported to be less likely to antiport K^+, dDATs, which are functionally similar to hDATs (Porzgen et al., 2001), are capable of antiporting K^+, which in turn increases DA uptake rate (Schmidt et al., 2022). Additionally, substrate binding to hDAT and dDAT is K^+ dependent (Schmidt et al., 2022).

These findings indicate that the hyperpolarised resting membrane potential of striatal DA axons might particularly support DAT-mediated currents, and that DAT-mediated changes to membrane potential may impact not only on DA uptake via DATs, but also DAT trafficking. Future experiments are necessary to test whether DAT function or trafficking is mediated by membrane voltage in mouse striatal DA axons.

5.4.5. Sex differences in DAT-mediated mechanisms

Whilst our data do not support any differences between sexes in DAT regulation of short-term plasticity in striatal DA release, sex differences are frequently reported relating to DAT function and DAT-mediated behaviours.

For example, using fast-scan cyclic voltammetry, Kuiper et al. (2024) demonstrated that the observation of sex differences in dopamine dynamics depend on species, striatal subregion, and parameter. In C57BL/6J mice, maximal DA uptake appears to be slightly faster across the striatum in females, compared to males, but no differences between sexes were observed in DA release (Kuiper et al., 2024). In agreement with this, also in C57BL/6 mice, females exhibit

a faster DA uptake rate, but DA release levels are equivalent between sexes (Brimblecombe et al., 2024). In Sprague Dawley rats, no sex differences were observed in maximal DA uptake rate, but DA release appeared to be slightly higher in males (Kuiper et al., 2024). Female CD-1 mice appear to exhibit higher striatal DAT function than males, as DA responses were larger in females in response to the DAT inhibitor, nomifensine (Bhatt & Dluzen, 2005).

Consistent with a general indication that females display increased DAT function, it has been reported that, in C57BL/6J mice, during the estrus phase of the female oestrous cycle, VTA DA neurons display enhanced activity compared to males or females in diestrus, which in turn drives posttranslational modifications to DATs, and augments cocaine potency at DATs in *ex vivo* preparations (Calipari et al., 2017). This was accompanied with enhanced preference for cocaine following conditioned place preference, compared to males or females in diestrus (Calipari et al., 2017). Similar findings have been reported in Sprague Dawley rats, where female rats displayed higher cocaine seeking compared to males, and females in estrus display augmented incubation of cocaine craving compared to females not in estrus (Nicolas et al., 2019). Following an amphetamine sensitisation protocol and subsequent amphetamine challenge, male, but not female, mice exhibit an increase in DAT endocytosis in the striatum, and a corresponding decrease in maximal DA uptake rate (Bagalkot & Sorkin, 2024).

However, sex or oestrous cycle differences are not consistently reported in DAT-related measures. For example, Alonso et al. (2022) did not find any significant impacts of sex or oestrus cycle phase in Sprague Dawley rats on cocaine self-administration or cocaine potency at DATs in *ex vivo* striatal slices. There were no significant differences in cocaine-induced increases in striatal DA release between male and female mice overexpressing α-synuclein, or their littermate controls (Threlfell et al., 2021). In agreement with these studies, no strong sex differences were apparent in any of our data. As recommended (e.g. Diester et

al., 2019; Garcia-Sifuentes & Maney, 2021), our data from male and female mice were pooled. Our data do show a trend towards augmented DAT function in female mice, and we are aware that our comparisons might be underpowered. It is also likely that the observation of sex differences depends on exact experimental measures and that sex differences do not apply to all aspects of DAT function.

Nevertheless, it is imperative to include both sexes in experiments. The inclusion of female animals does not increase experimental variability (Smarr & Kriegsfeld, 2022), rather, it is likely that male animals exhibit their own variability, meaning that variability in male biology is comparable with the variability in female biology (Mogil & Chanda, 2005). Sex differences may be over-reported in the biological sciences (Garcia-Sifuentes & Maney, 2021), thus we are cautious in interpreting the literature surrounding sex specific aspects of DAT function.

5.4.6. Summary

In summary, our data indicate that short-term plasticity in striatal DA release is governed by DATs in male and female mice, and is independent of DA uptake rate and DAT-mediated changes to DA release probability. Using a genetically-encoded fluorescent voltage indicator, we demonstrated that DATs generate depolarising currents following electrical stimulation in striatal DA axons. DATs promote repolarisation following hyperpolarisation in striatal DA axons, which reduces subsequent spike size, consistent with the observation that DATs promote short-term plasticity in DA release. Future experiments will determine whether this is the mechanism underlying DAT-mediated changes to short-term plasticity in striatal DA release, and whether DAT-mediated currents are transport-coupled or transport-uncoupled currents. GABA-Rs, particularly the $GABA_A$-R, also promotes membrane repolarisation following multiple stimulations. These data emphasise the complex, and important, roles of DATs in striatal DA re-release and axonal excitability.

Chapter 6.

General discussion

DA signalling in the striatum, from complex DA axonal arbours (Matsuda et al., 2009; Aransay et al., 2015a), is governed by a host of local neuromodulators, and mechanisms intrinsic to DA axons. Striatal DA signalling provides input to MSNs, which form the direct and indirect pathways of the basal ganglia, and subsequently signal to downstream nuclei (Bolam et al., 2000; Gittis & Kreitzer, 2012). Understanding the mechanisms posed to modulate striatal DA transmission is therefore critical to further our understanding of the roles and diseases of the basal ganglia.

The aims of this thesis were to explore whether DATs and GABA-Rs co-operate to govern striatal DA release, and to investigate whether DATs regulate axonal excitability. In Chapter 3, I showed that GABA-Rs support DAT-mediated changes to striatal DA release. In Chapter 4, I expanded on this line of enquiry and investigated the contribution of GIRK channels to the co-operation between DATs and GABA-Rs. In Chapter 5, I described how DATs modulate axonal membrane potential in a way that is consistent with DAT-mediated changes to striatal DA re-release. Here, I discuss the main findings in a wider context of striatal DA signalling in health and disease, and speculate on potential underlying mechanisms.

6.1. DATs and GABA-Rs co-operate to regulate striatal DA release

6.1.1. GABA-Rs promote DAT-mediated changes to DA release

Mesostriatal DA neurons are critical for action selection (Balleine & Ostlund, 2007; Howard et al., 2017) and reward learning (Schultz et al., 1997), and dysfunction in these neurons is associated with PD (Kish et al., 1988) and substance-use disorders (Robinson & Berridge, 1993). In C57BL/6 mice, it is estimated there are ~4,000-6,000 DA neurons in SNc and equivalent numbers in VTA per hemisphere (Nelson et al., 1996; Basso et al., 2024). In rats, differences in neuron numbers between SNc and VTA are more evident, with ~12,500 DA neurons in SNc, and ~20,000 DA neurons in VTA (Nair-Roberts et al., 2008). In humans, the

disparity between regions is even greater, with an estimated ~100,000-210,000 DA neurons originating in SNc and ~30,000-32,500 in VTA (Hirsch et al., 1988; McRitchie et al., 1997; Brichta & Greengard, 2014; Basso et al., 2024). Whilst midbrain DA neuron numbers are small compared to other neuron types in the brain, these DA neurons have an impressive reach. Mesostriatal DA neurons send vastly arbourised axons to the striatum, with each nigrostriatal axon thought to innervate, on average, ~2.7% of the striatum in rodents (Matsuda et al., 2009). GABAergic neurons comprise ~98% of striatal neurons, made up of ~95% MSNs, and ~2-3% GABA interneurons (Kemp, 1968; Tepper et al., 2007, 2010). A single nigrostriatal neuron, therefore, has the potential to influence ~75,000 GABA-containing striatal neurons (Matsuda et al., 2009). To look at it from another perspective, ~75,000 GABA neurons have the potential to influence the activity of one DA neuron. It is therefore unsurprising that striatal DA and GABA in the striatum are interdependent.

In Chapter 3, I demonstrated that striatal DA release in DLS is regulated by DATs and GABA-Rs, which co-operate to determine DA output. DATs on striatal DA axons mediate DA uptake, but the roles of DATs do not stop there; DATs also limit initial DA release, and govern short-term plasticity in DA release. DATs limit striatal DA release by immobilising a vesicle reserve pool, which is relieved upon pharmacological DAT inhibition (Venton et al., 2006; Kile et al., 2010). We found that the regulation of DA release by DATs is supported by activity at GABA-Rs. Antagonism of $GABA_A$-Rs and $GABA_B$-Rs attenuates cocaine-induced increases in striatal DA release, indicating that when GABA-Rs are active, cocaine-induced increases in DA release are promoted. The magnitude of single pulse-evoked DAT inhibitor-induced increases in DA release is indicative of the level of limitation DATs place on initial DA release. We therefore extrapolate that when striatal GABA-Rs are tonically active, they support DAT function. Though at first the role of GABA-Rs in supporting DATs may seem counterintuitive to the canonical inhibitory influence of GABA, DATs are also inhibitory, limiting initial release

and curtailing the extracellular lifetime of DA. GABA-Rs are therefore supporting another inhibitory mechanism, promoting further limitations on neurotransmitter release.

Surprisingly, activity at GABA-Rs does not appear to influence DA uptake. This supports the idea that the roles of DATs can be dissociated, and therefore differentially regulated. We observed that whilst GABA-Rs appear to robustly support DAT function in DLS, this is not the case in NAcC. Under several conditions (2.5 mM $[Ca^{2+}]_o$, 1.2 mM $[Ca^{2+}]_o$, GIRK channel inhibition), antagonism of GABA-Rs produced no, or minimal, effect on cocaine-induced increases in DA release. These regional differences may be related to the biology of vulnerable versus resistant DA neurons in PD. In DLS, GABA-R agonism produces no effect on cocaine-induced increases in DA release unpublished observations, Dr. E. Lopes, Cragg lab), but this has not yet been investigated in NAcC. Perhaps GABA-R activity differs between striatal regions, and agonism of GABA-Rs in NAcC would unveil a co-operation between DATs and GABA-Rs. Future experiments should focus on these regional differences, because many aspects of biology differ between DLS and NAcC DA axons, and future investigations into regional differences could elucidate which mechanisms are involved in this co-operativity between DATs and GABA-Rs.

6.1.2. Involvement of GIRK channels and K^+ handling

In Chapter 4, I investigated a role for GIRK channels in the control of striatal DA release by DATs and GABA-Rs. Pharmacological inhibition of GIRK channels prevented GABA-R antagonists from increasing DA release, and in DLS, attenuated the effect of cocaine on DA release. These results indicate that GIRK channels support GABA-R and DAT function. Furthermore, in DLS, GIRK channel inhibition drastically reduced the impact of GABA-Rs on cocaine-induced increases in DA release. These results indicate that GABA-Rs function via GIRK channels to modulate DAT function. However, surprisingly, a genetic approach to

knockdown, or knockout, GIRK2 channels on DA neurons did not parallel results obtained with the pharmacological inhibitor. Possible explanations for this were explored in Chapter 4.

The higher expression of GIRK channels in SNc than VTA DA neurons (Schein et al., 1998; Chung et al., 2005; Poulin et al., 2014) is consistent with the finding that GABA-Rs support DAT-mediated changes to DA release in DLS, but not in NAcC. K^+ flux through GIRK channels, generated by tonic activation of $GABA_B$-Rs in striatal DA axons (Lopes et al., 2019; Roberts et al., 2020), could promote DAT function. K^+ antiporting by DATs facilitates uptake rate (Schmidt et al., 2022), which indicates that the K^+ gradient could be an important factor in DAT functionality. DATs colocalise with $K_V7.2/7.3$ channels, potentially to limit transport-mediated depolarising influences on membrane potential (Bartolomé-Martín et al., 2019). In fact, DATs and GABA-Rs are required for K^+-mediated changes to short-term plasticity in striatal DA release (Condon et al., 2019; unpublished data, Dr. E. Lopes, Cragg lab), strongly implicating K^+ homeostasis in any interaction between DATs and GABA-Rs. VGKC inhibition promotes STD in striatal DA release (Condon et al., 2019). However, changes in $[K^+]_o$ do not affect single pulse evoked $[DA]_o$ (Condon et al., 2019), therefore, co-operativity between DATs and GABA-Rs may not be via K^+-mediated mechanisms. Furthering the investigation of the contribution of GIRK channels, or other K^+-mediated mechanisms, to the control of striatal DA release by DATs and GABA-Rs is challenging, due to the limited tools available. Promoting GABA-R activity with agonists does not modulate DAT function (unpublished data, Dr. E. Lopes, Cragg lab), therefore viral overexpression of GIRK channels does not appear to be a useful strategy, although it could yield useful data. Testing for GIRK channel expression of all GIRK channel subtypes in GIRK2 cKD or cKO animals would assist in the interpretation of data collected thus far. Though we did not test any other mediators of co-operation between DATs and GABA-Rs beside GIRK channels, there are several potential candidates, which will be discussed in Section 6.3.

6.1.3. Applicability to other receptor subtypes

Could the cooperativity between GABA-Rs and DATs be extended to other receptors that are structurally or functionally similar to GABA-Rs? It is certainly plausible that other receptors on striatal DA axons also modulate DAT function. If $GABA_A$-Rs alone support DAT function, this could be extended to other ionotropic receptors that function as Cl^- channels, such as ionotropic glycine receptors. Glycine attenuates striatal DA release, likely through ionotropic receptors located on DA axons, though studying ionotropic glycine receptor function can be difficult due to rapid receptor desensitisation (unpublished data, Dr. R. Anand, Cragg lab). On the other hand, if $GABA_B$-Rs alone modulate DAT function, the same could be true for other GPCRs that couple to GIRK channels, such as D_2-like-Rs, or GPCRs that could to VGCCs, such as metabotropic glutamate receptors. In Chapter 3, we used a D_2-like-R antagonist to test whether GABA-R modulation of cocaine-induced increases in DA release was due to a striatal circuit-mediated effect. Although this was not intended to test whether D_2-like-Rs modulate DAT-mediated changes to DA release, these experiments indirectly tested that hypothesis. We did not observe an attenuation in cocaine-induced increases in release in the presence of a D_2-like-R antagonist, indicating that D_2-like-Rs do not support DAT-mediated changes to DA release probability. Unpublished data from the Cragg lab indicates that metabotropic glutamate receptors do not have much of an impact on striatal DA release, but these data do not preclude the possibility that activation of these receptors could support DAT function. To test whether any of these receptors impact on DAT function, it is important to first determine which receptors are localised on striatal DA axons, and then pharmacologically test sensible receptor candidates.

If DAT function, however, is supported by a mechanism involving integration between $GABA_A$-Rs and $GABA_B$-Rs, it is less likely to be extended to other receptors on striatal DA axons. In that case, both ionotropic and metabotropic receptors would need to be expressed, and

together support DAT function. Future experiments should interrogate the possibility that these mechanisms can be extended to other receptors, or even other monoamine transporters, for example in norepinephrine- or 5-HT-containing axons.

6.1.4. DA-GABA co-release from striatal DA axons

Striatal DA axons co-release GABA to dampen striatal output (Tritsch et al., 2012), the involvement of which has not been accounted for in this thesis. GABA is likely co-stored in a portion of DA-containing vesicles, as GABA co-release from striatal DA axons is dependent on the vesicular transporter for DA, the vesicular monoamine transporter 2 (VMAT2) (Tritsch et al., 2012), and GABA is found in ~11% of VMAT2-positive dorsal striatal axons, exhibiting close co-localisation that is likely characteristic of co-storage (Stensrud et al., 2014). ~70% of GABA co-released from DA neurons in dorsal striatum is synthesised from putrescine in an aldehyde dehydrogenase (ALDH) 1a1-dependent manner, rather than through canonical synthesis via glutamate decarboxylase (GAD) 65 or 67 (J.-I. Kim et al., 2015). ALDH1a1 inhibition does not prevent an increase in striatal DA release upon application of GABA antagonists, demonstrating that GABA co-release from DA axons is not responsible for the tonic GABAergic inhibition of DA axons in the striatum (Roberts et al., 2020). Rather, tonic GABAergic inhibition of striatal DA transmission is dependent on a GAD-dependent source of GABA (Roberts et al., 2020).

Though GABA co-release from striatal DA axons does not contribute to single pulse-evoked DA release, GABA co-release may inhibit DA release arising from a stimulus train. The $GABA_A$-R antagonist, picrotoxin, increases DA release in DLS and NAcC to a greater extent when DA axons are optogenetically stimulated with train stimulation, than single pulse stimulation (Patel et al., 2024). If GAT1 is conditionally knocked out in DA neurons, the magnitude to which picrotoxin increases DA release is no longer dependent on stimulation paradigm (Patel et al., 2024). These findings indicate that GABA co-release from DA axons can be

autoinhibitory, limiting DA release (and potentially further GABA co-release) arising from subsequent stimulation (Patel et al., 2024). In agreement with previous demonstrations that midbrain DA somas express GATs (Tritsch et al., 2014), uptake of GABA through GATs on striatal DA axons plays a role in GABA co-release from DA axons, and subsequently inhibits DA release (Patel et al., 2024). However, striatal DA axons do not appear to express GATs (Roberts et al., 2020), indicating that the mechanisms responsible for synthesis or uptake of GABA may differ between somatodendritic and axonal compartments in midbrain DA neurons.

Although GABA and DA are co-released by striatal DA axons, no correlation between DA and GABA release from striatal DA axons exists, and release of each transmitter is differentially regulated (Zych & Ford, 2022). In dorsal striatum, VMAT2 inhibition with reserpine preferentially affects DA, over GABA, release (Zych & Ford, 2022). DA transmission is more sensitive to changes in Ca^{2+}, has looser coupling between Ca^{2+} entry and vesicular Ca^{2+} sensors, and exhibits higher re-release probability (Zych & Ford, 2022). DA transmission is inhibited more strongly by D_2-like-Rs, $GABA_B$-Rs, and κ-opioid receptors, than GABA transmission (Zych & Ford, 2022). The differential regulation of each transmitter indicates that vesicle pools are functionally or spatially segregated (Zych & Ford, 2022). Though DATs limit DA release by vesicle mobilisation (Venton et al., 2006; Kile et al., 2010), the same is not true for GABA release, as postsynaptic GABA currents on MSNs are unaffected by DAT inhibition (Kim et al., 2015; unpublished data, Dr. M. Condon, Cragg lab). Postsynaptic GABA currents exhibit STD following paired-pulses at IPIs of 100 ms, and unlike STD in DA release, this STD in GABA release is unaffected by DAT inhibition (unpublished data, Dr. M. Condon, Cragg lab). Taken together, whilst striatal DA axons co-release GABA, different properties of transmitter release and regulation make it difficult to infer whether manipulations to striatal DA release also affect GABA co-release.

Could GABA co-release from DA neurons play a role in the convergent regulation of DA release by DATs and GABA-Rs? If GABA is co-released from striatal DA axons upon single-pulse stimulation, we would not expect that this co-released GABA to have an impact on the next single pulse-evoked DA release event 2.5 minutes later, as GABA would likely have diffused or be taken up by GATs. However, if co-released GABA somehow did impact single pulse-evoked DA release 2.5 minutes later, we would expect this GABA to inhibit DA release, and therefore, the presence of GABA-R antagonists would preclude this inhibition by GABA. In this scenario, cocaine-induced increases in DA release would be augmented in the presence of GABA-R antagonists. On the contrary, we found that the presence of GABA-R antagonists attenuated cocaine-induced increases in DA release. The involvement of GABA co-release is plausible if GABA co-released from striatal DA axons acts by disinhibition of DA release. GABA, co-released with DA, may inhibit GABA-containing striatal neurons such as MSNs or GABAergic interneurons, to attenuate striatal GABA tone and subsequently augment DA release. Under this scenario, GABA-R antagonists would prevent an augmentation in DA release. This explanation remains unlikely however, due to the fact that the impact of GABA co-released from a single stimulation would have to persist for a minimum of 2.5 minutes, to regulate subsequent DA release. GABA co-release from DA axons does not affect single pulse-evoked DA release (Roberts et al., 2020). Monitoring of striatal GABA, for example, with the fluorescent GABA indicator, iGABASnFR (Marvin et al., 2019), would help to elucidate any changes to striatal GABA tone.

6.1.5. Heterogeneity across the striatum

Heterogeneity across the striatum might affect the interpretation of our data. There is potential for heterogeneity to exist across many aspects, including DA neuron subtype, DAT expression levels, tonic GABA levels, DA neuron co-release capabilities, and the structure of DA release sites.

Several molecularly distinct midbrain DA neuron subtypes have been identified, beyond the distinction between DA neurons originating in the SNc and VTA. A recent suggestion is that there are broadly seven distinct subtypes; *Aldh1a1*- and *Sox6*-positive, *Aldh1a1*-negative and *Sox6*-positive, *Vglut2*-positive (SNc only), *Vglut2*-positive (VTA only), *Vgat*-positive, *Aldh1a1*-positive and *Otx2*-positive, as well as a *Vip*-positive cluster which are predominantly in the retrorubral area, rather than SNc or VTA (Poulin et al., 2020). In addition, there are some poorly defined subtypes which require further characterisation (Poulin et al., 2020). Within these DA neuron subtypes, neurons can be further distinguished. For example, *Anxa1*-expressing DA neurons have been found to reside within the *Aldh1a1*-positive cluster (Azcorra et al., 2023). These molecularly distinct DA neuron subtypes might have implications for data obtained across the striatum. *Vglut2*-positive SNc DA neurons are thought to project to the anterior and intermediate DLS, but not posterior DLS (Poulin et al., 2018). *Aldh1a1*- and *Sox6*-positive SNc DA neurons, on the other hand, project to the DLS across the anterior-posterior axis, with the most dense projections to anterior and intermediate DLS (Poulin et al., 2018). *Aldh1a1*-negative and *Sox6*-positive neurons from the VTA are thought to be the predominant projection to NAcC (Poulin et al., 2018). In general, *ex vivo* recordings in coronal striatal slices presented in this thesis were spread across the anterior-posterior axis, though the majority of observations likely were obtained from intermediate DLS, rather than anterior or posterior. For FSCV experiments, careful notes were taken with regard to the position of the stimulating and recording electrodes, and no differences were observed in data obtained from different positions. It is possible, however, that subtle differences do exist, which could be apparent with carefully-designed experiments to probe regional heterogeneity. The *Vglut2*-positive SNc DA neurons which project to anterior and intermediate DLS (Poulin et al., 2018) are selectively vulnerable to neurodegeneration (Buck et al., 2022). Perhaps these are the neurons which have the densest DAT expression levels. DAT mRNA and gene expression levels are higher in SNc DA

neurons compared to VTA DA neurons (Haber et al., 1995; Poulin et al., 2014). However, the use of DAT^{IREcre} mice in cell profiling experiments might not allow accurate calculations as to DAT density per neuron subtype, because and DAT^{IREScre} heterozygous mice exhibit a 17% decrease in DAT expression levels (Bäckman et al., 2006). We anticipate, however, that decreased DAT expression in DAT^{IREcre} mice will similarly affect SNc and VTA DA neurons.

Heterogeneity in DAT expression levels, or DAT function, likely affect the outcome of our data obtained in DLS and NAcC. We hypothesised that whilst activity at GABA-Rs promotes DAT function in DLS (Chapter 3), GABA-Rs do not robustly regulate DAT function in NAcC, due to less DAT expression in NAcC, compared to DLS. However, even in DAT^{IREcre} heterozygous mice, which have a 17% decrease in DAT expression levels compared to wildtype mice, activity at GABA-Rs strongly supported DAT-mediated changes to DA release in DLS (Fig. 3.8). We cannot rule out the possibility that whilst DAT expression levels do not appear to directly affect a co-operation between DATs and GABA-Rs, perhaps DAT function differs between DLS and NAcC, in a manner which permits or prevents regulation by GABA-Rs. We speculate that differences in membrane voltage dynamics between DLS and NAcC, are at least in part, due to variability in DAT expression levels or DAT function. DLS DA axons tend to exhibit a rebound depolarisation following a spike, whilst NAcC DA axons do not (Chapter 5). The rebound depolarisation is abolished in the presence of DAT inhibitors (e.g.. Fig. 5.12). DAT inhibition produces a prolonged hyperpolarised state following a spike in both DLS and NAcC, but only in DLS is the AHP amplitude changed following DAT inhibition. We propose that the increased DAT levels in DLS promote a shallow AHP and rebound depolarisation, consistent with the depolarising abilities of DATs (Sonders et al., 1997), whereas the decreased DAT levels in NAcC permit a deep AHP and are not sufficient to generate a rebound depolarisation. Future experiments are required to directly test the involvement of DATs in membrane potential dynamics in different striatal sub-regions.

Differential GABA tone and GABA co-release between striatal sub-regions might also have implications for our data. Whilst GABA-R antagonists increase striatal DA release by approximately 25% in both DLS and NAcC, indicating no regional differences in ambient GABA tone, GAT inhibition significantly decreases DA release only in DLS, and not in NAcC (Roberts et al., 2020). This disparity between regions indicates that GABA tone in NAcC is not strongly regulated by GATs. Consistent with this interpretation, GAT-1 and GAT-3 protein expression levels are higher in DLS than NAcC (Roberts et al., 2020). Direct measurements of GABA tone and how this tone might differ between striatal subregions, is difficult, however. Fluorescent tools such as iGABASnFR (Marvin et al., 2019) tend to be useful in making relative measurements, but cannot necessarily reliably read out absolute levels. Furthermore, the high levels of ambient GABA in striatum mean it is difficult to make measurements with such tools without saturation of the fluorescent sensor (personal correspondence). GABA from low threshold spiking GABA interneurons, which are tonically active in slice preparations (Beatty et al., 2012), inhibit DMS DA release (Holly et al., 2021). It is not yet clear what contribution these interneurons make to overall GABA tone. Whilst several different GABA interneuron types exist in the striatum (Section 1.2.2), most of these have been identified in the dorsal striatum, and it is not clear if all subtypes also exist in NAcC. NAcC contains fast spiking interneurons and low threshold spiking interneurons, but ambiguity exists regarding other subtypes (Tepper et al., 2010; Schall et al., 2021). Parvalbumin positive GABA interneurons exhibit a medial-lateral gradient in expression, with the most dense expression in DLS (Luk & Sadikot, 2001; Fino et al., 2018). If in fact GABA interneuron expression differs between DLS and NAcC, this might impact our findings, particularly when interpreting the impact of GABA transmission on DA axon membrane potential. Future investigations are required to determine how GABA signalling might differ across the striatum, and how this impacts on striatal DA release.

GABA co-release appears to similarly inhibit phasic striatal DA release in DLS and NAcC (Patel et al., 2024), indicating that co-release might not greatly differ between SNc and VTA DA neurons. On the other hand, glutamate co-release, appears to differ between striatal subregions. Dopamine axons in NAcSh, but not dorsal striatum, co-release glutamate (Stuber et al., 2010). This subpopulation of dopamine neurons appears to selectively project to NAcSh, rather than NAcC, however (Mingote et al., 2019) so therefore might not impact our interpretation of data between DLS and NAcC.

The consensus is that the predominant form of DA release sites in striatum are 'en passant' varicosities on axons (Sulzer et al., 2016; Liu & Kaeser, 2019). It has been suggested, however, that midbrain DA neurons form distinct synapse types in striatum, including 'en passant' symmetric synapses, as well as asymmetric synapses, or no membrane specialisations (Pickel et al., 1981; Hattori et al., 1991). Furthermore, classical axon terminals may exist, which do not easily stain for tyrosine hydroxylase, but can be labelled with ^{3}H-proteins (Hattori et al., 1991). Striatal DA axons might also form axo-axonic connections with other DA axons, and other non-DA-containing axons (Pickel et al., 1981). A recent study identified a number of striatal DA release sites closely apposed to dendrites on MSNs, forming a 'classical-like' synapse (Kim et al., 2023). Furthermore, the ultrastructure of striatal DA axons share many features of classical synapses, to achieve temporally precise signalling (Bulumulla et al., 2024). We speculate that our *ex vivo* recordings therefore include measurements from distinct DA synapse types in the same recording region, because we did not have single-axon resolution. Measurements obtained with FSCV and ASAP5 imaging were across a population of striatal DA axons. It is plausible that, if we could achieve single-axon resolution, or single-synapse resolution, that regulation of DA release and membrane potential dynamics would differ between synapse types. We speculate that the inhibition on striatal DA release by GABA would predominantly affect DA release-sites that are 'en passant' and operate via volume transmission. DA release sites closely apposed to target neurons,

however, might be less vulnerable to strong regulation by GABA, particularly via $GABA_B$-Rs, and other sources of regulation. It is unknown whether there is variability in how DATs mediate DA release between release site types. Whilst data presented in this thesis likely cancels out any contributions from distinct DA release site types, future experiments could probe how regulation of DA release differs between 'en passant' and 'classical-like' synapses.

In summary, there is potential for much heterogeneity across the striatum, and within DA neurons. Future experiments are imperative to determine how this heterogeneity impacts striatal DA release, and what impact this could have on downstream signalling in the basal ganglia.

6.2. DATs are electrogenic and promote depolarising currents in striatal DA axons

6.2.1. DAT-mediated currents in striatal DA axons

DATs are electrogenic and generate currents greater than predicted for a transporter with a fixed stoichiometry of 1 DA/2 Na^+/1 Cl^- (Sonders et al., 1997; Ingram et al., 2002). DAT-mediated DA uptake generates a transport-coupled, depolarising inward current (Sonders et al., 1997; Carvelli et al., 2004), which increases DA neuron excitability (Ingram et al., 2002). DATs also generate transport-uncoupled currents, which may or may not be distinct from a leak current (Sonders et al., 1997; Carvelli et al., 2004; Meinild et al., 2004; Rodriguez-Menchaca et al., 2012). Aside from increasing neuronal excitability in cultured rat neurons (Ingram et al., 2002), and the interaction with syntaxin 1A in *C. elegans* (Carvelli et al., 2008), the physiological and functional consequences of these DAT-mediated currents are not well understood. In Chapter 5, using a newly developed genetically-encoded fluorescent voltage indicator in a population of mouse striatal DA axons, I demonstrated that DAT-mediated currents assist with membrane repolarisation following action potentials, and limit subsequent action potential size. In DLS, DAT inhibition augments AHP amplitude, and

prolongs time to repolarisation following the AHP. In NAcC, DAT inhibition does not affect AHP amplitude, likely due to the deep AHP already present in NAcC signals when DATs are active. DAT inhibition does prolong time to repolarisation following the AHP in NAcC. The prolonged time to membrane repolarisation observed in both regions under DAT inhibition is consistent with DATs generating depolarising currents. Our data indicate that striatal DATs support axonal membrane depolarisation following an action potential. Data collected thus far are bulk signals from populations of axons, but in the future, to image dynamics at the level of a single axon, multi-photon imaging could be used.

6.2.2. Transport-coupled or transport-uncoupled currents?

DA uptake through DATs generates a transport-coupled, depolarising inward current (Sonders et al., 1997; Carvelli et al., 2004). DATs also exhibit channel-like behaviour and generate transport-uncoupled currents, which might constitute a leak current (Sonders et al., 1997; Carvelli et al., 2004; Meinild et al., 2004; Rodriguez-Menchaca et al., 2012).

We observed DAT-mediated currents following electrical stimulation in striatal DA axons in DLS and NAcC. Whether these DAT-mediated currents in striatal DA axons are associated with translocation of DA or not, remains to be elucidated. In aCSF lacking $[Ca^{2+}]_o$, cocaine-induced changes to membrane potential were prevented. However, these data are non-straightforward to interpret, because the absence of $[Ca^{2+}]_o$ alone will alter membrane excitability. Future experiments are required to determine whether DATs generate transport-coupled or transport-uncoupled currents in striatal DA neurons. One approach would be to inhibit VMAT2 and prevent DA release, but there is a possibility that this could result in reversal of DATs due to toxic levels of cytosolic DA, and induce DA efflux via DATs. An elegant approach could be to deliver tetanus toxin light chain conditionally to DA neurons, to specifically abolish exocytosis of DA, and therefore DA uptake. If DAT-mediated currents

remain following tetanus toxin light chain administration, it is likely that DAT-mediated currents are transport-uncoupled.

Transport-uncoupled Cl^- currents via DATs increase neuronal firing rate (Ingram et al., 2002). In oocytes expressing hDAT, these uncoupled currents are inhibited by DA (Sonders et al., 1997), but potentiated by DA in rat cultured neurons (Ingram et al., 2002). In mouse, therefore, it is plausible that these uncoupled currents are not inhibited by DA. In both hDAT and rDAT, transport-uncoupled currents are blocked by cocaine, which results in membrane hyperpolarisation (Sonders et al., 1997; Ingram et al., 2002). It is likely that, if both types of current are generated in our experiments, cocaine will inhibit transport-coupled and -uncoupled currents. Transport-uncoupled currents in particular, are thought to be important for neuron excitability (Ingram et al., 2002; Sulzer & Galli, 2003). If conductances mediated by Cl^- appear important, future experiments to DA neuron function, future experiments could utilise a fluorescent intracellular Cl^- indicator.

It is unclear however, whether transport-independent currents will impact on short-term plasticity in DA release. It has been reported that α-synuclein potentiates transport-uncoupled currents (Swant et al., 2011). However, in mice overexpressing α-synuclein, STF is only minimally affected, and STD is unaffected (Threlfell et al., 2021). Our data indicate that DAT-mediated currents are consistent with DATs governing STD, therefore, if DATs do govern STD via changing axon excitability, it is most likely that the currents we have observed are transport-coupled. Future experiments will contribute to our understanding of the contexts in which DAT-mediated currents occur, and their relevance to physiology. Whilst DAT-mediated currents are consistent with the electrogenic and channel-like properties of DATs (Sonders et al., 1997; Carvelli et al., 2004), it is possible that DATs couple to other channels to regulate DA axon excitability. Some of these potential regulatory partners are discussed below.

6.2.3. Can all regulation of striatal DA release be explained by membrane potential dynamics?

In Chapter 5, I investigated whether DATs, GABA-Rs and GIRK channels shape axonal membrane potential, using the ASAP5 voltage indicator (Hao et al., 2024) across a population of striatal DA axons. Data indicate that activity at DATs strongly promotes repolarisation of the axonal membrane after hyperpolarisation, and regulates subsequent action potential size, independent of D_2-like-R activation. Activity at $GABA_A$- and $GABA_B$-Rs also contributes to membrane repolarisation after hyperpolarisation, particularly following more than one action potential. Activity at GIRK channels does not appear to robustly modify DA axon membrane potential. The ASAP5 voltage indicator (Hao et al., 2024) is a powerful tool for assessing membrane potential dynamics, and allows insight into electrical activity across previously inaccessible axons. I will now consider how much of the published evidence for the regulation of striatal DA release could be explained by regulation of axonal membrane potential.

DATs are known to limit striatal DA release probability by immobilising a portion of the vesicle pool when DATs are active (Venton et al., 2006; Kile et al., 2010). DAT inhibition increases striatal DA release probability by mobilising these (Venton et al., 2006; Kile et al., 2010). Changes in axonal membrane voltage appear to fail to account for this increase in striatal DA release upon application of pharmacological DAT inhibitors, presumably because vesicle immobilisation by DATs is downstream of membrane voltage. DAT inhibition with cocaine does not significantly increase spike height or AUC in DLS or NAcC (Fig. 5.12), in fact, if any changes are present, spike size is slightly decreased in the presence of cocaine. However, it is not implausible that the prolonged hyperpolarised state following the spike in the presence of DAT inhibitors affects axonal Ca^{2+} influx, synapsin activity, and DA release. In the basolateral amygdala, Ca^{2+} activated K^+ channels mediate a hyperpolarised state following a

burst of action potentials, and the presence of this afterhyperpolarisation attenuates EPSPs and slightly minimises dendritic Ca^{2+} influx (Power et al., 2011). At the calyx of Held, however, absolute membrane potential following an action potential-like stimulus has only minimal effects on the VGCC response or EPSC (Clarke et al., 2016). It therefore likely depends on intrinsic factors of a given neuron, whether an afterhyperpolarisation will affect neurotransmitter release, and this is currently not known for striatal DA axons.

Whether or not the post-spike membrane potential impacts striatal DA release is also a consideration when interpreting the effects of GABA-R activity on DA axon activation. Striatal GABA inhibits DA release via $GABA_A$-Rs and $GABA_B$-Rs (Pitman et al., 2014; Brodnik et al., 2019; Lopes et al., 2019; Roberts et al., 2020). Using patch-clamp electrophysiology at the main branch of a DA axon in the medial forebrain bundle, activation of $GABA_A$-Rs attenuates action potential amplitude (Kramer et al., 2020). However, we did not observe a significant augmentation of spike height or spike AUC upon $GABA_A$-R inhibition when measuring changes in membrane potential across a population of striatal DA axons (Fig. 5.22 & 5.23). The presence of GABA-R antagonists, however, modifies the post-spike membrane potential (Fig. 5.22 & 5.23), indicating that GABA-Rs might also modulate DA axon membrane potential on a slightly slower timescale immediately following an action potential. Changes to axonal membrane potential following an action potential will have consequences for excitability and subsequent spiking. If we assume that post-spike membrane potential will have implications for VGCC recruitment, axonal Ca^{2+} entry, and vesicle recruitment, then DAT- and GABA-mediated changes to DA axon membrane potential might indeed be able to explain changes to striatal DA release. However, DAT inhibition and GABA-R antagonists produce a more hyperpolarised state following the spike, which might not be consistent with the increased release probability in DAT inhibitors and GABA-R antagonists.

Striatal DA release is modulated by several other players in the striatum, which were not yet considered in this thesis. Striatal DA release is attenuated by adenosine acting at A_1Rs (Roberts et al., 2022), and feasibly, this attenuation could be explained by an impact on DA axon membrane potential. Although A_1Rs are GPCRs, these receptors activate two-pore-domain K^+ channels in mitral olfactory neurons (Rotermund et al., 2018) and VGCCs in *Xenopus* oocytes (Brown & Dale, 2000) and basolateral amygdala neurons (McCool & Farroni, 2001). Hyperpolarisation induced by A_1R activation and subsequent K^+ and Ca^{2+} channel modulation could therefore explain the inhibition of striatal DA release by adenosine A_1R activation.

Substance P increases striatal DA release in striosomes, decreases striatal DA release at boundaries between striosome and matrix, and does not impact striatal DA release in matrices (Brimblecombe & Cragg, 2015). Substance P acts via NK_1 GPCRs (Maggi, 1995), and is associated with membrane depolarisation via Transient Receptor Potential (TRP) channels in noradrenergic parietal cortex neurons (Min et al., 2008, 2009). NK_1 receptor activation is also depolarising in cortical neuronal nitric oxide synthase-containing neurons (Dittrich et al., 2012) and increases excitability and firing rate in the dorsal raphe nucleus (Conley et al., 2002). Therefore, the increase in striatal DA release in striosomal compartments might be due to axonal membrane depolarisation via NK_1 receptors. However, substance P decreases DA release at boundaries between striosome and matrix (Brimblecombe & Cragg, 2015). This may in fact also be explained by effects on membrane potential. In vagal afferent neurons, substance P or NK_1 receptor agonism is hyperpolarising (Jafri & Weinreich, 1996). Perhaps substance P has opposing effects on DA axon membrane potential, dependent on location within striosome or matrix, or indeed the boundary between the two, which then regulates DA release bidirectionally.

The VGSC inhibitor, lidocaine, decreases DA release by ~30% in DLS (Condon et al., 2019). In preliminary experiments presented in this thesis, lidocaine also decreased DA release in DLS, albeit to a smaller extent (Fig. 5.13G). Unexpectedly, lidocaine did not have any effect on membrane potential in striatal DA axons when measured using the ASAP5 voltage indicator (Hao et al., 2024). Either ASAP5 is not sensitive enough to small magnitude, fast, changes in membrane potential across a population of DA axons, or, lidocaine acts at another cell type to indirectly decrease striatal DA. For example, the magnitude of attenuation in DA release by lidocaine mirrors the magnitude of attenuation by $GABA_A$- or $GABA_B$-R agonism (Lopes et al., 2019). It is plausible that lidocaine acts on a distinct cell type to disinhibit GABA, leading to increased GABA tone, and therefore attenuated DA signalling. This speculation can be tested by using tools such as iGABASnFR (Marvin et al., 2019) to detect changes in striatal GABA in response to application of lidocaine.

The VGKC inhibitor, 4-AP, increases striatal DA release (M. D. Condon et al., 2019). This observation can easily be explained by changes to axonal membrane potential. We observed that 4-AP, as expected, widens action potentials in striatal DA axons, in both DLS and NAcC (Fig. 5.7B, D). Action potential widening is consistent with increased neurotransmitter release. Therefore, changes to striatal DA release can be explained entirely by membrane voltage.

In DLS, striatal DA release is supported by T-type, P/Q-type, N-type, and LTCCs, whereas in NAcC, DA release is predominantly supported by only P/Q-type and N-type VGCCs (M. D. Condon et al., 2019). Recent evidence demonstrates that the control of DA release by LTCCs co-varies with Parkinson's disease risk factors, such as sex, DAT levels, and DA neuron subtype (Brimblecombe et al., 2024). However, LTCC inhibition does not affect SNc DA neuron pacemaking (Guzman et al., 2009). It is therefore possible that the effects of LTCC inhibiton on striatal DA release are downstream of membrane voltage, and instead affect

axonal Ca^{2+} entry. It appears likely that a relationship between LTCCs and DA release is more complex, however, due to the observation that DAT-mediated depolarisations activate LTCCs (Cameron et al., 2015). Perhaps, LTCCs support DA release via a complex interaction with DATs and membrane potential. DATs generate depolarising currents immediately following an action potential (Fig. 5.12), which are expected to then rapidly activate LTCCs (Cameron et al., 2015). LTCCs might then mediate further depolarising currents to support axonal Ca^{2+} entry and DA release from even a single action potential. Whilst LTCC inhibition does not affect affect pacemaking in SNc (Guzman et al., 2009), it is possible that the thin, branched morphology of DA axons renders axonal membrane potential dynamics more susceptible to changes in VGCC activity, than at the soma. Future experiments are necessary to test these possibilities.

Although assessing membrane potential dynamics in striatal axons might not be sufficient to explain all published evidence for the local regulation of striatal DA release, it is plausible that many observations can be explained by changes to axonal activation. If indeed the post-spike membrane potential has implications for VGCC recruitment, Ca^{2+} entry, and DA release, then it is possible that changes to membrane potential are sufficient to explain the majority of local regulation of DA signalling. In any case, assessing axonal membrane potential remains a powerful technique to understand DA axon physiology, and particularly to detect subthreshold events which might have implications for subsequent spiking. Future in-depth experiments will test the capabilities of measuring membrane potential to explain changes to DA release in the striatum, as well as neurotransmitter release from various other cell types, particularly those with fine structures which are currently inaccessible with patch clamp electrophysiology.

6.3. Potential mechanisms underlying DAT and GABA-R function in regulating DA release and axonal excitability

6.3.1. Vesicle immobilisation

The ability of GABA-Rs to support DAT-mediated changes to single pulse-evoked DA release points to a potential involvement of vesicle mobilisation. DATs immobilise a synapsin-dependent vesicle reserve pool in DA neurons, which is mobilised for release when DAT inhibitors are present (Venton et al., 2006; Kile et al., 2010). Striatal DA release from synapsin TKO mice is elevated compared to wild-type mice, and DAT inhibitors do not increase DA release in synapsin TKO mice (Venton et al., 2006; Kile et al., 2010). These results indicate that DATs require synapsins to interact with the vesicle pool. Any mechanism, therefore, which modulates the impact of DATs on initial release probability, could be interacting with the vesicle pool. We showed that GABA-R antagonism attenuated the effect of DAT inhibitors on striatal DA release, indicating that activity at GABA-Rs supports DAT-mediated changes to initial DA release. Future experiments should test whether activity at GABA-Rs supports DATs in mobilising a vesicle reserve pool. One approach to test this would be to apply long stimulation trains to release and deplete the readily-releasable vesicle pool, and test whether the presence of GABA-R antagonists still attenuates the effect of cocaine on DA release. If depletion of the readily-releasable vesicle pool results in the same amount of DA released, regardless of whether GABA-R antagonists are present, this would indicate that GABA-Rs do not support DAT-mediated vesicle immobilisation. On the other hand, if depletion of the readily-releasable vesicle pool results in less DA released in the presence of GABA-R antagonists, this would support the idea that GABA-Rs are involved in vesicle pool modifications by DATs. Results could be confounded, however, by any other mechanisms involved in the co-operation between DATs and GABA-Rs. Furthermore, GABA-Rs may not directly interact with the vesicle pool, but instead with synapsins. Experiments could be

conducted in synapsin TKO mice, but would be difficult to interpret due to the lack of any effect of cocaine on initial DA release in these mice. Perhaps GABA-Rs act in parallel to DATs, immobilising the same vesicle reserve pool, which is released upon application of GABA-Rs, thus reducing the number of vesicles available for DATs to immobilise. This explanation seems unlikely however, as the mechanisms via which GABA-Rs limit neurotransmitter release are well-characterised. Future work is required to test whether GABA-Rs interact with synapsins, or the vesicle pool, to modulate DAT function.

6.3.2. Na^+ leak channels (NALCN)

NALCN is present on SNc and VTA DA cell bodies, particularly localised to proximal dendritic compartments, where these channels mediate pacemaking behaviour (Khaliq & Bean, 2010; Philippart & Khaliq, 2018; Um et al., 2021; Hahn et al., 2023; Cobb-Lewis et al., 2023; Wang et al., 2024). In SNc DA neurons, NALCN-mediated currents are potentiated in low $[Ca^{2+}]_o$ (Philippart & Khaliq, 2018). Loss of NALCN drastically reduces pacemaking activity, demonstrating that NALCN contribute to the generation of spontaneous activity in SNc DA neurons (Philippart & Khaliq, 2018). NALCN can forms complexes with GPCRs, and activation of GPCRs can modulate NALCN activity (Cochet-Bissuel et al., 2014).

NALCN on SNc DA neurons are inhibited upon activation of D_2-like-Rs and $GABA_B$-Rs (Philippart & Khaliq, 2018), a finding which could plausibly be extended to other $G_{i/o}$-coupled GPCRs. The authors suggest that NALCN are a third mediator via which $G_{i/o}$-coupled GPCRs decrease neuronal excitability, in addition to VGCCs and GIRK channels (Philippart & Khaliq, 2018). To test whether $GABA_B$-Rs modulate NALCN-mediated currents independent of GIRK channel signalling, the authors use tertiapin-Q and Ba^{2+} to inhibit GIRK channels, and show that the $GABA_B$-R agonist, baclofen, still slows firing in DA neurons, an effect which is abolished in mice lacking NALCN (Philippart & Khaliq, 2018). Whilst data obtained from mice lacking NALCN is promising, the results are possibly confounded by poor pharmacological

tools to target GIRK channels. Tertiapin-Q binds only to GIRK1 containing heterotetramers (Jin & Lu, 1998; Jin et al., 1999; Kanjhan et al., 2005), yet SNc DA neurons express only GIRK2 homotetramers (Inanobe, Yoshimoto, et al., 1999; del Burgo et al., 2008; Lüscher & Slesinger, 2010). Ba^{2+} is a non-selective tool which acts as a channel blocker at a large number of K^+ channels (British Pharmacological Society Guide to Pharmacology). Regardless of whether $GABA_B$-R activation inhibits NALCN independent of GIRK channels, these findings demonstrate a functional relationship between $GABA_B$-Rs and NALCN in midbrain DA neurons.

NALCN expression in the dendritic compartment renders SNc DA neurons highly excitable (Cobb-Lewis et al., 2023; Hahn et al., 2023). Plausibly, any mechanism which affects Na^+ conductance in DA neurons may also modulate DAT function. DATs are members of the NSS family, translocating DA with two Na^+ ions and one Cl^- ion (Krueger, 1990; McElvain & Schenk, 1992; Gu et al., 1994). DATs exhibit channel-like behaviour, generating depolarising currents larger than predicted for this fixed stoichiometry (Sonders et al., 1997; Ingram et al., 2002; Carvelli et al., 2004). DATs are also thought to mediate a Na^+ leak conductance (Sonders et al., 1997; Carvelli et al., 2004; Rodriguez-Menchaca et al., 2011). Our data indicate that activity at GABA-Rs promotes DAT function. In the context of NALCN, $GABA_B$-R activation inhibits NALCN (Philippart & Khaliq, 2018), but it is unclear what effect, if any, $GABA_B$-R inactivation has on NALCN. It is also not known whether $GABA_A$-Rs functionally interact with NALCN. If NALCN is involved in a co-operation between DATs and GABA-Rs, activity at GABA-Rs would inhibit NALCN conductances, which would promote DAT function. Since DATs and NALCN appear to function in parallel, it seems unlikely that NALCN inhibition would promote DAT function. Nevertheless, this could be tested by pharmacologically inhibiting NALCN, then applying a DAT inhibitor, to test whether results parallel those in the presence of GABA-R antagonists. It is important to note it is not yet known whether NALCN is expressed on DA axons in the striatum, or whether expression is restricted to somatodendritic regions.

6.3.3. Hyperpolarisation-activated cyclic nucleotide-gated (HCN) channels

HCN channels are, as the name indicates, activated by hyperpolarisation and are generally thought to be open at resting membrane potential (Benarroch, 2013). HCN channels are permeable to Na^+ and K^+, generating currents known as I_h currents, which regulate not only resting membrane potential, but also signal integration in dendrites, and oscillatory behaviour (Biel et al., 2009; Benarroch, 2013). HCN channels are present on midbrain DA neurons (Mercuri et al., 1995; Neuhoff et al., 2002; Cobb-Lewis et al., 2023; Wang et al., 2024), but generally do not contribute to spontaneous activity (Mercuri et al., 1995; Cobb-Lewis et al., 2023; Wang et al., 2024), apart from in SNc, calbindin-D28k negative, DA neurons (Neuhoff et al., 2002). HCN channels typically depolarise, but depending on the cell type and other effector mechanisms, HCN channels can lead to excitation or inhibition (Kase & Imoto, 2012).

In the soma of SNc and VTA DA neurons, HCN channels regulate AHP amplitude and duration (Lammel et al., 2008; Wanat et al., 2008; Chu & Zhen, 2010). Pharmacological inhibition of I_h currents in VTA neurons increases AHP amplitude and prolongs duration of membrane repolarisation (Wanat et al., 2008), somewhat mirroring the effects we observed with cocaine on axonal membrane potential. On the other hand, ethanol promotes HCN channel function in DA neurons, leading to reduced AHP amplitude and duration (Okamoto et al., 2006).

In VTA DA neurons, HCN channels form structural complexes with $GABA_B$-Rs (Pérez-Garci et al., 2025). HCN channel-mediated I_h currents are generated upon membrane hyperpolarisation by either $GABA_A$-Rs or $GABA_B$-Rs (Pérez-Garci et al., 2025). $GABA_A$-R-mediated HCN channel activation depends, at least in part, on colocalization of HCN channels and $GABA_B$-Rs (Pérez-Garci et al., 2025), supporting the idea that $GABA_A$-R or $GABA_B$-R function is somewhat interdependent. I_h current activation attenuates neuronal inhibition produced by GABA-mediated hyperpolarisation in VTA DA neurons (Pérez-Garci et

al., 2025). Disruptions to $GABA_B$-R and HCN channel complexes prolongs GABAergic inhibition of DA neurons, and heightens anxiety-like behaviour (Pérez-Garci et al., 2025). To our knowledge, no direct actions of HCN channels and DATs have been reported. Bath application of cocaine decreases of I_h current activation in VTA DA neurons, yet cocaine self-administration enhances I_h current activation (Mu et al., 2023). The authors speculate that modulation of I_h current by cocaine is via D_2-like-Rs, rather than via a direct interaction with DATs (Mu et al., 2023). Since HCN channels are activated upon membrane hyperpolarisation by GABA at the soma, we would expect, if HCN channels are expressed in DA axons, that the same is true in axons. GABA-Rs are tonically activated by GABA in the striatum (Lopes et al., 2019; Roberts et al., 2020), therefore, we might expect that HCN channels are also frequently active. We speculate that activation of HCN channels may promote DAT function. The presence of GABA-R antagonists would prevent GABA-mediated hyperpolarisations that activate HCN channels, thereby attenuating DAT function. Whilst purely speculative at the moment, future experiments could inhibit HCN channels and test for any impact on DAT function.

If HCN channels are depolarising in striatal DA axons, they could be working in parallel, or to support, DAT-mediated depolarisations. When HCN channels are inhibited, AHP amplitude and duration are increased in VTA DA neurons (Wanat et al., 2008). We observed the same pattern for DATs in striatal DA axons using voltage indicator imaging; DAT inhibition increases AHP amplitude in DLS and prolongs AHP duration in DLS and NAcC. HCN channels may therefore not only be implicated in the co-operation between DATs and GABA-Rs, but also in DAT-mediated currents and DA re-release. Future experiments should test the impact of inhibiting HCN channels on membrane potential in striatal DA axons, and whether this interacts with DAT-mediated currents.

6.3.4. LTCCs

Depolarisation associated with DA uptake through DATs can activate LTCCs (Cameron et al., 2015). Amphetamine-induced DA depolarisations through DATs also activates LTCCs, more potently than DA uptake (Cameron et al., 2015). Furthermore, DAT inward currents can activate LTCCs even in the absence of DA or amphetamine (Cameron et al., 2015). These findings demonstrate a functional relationship between DATs and LTCCs. The LTCC inhibitor, isradipine, modulates striatal DA release only when DATs are active, indicating that DATs support LTCC function (Brimblecombe et al., 2024). If DAT-mediated depolarisations activate LTCCs, LTCCs may contribute to axonal membrane repolarisation following hyperpolarisation. LTCC activation generally requires a large membrane depolarisation however (Lipscombe et al., 2004; Snutch, 2009), so it is plausible that LTCCs are not activated during DAT-mediated depolarisations following a single spike in membrane potential. Significant functional variability does exist among LTCCs however, and certain subtypes, such as $Ca_V1.3$ and 1.4, do not require such large depolarisations (Lipscombe et al., 2004). Activation of LTCCs upon DAT-mediated depolarisations, allowing LTCCs to support striatal DA release (Brimblecombe et al., 2024), may offset some of the DAT-mediated limitations on subsequent DA release. Future investigations could test whether LTCCs significantly contribute to DA axon excitability, and if so, whether LTCC currents are activated upon DAT-mediated depolarisations.

6.3.5. Ca^{2+} activated K^+ channels

The family of Ca^{2+} activated K^+ channels include BK (big conductance), SK (small conductance), and IK (intermediate conductance) channels, though BK and SK channels are the only forms predominantly expressed in the brain (Latorre et al., 1989; Sah, 1996; Sah & Faber, 2002) IK channels have been identified in the hippocampus, however (Turner et al., 2015). Ca^{2+} entry through VGCCs activates BK and SK channels (Sah, 1996; Sah & Faber,

2002). BK channels mediate the voltage-sensitive I_C current, which, in some neurons, is responsible for membrane repolarisation during the action potential downstroke (Sah, 1996). SK channels mediate a current which is not voltage sensitive, and has been defined, at least in some cases, as I_{AHP} (Sah, 1996; Sah & Faber, 2002). Neuronal action potentials are generally followed by a fast AHP (fAHP), then a medium AHP (mAHP), and a slow AHP (sAHP), although the existence and kinetics differ across neuron types (Sah & Faber, 2002). The fAHP is thought to be due to BK channel activation, and the mAHP is thought to be due to SK channel conductances (Sah & Faber, 2002). The sAHP most commonly occurs only following a train of action potentials, although it has been described to follow single action potentials on occasion (Sah & McLachlan, 1991; Sah & Faber, 2002). Mechanisms underlying the sAHP are not fully understood, and may be due to an interaction between IK channels, LTCCs, ryanodine receptors, and the Na^+/K^+ pump (Sahu & Turner, 2021). The modulation of the AHP, particularly in DLS, by cocaine, indicates a possible role for Ca^{2+} activated K^+ channels.

SNc DA neurons have been shown to exhibit a fAHP, mAHP, and sAHP (Wolfart et al., 2001; Kimm et al., 2015). In the somatic region of SNc DA neurons, BK channels inhibition increases action potential width but paradoxically increases the fAHP amplitude, though this is likely due to increased K_V2 channel activation upon BK channel inhibition (Kimm et al., 2015). BK channel inhibition increases firing rate in SNc DA neurons (Kimm et al., 2015). At the soma of VTA DA neurons, genetic ablation of BK channels increases action potential width and reduces fAHP amplitude, and increases firing rate (Juarez et al., 2023). SK channel expression has been shown to differ between SNc and VTA DA neurons (Wolfart et al., 2001). At the soma of SNc neurons, SK channels are responsible for the mAHP, and firing rate (Wolfart et al., 2001). SK channels are expressed in lower levels in VTA DA neurons, and do not contribute to the firing rate (Wolfart et al., 2001). In SNc DA neurons, positive allosteric modulation of SK channels deepens and prolongs the AHP, whereas inhibiting SK channels

has the opposite effect (Higgs et al., 2023). SK channel inhibition in VTA DA neurons reduces AHP amplitude and duration (Blankenship et al., 2023).

Together, these data indicate a strong role for BK and SK channels in the action potential waveform and firing rate in the somatic region of SNc and VTA DA neurons. It is currently unclear whether these channels are expressed and contribute to the action potential waveform in DA axons, though it seems likely. ASAP5 signals in DLS appear to have a fAHP, then a rapid rebound depolarisation. ASAP5 signals from NAcC DA axons exhibit a more pronounced and prolonged AHP. Upon DAT inhibition, the AHP amplitude is increased in DLS, and the rebound depolarisation is lost. In NAcC, DAT inhibition does not affect the immediate AHP amplitude, but prolongs membrane repolarisation on a longer timescale. The mAHP in SNC DA neurons is at its peak within ~50 ms following stimulation, and decayed over 100-200 ms (Wolfart et al., 2001), the timing of which is similar to what we observed in DLS DA axons in the presence of cocaine. Furthermore, signals obtained in 0 mM $[Ca^{2+}]_o$ demonstrated a loss of the rebound depolarisation in DLS, and the deep AHP in NAcC, implicating Ca^{2+} channels in these components. To test for the involvement of BK or SK channels in the action potential waveform, and any interaction with DATs, experiments could be carried out using pharmacological inhibitors or positive allosteric modulators of these channels.

6.3.6. Phosphatidylinositol-4,5-bisphosphate (PIP_2)

PIP_2 is a glycerophospholipid with varied roles in intracellular trafficking, membrane organisation, and regulation of ion channels (Mandal, 2020; Tariq & Luikart, 2021). PIP_2 is implicated in the regulation of several potentially relevant mechanisms. In DA neurons, DATs are clustered in nanodomains that overlap with PIP_2 expression (Lycas et al., 2022), and cholesterol (Rahbek-Clemmensen et al., 2017). DATs organised in these clusters preferentially adopt an inward-facing conformation, whereas unclustered DATs adopt an

outward-facing conformation (Lycas et al., 2022). Clustering of DATs into PIP_2-containing nanodomains is regulated by membrane excitability, D_2-like-Rs and VGCCs (Lycas et al., 2022). A DAT variant with a modified C terminus and PDZ binding domain (DAT-AAA) exhibits in nanodomains more often, and exhibits altered DAT function (Sørensen et al., 2021). PIP_2 binds to DATs and supports amphetamine actions at DATs (Hamilton et al., 2014; Khelashvili et al., 2015; Belovich et al., 2021). Perhaps, PIP_2 also supports actions of cocaine at DATs. Like DATs, $GABA_A$-Rs appear to bind PIP_2 molecules, which may be important for $GABA_A$-R distribution (Laverty et al., 2019). Further implicating PIP_2, GIRK2 channels are regulated by PIP_2 and cholesterol (Mathiharan et al., 2021). Like DATs, GIRK2 channels exhibit a cholesterol binding site, and PIP_2 interactions with GIRK channels are supported by binding of cholesterol (Mathiharan et al., 2021). PIP2 promotes HCN channel function (Pian et al., 2007). Perhaps interactions between DATs and GABA-Rs are linked to their expression in the same PIP_2-containing nanodomains.

It is most likely that several mechanisms are implicated in the control of DA release by DATs and GABA-Rs. In pyramidal neurons, a combination of inwardly rectifying K+ channels (which are modulated by PIP_2 (Hansen et al., 2011)), K^+ leak channels, and HCN, mediate excitability in dendrites (Day et al., 2005). Perhaps a similar combination of factors govern DA axon excitability, and therefore DAT and GABA-R function.

6.4. Investigating DAT-GABA co-operativity in disease and *in vivo*

6.4.1. Translatability to *in vivo* contexts

Whilst conducting experiments in *ex vivo* brain slice preparations is advantageous for expanding our understanding of the mechanisms underlying DA transmission, this experimental approach has its limitations. *Ex vivo* striatal slices do not contain the somatodendritic compartments of midbrain DA neurons. Therefore, DA axons within the

striatum are ‘silent’ and do not fire action potentials, unless stimulated electrically or optogenetically. This contrasts with midbrain DA neurons *in vivo*, which are understood to exhibit tonic activity in the range of 1-10 Hz (Grace & Bunney, 1983a; Freeman et al., 1985). Upon the presence of salient stimuli, midbrain DA neurons exhibit a burst firing pattern in the range of 20-40 Hz, although frequencies of up to 100 Hz are occasionally reached (Grace & Bunney, 1984; Hyland et al., 2002). A proportion of DA neurons in the SNc are understood to be ‘silent’, although this population likely only makes up 2% of SNc DA neurons at most (Dai & Tepper, 1998). However, SNc DA neurons exhibit vast arbourisations in the striatum, with each nigrostriatal axon thought to innervate, on average, 2.7% of the striatum in rodents (Matsuda et al., 2009). Therefore, even small populations of midbrain DA neurons may have profound impact on striatal activity.

Whilst electrical stimulation paradigms used in this thesis consisted of single- or paired-pulses only, and did not include any longer pulse trains, paired-pulse bursts are in fact very relevant to an *in vivo* context, particularly in response to salient stimuli. The most common number of action potentials in a burst in SNc DA neurons is two action potentials, with the overall average burst consisting of three to four action potentials (Grace & Bunney, 1984). An *ex vivo* preparation is therefore useful to determine how much DA might be released in striatum by subsequent action potential. Nonetheless, the majority of midbrain DA neurons *in vivo* are tonically active, which is not the case in *ex vivo* striatal slices. It is therefore likely that the concentration of DA released in response to a single electrical stimulation, is higher than that which would be achieved *in vivo* from a tonically active DA neuron. Midbrain DA neurons tend to fire in an irregular manner, with an inter-spike interval of around 200-250 ms for irregularly firing, single spiking neurons (Grace & Bunney, 1984). DA neurons which exhibit bursting behaviour have an inter-spike interval of less than 75 ms (Grace & Bunney, 1984).

We speculate that the majority of midbrain neurons are firing irregularly every ~200 ms, and therefore are likely exhibiting STD. We therefore propose, in light of data presented in this thesis, that under 'normal' conditions, DATs support STD in striatal DA release, potentially by operating depolarising currents following each action potential. However, when DATs are inhibited, such as in the case of drug taking, STD will be relieved, potentially due to the hyperpolarised state following each action potential, and therefore striatal DA concentrations will be higher from each subsequent action potential. Furthermore, in cases where DAT function might be augmented, such as in early Parkinson's disease (Threlfell et al., 2021), striatal DA concentrations will be attenuated from each subsequent action potential, promoting a hypo-DA state.

In the case of midbrain DA neuron bursts, particularly those occurring at a frequency greater than ~50 Hz, we speculate that DAT activity supports axonal Ca^{2+} handling in a manner which promotes augmented striatal DA release from a subsequent action potential. This might operate particularly in neurons originating in VTA and projecting to NAcC, due to the prominent STF at firing frequencies of ≥25 Hz, and might be highly relevant to the context of drug-taking and drug-seeking.

Finally, if electrical coupling is present in midbrain DA neurons, our *ex vivo* observations following field stimulation, might be applicable to DA neurons *in vivo*. DA neurons form dendro-dendritic synapses with one another in SNc and VTA (Wilson et al., 1977; Bayer & Pickel, 1990), and likely form axo-axonic synapses with one another in the striatum (Pickel et al., 1981). Electrical coupling has been reported for DA neurons in the striatum (Grace & Bunney, 1983b; Vandecasteele et al., 2005, 2008). We speculate that DATs will have a profound impact on striatal DA signalling if electrical activity in neighbouring DA axons is coupled under certain conditions. Future experiments are necessary to explore the relevance of observations obtained in *ex vivo* preparations to DA neuron activity *in vivo*.

6.4.2. Substance use disorders

Studies exploring the impact of GABA-R signalling on psychostimulant-mediated behaviours, largely focus on the role of $GABA_B$-Rs, rather than $GABA_A$-Rs. Intra-VTA infusion of the $GABA_B$-R agonist, baclofen, prevents cocaine-induced locomotion (Kalivas et al., 1990) and attenuates cocaine self-administration (Shoaib et al., 1998; Brebner et al., 2000). Striatal baclofen infusions attenuate cocaine self-administration (Shoaib et al., 1998; Brebner et al., 2000), as do systemic baclofen injections (Di Ciano & Everitt, 2003). Systemic baclofen attenuates amphetamine self-administration and prevents amphetamine-induced increases in DA efflux in NAc (Brebner et al., 2005). Striatal drug infusions in particular could plausibly be attenuating striatal GABA release by acting at $GABA_B$-Rs on GABA-containing neurons, and have a net effect of decreasing GABAergic inhibition of DA axons. From this perspective, these behavioural results could be consistent with our finding that attenuating GABAergic inhibition of DA axons decreases the effect of cocaine on DA release.

However, systemic or intracranial drug infusions lack specificity, making it difficult to interpret the mechanisms underlying the resultant behaviour. Updated tools have paved the way for a more accurate dissection of mechanisms. Viral deletion of $GABA_B$-Rs in VTA DA neurons increases cocaine-induced increases in locomotor behaviour in a mixed-sex cohort (Edwards et al., 2017). Similarly, $GABA_B$-R (and D_2-R) genetic ablation in VTA DA neurons potentiates cocaine-induced locomotion, in male, but not female, mice (DeBaker et al., 2021). These results indicate that $GABA_B$-R activation attenuates the behavioural effects of cocaine, consistent with findings that GIRK channel ablation augments cocaine-associated behaviours. SNX27 knockout reduces $GABA_B$-R mediated GIRK currents, and enhances cocaine-induced locomotor activity (Munoz & Slesinger, 2014). The impact of GIRK channels on cocaine-associated behaviours may depend on GIRK channel subunit composition, however. Overexpression of GIRK2c in VTA DA neurons reduces cocaine-induced locomotor

activity, whereas overexpression of GIRK3 enhances cocaine-induced locomotor activity (McCall et al., 2019).

An attenuation of cocaine potency by $GABA_B$-Rs is not necessarily consistent with our findings that GABA-Rs support DAT function, and therefore promote the effect of cocaine at DATs. However, our experiments were conducted in the striatum, excluding DA somatodendritic influence, or influence from GABAergic circuits in the midbrain. Furthermore, interpreting directionality between cocaine potency at DATs, cocaine intake, and behavioural effects, is non-trivial. On one hand, high cocaine potency at DATs is associated with high cocaine intake, and rates of intake (Alonso et al., 2022), potentially because the rewarding effects of cocaine have been amplified. On the other hand, lower cocaine potency may require animals to self-administer higher amounts of cocaine, to achieve the desired effect. In behavioural experiments, the pattern of intake is thought to be a key factor in determining cocaine potency, tolerance, and sensitisation (Calipari et al., 2013), and DA release in response to drug-related cues (Burgeno et al., 2023). Therefore, initial cocaine potency will impact the rate of intake, and subsequently, the rate of intake will impact cocaine potency at DATs. Unravelling directionality is complex. Critically, we did not find evidence that GABA-Rs change DA uptake. Perhaps, uptake rate is particularly influential for cocaine-associated behaviours. To test for a co-operation between DATs and GABA-Rs *in vivo*, we would suggest targeting of both $GABA_A$- and $GABA_B$-Rs, because in our *ex vivo* preparation, this combination of pharmacology decreases cocaine-induced DA release. Using techniques such as drugs acutely restricted by tethering (DART; Shields et al., 2017, 2024), will assist in specifically targeting GABA-Rs on DA neurons. Furthermore, a sensible initial approach could be to use an anaesthetised preparation, to test whether GABA-R antagonists also attenuate cocaine-induced DA release in the intact brain, before transitioning to behaviour. Finally, we observed a robust relationship between DATs and GABA-Rs in DLS only, and not in NAcC. Most, if not all, of the behavioural studies above have

been conducted on VTA DA neurons, which predominantly project to NAcC. This is an important consideration in interpreting the behavioural relevance of the *ex vivo* data in this thesis.

6.4.3. Parkinson's disease

SNc DA neurons are selectively affected in PD, whilst the neighbouring VTA DA neurons remain generally unafflicted. DATs are implicated in this selective vulnerability; brains of PD patients exhibit attenuated DAT density, and DA uptake is increased in early stages of PD (Lee et al., 2000; Sossi et al., 2010; Bu et al., 2021). DAT mRNA and gene expression levels are higher in DA neurons which project from SNc to DLS, compared to those which project from VTA to NAcC (Haber et al., 1995; Poulin et al., 2014). Additionally, DATs provide an entry route for toxic substances to enter DA neurons (Lohr et al., 2017), which may interact with DAT genetic variants (Ritz et al., 2009), making the DAT-enriched SNc DA neurons particularly vulnerable to disease.

SNCA-OVX mice, which overexpress human α-synuclein (Janezic et al., 2013), exhibit a potentiated DAT function in DLS, with smaller single pulse evoked DA release, faster DA uptake rates, and larger cocaine-induced increases to DA release, compared to controls (Threlfell et al., 2021). These mice also display increased striatal GABA tone in DLS, due to lower GAT expression, which provides stronger tonic inhibition of DA axons compared to controls (Roberts et al., 2020). NAcC GABA tone remained unaffected in these mice (Roberts et al., 2020). How might this relate to the convergent regulation of DA release by DATs and GABA-Rs? In DLS, under a variety of conditions, GABA-Rs support DAT-mediated changes to DA release, whereas in NAcC, there was a distinct lack of a strong role for GABA-RS in DAT-mediated changes to DA signalling. These findings may be related to vulnerable versus resistant DA neuron populations in Parkinson's disease. It seems plausible that there are a variety of mechanisms, possibly involving Ca^{2+} buffering, in NAcC DA neurons which are

neuroprotective. Perhaps, DAT function in NAcC DA neurons is not changed by activity at GABA-Rs, as mechanisms intrinsic to NAcC DA neurons 'protect' them from regulation, and thus dysregulation and degeneration. The strong modulation of DAT function, and therefore DA axon function, by GABA-Rs in DLS may be a symptom, or driver, of vulnerability in these neurons. Future experiments should investigate whether the co-operation between DATs and GABA-Rs in DLS is affected in *SNCA*-OVX mice. Furthermore, in Chapter 4, we found that GIRK channel inhibition attenuates increases in DA release by cocaine, and GABA-R antagonists. Future experiments should test whether inhibition of GIRK channels in DLS 'normalises' the effect of cocaine and GABA-R antagonists in *SNCA*-OVX mice.

DATs express binding sites for α-synuclein, and presence of α-synuclein modulates DAT function (Lee et al., 2001; Swant et al., 2011). In cultured neurons, the presence of α-synuclein reduces DA uptake, but increases transport-uncoupled, Cl^- dependent, currents via DATs (Swant et al., 2011). This increase in transport-uncoupled currents was prevented by DAT inhibition (Swant et al., 2011). Subsequent experiments should test whether DAT-mediated currents in striatal DA axons are altered in the *SNCA*-OVX mouse model, bearing in mind that STD in DA release is unaffected in these mice (Threlfell et al., 2021), and it could be technically challenging to observe transport-uncoupled currents. Rather, α-synuclein appears to selectively affect STF, and there are conflicting results about whether STF is augmented (Chadchankar & Yavich, 2011) or attenuated (Threlfell et al., 2021). Aside from the strong implication for DATs in PD, HCN channel function appears to be attenuated in PD (DiFrancesco & DiFrancesco, 2015), and LTCC function co-varies with PD risk factors (Brimblecombe et al., 2024). It is therefore imperative to investigate the regulatory partners of DATs, and test whether dysfunction in these relationships could contribute to disease, such as PD.

Here, we have identified GABA-Rs as regulatory partners of DATs. Ultimately, the goal of this pre-clinical research is to translate to humans, and recently, it was found that GABAergic, rather than cholinergic, control of striatal DA release is particularly dominant in non-human primates (Shin et al., 2025). In the mouse striatum, DA release is heavily regulated by ACh from cholinergic interneurons (ChIs), acting at nAChRs on DA axons (Rice & Cragg, 2004; H. Zhang & Sulzer, 2004; Threlfell et al., 2012; Kramer et al., 2022; Liu et al., 2022). Throughout this thesis, confounding effects from ACh were mitigated by the presence of the nAChR antagonist, DHβE. Investigating local regulation of DA release whilst preventing modulation from ACh is essential for several reasons. ChIs pause their firing *in vivo* when DA neurons burst (Aosaki et al., 1994; Morris et al., 2004; Cragg, 2006; Aosaki et al., 2010), and nAChRs rapidly desensitise in response to substrates (Katz & Thesleff, 1957; Ochoa et al., 1989; Zhou et al., 2001; Quick & Lester, 2002; Rice & Cragg, 2004). Furthermore, it has now been demonstrated that, in the primate striatum, local regulation of DA release is predominantly mediated by GABA, rather than ACh (Shin et al., 2025). Co-application of $GABA_A$- and $GABA_B$-R antagonists increase DA release to a further extent in macaque striatum, compared to mouse, indicating that GABA tone exerts more control over DA axons in primates (Shin et al., 2025). This study underpins the translational possibilities, and relevance, of investigating GABAergic regulation of striatal DA release, and investigating how GABAergic mechanisms interact with other intrinsic mechanisms on striatal DA axons, such as DATs.

6.5. Conclusions

In this thesis, I investigated the regulation of striatal DA release and axonal excitability by DATs, and the involvement of GABA-Rs and GIRK channels. I demonstrated that GABA-Rs support DAT-mediated limitations on initial DA release in DLS, but not in NAcC. I showed that GIRK channels might be involved in the control of DA release by DATs and GABA-Rs. Furthermore, I demonstrated that DAT-mediated currents in striatal DA axons are consistent

with the observation that, following initial release, DATs limit axonal re-activation and subsequent DA release. These findings indicate that striatal DA axons integrate information from DATs and GABA-Rs to determine DA release, and that DATs regulate axonal excitability. The results in this thesis contribute to our understanding of striatal DA axon function.

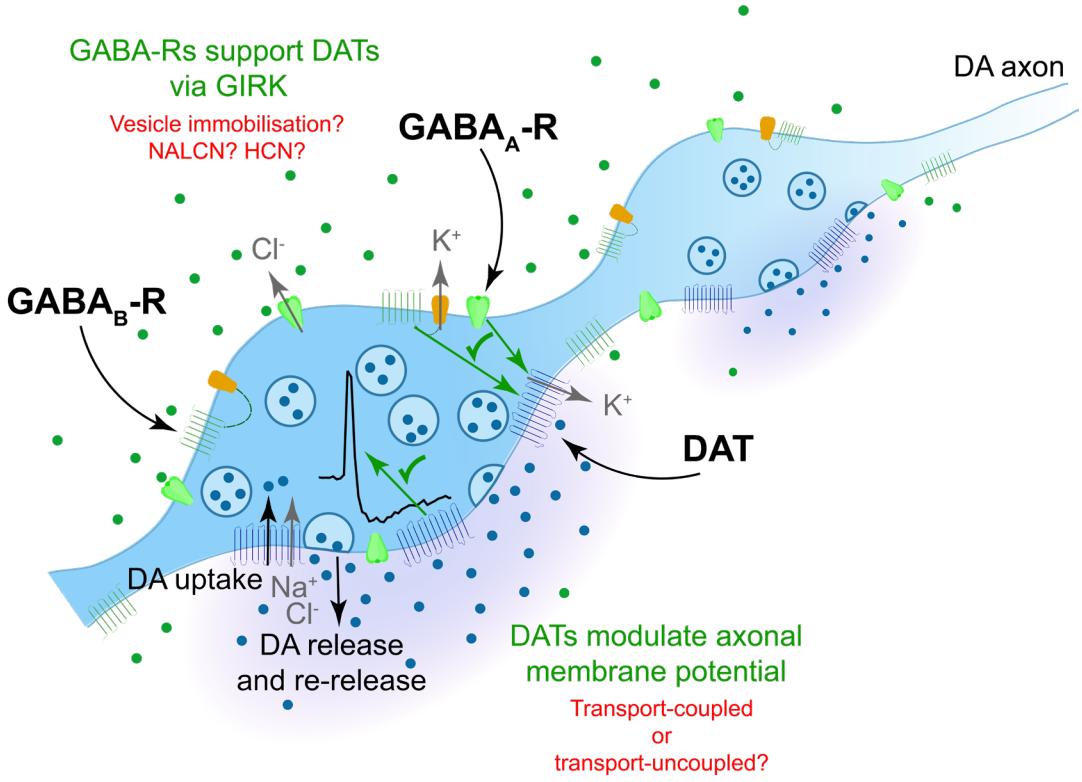

Figure 6.1. DATs co-operate with GABA-Rs and modulate axonal excitability
Simplified schematic of striatal DA axon, expressing DATs, $GABA_A$-Rs and $GABA_B$-Rs. GABA-Rs support DAT-mediated changes to DA release, possibly via GIRK channels (shown coupled with $GABA_B$-Rs). DATs mediate depolarising currents to modify axonal membrane potential. Future directions are in red.

References

Abeliovich, A., Schmitz, Y., Fariñas, I., Choi-Lundberg, D., Ho, W.-H., Castillo, P. E., Shinsky, N., Verdugo, J. M. G., Armanini, M., Ryan, A., Hynes, M., Phillips, H., Sulzer, D., & Rosenthal, A. (2000). Mice Lacking α-Synuclein Display Functional Deficits in the Nigrostriatal Dopamine System. *Neuron*, *25*(1), 239–252. https://doi.org/10.1016/S0896-6273(00)80886-7

Acevedo-Rodriguez, A., Zhang, L., Zhou, F., Gong, S., Gu, H., De Biasi, M., Zhou, F.-M., & Dani, J. A. (2014). Cocaine inhibition of nicotinic acetylcholine receptors influences dopamine release. *Frontiers in Synaptic Neuroscience*, *6*. https://doi.org/10.3389/fnsyn.2014.00019

Agnew, W. S. (1984). Voltage-Regulated Sodium Channel Molecules. *Annual Review of Physiology*, *46*(Volume 46,), 517–530. https://doi.org/10.1146/annurev.ph.46.030184.002505

Albin, R. L., Young, A. B., & Penney, J. B. (1989). The functional anatomy of basal ganglia disorders. *Trends in Neurosciences*, *12*(10), 366–375. https://doi.org/10.1016/0166-2236(89)90074-X

Alle, H., & Geiger, J. R. P. (2006). Combined Analog and Action Potential Coding in Hippocampal Mossy Fibers. *Science*, *311*(5765), 1290–1293. https://doi.org/10.1126/science.1119055

Alonso, I. P., O'Connor, B. M., Bryant, K. G., Mandalaywala, R. K., & España, R. A. (2022). Incubation of cocaine craving coincides with changes in dopamine terminal neurotransmission. *Addiction Neuroscience*, *3*, 100029. https://doi.org/10.1016/j.addicn.2022.100029

Amico, C., Marchetti, C., Nobile, M., & Usai, C. (1995). Pharmacological types of calcium channels and their modulation by baclofen in cerebellar granules. *The Journal of*

Neuroscience, *15*(4), 2839–2848. https://doi.org/10.1523/JNEUROSCI.15-04-02839.1995

Ammari, R., Lopez, C., Fiorentino, H., Gonon, F., & Hammond, C. (2009). A mouse juvenile or adult slice with preserved functional nigro-striatal dopaminergic neurons. *Neuroscience*, *159*(1), 3–6. https://doi.org/10.1016/j.neuroscience.2008.10.051

Anwar, H., Li, X., Bucher, D., & Nadim, F. (2017). Functional roles of short-term synaptic plasticity with an emphasis on inhibition. *Current Opinion in Neurobiology*, *43*, 71–78. https://doi.org/10.1016/j.conb.2017.01.002

Aosaki, T., Graybiel, A. M., & Kimura, M. (1994). Effect of the Nigrostriatal Dopamine System on Acquired Neural Responses in the Striatum of Behaving Monkeys. *Science*, *265*(5170), 412–415. https://doi.org/10.1126/science.8023166

Aosaki, T., Miura, M., Suzuki, T., Nishimura, K., & Masuda, M. (2010). Acetylcholine–dopamine balance hypothesis in the striatum: An update. *Geriatrics & Gerontology International*, *10*, S148–S157. https://doi.org/10.1111/j.1447-0594.2010.00588.x

Aransay, A., Rodríguez-López, C., García-Amado, M., Clascá, F., & Prensa, L. (2015a). Long-range projection neurons of the mouse ventral tegmental area: A single-cell axon tracing analysis. *Frontiers in Neuroanatomy*, *9*. https://doi.org/10.3389/fnana.2015.00059

Aransay, A., Rodríguez-López, C., García-Amado, M., Clascá, F., & Prensa, L. (2015b). Long-range projection neurons of the mouse ventral tegmental area: A single-cell axon tracing analysis. *Frontiers in Neuroanatomy*, *9*. https://doi.org/10.3389/fnana.2015.00059

Arien, H., Wiser, O., Arkin, I. T., Leonov, H., & Atlas, D. (2003). Syntaxin 1A Modulates the Voltage-gated L-type Calcium Channel (Cav1.2) in a Cooperative Manner*. *Journal of Biological Chemistry*, *278*(31), 29231–29239. https://doi.org/10.1074/jbc.M301401200

Armstrong, C. M., & Bezanilla, F. (1973). Currents Related to Movement of the Gating Particles of the Sodium Channels. *Nature*, *242*(5398), 459–461. https://doi.org/10.1038/242459a0

Azcorra, M., Gaertner, Z., Davidson, C., He, Q., Kim, H., Nagappan, S., Hayes, C. K., Ramakrishnan, C., Fenno, L., Kim, Y. S., Deisseroth, K., Longnecker, R., Awatramani, R., & Dombeck, D. A. (2023). Unique functional responses differentially map onto genetic subtypes of dopamine neurons. *Nature Neuroscience*, *26*(10), 1762–1774. https://doi.org/10.1038/s41593-023-01401-9

Bäckman, C. M., Malik, N., Zhang, Y., Shan, L., Grinberg, A., Hoffer, B. J., Westphal, H., & Tomac, A. C. (2006). Characterization of a mouse strain expressing Cre recombinase from the 3' untranslated region of the dopamine transporter locus. *Genesis*, *44*(8), 383–390. https://doi.org/10.1002/dvg.20228

Balana, B., Maslennikov, I., Kwiatkowski, W., Stern, K. M., Bahima, L., Choe, S., & Slesinger, P. A. (2011). Mechanism underlying selective regulation of G protein-gated inwardly rectifying potassium channels by the psychostimulant-sensitive sorting nexin 27. *Proceedings of the National Academy of Sciences*, *108*(14), 5831–5836. https://doi.org/10.1073/pnas.1018645108

Balleine, B. W., & Ostlund, S. B. (2007). Still at the Choice-Point. *Annals of the New York Academy of Sciences*, *1104*(1), 147–171. https://doi.org/10.1196/annals.1390.006

Bamford, I. J., & Bamford, N. S. (2019). The Striatum's Role in Executing Rational and Irrational Economic Behaviors. *The Neuroscientist : A Review Journal Bringing Neurobiology, Neurology and Psychiatry*, *25*(5), 475–490. https://doi.org/10.1177/1073858418824256

Bang, D., Kishida, K. T., Lohrenz, T., White, J. P., Laxton, A. W., Tatter, S. B., Fleming, S. M., & Montague, P. R. (2020). Sub-second Dopamine and Serotonin Signaling in Human

Striatum during Perceptual Decision-Making. *Neuron*, *108*(5), 999-1010.e6. https://doi.org/10.1016/j.neuron.2020.09.015

Barbeau, A. (1969). L-Dopa Therapy in Parkinson's Disease. *Canadian Medical Association Journal*, *101*(13), 59–68.

Barroso-Flores, J., Herrera-Valdez, M. A., Galarraga, E., & Bargas, J. (2017). Models of Short-Term Synaptic Plasticity. In R. von Bernhardi, J. Eugenín, & K. J. Muller (Eds.), *The Plastic Brain* (pp. 41–57). Springer International Publishing. https://doi.org/10.1007/978-3-319-62817-2_3

Barroso-Flores, J., Herrera-Valdez, M. A., Lopez-Huerta, V. G., Galarraga, E., & Bargas, J. (2015a). Diverse Short-Term Dynamics of Inhibitory Synapses Converging on Striatal Projection Neurons: Differential Changes in a Rodent Model of Parkinson's Disease. *Neural Plasticity*, *2015*(1), 573543. https://doi.org/10.1155/2015/573543

Barroso-Flores, J., Herrera-Valdez, M. A., Lopez-Huerta, V. G., Galarraga, E., & Bargas, J. (2015b). Diverse Short-Term Dynamics of Inhibitory Synapses Converging on Striatal Projection Neurons: Differential Changes in a Rodent Model of Parkinson's Disease. *Neural Plasticity*, *2015*(1), 573543. https://doi.org/10.1155/2015/573543

Bartolomé-Martín, D., Ibáñez, I., Piniella, D., Martínez-Blanco, E., Pelaz, S. G., & Zafra, F. (2019). Identification of potassium channel proteins Kv7.2/7.3 as common partners of the dopamine and glutamate transporters DAT and GLT-1. *Neuropharmacology*, *161*, 107568. https://doi.org/10.1016/j.neuropharm.2019.03.011

Basso, V., Döbrössy, M. D., Thompson, L. H., Kirik, D., Fuller, H. R., & Gates, M. A. (2024). State of the Art in Sub-Phenotyping Midbrain Dopamine Neurons. *Biology*, *13*(9), Article 9. https://doi.org/10.3390/biology13090690

Baur, J. E., Kristensen, E. W., May, L. J., Wiedemann, D. J., & Wightman, R. Mark. (1988). Fast-scan voltammetry of biogenic amines. *Analytical Chemistry*, *60*(13), 1268–1272. https://doi.org/10.1021/ac00164a006

Baxter, G., Kennett, G., Blackburn, T., & Blaney, F. (1995). 5-HT2 receptor subtypes: A family re-united? *Trends in Pharmacological Sciences*, *16*(3), 105–110. https://doi.org/10.1016/S0165-6147(00)88991-9

Bayer, V. E., & Pickel, V. M. (1990). Ultrastructural localization of tyrosine hydroxylase in the rat ventral tegmental area: Relationship between immunolabeling density and neuronal associations. *The Journal of Neuroscience: The Official Journal of the Society for Neuroscience*, *10*(9), 2996–3013. https://doi.org/10.1523/JNEUROSCI.10-09-02996.1990

Beatty, J. A., Sullivan, M. A., Morikawa, H., & Wilson, C. J. (2012). Complex autonomous firing patterns of striatal low-threshold spike interneurons. *Journal of Neurophysiology*, *108*(3), 771–781. https://doi.org/10.1152/jn.00283.2012

Beaulieu, J.-M., Espinoza, S., & Gainetdinov, R. R. (2015). Dopamine receptors – IUPHAR Review 13. *British Journal of Pharmacology*, *172*(1), 1–23. https://doi.org/10.1111/bph.12906

Beaulieu, J.-M., & Gainetdinov, R. R. (2011). The Physiology, Signaling, and Pharmacology of Dopamine Receptors. *Pharmacological Reviews*, *63*(1), 182–217. https://doi.org/10.1124/pr.110.002642

Beaver, M. L., & Evans, R. C. (2025). Muscarinic Receptor Activation Preferentially Inhibits Rebound in Vulnerable Dopaminergic Neurons. *Journal of Neuroscience*, *45*(16). https://doi.org/10.1523/JNEUROSCI.1443-24.2025

Beckstead, M. J., Ford, C. P., Phillips, P. E. M., & Williams, J. T. (2007). Presynaptic regulation of dendrodendritic dopamine transmission. *European Journal of Neuroscience*, *26*(6), 1479–1488. https://doi.org/10.1111/j.1460-9568.2007.05775.x

Beery, A. K., & Zucker, I. (2011). Sex bias in neuroscience and biomedical research. *Neuroscience & Biobehavioral Reviews*, *35*(3), 565–572. https://doi.org/10.1016/j.neubiorev.2010.07.002

Belovich, A. N., Aguilar, J. I., Mabry, S. J., Cheng, M. H., Zanella, D., Hamilton, P. J., Stanislowski, D. J., Shekar, A., Foster, J. D., Bahar, I., Matthies, H. J. G., & Galli, A. (2021). A network of phosphatidylinositol (4,5)-bisphosphate (PIP2) binding sites on the dopamine transporter regulates amphetamine behavior in Drosophila Melanogaster. *Molecular Psychiatry*, *26*(8), 4417–4430. https://doi.org/10.1038/s41380-019-0620-0

Ben-Ari, Y., Cherubini, E., Corradetti, R., & Gaiarsa, J. L. (1989). Giant synaptic potentials in immature rat CA3 hippocampal neurones. *The Journal of Physiology*, *416*(1), 303–325. https://doi.org/10.1113/jphysiol.1989.sp017762

Benarroch, E. (2016, April 19). *Intrinsic circuits of the striatum*. Neurology. https://www.neurology.org/doi/10.1212/WNL.0000000000002599

Benarroch, E. E. (2013). HCN channels. *Neurology*, *80*(3), 304–310. https://doi.org/10.1212/WNL.0b013e31827dec42

Benoit-Marand, M., Borrelli, E., & Gonon, F. (2001). Inhibition of Dopamine Release Via Presynaptic D2 Receptors: Time Course and Functional Characteristics In Vivo. *Journal of Neuroscience*, *21*(23), 9134–9141. https://doi.org/10.1523/JNEUROSCI.21-23-09134.2001

Berke, J. D., & Hyman, S. E. (2000). Addiction, Dopamine, and the Molecular Mechanisms of Memory. *Neuron*, *25*(3), 515–532. https://doi.org/10.1016/S0896-6273(00)81056-9

Bettler, B., Kaupmann, K., Mosbacher, J., & Gassmann, M. (2004). Molecular Structure and Physiological Functions of GABAB Receptors. *Physiological Reviews*, *84*(3), 835–867. https://doi.org/10.1152/physrev.00036.2003

Beuming, T., Kniazeff, J., Bergmann, M. L., Shi, L., Gracia, L., Raniszewska, K., Newman, A. H., Javitch, J. A., Weinstein, H., Gether, U., & Loland, C. J. (2008). The binding sites for cocaine and dopamine in the dopamine transporter overlap. *Nature Neuroscience*, *11*(7), 780–789. https://doi.org/10.1038/nn.2146

Biel, M., Wahl-Schott, C., Michalakis, S., & Zong, X. (2009). Hyperpolarization-Activated Cation Channels: From Genes to Function. *Physiological Reviews*, *89*(3), 847–885. https://doi.org/10.1152/physrev.00029.2008

Björklund, A., & Dunnett, S. B. (2007). Dopamine neuron systems in the brain: An update. *Trends in Neurosciences*, *30*(5), 194–202. https://doi.org/10.1016/j.tins.2007.03.006

Blankenship, H. E., Carter, K. A., Cassidy, N. T., Markiewicz, A. N., Thellmann, M. I., Sharpe, A. L., Freeman, W. M., & Beckstead, M. J. (2023). VTA dopamine neurons are hyperexcitable in 3xTg-AD mice due to casein kinase 2-dependent SK channel dysfunction. *bioRxiv*, 2023.11.16.567486. https://doi.org/10.1101/2023.11.16.567486

Blatow, M., Caputi, A., Burnashev, N., Monyer, H., & Rozov, A. (2003). Ca2+ Buffer Saturation Underlies Paired Pulse Facilitation in Calbindin-D28k-Containing Terminals. *Neuron*, *38*(1), 79–88. https://doi.org/10.1016/S0896-6273(03)00196-X

Blythe, S. N., Wokosin, D., Atherton, J. F., & Bevan, M. D. (2009). Cellular Mechanisms Underlying Burst Firing in Substantia Nigra Dopamine Neurons. *Journal of Neuroscience*, *29*(49), 15531–15541. https://doi.org/10.1523/JNEUROSCI.2961-09.2009

Bogen, I. L., Boulland, J.-L., Mariussen, E., Wright, M. S., Fonnum, F., Kao, H.-T., & Walaas, S. I. (2006). Absence of synapsin I and II is accompanied by decreases in vesicular transport of specific neurotransmitters. *Journal of Neurochemistry*, *96*(5), 1458–1466. https://doi.org/10.1111/j.1471-4159.2005.03636.x

Bolam, J. P., Hanley, J. J., Booth, P. a. C., & Bevan, M. D. (2000). Synaptic organisation of the basal ganglia. *Journal of Anatomy*, *196*(4), 527–542. https://doi.org/10.1046/j.1469-7580.2000.19640527.x

Bolam, J. P., Wainer, B. H., & Smith, A. D. (1984). Characterization of cholinergic neurons in the rat neostriatum. A combination of choline acetyltransferase

immunocytochemistry, Golgi-impregnation and electron microscopy. *Neuroscience*, *12*(3), 711–718. https://doi.org/10.1016/0306-4522(84)90165-9

Borre, L., Andreassen, T. F., Shi, L., Weinstein, H., & Gether, U. (2014). The Second Sodium Site in the Dopamine Transporter Controls Cation Permeation and Is Regulated by Chloride. *The Journal of Biological Chemistry*, *289*(37), 25764–25773. https://doi.org/10.1074/jbc.M114.574269

Boumhaouad, S., Makowicz, E. A., Choi, S., Bouhaddou, N., Balla, J., Taghzouti, K., Sulzer, D., & Mosharov, E. V. (2025). Regulation of Dopamine Release by Tonic Activity Patterns in the Striatal Brain Slice. *ACS Chemical Neuroscience*, *16*(3), 303–310. https://doi.org/10.1021/acschemneuro.4c00323

Bourne, J. A. (2001). SCH 23390: The First Selective Dopamine D1-Like Receptor Antagonist. *CNS Drug Reviews*, *7*(4), 399–414. https://doi.org/10.1111/j.1527-3458.2001.tb00207.x

Branch, S. Y., & Beckstead, M. J. (2012). Methamphetamine produces bidirectional, concentration-dependent effects on dopamine neuron excitability and dopamine-mediated synaptic currents. *Journal of Neurophysiology*, *108*(3), 802–809. https://doi.org/10.1152/jn.00094.2012

Brebner, K., Ahn, S., & Phillips, A. G. (2005). Attenuation of d-amphetamine self-administration by baclofen in the rat: Behavioral and neurochemical correlates. *Psychopharmacology*, *177*(4), 409–417. https://doi.org/10.1007/s00213-004-1968-6

Brebner, K., Phelan, R., & Roberts, D. C. S. (2000). Intra-VTA Baclofen Attenuates Cocaine Self-Administration on a Progressive Ratio Schedule of Reinforcement. *Pharmacology Biochemistry and Behavior*, *66*(4), 857–862. https://doi.org/10.1016/S0091-3057(00)00286-0

Brichta, L., & Greengard, P. (2014). Molecular determinants of selective dopaminergic vulnerability in Parkinson's disease: An update. *Frontiers in Neuroanatomy*, *8*. https://doi.org/10.3389/fnana.2014.00152

Briggs, C. A., Pollock, N. J., Frail, D. E., Paxson, C. L., Rakowski, R. F., Kang, C. H., & Kebabian, J. W. (1991). Activation of the 5-HT1c receptor expressed in Xenopus oocytes by the benzazepines SCH 23390 and SKF 38393. *British Journal of Pharmacology*, *104*(4), 1038–1044. https://doi.org/10.1111/j.1476-5381.1991.tb12546.x

Brill-Weil, S. G., Kramer, P. F., Yanez, A., Clever, F. H., Zhang, R., & Khaliq, Z. M. (2024). *Presynaptic GABAA receptors control integration of nicotinic input onto dopaminergic axons in the striatum* (p. 2024.06.25.600616). bioRxiv. https://doi.org/10.1101/2024.06.25.600616

Brimblecombe, K. R., Connor-Robson, N., Bataille, C. J. R., Roberts, B. M., Gracie, C., O'Connor, B., te Water Naude, R., Karthik, G., Russell, A. J., Wade-Martins, R., & Cragg, S. J. (2024). Inhibition of striatal dopamine release by the L-type calcium channel inhibitor isradipine co-varies with risk factors for Parkinson's. *European Journal of Neuroscience*, *59*(6), 1242–1259. https://doi.org/10.1111/ejn.16180

Brimblecombe, K. R., & Cragg, S. J. (2015). Substance P Weights Striatal Dopamine Transmission Differently within the Striosome-Matrix Axis. *Journal of Neuroscience*, *35*(24), 9017–9023. https://doi.org/10.1523/JNEUROSCI.0870-15.2015

Brimblecombe, K. R., & Cragg, S. J. (2017). The Striosome and Matrix Compartments of the Striatum: A Path through the Labyrinth from Neurochemistry toward Function. *ACS Chemical Neuroscience*, *8*(2), 235–242. https://doi.org/10.1021/acschemneuro.6b00333

Brimblecombe, K. R., Gracie, C. J., Platt, N. J., & Cragg, S. J. (2015). Gating of dopamine transmission by calcium and axonal N-, Q-, T- and L-type voltage-gated calcium

channels differs between striatal domains. *The Journal of Physiology*, *593*(4), 929–946. https://doi.org/10.1113/jphysiol.2014.285890

Brimblecombe, K. R., Vietti-Michelina, S., Platt, N. J., Kastli, R., Hnieno, A., Gracie, C. J., & Cragg, S. J. (2019). Calbindin-D28K Limits Dopamine Release in Ventral but Not Dorsal Striatum by Regulating Ca2+ Availability and Dopamine Transporter Function. *ACS Chemical Neuroscience*, *10*(8), 3419–3426. https://doi.org/10.1021/acschemneuro.9b00325

Brodnik, Z. D., Batra, A., Oleson, E. B., & España, R. A. (2019). Local GABAA Receptor-Mediated Suppression of Dopamine Release within the Nucleus Accumbens. *ACS Chemical Neuroscience*, *10*(4), 1978–1985. https://doi.org/10.1021/acschemneuro.8b00268

Brodnik, Z. D., Xu, W., Batra, A., Lewandowski, S. I., Ruiz, C. M., Mortensen, O. V., Kortagere, S., Mahler, S. V., & España, R. A. (2020). Chemogenetic Manipulation of Dopamine Neurons Dictates Cocaine Potency at Distal Dopamine Transporters. *Journal of Neuroscience*, *40*(45), 8767–8779. https://doi.org/10.1523/JNEUROSCI.0894-20.2020

Brody, D. L., & Yue, D. T. (2000). Release-Independent Short-Term Synaptic Depression in Cultured Hippocampal Neurons. *Journal of Neuroscience*, *20*(7), 2480–2494. https://doi.org/10.1523/JNEUROSCI.20-07-02480.2000

Brown, P., & Dale, N. (2000). Adenosine A1 receptors modulate high voltage-activated Ca2+ currents and motor pattern generation in the Xenopus embryo. *The Journal of Physiology*, *525*(Pt 3), 655–667. https://doi.org/10.1111/j.1469-7793.2000.00655.x

Bu, M., Farrer, M. J., & Khoshbouei, H. (2021). Dynamic control of the dopamine transporter in neurotransmission and homeostasis. *Npj Parkinson's Disease*, *7*(1), 1–11. https://doi.org/10.1038/s41531-021-00161-2

Buck, S. A., Erickson-Oberg, M. Q., Bhatte, S. H., McKellar, C. D., Ramanathan, V. P., Rubin, S. A., & Freyberg, Z. (2022). Roles of VGLUT2 and Dopamine/Glutamate Co-

Transmission in Selective Vulnerability to Dopamine Neurodegeneration. *ACS Chemical Neuroscience*, *13*(2), 187–193. https://doi.org/10.1021/acschemneuro.1c00741

Bulumulla, C., Walpita, D., Iyer, N., Eddison, M., Patel, R., Alcor, D., Ackerman, D., & Beyene, A. G. (2024). *Synaptic Specializations at Dopamine Release Sites Orchestrate Efficient and Precise Neuromodulatory Signaling* (p. 2024.09.16.613338). bioRxiv. https://doi.org/10.1101/2024.09.16.613338

Burgeno, L. M., Farero, R. D., Murray, N. L., Panayi, M. C., Steger, J. S., Soden, M. E., Evans, S. B., Sandberg, S. G., Willuhn, I., Zweifel, L. S., & Phillips, P. E. M. (2023). *Cocaine Seeking And Taking Are Oppositely Regulated By Dopamine* (p. 2023.04.09.536189). bioRxiv. https://doi.org/10.1101/2023.04.09.536189

Burton, A. C., Nakamura, K., & Roesch, M. R. (2015). From ventral-medial to dorsal-lateral striatum: Neural correlates of reward-guided decision-making. *Neurobiology of Learning and Memory*, *117*, 51–59. https://doi.org/10.1016/j.nlm.2014.05.003

Cai, X., Liu, C., Tsutsui-Kimura, I., Lee, J.-H., Guo, C., Banerjee, A., Lee, J., Amo, R., Xie, Y., Patriarchi, T., Li, Y., Watabe-Uchida, M., Uchida, N., & Kaeser, P. S. (2024). Dopamine dynamics are dispensable for movement but promote reward responses. *Nature*, *635*(8038), 406–414. https://doi.org/10.1038/s41586-024-08038-z

Caillé, I., Dumartin, B., & Bloch, B. (1996). Ultrastructural localization of D1 dopamine receptor immunoreactivity in rat striatonigral neurons and its relation with dopaminergic innervation. *Brain Research*, *730*(1), 17–31. https://doi.org/10.1016/0006-8993(96)00424-6

Calipari, E. S., Ferris, M. J., Zimmer, B. A., Roberts, D. C., & Jones, S. R. (2013). Temporal Pattern of Cocaine Intake Determines Tolerance vs Sensitization of Cocaine Effects at the Dopamine Transporter. *Neuropsychopharmacology*, *38*(12), 2385–2392. https://doi.org/10.1038/npp.2013.136

Calipari, E. S., Juarez, B., Morel, C., Walker, D. M., Cahill, M. E., Ribeiro, E., Roman-Ortiz, C., Ramakrishnan, C., Deisseroth, K., Han, M.-H., & Nestler, E. J. (2017a). Dopaminergic dynamics underlying sex-specific cocaine reward. *Nature Communications*, *8*(1), 13877. https://doi.org/10.1038/ncomms13877

Calipari, E. S., Juarez, B., Morel, C., Walker, D. M., Cahill, M. E., Ribeiro, E., Roman-Ortiz, C., Ramakrishnan, C., Deisseroth, K., Han, M.-H., & Nestler, E. J. (2017b). Dopaminergic dynamics underlying sex-specific cocaine reward. *Nature Communications*, *8*(1), 13877. https://doi.org/10.1038/ncomms13877

Cameron, K. N., Solis, E., Ruchala, I., De Felice, L. J., & Eltit, J. M. (2015). Amphetamine activates calcium channels through dopamine transporter-mediated depolarization. *Cell Calcium*, *58*(5), 457–466. https://doi.org/10.1016/j.ceca.2015.06.013

Cardozo, D. L., & Bean, B. P. (1995). Voltage-dependent calcium channels in rat midbrain dopamine neurons: Modulation by dopamine and GABAB receptors. *Journal of Neurophysiology*, *74*(3), 1137–1148. https://doi.org/10.1152/jn.1995.74.3.1137

Carvelli, L., Blakely, R. D., & DeFelice, L. J. (2008). Dopamine transporter/syntaxin 1A interactions regulate transporter channel activity and dopaminergic synaptic transmission. *Proceedings of the National Academy of Sciences*, *105*(37), 14192–14197. https://doi.org/10.1073/pnas.0802214105

Carvelli, L., McDonald, P. W., Blakely, R. D., & DeFelice, L. J. (2004). Dopamine transporters depolarize neurons by a channel mechanism. *Proceedings of the National Academy of Sciences*, *101*(45), 16046–16051. https://doi.org/10.1073/pnas.0403299101

Catterall, W. A. (2000). From Ionic Currents to Molecular Mechanisms: The Structure and Function of Voltage-Gated Sodium Channels. *Neuron*, *26*(1), 13–25. https://doi.org/10.1016/S0896-6273(00)81133-2

Catterall, W. A. (2012). Voltage-gated sodium channels at 60: Structure, function and pathophysiology. *The Journal of Physiology*, *590*(11), 2577–2589. https://doi.org/10.1113/jphysiol.2011.224204

Cesca, F., Baldelli, P., Valtorta, F., & Benfenati, F. (2010). The synapsins: Key actors of synapse function and plasticity. *Progress in Neurobiology*, *91*(4), 313–348. https://doi.org/10.1016/j.pneurobio.2010.04.006

Chadchankar, H., & Yavich, L. (2011). Sub-regional differences and mechanisms of the short-term plasticity of dopamine overflow in striatum in mice lacking alpha-synuclein. *Brain Research*, *1423*, 67–76. https://doi.org/10.1016/j.brainres.2011.09.026

Chamberland, S., Yang, H. H., Pan, M. M., Evans, S. W., Guan, S., Chavarha, M., Yang, Y., Salesse, C., Wu, H., Wu, J. C., Clandinin, T. R., Toth, K., Lin, M. Z., & St-Pierre, F. (2017). Fast two-photon imaging of subcellular voltage dynamics in neuronal tissue with genetically encoded indicators. *eLife*, *6*, e25690. https://doi.org/10.7554/eLife.25690

Charara, A., Heilman, C., Levey, A. I., & Smith, Y. (1999). Pre- and postsynaptic localization of GABAB receptors in the basal ganglia in monkeys. *Neuroscience*, *95*(1), 127–140. https://doi.org/10.1016/S0306-4522(99)00409-1

Chebib, M., & Johnston, G. A. R. (1999). The 'Abc' of Gaba Receptors: A Brief Review. *Clinical and Experimental Pharmacology and Physiology*, *26*(11), 937–940. https://doi.org/10.1046/j.1440-1681.1999.03151.x

Chen, H., Xia, Z., Dong, J., Huang, B., Zhang, J., Zhou, F., Yan, R., Shi, Y., Gong, J., Jiang, J., Huang, Z., & Jiang, D. (2024). Structural mechanism of voltage-gated sodium channel slow inactivation. *Nature Communications*, *15*(1), 3691. https://doi.org/10.1038/s41467-024-48125-3

Chen, T.-W., Wardill, T. J., Sun, Y., Pulver, S. R., Renninger, S. L., Baohan, A., Schreiter, E. R., Kerr, R. A., Orger, M. B., Jayaraman, V., Looger, L. L., Svoboda, K., & Kim, D. S. (2013).

Ultrasensitive fluorescent proteins for imaging neuronal activity. *Nature*, *499*(7458), 295–300. https://doi.org/10.1038/nature12354

Christie, J. M., Chiu, D. N., & Jahr, C. E. (2011). Ca2+-dependent enhancement of release by subthreshold somatic depolarization. *Nature Neuroscience*, *14*(1), 62–68. https://doi.org/10.1038/nn.2718

Chu, H., & Zhen, X. (2010). Hyperpolarization-activated, cyclic nucleotide-gated (HCN) channels in the regulation of midbrain dopamine systems. *Acta Pharmacologica Sinica*, *31*(9), 1036–1043. https://doi.org/10.1038/aps.2010.105

Chung, C. Y., Seo, H., Sonntag, K. C., Brooks, A., Lin, L., & Isacson, O. (2005). Cell type-specific gene expression of midbrain dopaminergic neurons reveals molecules involved in their vulnerability and protection. *Human Molecular Genetics*, *14*(13), 1709–1725. https://doi.org/10.1093/hmg/ddi178

Chung, S., Li, X., & Nelson, S. B. (2002). Short-Term Depression at Thalamocortical Synapses Contributes to Rapid Adaptation of Cortical Sensory Responses In Vivo. *Neuron*, *34*(3), 437–446. https://doi.org/10.1016/S0896-6273(02)00659-1

Ciano, P. D., & Everitt, B. J. (2003). The GABAB Receptor Agonist Baclofen Attenuates Cocaine- and Heroin-Seeking Behavior by Rats. *Neuropsychopharmacology*, *28*(3), 510–518. https://doi.org/10.1038/sj.npp.1300088

Clark, B., & Häusser, M. (2006). Neural Coding: Hybrid Analog and Digital Signalling in Axons. *Current Biology*, *16*(15), R585–R588. https://doi.org/10.1016/j.cub.2006.07.007

Clark, P. J., & España, R. A. (2023). Fast Scan Cyclic Voltammetry to Assess Dopamine Function: From Circuits to Behavior. In J. A. Fuentealba-Evans & P. Henny (Eds.), *Dopaminergic System Function and Dysfunction: Experimental Approaches* (pp. 249–281). Springer US. https://doi.org/10.1007/978-1-0716-2799-0_11

Clarke, S. G., Scarnati, M. S., & Paradiso, K. G. (2016). Neurotransmitter Release Can Be Stabilized by a Mechanism That Prevents Voltage Changes Near the End of Action

Potentials from Affecting Calcium Currents. *The Journal of Neuroscience*, *36*(45), 11559–11572. https://doi.org/10.1523/JNEUROSCI.0066-16.2016

Cobb-Lewis, D. E., Sansalone, L., & Khaliq, Z. M. (2023). Contributions of the Sodium Leak Channel NALCN to Pacemaking of Medial Ventral Tegmental Area and Substantia Nigra Dopaminergic Neurons. *Journal of Neuroscience*, *43*(41), 6841–6853. https://doi.org/10.1523/JNEUROSCI.0930-22.2023

Cochet-Bissuel, M., Lory, P., & Monteil, A. (2014). The sodium leak channel, NALCN, in health and disease. *Frontiers in Cellular Neuroscience*, *8*, 132. https://doi.org/10.3389/fncel.2014.00132

Coddington, L. T., & Dudman, J. T. (2019). Learning from Action: Reconsidering Movement Signaling in Midbrain Dopamine Neuron Activity. *Neuron*, *104*(1), 63–77. https://doi.org/10.1016/j.neuron.2019.08.036

Condon, A. F., Asad, N., Dore, T. M., & Williams, J. T. (2022). Co-activation of GPCRs facilitate GIRK-dependent current. *The Journal of Physiology*, *600*(22), 4881–4895. https://doi.org/10.1113/JP283590

Condon, M. D., Platt, N. J., Zhang, Y.-F., Roberts, B. M., Clements, M. A., Vietti-Michelina, S., Tseu, M.-Y., Brimblecombe, K. R., Threlfell, S., Mann, E. O., & Cragg, S. J. (2019). Plasticity in striatal dopamine release is governed by release-independent depression and the dopamine transporter. *Nature Communications*, *10*(1), 4263. https://doi.org/10.1038/s41467-019-12264-9

Conley, R. K., Cumberbatch, M. J., Mason, G. S., Williamson, D. J., Harrison, T., Locker, K., Swain, C., Maubach, K., O'Donnell, R., Rigby, M., Hewson, L., Smith, D., & Rupniak, N. M. J. (2002). Substance P (Neurokinin 1) Receptor Antagonists Enhance Dorsal Raphe Neuronal Activity. *Journal of Neuroscience*, *22*(17), 7730–7736. https://doi.org/10.1523/JNEUROSCI.22-17-07730.2002

Coombs, J. S., Curtis, D. R., & Eccles, J. C. (1957). The interpretation of spike potentials of motoneurones. *The Journal of Physiology*, *139*(2), 198–231. https://doi.org/10.1113/jphysiol.1957.sp005887

Costa, K. M., Schenkel, D., & Roeper, J. (2021). Sex-dependent alterations in behavior, drug responses and dopamine transporter expression in heterozygous DAT-Cre mice. *Scientific Reports*, *11*(1), 3334. https://doi.org/10.1038/s41598-021-82600-x

Cragg, S. J. (2003). Variable Dopamine Release Probability and Short-Term Plasticity between Functional Domains of the Primate Striatum. *Journal of Neuroscience*, *23*(10), 4378–4385. https://doi.org/10.1523/JNEUROSCI.23-10-04378.2003

Cragg, S. J. (2006). Meaningful silences: How dopamine listens to the ACh pause. *Trends in Neurosciences*, *29*(3), 125–131. https://doi.org/10.1016/j.tins.2006.01.003

Cragg, S. J., & Rice, M. E. (2004). DAncing past the DAT at a DA synapse. *Trends in Neurosciences*, *27*(5), 270–277. https://doi.org/10.1016/j.tins.2004.03.011

Crittenden, J. R., & Graybiel, A. M. (2011). Basal Ganglia Disorders Associated with Imbalances in the Striatal Striosome and Matrix Compartments. *Frontiers in Neuroanatomy*, *5*. https://doi.org/10.3389/fnana.2011.00059

Cruz, H. G., Ivanova, T., Lunn, M.-L., Stoffel, M., Slesinger, P. A., & Lüscher, C. (2004). Bi-directional effects of GABAB receptor agonists on the mesolimbic dopamine system. *Nature Neuroscience*, *7*(2), 153–159. https://doi.org/10.1038/nn1181

Da Cunha, C., McKimm, E., Da Cunha, R. M., Boschen, S. L., Redgrave, P., & Blaha, C. D. (2017). Mechanism for optimization of signal-to-noise ratio of dopamine release based on short-term bidirectional plasticity. *Brain Research*, *1667*, 68–73. https://doi.org/10.1016/j.brainres.2017.05.002

Daberkow, D. P., Brown, H. D., Bunner, K. D., Kraniotis, S. A., Doellman, M. A., Ragozzino, M. E., Garris, P. A., & Roitman, M. F. (2013). Amphetamine Paradoxically Augments

Exocytotic Dopamine Release and Phasic Dopamine Signals. *Journal of Neuroscience*, *33*(2), 452–463. https://doi.org/10.1523/JNEUROSCI.2136-12.2013

Dai, M., & Tepper, J. M. (1998). Do silent dopaminergic neurons exist in rat substantia nigra *in vivo*? *Neuroscience*, *85*(4), 1089–1099. https://doi.org/10.1016/S0306-4522(97)00615-5

Day, M., Carr, D. B., Ulrich, S., Ilijic, E., Tkatch, T., & Surmeier, D. J. (2005). Dendritic Excitability of Mouse Frontal Cortex Pyramidal Neurons Is Shaped by the Interaction among HCN, Kir2, and Kleak Channels. *Journal of Neuroscience*, *25*(38), 8776–8787. https://doi.org/10.1523/JNEUROSCI.2650-05.2005

De Camilli, P., Harris, S. M., Huttner, W. B., & Greengard, P. (1983). *Synapsin I (Protein I), a nerve terminal-specific phosphoprotein. II. Its specific association with synaptic vesicles demonstrated by immunocytochemistry in agarose-embedded synaptosomes. | Journal of Cell Biology | Rockefeller University Press*. https://rupress.org/jcb/article/96/5/1355/59233/Synapsin-I-Protein-I-a-nerve-terminal-specific

DeBaker, M. C., Velasco, E. M. F. de, McCall, N. M., Lee, A. M., & Wickman, K. (2021). Differential Impact of Inhibitory G-Protein Signaling Pathways in Ventral Tegmental Area Dopamine Neurons on Behavioral Sensitivity to Cocaine and Morphine. *eNeuro*, *8*(2). https://doi.org/10.1523/ENEURO.0081-21.2021

Debanne, D. (2004). Information processing in the axon. *Nature Reviews Neuroscience*, *5*(4), 304–316. https://doi.org/10.1038/nrn1397

Debanne, D., Guérineau, N. C., Gähwiler, B. H., & Thompson, S. M. (1997). Action-potential propagation gated by an axonal IA-like K+ conductance in hippocampus. *Nature*, *389*(6648), 286–289. https://doi.org/10.1038/38502

Deken, S. L., Beckman, M. L., Boos, L., & Quick, M. W. (2000a). Transport rates of GABA transporters: Regulation by the N-terminal domain and syntaxin 1A. *Nature Neuroscience*, *3*(10), 998–1003. https://doi.org/10.1038/79939

Deken, S. L., Beckman, M. L., Boos, L., & Quick, M. W. (2000b). Transport rates of GABA transporters: Regulation by the N-terminal domain and syntaxin 1A. *Nature Neuroscience*, *3*(10), 998–1003. https://doi.org/10.1038/79939

del Burgo, L. S., Cortes, R., Mengod, G., Zarate, J., Echevarria, E., & Salles, J. (2008). Distribution and neurochemical characterization of neurons expressing GIRK channels in the rat brain. *Journal of Comparative Neurology*, *510*(6), 581–606. https://doi.org/10.1002/cne.21810

DeLong, M. R. (1990). Primate models of movement disorders of basal ganglia origin. *Trends in Neurosciences*, *13*(7), 281–285. https://doi.org/10.1016/0166-2236(90)90110-V

DeLong, M. R., & Wichmann, T. (2007). Circuits and Circuit Disorders of the Basal Ganglia. *Archives of Neurology*, *64*(1), 20–24. https://doi.org/10.1001/archneur.64.1.20

Descarries, L., Watkins, K. C., Garcia, S., Bosler, O., & Doucet, G. (1996). Dual character, asynaptic and synaptic, of the dopamine innervation in adult rat neostriatum: A quantitative autoradiographic and immunocytochemical analysis. *Journal of Comparative Neurology*, *375*(2), 167–186. https://doi.org/10.1002/(SICI)1096-9861(19961111)375:2<167::AID-CNE1>3.0.CO;2-0

Deschênes, M., & Landry, P. (1980). Axonal branch diameter and spacing of nodes in the terminal arborization of identified thalamic and cortical neurons. *Brain Research*, *191*(2), 538–544. https://doi.org/10.1016/0006-8993(80)91302-5

DiFrancesco, J. C., & DiFrancesco, D. (2015). Dysfunctional HCN ion channels in neurological diseases. *Frontiers in Cellular Neuroscience*, *9*. https://doi.org/10.3389/fncel.2015.00071

Dittrich, L., Heiss, J. E., Warrier, D. R., Perez, X. A., Quik, M., & Kilduff, T. S. (2012). Cortical nNOS neurons co-express the NK1 receptor and are depolarized by Substance P in multiple mammalian species. *Frontiers in Neural Circuits*, *6*. https://doi.org/10.3389/fncir.2012.00031

Dodson, P. D., Dreyer, J. K., Jennings, K. A., Syed, E. C. J., Wade-Martins, R., Cragg, S. J., Bolam, J. P., & Magill, P. J. (2016). Representation of spontaneous movement by dopaminergic neurons is cell-type selective and disrupted in parkinsonism. *Proceedings of the National Academy of Sciences*, *113*(15), E2180–E2188. https://doi.org/10.1073/pnas.1515941113

Edwards, N. J., Tejeda, H. A., Pignatelli, M., Zhang, S., McDevitt, R. A., Wu, J., Bass, C. E., Bettler, B., Morales, M., & Bonci, A. (2017). Circuit specificity in the inhibitory architecture of the VTA regulates cocaine-induced behavior. *Nature Neuroscience*, *20*(3), 438–448. https://doi.org/10.1038/nn.4482

Ehringer, H., & Hornykiewicz, O. (1960). Verteilung Von Noradrenalin Und Dopamin (3-Hydroxytyramin) Im Gehirn Des Menschen Und Ihr Verhalten Bei Erkrankungen Des Extrapyramidalen Systems. *Klinische Wochenschrift*, *38*(24), 1236–1239. https://doi.org/10.1007/BF01485901

El-Brolosy, M. A., & Stainier, D. Y. R. (2017). Genetic compensation: A phenomenon in search of mechanisms. *PLOS Genetics*, *13*(7), e1006780. https://doi.org/10.1371/journal.pgen.1006780

Ellerkmann, R. K., Riazanski, V., Elger, C. E., Urban, B. W., & Beck, H. (2001). Slow recovery from inactivation regulates the availability of voltage-dependent Na+ channels in hippocampal granule cells, hilar neurons and basket cells. *The Journal of Physiology*, *532*(2), 385–397. https://doi.org/10.1111/j.1469-7793.2001.0385f.x

Eriksen, J., Jørgensen, T. N., & Gether, U. (2010). Regulation of dopamine transporter function by protein-protein interactions: New discoveries and methodological challenges.

Journal of Neurochemistry, *113*(1), 27–41. https://doi.org/10.1111/j.1471-4159.2010.06599.x

Ernst, M., Bruckner, S., Boresch, S., & Sieghart, W. (2005). Comparative Models of GABAA Receptor Extracellular and Transmembrane Domains: Important Insights in Pharmacology and Function. *Molecular Pharmacology*, *68*(5), 1291–1300. https://doi.org/10.1124/mol.105.015982

Erreger, K., Grewer, C., Javitch, J. A., & Galli, A. (2008). Currents in Response to Rapid Concentration Jumps of Amphetamine Uncover Novel Aspects of Human Dopamine Transporter Function. *Journal of Neuroscience*, *28*(4), 976–989. https://doi.org/10.1523/JNEUROSCI.2796-07.2008

España, R. A., Roberts, D. C. S., & Jones, S. R. (2008). Short-acting cocaine and long-acting GBR-12909 both elicit rapid dopamine uptake inhibition following intravenous delivery. *Neuroscience*, *155*(1), 250–257. https://doi.org/10.1016/j.neuroscience.2008.05.022

Evans, R. C., Zhu, M., & Khaliq, Z. M. (2017). Dopamine Inhibition Differentially Controls Excitability of Substantia Nigra Dopamine Neuron Subpopulations through T-Type Calcium Channels. *Journal of Neuroscience*, *37*(13), 3704–3720. https://doi.org/10.1523/JNEUROSCI.0117-17.2017

Evans, S. W., Shi, D.-Q., Chavarha, M., Plitt, M. H., Taxidis, J., Madruga, B., Fan, J. L., Hwang, F.-J., van Keulen, S. C., Suomivuori, C.-M., Pang, M. M., Su, S., Lee, S., Hao, Y. A., Zhang, G., Jiang, D., Pradhan, L., Roth, R. H., Liu, Y., … Lin, M. Z. (2023). A positively tuned voltage indicator for extended electrical recordings in the brain. *Nature Methods*, *20*(7), 1104–1113. https://doi.org/10.1038/s41592-023-01913-z

Farrant, M., & Nusser, Z. (2005). Variations on an inhibitory theme: Phasic and tonic activation of GABAA receptors. *Nature Reviews Neuroscience*, *6*(3), 215–229. https://doi.org/10.1038/nrn1625

Faustini, G., Longhena, F., Muscò, A., Bono, F., Parrella, E., La Via, L., Barbon, A., Pizzi, M., Onofri, F., Benfenati, F., Missale, C., Memo, M., Zizioli, D., & Bellucci, A. (2022). Synapsin III Regulates Dopaminergic Neuron Development in Vertebrates. *Cells*, *11*(23), Article 23. https://doi.org/10.3390/cells11233902

Feng, J., Chi, P., Blanpied, T. A., Xu, Y., Magarinos, A. M., Ferreira, A., Takahashi, R. H., Kao, H.-T., McEwen, B. S., Ryan, T. A., Augustine, G. J., & Greengard, P. (2002). Regulation of Neurotransmitter Release by Synapsin III. *The Journal of Neuroscience*, *22*(11), 4372–4380. https://doi.org/10.1523/JNEUROSCI.22-11-04372.2002

Ferreira, A., Kao, H.-T., Feng, J., Rapoport, M., & Greengard, P. (2000). Synapsin III: Developmental Expression, Subcellular Localization, and Role in Axon Formation. *The Journal of Neuroscience*, *20*(10), 3736–3744. https://doi.org/10.1523/JNEUROSCI.20-10-03736.2000

Fino, E., Vandecasteele, M., Perez, S., Saudou, F., & Venance, L. (2018). Region-specific and state-dependent action of striatal GABAergic interneurons. *Nature Communications*, *9*(1), 3339. https://doi.org/10.1038/s41467-018-05847-5

Fioravante, D., & Regehr, W. G. (2011). Short-term forms of presynaptic plasticity. *Current Opinion in Neurobiology*, *21*(2), 269–274. https://doi.org/10.1016/j.conb.2011.02.003

Fog, J. U., Khoshbouei, H., Holy, M., Owens, W. A., Vaegter, C. B., Sen, N., Nikandrova, Y., Bowton, E., McMahon, D. G., Colbran, R. J., Daws, L. C., Sitte, H. H., Javitch, J. A., Galli, A., & Gether, U. (2006). Calmodulin Kinase II Interacts with the Dopamine Transporter C Terminus to Regulate Amphetamine-Induced Reverse Transport. *Neuron*, *51*(4), 417–429. https://doi.org/10.1016/j.neuron.2006.06.028

Forn, J., & Greengard, P. (1978). Depolarizing agents and cyclic nucleotides regulate the phosphorylation of specific neuronal proteins in rat cerebral cortex slices. *Proceedings of the National Academy of Sciences*, *75*(10), 5195–5199. https://doi.org/10.1073/pnas.75.10.5195

Freeman, A. S., Meltzer, L. T., & Bunney, B. S. (1985). Firing properties of substantia nigra dopaminergic neurons in freely moving rats. *Life Sciences*, *36*(20), 1983–1994. https://doi.org/10.1016/0024-3205(85)90448-5

Fuortes, M. G. F., Frank, K., & Becker, M. C. (1957). STEPS IN THE PRODUCTION OF MOTONEURON SPIKES. *Journal of General Physiology*, *40*(5), 735–752. https://doi.org/10.1085/jgp.40.5.735

Gainetdinov, R. R., Jones, S. R., & Caron, M. G. (1999). Functional hyperdopaminergia in dopamine transporter knock-out mice. *Biological Psychiatry*, *46*(3), 303–311. https://doi.org/10.1016/S0006-3223(99)00122-5

Garcia-Olivares, J., Torres-Salazar, D., Owens, W. A., Baust, T., Siderovski, D. P., Amara, S. G., Zhu, J., Daws, L. C., & Torres, G. E. (2013). Inhibition of Dopamine Transporter Activity by G Protein βγ Subunits. *PLOS ONE*, *8*(3), e59788. https://doi.org/10.1371/journal.pone.0059788

Gerfen, C. R., Baimbridge, K. G., & Miller, J. J. (1985). The neostriatal mosaic: Compartmental distribution of calcium-binding protein and parvalbumin in the basal ganglia of the rat and monkey. *Proceedings of the National Academy of Sciences*, *82*(24), 8780–8784. https://doi.org/10.1073/pnas.82.24.8780

Ghit, A., Assal, D., Al-Shami, A. S., & Hussein, D. E. E. (2021). GABAA receptors: Structure, function, pharmacology, and related disorders. *Journal of Genetic Engineering and Biotechnology*, *19*(1), 123. https://doi.org/10.1186/s43141-021-00224-0

Gingrich, J. A., & Caron, M. G. (1993). Recent Advances in the Molecular Biology of Dopamine Receptors. *Annual Review of Neuroscience*, *16*(Volume 16, 1993), 299–321. https://doi.org/10.1146/annurev.ne.16.030193.001503

Giros, B., Jaber, M., Jones, S. R., Wightman, R. M., & Caron, M. G. (1996). Hyperlocomotion and indifference to cocaine and amphetamine in mice lacking the dopamine transporter. *Nature*, *379*(6566), 606–612. https://doi.org/10.1038/379606a0

Giros, B., Martres, M.-P., Pilon, C., Sokoloff, P., & Schwartz, J.-C. (1991). Shorter variants of the D3 dopamine receptor produced through various patterns of alternative splicing. *Biochemical and Biophysical Research Communications*, *176*(3), 1584–1592. https://doi.org/10.1016/0006-291X(91)90469-N

Giros, B., Sokoloff, P., Martres, M.-P., Riou, J.-F., Emorine, L. J., & Schwartz, J.-C. (1989). Alternative splicing directs the expression of two D2 dopamine receptor isoforms. *Nature*, *342*(6252), 923–926. https://doi.org/10.1038/342923a0

Gittis, A. H., & Kreitzer, A. C. (2012). Striatal microcircuitry and movement disorders. *Trends in Neurosciences*, *35*(9), 557–564. https://doi.org/10.1016/j.tins.2012.06.008

Goldberg, J. A., & Wilson, C. J. (2016). Chapter 7—The Cholinergic Interneuron of the Striatum. In H. Steiner & K. Y. Tseng (Eds.), *Handbook of Behavioral Neuroscience* (Vol. 24, pp. 137–155). Elsevier. https://doi.org/10.1016/B978-0-12-802206-1.00007-6

Goldin, A. L. (2003). Mechanisms of sodium channel inactivation. *Current Opinion in Neurobiology*, *13*(3), 284–290. https://doi.org/10.1016/S0959-4388(03)00065-5

Grace, A. A., & Bunney, B. S. (1983a). Intracellular and extracellular electrophysiology of nigral dopaminergic neurons—1. Identification and characterization. *Neuroscience*, *10*(2), 301–315. https://doi.org/10.1016/0306-4522(83)90135-5

Grace, A. A., & Bunney, B. S. (1983b). Intracellular and extracellular electrophysiology of nigral dopaminergic neurons—3. Evidence for electrotonic coupling. *Neuroscience*, *10*(2), 333–348. https://doi.org/10.1016/0306-4522(83)90137-9

Grace, A. A., & Bunney, B. S. (1984). The control of firing pattern in nigral dopamine neurons: Burst firing. *Journal of Neuroscience*, *4*(11), 2877–2890. https://doi.org/10.1523/JNEUROSCI.04-11-02877.1984

Grace, A. A., Floresco, S. B., Goto, Y., & Lodge, D. J. (2007). Regulation of firing of dopaminergic neurons and control of goal-directed behaviors. *Trends in Neurosciences*, *30*(5), 220–227. https://doi.org/10.1016/j.tins.2007.03.003

Grace, A. A., & Onn, S.-P. (n.d.). *Morphology and Electrophysiological Properties of Immunocytochemically Identified Rat Dopamine Neurons Recorded in wifro*.

Grandy, D. K., Zhou, Q. Y., Allen, L., Litt, R., Magenis, R. E., Civelli, O., & Litt, M. (1990). A human D1 dopamine receptor gene is located on chromosome 5 at q35.1 and identifies an EcoRI RFLP. *American Journal of Human Genetics*, *47*(5), 828–834.

Graveland, G. A., & Difiglia, M. (1985). The frequency and distribution of medium-sized neurons with indented nuclei in the primate and rodent neostriatum. *Brain Research*, *327*(1), 307–311. https://doi.org/10.1016/0006-8993(85)91524-0

Greengard, P., Valtorta, F., Czernik, A. J., & Benfenati, F. (1993). Synaptic Vesicle Phosphoproteins and Regulation of Synaptic Function. *Science*, *259*(5096), 780–785. https://doi.org/10.1126/science.8430330

Grouleff, J., Ladefoged, L. K., Koldsø, H., & Schiøtt, B. (2015). Monoamine transporters: Insights from molecular dynamics simulations. *Frontiers in Pharmacology*, *6*. https://doi.org/10.3389/fphar.2015.00235

Gu, H., Wall, S. C., & Rudnick, G. (1994). Stable expression of biogenic amine transporters reveals differences in inhibitor sensitivity, kinetics, and ion dependence. *The Journal of Biological Chemistry*, *269*(10), 7124–7130.

Gulley, J. M., & Zahniser, N. R. (2003). Rapid regulation of dopamine transporter function by substrates, blockers and presynaptic receptor ligands. *European Journal of Pharmacology*, *479*(1), 139–152. https://doi.org/10.1016/j.ejphar.2003.08.064

Guzman, J. N., Sánchez-Padilla, J., Chan, C. S., & Surmeier, D. J. (2009). Robust Pacemaking in Substantia Nigra Dopaminergic Neurons. *Journal of Neuroscience*, *29*(35), 11011–11019. https://doi.org/10.1523/JNEUROSCI.2519-09.2009

Guzman, J. N., Sanchez-Padilla, J., Wokosin, D., Kondapalli, J., Ilijic, E., Schumacker, P. T., & Surmeier, D. J. (2010). Oxidant stress evoked by pacemaking in dopaminergic neurons

is attenuated by DJ-1. *Nature*, *468*(7324), 696–700. https://doi.org/10.1038/nature09536

Haber, S. N., Ryoo, H., Cox, C., & Lu, W. (1995). Subsets of midbrain dopaminergic neurons in monkeys are distinguished by different levels of mRNA for the dopamine transporter: Comparison with the mRNA for the D2 receptor, tyrosine hydroxylase and calbindin immunoreactivity. *Journal of Comparative Neurology*, *362*(3), 400–410. https://doi.org/10.1002/cne.903620308

Hahn, S., Um, K. B., Kim, S. W., Kim, H. J., & Park, M. K. (2023). Proximal dendritic localization of NALCN channels underlies tonic and burst firing in nigral dopaminergic neurons. *The Journal of Physiology*, *601*(1), 171–193. https://doi.org/10.1113/JP283716

Hamilton, P. J., Belovich, A. N., Khelashvili, G., Saunders, C., Erreger, K., Javitch, J. A., Sitte, H. H., Weinstein, H., Matthies, H. J. G., & Galli, A. (2014). PIP2 regulates psychostimulant behaviors through its interaction with a membrane protein. *Nature Chemical Biology*, *10*(7), 582–589. https://doi.org/10.1038/nchembio.1545

Hansen, S. B., Tao, X., & MacKinnon, R. (2011). Structural basis of PIP2 activation of the classical inward rectifier K+ channel Kir2.2. *Nature*, *477*(7365), 495–498. https://doi.org/10.1038/nature10370

Hao, Y. A., Lee, S., Roth, R. H., Natale, S., Gomez, L., Taxidis, J., O'Neill, P. S., Villette, V., Bradley, J., Wang, Z., Jiang, D., Zhang, G., Sheng, M., Lu, D., Boyden, E., Delvendahl, I., Golshani, P., Wernig, M., Feldman, D. E., … Lin, M. Z. (2024). A fast and responsive voltage indicator with enhanced sensitivity for unitary synaptic events. *Neuron*, *112*(22), 3680-3696.e8. https://doi.org/10.1016/j.neuron.2024.08.019

Hassel, B., Iversen, E. G., Gjerstad, L., & Taubøll, E. (2001). Up-regulation of hippocampal glutamate transport during chronic treatment with sodium valproate. *Journal of Neurochemistry*, *77*(5), 1285–1292. https://doi.org/10.1046/j.1471-4159.2001.00349.x

Hattori, T., Takada, M., Moriizumi, T., & Van Der Kooy, D. (1991). Single dopaminergic nigrostriatal neurons form two chemically distinct synaptic types: Possible transmitter segregation within neurons. *Journal of Comparative Neurology*, *309*(3), 391–401. https://doi.org/10.1002/cne.903090308

He, Y., Zorumski, C. F., & Mennerick, S. (2002). Contribution of Presynaptic Na+ Channel Inactivation to Paired-Pulse Synaptic Depression in Cultured Hippocampal Neurons. *Journal of Neurophysiology*, *87*(2), 925–936. https://doi.org/10.1152/jn.00225.2001

Hersch, S. M., Ciliax, B. J., Gutekunst, C. A., Rees, H. D., Heilman, C. J., Yung, K. K., Bolam, J. P., Ince, E., Yi, H., & Levey, A. I. (1995). Electron microscopic analysis of D1 and D2 dopamine receptor proteins in the dorsal striatum and their synaptic relationships with motor corticostriatal afferents. *Journal of Neuroscience*, *15*(7), 5222–5237. https://doi.org/10.1523/JNEUROSCI.15-07-05222.1995

Hersch, S. M., Yi, H., Heilman, C. J., Edwards, R. H., & Levey, A. I. (1997). Subcellular localization and molecular topology of the dopamine transporter in the striatum and substantia nigra. *Journal of Comparative Neurology*, *388*(2), 211–227. https://doi.org/10.1002/(SICI)1096-9861(19971117)388:2<211::AID-CNE3>3.0.CO;2-4

Higgs, M. H., Jones, J. A., Wilson, C. J., & Beckstead, M. J. (2023). SK and Kv4 Channels Limit Spike Timing Perturbations in Pacemaking Dopamine Neurons. *eNeuro*, *10*(4). https://doi.org/10.1523/ENEURO.0445-22.2023

Hilfiker, S., Pieribone, V. A., Czernik, A. J., Kao, H.-T., Augustine, G. J., & Greengard, P. (1999). Synapsins as regulators of neurotransmitter release. *Philosophical Transactions of the Royal Society of London. Series B: Biological Sciences*, *354*(1381), 269–279. https://doi.org/10.1098/rstb.1999.0378

Hirsch, E., Graybiel, A. M., & Agid, Y. A. (1988). Melanized dopaminergic neurons are differentially susceptible to degeneration in Parkinson's disease. *Nature*, *334*(6180), 345–348. https://doi.org/10.1038/334345a0

Hodgkin, A. L., & Huxley, A. F. (1952a). Currents carried by sodium and potassium ions through the membrane of the giant axon of Loligo. *The Journal of Physiology*, *116*(4), 449–472. https://doi.org/10.1113/jphysiol.1952.sp004717

Hodgkin, A. L., & Huxley, A. F. (1952b). The components of membrane conductance in the giant axon of Loligo. *The Journal of Physiology*, *116*(4), 473–496. https://doi.org/10.1113/jphysiol.1952.sp004718

Holly, E. N., Davatolhagh, M. F., España, R. A., & Fuccillo, M. V. (2021). Striatal low-threshold spiking interneurons locally gate dopamine. *Current Biology*, *31*(18), 4139-4147.e6. https://doi.org/10.1016/j.cub.2021.06.081

Honda, I., Araki, K., Honda, S., Soeda, F., Shin, M.-C., Misumi, S., Yamamura, K., & Takahama, K. (2018). Deletion of GIRK2 subunit containing GIRK channels of neurons expressing dopamine transporter decrease immobility time on forced swimming in mice. *Neuroscience Letters*, *665*, 140–146. https://doi.org/10.1016/j.neulet.2017.11.028

Hong, W. C., & Amara, S. G. (2010). Membrane Cholesterol Modulates the Outward Facing Conformation of the Dopamine Transporter and Alters Cocaine Binding*. *Journal of Biological Chemistry*, *285*(42), 32616–32626. https://doi.org/10.1074/jbc.M110.150565

Hosaka, M., & Südhof, T. C. (1998a). Synapsin III, a Novel Synapsin with an Unusual Regulation by Ca2+*. *Journal of Biological Chemistry*, *273*(22), 13371–13374. https://doi.org/10.1074/jbc.273.22.13371

Hosaka, M., & Südhof, T. C. (1998b). Synapsins I and II Are ATP-binding Proteins with Differential Ca2+ Regulation*. *Journal of Biological Chemistry*, *273*(3), 1425–1429. https://doi.org/10.1074/jbc.273.3.1425

Howard, C. D., Li, H., Geddes, C. E., & Jin, X. (2017). Dynamic Nigrostriatal Dopamine Biases Action Selection. *Neuron*, *93*(6), 1436-1450.e8. https://doi.org/10.1016/j.neuron.2017.02.029

Howe, M. W., & Dombeck, D. A. (2016). Rapid signalling in distinct dopaminergic axons during locomotion and reward. *Nature*, *535*(7613), 505–510. https://doi.org/10.1038/nature18942

Huang, C. K., Browning, M. D., & Greengard, P. (1982). Purification and characterization of protein IIIb, a mammalian brain phosphoprotein. *Journal of Biological Chemistry*, *257*(11), 6524–6528. https://doi.org/10.1016/S0021-9258(20)65173-0

Humphrey, P. P. A., Hartig, P., & Hoyer, D. (1993). A proposed new nomenclature for 5-HT receptors. *Trends in Pharmacological Sciences*, *14*(6), 233–236. https://doi.org/10.1016/0165-6147(93)90016-D

Huttner, W. B., & Greengard, P. (1979). Multiple phosphorylation sites in protein I and their differential regulation by cyclic AMP and calcium. *Proceedings of the National Academy of Sciences*, *76*(10), 5402–5406. https://doi.org/10.1073/pnas.76.10.5402

Huttner, W. B., Schiebler, W., Greengard, P., & De Camilli, P. (1983). *Synapsin I (protein I), a nerve terminal-specific phosphoprotein. III. Its association with synaptic vesicles studied in a highly purified synaptic vesicle preparation—PubMed*. https://pubmed.ncbi.nlm.nih.gov/6404912/

Hyland, B. I., Reynolds, J. N. J., Hay, J., Perk, C. G., & Miller, R. (2002). Firing modes of midbrain dopamine cells in the freely moving rat. *Neuroscience*, *114*(2), 475–492. https://doi.org/10.1016/S0306-4522(02)00267-1

Inanobe, A., Horio, Y., Fujita, A., Tanemoto, M., Hibino, H., Inageda, K., & Kurachi, Y. (1999). Molecular cloning and characterization of a novel splicing variant of the Kir3.2 subunit predominantly expressed in mouse testis. *The Journal of Physiology*, *521*(1), 19–30. https://doi.org/10.1111/j.1469-7793.1999.00019.x

Inanobe, A., Yoshimoto, Y., Horio, Y., Morishige, K.-I., Hibino, H., Matsumoto, S., Tokunaga, Y., Maeda, T., Hata, Y., Takai, Y., & Kurachi, Y. (1999). Characterization of G-Protein-Gated K+ Channels Composed of Kir3.2 Subunits in Dopaminergic Neurons of the Substantia Nigra. *Journal of Neuroscience*, *19*(3), 1006–1017. https://doi.org/10.1523/JNEUROSCI.19-03-01006.1999

Ingram, S. L., & Amara, S. G. (2000). Arachidonic Acid Stimulates a Novel Cocaine-Sensitive Cation Conductance Associated with the Human Dopamine Transporter. *Journal of Neuroscience*, *20*(2), 550–557. https://doi.org/10.1523/JNEUROSCI.20-02-00550.2000

Ingram, S. L., Prasad, B. M., & Amara, S. G. (2002). Dopamine transporter–mediated conductances increase excitability of midbrain dopamine neurons. *Nature Neuroscience*, *5*(10), 971–978. https://doi.org/10.1038/nn920

Isomoto, S., Kondo, C., Takahashi, N., Matsumoto, S., Yamada, M., Takumi, T., Horio, Y., & Kurachi, Y. (1996). A Novel Ubiquitously Distributed Isoform of GIRK2 (GIRK2B) Enhances GIRK1 Expression of the G-Protein-Gated K+ Current in*Xenopus*Oocytes. *Biochemical and Biophysical Research Communications*, *218*(1), 286–291. https://doi.org/10.1006/bbrc.1996.0050

Jafri, M. S., & Weinreich, D. (1996). Substance P hyperpolarizes vagal sensory neurones of the ferret. *The Journal of Physiology*, *493*(Pt 1), 157–166. https://doi.org/10.1113/jphysiol.1996.sp021371

Janezic, S., Threlfell, S., Dodson, P. D., Dowie, M. J., Taylor, T. N., Potgieter, D., Parkkinen, L., Senior, S. L., Anwar, S., Ryan, B., Deltheil, T., Kosillo, P., Cioroch, M., Wagner, K., Ansorge, O., Bannerman, D. M., Bolam, J. P., Magill, P. J., Cragg, S. J., & Wade-Martins, R. (2013a). Deficits in dopaminergic transmission precede neuron loss and dysfunction in a new Parkinson model. *Proceedings of the National Academy of Sciences*, *110*(42), E4016–E4025. https://doi.org/10.1073/pnas.1309143110

Janezic, S., Threlfell, S., Dodson, P. D., Dowie, M. J., Taylor, T. N., Potgieter, D., Parkkinen, L., Senior, S. L., Anwar, S., Ryan, B., Deltheil, T., Kosillo, P., Cioroch, M., Wagner, K., Ansorge, O., Bannerman, D. M., Bolam, J. P., Magill, P. J., Cragg, S. J., & Wade-Martins, R. (2013b). Deficits in dopaminergic transmission precede neuron loss and dysfunction in a new Parkinson model. *Proceedings of the National Academy of Sciences*, *110*(42), E4016–E4025. https://doi.org/10.1073/pnas.1309143110

Jembrek, M. J., & Vlainic, J. (2015). GABA Receptors: Pharmacological Potential and Pitfalls. *Current Pharmaceutical Design*, *21*(34), 4943–4959. https://doi.org/10.2174/1381612821666150914121624

Jeremic, D., Sanchez-Rodriguez, I., Jimenez-Diaz, L., & Navarro-Lopez, J. D. (2021). Therapeutic potential of targeting G protein-gated inwardly rectifying potassium (GIRK) channels in the central nervous system. *Pharmacology & Therapeutics*, *223*, 107808. https://doi.org/10.1016/j.pharmthera.2021.107808

Jin, W., Klem, A. M., Lewis, J. H., & Lu, Z. (1999). Mechanisms of Inward-Rectifier K+ Channel Inhibition by Tertiapin-Q. *Biochemistry*, *38*(43), 14294–14301. https://doi.org/10.1021/bi991206j

Jin, W., & Lu, Z. (1998). A Novel High-Affinity Inhibitor for Inward-Rectifier K+ Channels. *Biochemistry*, *37*(38), 13291–13299. https://doi.org/10.1021/bi981178p

John, C. E., & Jones, S. R. (2007). Voltammetric characterization of the effect of monoamine uptake inhibitors and releasers on dopamine and serotonin uptake in mouse caudate-putamen and substantia nigra slices. *Neuropharmacology*, *52*(8), 1596–1605. https://doi.org/10.1016/j.neuropharm.2007.03.004

Jones, K. A., Borowsky, B., Tamm, J. A., Craig, D. A., Durkin, M. M., Dai, M., Yao, W.-J., Johnson, M., Gunwaldsen, C., Huang, L.-Y., Tang, C., Shen, Q., Salon, J. A., Morse, K., Laz, T., Smith, K. E., Nagarathnam, D., Noble, S. A., Branchek, T. A., & Gerald, C.

(1998). GABAB receptors function as a heteromeric assembly of the subunits GABABR1 and GABABR2. *Nature*, *396*(6712), 674–679. https://doi.org/10.1038/25348

Jones, K. T., Zhen, J., & Reith, M. E. A. (2012). Importance of cholesterol in dopamine transporter function. *Journal of Neurochemistry*, *123*(5), 700–715. https://doi.org/10.1111/jnc.12007

Juarez, B., Kong, M.-S., Jo, Y. S., Elum, J. E., Yee, J. X., Ng-Evans, S., Cline, M., Hunker, A. C., Quinlan, M. A., Baird, M. A., Elerding, A. J., Johnson, M., Ban, D., Mendez, A., Goodwin, N. L., Soden, M. E., & Zweifel, L. S. (2023). Temporal scaling of dopamine neuron firing and dopamine release by distinct ion channels shape behavior. *Science Advances*, *9*(32), eadg8869. https://doi.org/10.1126/sciadv.adg8869

Kaeser, P. S., & Regehr, W. G. (2014). Molecular Mechanisms for Synchronous, Asynchronous, and Spontaneous Neurotransmitter Release. *Annual Review of Physiology*, *76*(Volume 76, 2014), 333–363. https://doi.org/10.1146/annurev-physiol-021113-170338

Kaila, K. (1994). Ionic basis of GABAA receptor channel function in the nervous system. *Progress in Neurobiology*, *42*(4), 489–537. https://doi.org/10.1016/0301-0082(94)90049-3

Kaila, K., Voipio, J., Paalasmaa, P., Pasternack, M., & Deisz, R. A. (1993). The role of bicarbonate in GABAA receptor-mediated IPSPs of rat neocortical neurones. *The Journal of Physiology*, *464*(1), 273–289. https://doi.org/10.1113/jphysiol.1993.sp019634

Kalivas, P. W., Duffy, P., & Eberhardt, H. (1990). Modulation of A10 dopamine neurons by gamma-aminobutyric acid agonists. *The Journal of Pharmacology and Experimental Therapeutics*, *253*(2), 858–866. https://doi.org/10.1016/S0022-3565(25)13057-7

Kanjhan, R., Coulson, E. J., Adams, D. J., & Bellingham, M. C. (2005). Tertiapin-Q Blocks Recombinant and Native Large Conductance K+ Channels in a Use-Dependent

Manner. *The Journal of Pharmacology and Experimental Therapeutics*, *314*(3), 1353–1361. https://doi.org/10.1124/jpet.105.085928

Kao, H.-T., Porton, B., Czernik, A. J., Feng, J., Yiu, G., Häring, M., Benfenati, F., & Greengard, P. (1998). A third member of the synapsin gene family. *Proceedings of the National Academy of Sciences*, *95*(8), 4667–4672. https://doi.org/10.1073/pnas.95.8.4667

Karschin, C., Dißmann, E., Stühmer, W., & Karschin, A. (1996). IRK(1–3) and GIRK(1–4) Inwardly Rectifying K+Channel mRNAs Are Differentially Expressed in the Adult Rat Brain. *Journal of Neuroscience*, *16*(11), 3559–3570. https://doi.org/10.1523/JNEUROSCI.16-11-03559.1996

Kase, D., & Imoto, K. (2012). The Role of HCN Channels on Membrane Excitability in the Nervous System. *Journal of Signal Transduction*, *2012*(1), 619747. https://doi.org/10.1155/2012/619747

Katz, B., & Miledi, R. (1968). The role of calcium in neuromuscular facilitation. *The Journal of Physiology*, *195*(2), 481–492. https://doi.org/10.1113/jphysiol.1968.sp008469

Katz, B., & Thesleff, S. (1957). A study of the 'desensitization' produced by acetylcholine at the motor end-plate. *The Journal of Physiology*, *138*(1), 63–80. https://doi.org/10.1113/jphysiol.1957.sp005838

Kaupmann, K., Malitschek, B., Schuler, V., Heid, J., Froestl, W., Beck, P., Mosbacher, J., Bischoff, S., Kulik, A., Shigemoto, R., Karschin, A., & Bettler, B. (1998). GABAB-receptor subtypes assemble into functional heteromeric complexes. *Nature*, *396*(6712), 683–687. https://doi.org/10.1038/25360

Kebabian, J. W. (1978). Multiple classes of dopamine receptors in mammalian central nervous system: The involvement of dopamine-sensitive adenylyl cyclase. *Life Sciences*, *23*(5), 479–483. https://doi.org/10.1016/0024-3205(78)90157-1

Kebabian, J. W., & Calne, D. B. (1979). Multiple receptors for dopamine. *Nature*, *277*(5692), 93–96. https://doi.org/10.1038/277093a0

Keighron, J. D., Bonaventura, J., Li, Y., Yang, J.-W., DeMarco, E. M., Hersey, M., Cao, J., Sandtner, W., Michaelides, M., Sitte, H. H., Newman, A. H., & Tanda, G. (2023). Interactions of calmodulin kinase II with the dopamine transporter facilitate cocaine-induced enhancement of evoked dopamine release. *Translational Psychiatry*, *13*(1), 1–10. https://doi.org/10.1038/s41398-023-02493-4

Kemp, J. M. (1968). Observations on the caudate nucleus of the cat impregnated with the Golgi method. *Brain Research*, *11*(2), 467–470. https://doi.org/10.1016/0006-8993(68)90043-7

Khakh, B. S. (2019). Astrocyte–Neuron Interactions in the Striatum: Insights on Identity, Form, and Function. *Trends in Neurosciences*, *42*(9), 617–630. https://doi.org/10.1016/j.tins.2019.06.003

Khaliq, Z. M., & Bean, B. P. (2010). Pacemaking in Dopaminergic Ventral Tegmental Area Neurons: Depolarizing Drive from Background and Voltage-Dependent Sodium Conductances. *Journal of Neuroscience*, *30*(21), 7401–7413. https://doi.org/10.1523/JNEUROSCI.0143-10.2010

Khelashvili, G., Stanley, N., Sahai, M. A., Medina, J., LeVine, M. V., Shi, L., De Fabritiis, G., & Weinstein, H. (2015). Spontaneous Inward Opening of the Dopamine Transporter Is Triggered by PIP2-Regulated Dynamics of the N-Terminus. *ACS Chemical Neuroscience*, *6*(11), 1825–1837. https://doi.org/10.1021/acschemneuro.5b00179

Kilb, W. (2021). When Are Depolarizing GABAergic Responses Excitatory? *Frontiers in Molecular Neuroscience*, *14*. https://doi.org/10.3389/fnmol.2021.747835

Kile, B. M., Guillot, T. S., Venton, B. J., Wetsel, W. C., Augustine, G. J., & Wightman, R. M. (2010). Synapsins Differentially Control Dopamine and Serotonin Release. *Journal of Neuroscience*, *30*(29), 9762–9770. https://doi.org/10.1523/JNEUROSCI.2071-09.2010

Kim, H.-J., Hwang, B., Reva, M., Lee, J., Lee, B. E., Lee, Y., Cho, E. J., Jeong, M., Lee, S. E., Myung, K., Baik, J.-H., Park, J.-H., & Kim, J.-I. (2023). GABAergic-like dopamine

synapses in the brain. *Cell Reports*, *42*(10), 113239. https://doi.org/10.1016/j.celrep.2023.113239

Kim, J.-I., Ganesan, S., Luo, S. X., Wu, Y.-W., Park, E., Huang, E. J., Chen, L., & Ding, J. B. (2015). Aldehyde dehydrogenase 1a1 mediates a GABA synthesis pathway in midbrain dopaminergic neurons. *Science*. https://doi.org/10.1126/science.aac4690

Kimm, T., Khaliq, Z. M., & Bean, B. P. (2015). Differential Regulation of Action Potential Shape and Burst-Frequency Firing by BK and Kv2 Channels in Substantia Nigra Dopaminergic Neurons. *Journal of Neuroscience*, *35*(50), 16404–16417. https://doi.org/10.1523/JNEUROSCI.5291-14.2015

Kish, S. J., Shannak, K., & Hornykiewicz, O. (1988). Uneven Pattern of Dopamine Loss in the Striatum of Patients with Idiopathic Parkinson's Disease. *New England Journal of Medicine*, *318*(14), 876–880. https://doi.org/10.1056/NEJM198804073181402

Kishida, K. T., Saez, I., Lohrenz, T., Witcher, M. R., Laxton, A. W., Tatter, S. B., White, J. P., Ellis, T. L., Phillips, P. E. M., & Montague, P. R. (2016). Subsecond dopamine fluctuations in human striatum encode superposed error signals about actual and counterfactual reward. *Proceedings of the National Academy of Sciences*, *113*(1), 200–205. https://doi.org/10.1073/pnas.1513619112

Kishida, K. T., Sandberg, S. G., Lohrenz, T., Comair, Y. G., Sáez, I., Phillips, P. E. M., & Montague, P. R. (2011). Sub-Second Dopamine Detection in Human Striatum. *PLOS ONE*, *6*(8), e23291. https://doi.org/10.1371/journal.pone.0023291

Kobayashi, T., Ikeda, K., Ichikawa, T., Abe, S., Togashi, S., & Kumanishi, T. (1995). Molecular Cloning of a Mouse G-Protein-Activated K+ Channel (mGIRK1) and Distinct Distributions of 3 GIRK (GIRK1, 2 and 3) mRNAs in Mouse Brain. *Biochemical and Biophysical Research Communications*, *208*(3), 1166–1173. https://doi.org/10.1006/bbrc.1995.1456

Kotecki, L., Hearing, M., McCall, N. M., Velasco, E. M. F. de, Pravetoni, M., Arora, D., Victoria, N. C., Munoz, M. B., Xia, Z., Slesinger, P. A., Weaver, C. D., & Wickman, K. (2015). GIRK Channels Modulate Opioid-Induced Motor Activity in a Cell Type- and Subunit-Dependent Manner. *Journal of Neuroscience*, *35*(18), 7131–7142. https://doi.org/10.1523/JNEUROSCI.5051-14.2015

Koyrakh, L., Luján, R., Colón, J., Karschin, C., Kurachi, Y., Karschin, A., & Wickman, K. (2005). Molecular and Cellular Diversity of Neuronal G-Protein-Gated Potassium Channels. *Journal of Neuroscience*, *25*(49), 11468–11478. https://doi.org/10.1523/JNEUROSCI.3484-05.2005

Kozek, K. A., Du, Y., Sharma, S., Francis J. Prael, I. I. I., Spitznagel, B. D., Kharade, S. V., Denton, J. S., Hopkins, C. R., & Weaver, C. D. (2018). Discovery and Characterization of VU0529331, a Synthetic Small-Molecule Activator of Homomeric G Protein-Gated, Inwardly Rectifying, Potassium (GIRK) Channels. *ACS Chemical Neuroscience*. https://doi.org/10.1021/acschemneuro.8b00287

Kozek, K. A., Du, Y., Sharma, S., Prael, F. J. I., Spitznagel, B. D., Kharade, S. V., Denton, J. S., Hopkins, C. R., & Weaver, C. D. (2019). Discovery and Characterization of VU0529331, a Synthetic Small-Molecule Activator of Homomeric G Protein-Gated, Inwardly Rectifying, Potassium (GIRK) Channels. *ACS Chemical Neuroscience*, *10*(1), 358–370. https://doi.org/10.1021/acschemneuro.8b00287

Kramer, P. F., Brill-Weil, S. G., Cummins, A. C., Zhang, R., Camacho-Hernandez, G. A., Newman, A. H., Eldridge, M. A. G., Averbeck, B. B., & Khaliq, Z. M. (2022). Synaptic-like axo-axonal transmission from striatal cholinergic interneurons onto dopaminergic fibers. *Neuron*, *110*(18), 2949-2960.e4. https://doi.org/10.1016/j.neuron.2022.07.011

Kramer, P. F., Twedell, E. L., Shin, J. H., Zhang, R., & Khaliq, Z. M. (2020). Axonal mechanisms mediating γ-aminobutyric acid receptor type A (GABA-A) inhibition of striatal dopamine release. *eLife*, *9*, e55729. https://doi.org/10.7554/eLife.55729

Kramer, P. F., & Williams, J. T. (2016). Calcium Release from Stores Inhibits GIRK. *Cell Reports*, *17*(12), 3246–3255. https://doi.org/10.1016/j.celrep.2016.11.076

Krnjević, K., & Miledi, R. (1959). Presynaptic failure of neuromuscular propagation in rats. *The Journal of Physiology*, *149*(1), 1–22. https://doi.org/10.1113/jphysiol.1959.sp006321

Krueger, B. K. (1990). Kinetics and Block of Dopamine Uptake in Synaptosomes from Rat Caudate Nucleus. *Journal of Neurochemistry*, *55*(1), 260–267. https://doi.org/10.1111/j.1471-4159.1990.tb08847.x

Kuhr, W. G., & Wightman, R. M. (1986). Real-time measurement of dopamine release in rat brain. *Brain Research*, *381*(1), 168–171. https://doi.org/10.1016/0006-8993(86)90707-9

Kuiper, L. B., Dawes, M. H., West, A. M., DiMarco, E. K., Galante, E. V., Kishida, K. T., & Jones, S. R. (2024). Comparison of dopamine release and uptake parameters across sex, species and striatal subregions. *European Journal of Neuroscience*, *60*(6), 5113–5140. https://doi.org/10.1111/ejn.16495

Kuzhikandathil, E. V., & Oxford, G. S. (2002). Classic D1 Dopamine Receptor AntagonistR-(+)-7-Chloro-8-hydroxy-3-methyl-1-phenyl-2,3,4,5-tetrahydro-1H-3-benzazepine hydrochloride (SCH23390) Directly Inhibits G Protein-Coupled Inwardly Rectifying Potassium Channels. *Molecular Pharmacology*, *62*(1), 119–126. https://doi.org/10.1124/mol.62.1.119

Kuzhikandathil, E. V., Yu, W., & Oxford, G. S. (1998). Human Dopamine D3 and D2L Receptors Couple to Inward Rectifier Potassium Channels in Mammalian Cell Lines. *Molecular and Cellular Neuroscience*, *12*(6), 390–402. https://doi.org/10.1006/mcne.1998.0722

Labouèbe, G., Lomazzi, M., Cruz, H. G., Creton, C., Luján, R., Li, M., Yanagawa, Y., Obata, K., Watanabe, M., Wickman, K., Boyer, S. B., Slesinger, P. A., & Lüscher, C. (2007). RGS2 modulates coupling between GABAB receptors and GIRK channels in dopamine neurons of the ventral tegmental area. *Nature Neuroscience*, *10*(12), 1559–1568. https://doi.org/10.1038/nn2006

Lacey, M. G., Mercuri, N. B., & North, R. A. (1988). On the potassium conductance increase activated by GABAB and dopamine D2 receptors in rat substantia nigra neurones. *The Journal of Physiology*, *401*(1), 437–453. https://doi.org/10.1113/jphysiol.1988.sp017171

Ladera, C., Del Carmen Godino, M., Cabañero, M. J., Torres, M., Watanabe, M., Luján, R., & Sánchez-Prieto, J. (2008). Pre-synaptic GABAB receptors inhibit glutamate release through GIRK channels in rat cerebral cortex. *Journal of Neurochemistry*, *107*(6), 1506–1517. https://doi.org/10.1111/j.1471-4159.2008.05712.x

Lalive, A. L., Munoz, M. B., Bellone, C., Slesinger, P. A., Lüscher, C., & Tan, K. R. (2014). Firing Modes of Dopamine Neurons Drive Bidirectional GIRK Channel Plasticity. *Journal of Neuroscience*, *34*(15), 5107–5114. https://doi.org/10.1523/JNEUROSCI.5203-13.2014

Lammel, S., Hetzel, A., Häckel, O., Jones, I., Liss, B., & Roeper, J. (2008). Unique Properties of Mesoprefrontal Neurons within a Dual Mesocorticolimbic Dopamine System. *Neuron*, *57*(5), 760–773. https://doi.org/10.1016/j.neuron.2008.01.022

Latorre, R., Oberhauser, A., Labarca, P., & Alvarez, O. (1989). Varieties of calcium-activated potassium channels. *Annual Review of Physiology*, *51*, 385–399. https://doi.org/10.1146/annurev.ph.51.030189.002125

Laverty, D., Desai, R., Uchański, T., Masiulis, S., Stec, W. J., Malinauskas, T., Zivanov, J., Pardon, E., Steyaert, J., Miller, K. W., & Aricescu, A. R. (2019). Cryo-EM structure of the human α1β3γ2 GABAA receptor in a lipid bilayer. *Nature*, 10.1038/s41586-018-0833–0834. https://doi.org/10.1038/s41586-018-0833-4

Lavoie, B., & Parent, A. (1991). Dopaminergic neurons expressing calbindin in normal and parkinsonian monkeys. *NeuroReport*, *2*(10), 601.

Lebowitz, J. J., Kissiwaa, S. A., Engeln, K. A., Bowman, A. M., Williams, J. T., & Jackman, S. L. (2024). Synaptotagmin-7 Counteracts Short-Term Depression during Phasic Dopamine Release. *eNeuro*, *11*(3). https://doi.org/10.1523/ENEURO.0501-23.2024

Lebowitz, J. J., Pino, J. A., Mackie, P. M., Lin, M., Hurst, C., Divita, K., Collins, A. T., Koutzoumis, D. N., Torres, G. E., & Khoshbouei, H. (2019). Clustered Kv2.1 decreases dopamine transporter activity and internalization. *Journal of Biological Chemistry*, *294*(17), 6957–6971. https://doi.org/10.1074/jbc.RA119.007441

Lee, C., Mayfield, R. D., & Harris, R. A. (2010). Intron 4 Containing Novel GABAB1 Isoforms Impair GABAB Receptor Function. *PLOS ONE*, *5*(11), e14044. https://doi.org/10.1371/journal.pone.0014044

Lee, C. S., Samii, A., Sossi, V., Ruth, T. J., Schulzer, M., Holden, J. E., Wudel, J., Pal, P. K., De La Fuente-Fernandez, R., Calne, D. B., & Stoessl, A. J. (2000). In vivo positron emission tomographic evidence for compensatory changes in presynaptic dopaminergic nerve terminals in Parkinson's disease. *Annals of Neurology*, *47*(4), 493–503. https://doi.org/10.1002/1531-8249(200004)47:4<493::AID-ANA13>3.0.CO;2-4

Lee, F. J., Pei, L., Moszczynska, A., Vukusic, B., Fletcher, P. J., & Liu, F. (2007). Dopamine transporter cell surface localization facilitated by a direct interaction with the dopamine D2 receptor. *The EMBO Journal*, *26*(8), 2127–2136. https://doi.org/10.1038/sj.emboj.7601656

Lee, F. J. S., Liu, F., Pristupa, Z. B., & Niznik, H. B. (2001). Direct binding and functional coupling of α-synuclein to the dopamine transporters accelerate dopamine-induced apoptosis. *The FASEB Journal*, *15*(6), 916–926. https://doi.org/10.1096/fsb2fj000334com

Lesage, F., Duprat, F., Fink, M., Guillemare, E., Coppola, T., Lazdunski, M., & Hugnot, J.-P. (1994). Cloning provides evidence for a family of inward rectifier and G-protein coupled K+ channels in the brain. *FEBS Letters*, *353*(1), 37–42. https://doi.org/10.1016/0014-5793(94)01007-2

Lesage, F., Guillemare, E., Fink, M., Duprat, F., Heurteaux, C., Fosset, M., Romey, G., Barhanin, J., & Lazdunski, M. (1995). Molecular Properties of Neuronal G-protein-activated Inwardly Rectifying K+ Channels (*). *Journal of Biological Chemistry*, *270*(48), 28660–28667. https://doi.org/10.1074/jbc.270.48.28660

Liao, Y. J., Jan, Y. N., & Jan, L. Y. (1996). Heteromultimerization of G-Protein-Gated Inwardly Rectifying K+ Channel Proteins GIRK1 and GIRK2 and Their Altered Expression in weaver Brain. *Journal of Neuroscience*, *16*(22), 7137–7150. https://doi.org/10.1523/JNEUROSCI.16-22-07137.1996

Lipscombe, D., Helton, T. D., & Xu, W. (2004). L-Type Calcium Channels: The Low Down. *Journal of Neurophysiology*, *92*(5), 2633–2641. https://doi.org/10.1152/jn.00486.2004

Lisman, J. E. (1997). Bursts as a unit of neural information: Making unreliable synapses reliable. *Trends in Neurosciences*, *20*(1), 38–43. https://doi.org/10.1016/S0166-2236(96)10070-9

Liu, C., Cai, X., Ritzau-Jost, A., Kramer, P. F., Li, Y., Khaliq, Z. M., Hallermann, S., & Kaeser, P. S. (2022). An action potential initiation mechanism in distal axons for the control of dopamine release. *Science*. https://doi.org/10.1126/science.abn0532

Liu, C., & Kaeser, P. S. (2019). Mechanisms and regulation of dopamine release. *Current Opinion in Neurobiology*, *57*, 46–53. https://doi.org/10.1016/j.conb.2019.01.001

Lohr, K. M., Masoud, S. T., Salahpour, A., & Miller, G. W. (2017). Membrane transporters as mediators of synaptic dopamine dynamics: Implications for disease. *European Journal of Neuroscience*, *45*(1), 20–33. https://doi.org/10.1111/ejn.13357

Longhena, F., Faustini, G., Brembati, V., Pizzi, M., Benfenati, F., & Bellucci, A. (2021). An updated reappraisal of synapsins: Structure, function and role in neurological and psychiatric disorders. *Neuroscience & Biobehavioral Reviews*, *130*, 33–60. https://doi.org/10.1016/j.neubiorev.2021.08.011

Lopes, E. F., Roberts, B. M., Siddorn, R. E., Clements, M. A., & Cragg, S. J. (2019). Inhibition of Nigrostriatal Dopamine Release by Striatal GABAA and GABAB Receptors. *Journal of Neuroscience*, *39*(6), 1058–1065. https://doi.org/10.1523/JNEUROSCI.2028-18.2018

Lucy M. Palmer & Greg J. Stuart. (2006, February 8). *Site of Action Potential Initiation in Layer 5 Pyramidal Neurons | Journal of Neuroscience*. https://www.jneurosci.org/content/26/6/1854

Luján, R., Marron Fernandez de Velasco, E., Aguado, C., & Wickman, K. (2014). New insights into the therapeutic potential of Girk channels. *Trends in Neurosciences*, *37*(1), 20–29. https://doi.org/10.1016/j.tins.2013.10.006

Luk, K. C., & Sadikot, A. F. (2001). GABA promotes survival but not proliferation of parvalbumin-immunoreactive interneurons in rodent neostriatum: An in vivo study with stereology. *Neuroscience*, *104*(1), 93–103. https://doi.org/10.1016/S0306-4522(01)00038-0

Luo, H., Marron Fernandez de Velasco, E., & Wickman, K. (2022). Neuronal G protein-gated K+ channels. *American Journal of Physiology-Cell Physiology*, *323*(2), C439–C460. https://doi.org/10.1152/ajpcell.00102.2022

Lüscher, C., Jan, L. Y., Stoffel, M., Malenka, R. C., & Nicoll, R. A. (1997). G Protein-Coupled Inwardly Rectifying K+ Channels (GIRKs) Mediate Postsynaptic but Not Presynaptic Transmitter Actions in Hippocampal Neurons. *Neuron*, *19*(3), 687–695. https://doi.org/10.1016/S0896-6273(00)80381-5

Lüscher, C., & Slesinger, P. A. (2010). Emerging roles for G protein-gated inwardly rectifying potassium (GIRK) channels in health and disease. *Nature Reviews Neuroscience*, *11*(5), 301–315. https://doi.org/10.1038/nrn2834

Lycas, M. D., Ejdrup, A. L., Sørensen, A. T., Haahr, N. O., Jørgensen, S. H., Guthrie, D. A., Støier, J. F., Werner, C., Newman, A. H., Sauer, M., Herborg, F., & Gether, U. (2022). Nanoscopic dopamine transporter distribution and conformation are inversely regulated by excitatory drive and D2 autoreceptor activity. *Cell Reports*, *40*(13), 111431. https://doi.org/10.1016/j.celrep.2022.111431

Ma, D., Zerangue, N., Raab-Graham, K., Fried, S. R., Jan, Y. N., & Jan, L. Y. (2002). Diverse Trafficking Patterns Due to Multiple Traffic Motifs in G Protein-Activated Inwardly Rectifying Potassium Channels from Brain and Heart. *Neuron*, *33*(5), 715–729. https://doi.org/10.1016/S0896-6273(02)00614-1

Macdonald, R. L., & Olsen, R. W. (1994). GABAA Receptor Channels. *Annual Review of Neuroscience*, *17*(Volume 17, 1994), 569–602. https://doi.org/10.1146/annurev.ne.17.030194.003033

Maggi, C. A. (1995). The mammalian tachykinin receptors. *General Pharmacology: The Vascular System*, *26*(5), 911–944. https://doi.org/10.1016/0306-3623(94)00292-U

Mandal, K. (2020). Review of PIP2 in Cellular Signaling, Functions and Diseases. *International Journal of Molecular Sciences*, *21*(21), Article 21. https://doi.org/10.3390/ijms21218342

Margolis, E. B., Mitchell, J. M., Ishikawa, J., Hjelmstad, G. O., & Fields, H. L. (2008). Midbrain Dopamine Neurons: Projection Target Determines Action Potential Duration and Dopamine D2 Receptor Inhibition. *Journal of Neuroscience*, *28*(36), 8908–8913. https://doi.org/10.1523/JNEUROSCI.1526-08.2008

Markowitz, J. E., Gillis, W. F., Jay, M., Wood, J., Harris, R. W., Cieszkowski, R., Scott, R., Brann, D., Koveal, D., Kula, T., Weinreb, C., Osman, M. A. M., Pinto, S. R., Uchida, N.,

Linderman, S. W., Sabatini, B. L., & Datta, S. R. (2023). Spontaneous behaviour is structured by reinforcement without explicit reward. *Nature*, *614*(7946), 108–117. https://doi.org/10.1038/s41586-022-05611-2

Markram, H., Wang, Y., & Tsodyks, M. (1998). Differential signaling via the same axon of neocortical pyramidal neurons. *Proceedings of the National Academy of Sciences*, *95*(9), 5323–5328. https://doi.org/10.1073/pnas.95.9.5323

Marsden, C. D. (1982, May 1). *The mysterious motor function of the basal ganglia*. Neurology. https://www.neurology.org/doi/10.1212/WNL.32.5.514

Martel, J. C., & Gatti McArthur, S. (2020). Dopamine Receptor Subtypes, Physiology and Pharmacology: New Ligands and Concepts in Schizophrenia. *Frontiers in Pharmacology*, *11*. https://doi.org/10.3389/fphar.2020.01003

Martín-Belmonte, A., Aguado, C., Alfaro-Ruiz, R., Moreno-Martínez, A. E., de la Ossa, L., Aso, E., Gómez-Acero, L., Shigemoto, R., Fukazawa, Y., Ciruela, F., & Luján, R. (2022). Nanoscale alterations in GABAB receptors and GIRK channel organization on the hippocampus of APP/PS1 mice. *Alzheimer's Research & Therapy*, *14*(1), 136. https://doi.org/10.1186/s13195-022-01078-5

Marvin, J. S., Shimoda, Y., Magloire, V., Leite, M., Kawashima, T., Jensen, T. P., Kolb, I., Knott, E. L., Novak, O., Podgorski, K., Leidenheimer, N. J., Rusakov, D. A., Ahrens, M. B., Kullmann, D. M., & Looger, L. L. (2019). A genetically encoded fluorescent sensor for in vivo imaging of GABA. *Nature Methods*, *16*(8), 763–770. https://doi.org/10.1038/s41592-019-0471-2

Masson, J., Sagné, C., Hamon, M., & Mestikawy, S. E. (1999). Neurotransmitter Transporters in the Central Nervous System. *Pharmacological Reviews*, *51*(3), 439–464. https://doi.org/10.1016/S0031-6997(24)01414-5

Mathiharan, Y. K., Glaaser, I. W., Zhao, Y., Robertson, M. J., Skiniotis, G., & Slesinger, P. A. (2021). Structural insights into GIRK2 channel modulation by cholesterol and PIP2. *Cell Reports*, *36*(8), 109619. https://doi.org/10.1016/j.celrep.2021.109619

Matsuda, W., Furuta, T., Nakamura, K. C., Hioki, H., Fujiyama, F., Arai, R., & Kaneko, T. (2009). Single Nigrostriatal Dopaminergic Neurons Form Widely Spread and Highly Dense Axonal Arborizations in the Neostriatum. *Journal of Neuroscience*, *29*(2), 444–453. https://doi.org/10.1523/JNEUROSCI.4029-08.2009

Matz, O. C., Spocter, M., Matz, O. C., & Spocter, M. A. (2022). The Effect of Huntington's Disease on the Basal Nuclei: A Review. *Cureus*, *14*(4). https://doi.org/10.7759/cureus.24473

Mauna, J. C., Harris, S. S., Pino, J. A., Edwards, C. M., DeChellis-Marks, M. R., Bassi, C. D., Garcia-Olivares, J., Amara, S. G., Guajardo, F. G., Sotomayor-Zarate, R., Terminel, M., Castañeda, E., Vergara, M., Baust, T., Thiels, E., & Torres, G. E. (2019). G protein βγ subunits play a critical role in the actions of amphetamine. *Translational Psychiatry*, *9*(1), 1–11. https://doi.org/10.1038/s41398-019-0387-8

McCall, N. M., Kotecki, L., Dominguez-Lopez, S., Marron Fernandez de Velasco, E., Carlblom, N., Sharpe, A. L., Beckstead, M. J., & Wickman, K. (2017). Selective Ablation of GIRK Channels in Dopamine Neurons Alters Behavioral Effects of Cocaine in Mice. *Neuropsychopharmacology*, *42*(3), 707–715. https://doi.org/10.1038/npp.2016.138

McCall, N. M., Velasco, E. M. F. de, & Wickman, K. (2019). GIRK Channel Activity in Dopamine Neurons of the Ventral Tegmental Area Bidirectionally Regulates Behavioral Sensitivity to Cocaine. *Journal of Neuroscience*, *39*(19), 3600–3610. https://doi.org/10.1523/JNEUROSCI.3101-18.2019

McCool, B. A., & Farroni, J. S. (2001). A1 adenosine receptors inhibit multiple voltage-gated Ca2+ channel subtypes in acutely isolated rat basolateral amygdala neurons. *British Journal of Pharmacology*, *132*(4), 879–888. https://doi.org/10.1038/sj.bjp.0703884

Mcelvain, J. S., & Schenk, J. O. (1992). A multisubstrate mechanism of striatal dopamine uptake and its inhibition by cocaine. *Biochemical Pharmacology*, *43*(10), 2189–2199. https://doi.org/10.1016/0006-2952(92)90178-L

McRitchie, D. A., Cartwright, H. R., & Halliday, G. M. (1997). Specific A10 Dopaminergic Nuclei in the Midbrain Degenerate in Parkinson's Disease. *Experimental Neurology*, *144*(1), 202–213. https://doi.org/10.1006/exnr.1997.6418

Medrihan, L., Cesca, F., Raimondi, A., Lignani, G., Baldelli, P., & Benfenati, F. (2013). Synapsin II desynchronizes neurotransmitter release at inhibitory synapses by interacting with presynaptic calcium channels. *Nature Communications*, *4*(1), 1512. https://doi.org/10.1038/ncomms2515

Meinild, A.-K., Sitte, H. H., & Gether, U. (2004). Zinc Potentiates an Uncoupled Anion Conductance Associated with the Dopamine Transporter*. *Journal of Biological Chemistry*, *279*(48), 49671–49679. https://doi.org/10.1074/jbc.M407660200

Mercuri, N. B., Bonci, A., Calabresi, P., Stefani, A., & Bernardi, G. (1995). Properties of the Hyperpolarization-activated Cation Current Ih in Rat Midbrain Dopaminergic Neurons. *European Journal of Neuroscience*, *7*(3), 462–469. https://doi.org/10.1111/j.1460-9568.1995.tb00342.x

Michael, D. J., & Wightman, R. M. (1999). Electrochemical monitoring of biogenic amine neurotransmission in real time. *Journal of Pharmaceutical and Biomedical Analysis*, *19*(1), 33–46. https://doi.org/10.1016/S0731-7085(98)00145-9

Millan, M. J., Newman-Tancredi, A., Quentric, Y., & Cussac, D. (2001). The 'selective' dopamine D1 receptor antagonist, SCH23390, is a potent and high efficacy agonist at cloned human serotonin2C receptors. *Psychopharmacology*, *156*(1), 58–62. https://doi.org/10.1007/s002130100742

Millar, J., Stamford, J. A., Kruk, Z. L., & Wightman, R. M. (1985). Electrochemical, pharmacological and electrophysiological evidence of rapid dopamine release and

removal in the rat caudate nucleus following electrical stimulation of the median forebrain bundle. *European Journal of Pharmacology*, *109*(3), 341–348. https://doi.org/10.1016/0014-2999(85)90394-2

Min, M.-Y., Shih, P.-Y., Wu, Y.-W., Lu, H.-W., Lee, M.-L., & Yang, H.-W. (2009). Neurokinin 1 receptor activates transient receptor potential-like currents in noradrenergic A7 neurons in rats. *Molecular and Cellular Neuroscience*, *42*(1), 56–65. https://doi.org/10.1016/j.mcn.2009.05.006

Min, M.-Y., Wu, Y.-W., Shih, P.-Y., Lu, H.-W., Lin, C.-C., Wu, Y., Li, M.-J., & Yang, H.-W. (2008). Physiological and morphological properties of, and effect of substance P on, neurons in the A7 catecholamine cell group in rats. *Neuroscience*, *153*(4), 1020–1033. https://doi.org/10.1016/j.neuroscience.2008.03.011

Mingote, S., Amsellem, A., Kempf, A., Rayport, S., & Chuhma, N. (2019). Dopamine-glutamate neuron projections to the nucleus accumbens medial shell and behavioral switching. *Neurochemistry International*, *129*, 104482. https://doi.org/10.1016/j.neuint.2019.104482

Mirenowicz, J., & Schultz, W. (1996). Preferential activation of midbrain dopamine neurons by appetitive rather than aversive stimuli. *Nature*, *379*(6564), 449–451. https://doi.org/10.1038/379449a0

Mogenson, G. J., Jones, D. L., & Yim, C. Y. (1980). From motivation to action: Functional interface between the limbic system and the motor system. *Progress in Neurobiology*, *14*(2), 69–97. https://doi.org/10.1016/0301-0082(80)90018-0

Molochnikov, I., & Cohen, D. (2014). Hemispheric differences in the mesostriatal dopaminergic system. *Frontiers in Systems Neuroscience*, *8*. https://doi.org/10.3389/fnsys.2014.00110

Monsma, F. J., McVittie, L. D., Gerfen, C. R., Mahan, L. C., & Sibley, D. R. (1989). Multiple D2 dopamine receptors produced by alternative RNA splicing. *Nature*, *342*(6252), 926–929. https://doi.org/10.1038/342926a0

Morissette, M., Morin, N., Rouillard, C., & Di Paolo, T. (2018). Membrane cholesterol removal and replenishment affect rat and monkey brain monoamine transporters. *Neuropharmacology*, *133*, 289–306. https://doi.org/10.1016/j.neuropharm.2018.01.039

Morris, G., Arkadir, D., Nevet, A., Vaadia, E., & Bergman, H. (2004). Coincident but Distinct Messages of Midbrain Dopamine and Striatal Tonically Active Neurons. *Neuron*, *43*(1), 133–143. https://doi.org/10.1016/j.neuron.2004.06.012

Mortensen, O. V., & Amara, S. G. (2003a). Dynamic regulation of the dopamine transporter. *European Journal of Pharmacology*, *479*(1), 159–170. https://doi.org/10.1016/j.ejphar.2003.08.066

Mortensen, O. V., & Amara, S. G. (2003b). Dynamic regulation of the dopamine transporter. *European Journal of Pharmacology*, *479*(1), 159–170. https://doi.org/10.1016/j.ejphar.2003.08.066

Moschetta, M., Ravasenga, T., De Fusco, A., Maragliano, L., Aprile, D., Orlando, M., Sacchetti, S., Casagrande, S., Lignani, G., Fassio, A., Baldelli, P., & Benfenati, F. (2022). Ca2+ binding to synapsin I regulates resting Ca2+ and recovery from synaptic depression in nerve terminals. *Cellular and Molecular Life Sciences*, *79*(12), 600. https://doi.org/10.1007/s00018-022-04631-5

Mu, L., Liu, X., Yu, H., Vickstrom, C. R., Friedman, V., Kelly, T. J., Hu, Y., Su, W., Liu, S., Mantsch, J. R., & Liu, Q. (2023). cAMP-mediated upregulation of HCN channels in VTA dopamine neurons promotes cocaine reinforcement. *Molecular Psychiatry*, *28*(9), 3930–3942. https://doi.org/10.1038/s41380-023-02290-x

Munoz, M. B., Padgett, C. L., Rifkin, R., Terunuma, M., Wickman, K., Contet, C., Moss, S. J., & Slesinger, P. A. (2016). A Role for the GIRK3 Subunit in Methamphetamine-Induced Attenuation of GABAB Receptor-Activated GIRK Currents in VTA Dopamine Neurons. *Journal of Neuroscience*, *36*(11), 3106–3114. https://doi.org/10.1523/JNEUROSCI.1327-15.2016

Munoz, M. B., & Slesinger, P. A. (2014). Sorting Nexin 27 Regulation of G Protein-Gated Inwardly Rectifying K+ Channels Attenuates In Vivo Cocaine Response. *Neuron*, *82*(3), 659–669. https://doi.org/10.1016/j.neuron.2014.03.011

Nagy, A. (2000). Cre recombinase: The universal reagent for genome tailoring. *Genesis*, *26*(2), 99–109. https://doi.org/10.1002/(SICI)1526-968X(200002)26:2<99::AID-GENE1>3.0.CO;2-B

Nairn, A. C., & Greengard, P. (1987). Purification and characterization of Ca2+/calmodulin-dependent protein kinase I from bovine brain. *Journal of Biological Chemistry*, *262*(15), 7273–7281. https://doi.org/10.1016/S0021-9258(18)48233-6

Nair-Roberts, R. G., Chatelain-Badie, S. D., Benson, E., White-Cooper, H., Bolam, J. P., & Ungless, M. A. (2008). Stereological estimates of dopaminergic, GABAergic and glutamatergic neurons in the ventral tegmental area, substantia nigra and retrorubral field in the rat. *Neuroscience*, *152*(4–2), 1024–1031. https://doi.org/10.1016/j.neuroscience.2008.01.046

Nayeem, N., Green, T. P., Martin, I. L., & Barnard, E. A. (1994). Quaternary Structure of the Native GABAA Receptor Determined by Electron Microscopic Image Analysis. *Journal of Neurochemistry*, *62*(2), 815–818. https://doi.org/10.1046/j.1471-4159.1994.62020815.x

Neher, E., & Sakaba, T. (2008). Multiple Roles of Calcium Ions in the Regulation of Neurotransmitter Release. *Neuron*, *59*(6), 861–872. https://doi.org/10.1016/j.neuron.2008.08.019

Nelson, C. S., Marino, J. L., & Allen, C. N. (1997). Cloning and characterization of Kir3.1 (GIRK1) C-terminal alternative splice variants. *Molecular Brain Research*, *46*(1), 185–196. https://doi.org/10.1016/S0169-328X(96)00301-4

Nelson, E. l., Liang, C.-L., Sinton, C. m., & German, D. c. (1996). Midbrain dopaminergic neurons in the mouse: Computer-assisted mapping. *Journal of Comparative Neurology*, *369*(3), 361–371. https://doi.org/10.1002/(SICI)1096-9861(19960603)369:3<361::AID-CNE3>3.0.CO;2-3

Nepal, B., Das, S., Reith, M. E., & Kortagere, S. (2023). Overview of the structure and function of the dopamine transporter and its protein interactions. *Frontiers in Physiology*, *14*. https://doi.org/10.3389/fphys.2023.1150355

Neuhoff, H., Neu, A., Liss, B., & Roeper, J. (2002). Ih Channels Contribute to the Different Functional Properties of Identified Dopaminergic Subpopulations in the Midbrain. *Journal of Neuroscience*, *22*(4), 1290–1302. https://doi.org/10.1523/JNEUROSCI.22-04-01290.2002

Nirenberg, M. J., Chan, J., Pohorille, A., Vaughan, R. A., Uhl, G. R., Kuhar, M. J., & Pickel, V. M. (1997). The Dopamine Transporter: Comparative Ultrastructure of Dopaminergic Axons in Limbic and Motor Compartments of the Nucleus Accumbens. *Journal of Neuroscience*, *17*(18), 6899–6907. https://doi.org/10.1523/JNEUROSCI.17-18-06899.1997

Obeso, J. A., Rodriguez-Oroz, M. C., Stamelou, M., Bhatia, K. P., & Burn, D. J. (2014). The expanding universe of disorders of the basal ganglia. *The Lancet*, *384*(9942), 523–531. https://doi.org/10.1016/S0140-6736(13)62418-6

Ochoa, E. L. M., Chattopadhyay, A., & McNamee, M. G. (1989). Desensitization of the nicotinic acetylcholine receptor: Molecular mechanisms and effect of modulators. *Cellular and Molecular Neurobiology*, *9*(2), 141–178. https://doi.org/10.1007/BF00713026

Ofer, N., Shefi, O., & Yaari, G. (2017). Branching morphology determines signal propagation dynamics in neurons. *Scientific Reports*, *7*(1), 8877. https://doi.org/10.1038/s41598-017-09184-3

Okamoto, T., Harnett, M. T., & Morikawa, H. (2006). Hyperpolarization-Activated Cation Current (Ih) Is an Ethanol Target in Midbrain Dopamine Neurons of Mice. *Journal of Neurophysiology*, *95*(2), 619–626. https://doi.org/10.1152/jn.00682.2005

O'Leary, M. E., & Chahine, M. (2002). Cocaine binds to a common site on open and inactivated human heart (Nav1.5) sodium channels. *The Journal of Physiology*, *541*(3), 701–716. https://doi.org/10.1113/jphysiol.2001.016139

Olsen, R. W., & Sieghart, W. (2008). International Union of Pharmacology. LXX. Subtypes of γ-Aminobutyric AcidA Receptors: Classification on the Basis of Subunit Composition, Pharmacology, and Function. Update. *Pharmacological Reviews*, *60*(3), 243–260. https://doi.org/10.1124/pr.108.00505

Papa, M., Diewald, L., Carey, M. P., Esposito, F. J., Gironi Carnevale, U. A., & Sadile, A. G. (2002). A rostro-caudal dissociation in the dorsal and ventral striatum of the juvenile SHR suggests an anterior hypo- and a posterior hyperfunctioning mesocorticolimbic system. *Behavioural Brain Research*, *130*(1), 171–179. https://doi.org/10.1016/S0166-4328(01)00421-1

Patel, J. C., Sherpa, A. D., Melani, R., Witkovsky, P., Wiseman, M. R., O'Neill, B., Aoki, C., Tritsch, N. X., & Rice, M. E. (2024). GABA co-released from striatal dopamine axons dampens phasic dopamine release through autoregulatory GABAA receptors. *Cell Reports*, *43*(3), 113834. https://doi.org/10.1016/j.celrep.2024.113834

Patel, J., Trout, S. J., & Kruk, Z. L. (1992). Regional differences in evoked dopamine efflux in brain slices of rat anterior and posterior caudate putamen. *Naunyn-Schmiedeberg's Archives of Pharmacology*, *346*(3), 267–276. https://doi.org/10.1007/BF00173539

Patriarchi, T., Cho, J. R., Merten, K., Howe, M. W., Marley, A., Xiong, W.-H., Folk, R. W., Broussard, G. J., Liang, R., Jang, M. J., Zhong, H., Dombeck, D., von Zastrow, M., Nimmerjahn, A., Gradinaru, V., Williams, J. T., & Tian, L. (2018). Ultrafast neuronal imaging of dopamine dynamics with designed genetically encoded sensors. *Science*, *360*(6396), eaat4422. https://doi.org/10.1126/science.aat4422

Peerboom, C., & Wierenga, C. J. (2021). The postnatal GABA shift: A developmental perspective. *Neuroscience & Biobehavioral Reviews*, *124*, 179–192. https://doi.org/10.1016/j.neubiorev.2021.01.024

Penmatsa, A., & Gouaux, E. (2014). How LeuT shapes our understanding of the mechanisms of sodium-coupled neurotransmitter transporters. *The Journal of Physiology*, *592*(5), 863–869. https://doi.org/10.1113/jphysiol.2013.259051

Penmatsa, A., Wang, K. H., & Gouaux, E. (2013). X-ray structure of dopamine transporter elucidates antidepressant mechanism. *Nature*, *503*(7474), 85–90. https://doi.org/10.1038/nature12533

Pereira, D. B., Schmitz, Y., Mészáros, J., Merchant, P., Hu, G., Li, S., Henke, A., Lizardi-Ortiz, J. E., Karpowicz, R. J., Morgenstern, T. J., Sonders, M. S., Kanter, E., Rodriguez, P. C., Mosharov, E. V., Sames, D., & Sulzer, D. (2016). Fluorescent false neurotransmitter reveals functionally silent dopamine vesicle clusters in the striatum. *Nature Neuroscience*, *19*(4), 578–586. https://doi.org/10.1038/nn.4252

Pérez-Garci, E., Pysanenko, K., Rizzi, G., Studer, F., Ulrich, D., Fritzius, T., Früh, S., Porcu, A., Besseyrias, V., Melichar, A., Gassmann, M., Barkat, T. R., Tureček, R., Tan, K. R., & Bettler, B. (2025). Binding of HCN channels to GABAB receptors in dopamine neurons of the VTA limits synaptic inhibition and prevents the development of anxiety. *Neurobiology of Disease*, *206*, 106831. https://doi.org/10.1016/j.nbd.2025.106831

Perkins, K. L., & Wong, R. K. (1996). Ionic basis of the postsynaptic depolarizing GABA response in hippocampal pyramidal cells. *Journal of Neurophysiology*, *76*(6), 3886–3894. https://doi.org/10.1152/jn.1996.76.6.3886

Perreault, M. L., Hasbi, A., O'Dowd, B. F., & George, S. R. (2014). Heteromeric Dopamine Receptor Signaling Complexes: Emerging Neurobiology and Disease Relevance. *Neuropsychopharmacology*, *39*(1), 156–168. https://doi.org/10.1038/npp.2013.148

Phelps, P. E., Houser, C. R., & Vaughn, J. E. (1985). Immunocytochemical localization of choline acetyltransferase within the rat neostriatum: A correlated light and electron microscopic study of cholinergic neurons and synapses. *Journal of Comparative Neurology*, *238*(3), 286–307. https://doi.org/10.1002/cne.902380305

Philippart, F., & Khaliq, Z. M. (2018). Gi/o protein-coupled receptors in dopamine neurons inhibit the sodium leak channel NALCN. *eLife*, *7*, e40984. https://doi.org/10.7554/eLife.40984

Phillips, P. E. M., Hancock, P. J., & Stamford, J. A. (2002). Time window of autoreceptor-mediated inhibition of limbic and striatal dopamine release. *Synapse*, *44*(1), 15–22. https://doi.org/10.1002/syn.10049

Pian, P., Bucchi, A., DeCostanzo, A., Robinson, R. B., & Siegelbaum, S. A. (2007). Modulation of cyclic nucleotide-regulated HCN channels by PIP2 and receptors coupled to phospholipase C. *Pflügers Archiv - European Journal of Physiology*, *455*(1), 125–145. https://doi.org/10.1007/s00424-007-0295-2

Picetti, R., Saiardi, A., Samad, T. A., Bozzi, Y., Baik, J.-H., & Borrelli, E. (1997). Dopamine D2 Receptors in Signal Transduction and Behavior. *Critical Reviews™ in Neurobiology*, *11*(2–3). https://doi.org/10.1615/CritRevNeurobiol.v11.i2-3.20

Pickel, V. M., Beckley, S. C., Joh, T. H., & Reis, D. J. (1981). Ultrastructural immunocytochemical localization of tyrosine hydroxylase in the neostriatum. *Brain Research*, *225*(2), 373–385. https://doi.org/10.1016/0006-8993(81)90843-X

Pieribone, V. A., Porton, B., Rendon, B., Feng, J., Greengard, P., & Kao, H.-T. (2002). Expression of synapsin III in nerve terminals and neurogenic regions of the adult brain. *Journal of Comparative Neurology*, *454*(2), 105–114. https://doi.org/10.1002/cne.10417

Pin, J.-P., & Bettler, B. (2016). Organization and functions of mGlu and GABAB receptor complexes. *Nature*, *540*(7631), 60–68. https://doi.org/10.1038/nature20566

Pino, J. A., Nuñez-Vivanco, G., Hidalgo, G., Reyes Parada, M., Khoshbouei, H., & Torres, G. E. (2021). Identification of Critical Residues in the Carboxy Terminus of the Dopamine Transporter Involved in the G Protein βγ-Induced Dopamine Efflux. *Frontiers in Pharmacology*, *12*. https://doi.org/10.3389/fphar.2021.642881

Pirino, B. E., Hawks, A., Carpenter, B. A., Candelas, P. G., Gargiulo, A. T., Curtis, G. R., Karkhanis, A. N., & Barson, J. R. (2024). Kappa-opioid receptor stimulation in the nucleus accumbens shell and ethanol drinking: Differential effects by rostro-caudal location and level of drinking. *Neuropsychopharmacology*, *49*(10), 1550–1558. https://doi.org/10.1038/s41386-024-01850-1

Pissadaki, E. K., & Bolam, J. P. (2013). The energy cost of action potential propagation in dopamine neurons: Clues to susceptibility in Parkinson's disease. *Frontiers in Computational Neuroscience*, *7*. https://doi.org/10.3389/fncom.2013.00013

Pitman, K. A., Puil, E., & Borgland, S. L. (2014). GABAB modulation of dopamine release in the nucleus accumbens core. *European Journal of Neuroscience*, *40*(10), 3472–3480. https://doi.org/10.1111/ejn.12733

Poisson, C. L., Engel, L., & Saunders, B. T. (2021). Dopamine Circuit Mechanisms of Addiction-Like Behaviors. *Frontiers in Neural Circuits*, *15*. https://doi.org/10.3389/fncir.2021.752420

Poulin, J.-F., Caronia, G., Hofer, C., Cui, Q., Helm, B., Ramakrishnan, C., Chan, C. S., Dombeck, D., Deisseroth, K., & Awatramani, R. (2018). Mapping projections of molecularly defined dopamine neuron subtypes using intersectional genetic

approaches. *Nature Neuroscience*, *21*(9), 1260–1271. https://doi.org/10.1038/s41593-018-0203-4

Poulin, J.-F., Gaertner, Z., Moreno-Ramos, O. A., & Awatramani, R. (2020). Classification of Midbrain Dopamine Neurons Using Single-Cell Gene Expression Profiling Approaches. *Trends in Neurosciences*, *43*(3), 155–169. https://doi.org/10.1016/j.tins.2020.01.004

Poulin, J.-F., Zou, J., Drouin-Ouellet, J., Kim, K.-Y. A., Cicchetti, F., & Awatramani, R. B. (2014). Defining Midbrain Dopaminergic Neuron Diversity by Single-Cell Gene Expression Profiling. *Cell Reports*, *9*(3), 930–943. https://doi.org/10.1016/j.celrep.2014.10.008

Power, J. M., Bocklisch, C., Curby, P., & Sah, P. (2011). Location and Function of the Slow Afterhyperpolarization Channels in the Basolateral Amygdala. *Journal of Neuroscience*, *31*(2), 526–537. https://doi.org/10.1523/JNEUROSCI.1045-10.2011

Quick, M. W., & Lester, R. A. J. (2002). Desensitization of neuronal nicotinic receptors. *Journal of Neurobiology*, *53*(4), 457–478. https://doi.org/10.1002/neu.10109

Rahbek-Clemmensen, T., Lycas, M. D., Erlendsson, S., Eriksen, J., Apuschkin, M., Vilhardt, F., Jørgensen, T. N., Hansen, F. H., & Gether, U. (2017). Super-resolution microscopy reveals functional organization of dopamine transporters into cholesterol and neuronal activity-dependent nanodomains. *Nature Communications*, *8*(1), 740. https://doi.org/10.1038/s41467-017-00790-3

Rama, S., Zbili, M., Bialowas, A., Fronzaroli-Molinieres, L., Ankri, N., Carlier, E., Marra, V., & Debanne, D. (2015). Presynaptic hyperpolarization induces a fast analogue modulation of spike-evoked transmission mediated by axonal sodium channels. *Nature Communications*, *6*(1), 10163. https://doi.org/10.1038/ncomms10163

Rama, S., Zbili, M., & Debanne, D. (2018). Signal propagation along the axon. *Current Opinion in Neurobiology*, *51*, 37–44. https://doi.org/10.1016/j.conb.2018.02.017

Regehr, W. G. (2012a). Short-Term Presynaptic Plasticity. *Cold Spring Harbor Perspectives in Biology*, *4*(7), a005702. https://doi.org/10.1101/cshperspect.a005702

Regehr, W. G. (2012b). Short-Term Presynaptic Plasticity. *Cold Spring Harbor Perspectives in Biology*, *4*(7), a005702. https://doi.org/10.1101/cshperspect.a005702

Rice, M. E., & Cragg, S. J. (2004). Nicotine amplifies reward-related dopamine signals in striatum. *Nature Neuroscience*, *7*(6), 583–584. https://doi.org/10.1038/nn1244

Rice, M. E., & Cragg, S. J. (2008). Dopamine spillover after quantal release: Rethinking dopamine transmission in the nigrostriatal pathway. *Brain Research Reviews*, *58*(2), 303–313. https://doi.org/10.1016/j.brainresrev.2008.02.004

Rice, M. E., Cragg, S. J., & Greenfield, S. A. (1997). Characteristics of Electrically Evoked Somatodendritic Dopamine Release in Substantia Nigra and Ventral Tegmental Area In Vitro. *Journal of Neurophysiology*, *77*(2), 853–862. https://doi.org/10.1152/jn.1997.77.2.853

Rice, M. E., Patel, J. C., & Cragg, S. J. (2011). Dopamine release in the basal ganglia. *Neuroscience*, *198*, 112–137. https://doi.org/10.1016/j.neuroscience.2011.08.066

Richards, C. D., Shiroyama, T., & Kitai, S. T. (1997). Electrophysiological and immunocytochemical characterization of GABA and dopamine neurons in the substantia nigra of the rat. *Neuroscience*, *80*(2), 545–557. https://doi.org/10.1016/S0306-4522(97)00093-6

Richardson, B. D., Saha, K., Krout, D., Cabrera, E., Felts, B., Henry, L. K., Swant, J., Zou, M.-F., Newman, A. H., & Khoshbouei, H. (2016a). Membrane potential shapes regulation of dopamine transporter trafficking at the plasma membrane. *Nature Communications*, *7*(1), 10423. https://doi.org/10.1038/ncomms10423

Richardson, B. D., Saha, K., Krout, D., Cabrera, E., Felts, B., Henry, L. K., Swant, J., Zou, M.-F., Newman, A. H., & Khoshbouei, H. (2016b). Membrane potential shapes regulation of

dopamine transporter trafficking at the plasma membrane. *Nature Communications*, *7*(1), 10423. https://doi.org/10.1038/ncomms10423

Rifkin, R. A., Huyghe, D., Li, X., Parakala, M., Aisenberg, E., Moss, S. J., & Slesinger, P. A. (2018). GIRK currents in VTA dopamine neurons control the sensitivity of mice to cocaine-induced locomotor sensitization. *Proceedings of the National Academy of Sciences*, *115*(40), E9479–E9488. https://doi.org/10.1073/pnas.1807788115

Ritz, B. R., Manthripragada, A. D., Costello, S., Lincoln, S. J., Farrer, M. J., Cockburn, M., & Bronstein, J. (2009). Dopamine Transporter Genetic Variants and Pesticides in Parkinson's Disease. *Environmental Health Perspectives*, *117*(6), 964–969. https://doi.org/10.1289/ehp.0800277

Rizo, J. (2022). Molecular Mechanisms Underlying Neurotransmitter Release. *Annual Review of Biophysics*, *51*(Volume 51, 2022), 377–408. https://doi.org/10.1146/annurev-biophys-111821-104732

Roberts, B. M., Doig, N. M., Brimblecombe, K. R., Lopes, E. F., Siddorn, R. E., Threlfell, S., Connor-Robson, N., Bengoa-Vergniory, N., Pasternack, N., Wade-Martins, R., Magill, P. J., & Cragg, S. J. (2020). GABA uptake transporters support dopamine release in dorsal striatum with maladaptive downregulation in a parkinsonism model. *Nature Communications*, *11*(1), 4958. https://doi.org/10.1038/s41467-020-18247-5

Roberts, B. M., Lambert, E., Livesey, J. A., Wu, Z., Li, Y., & Cragg, S. J. (2022a). Dopamine Release in Nucleus Accumbens Is under Tonic Inhibition by Adenosine A1 Receptors Regulated by Astrocytic ENT1 and Dysregulated by Ethanol. *Journal of Neuroscience*, *42*(9), 1738–1751. https://doi.org/10.1523/JNEUROSCI.1548-21.2021

Roberts, B. M., Lambert, E., Livesey, J. A., Wu, Z., Li, Y., & Cragg, S. J. (2022b). Dopamine Release in Nucleus Accumbens Is under Tonic Inhibition by Adenosine A1 Receptors Regulated by Astrocytic ENT1 and Dysregulated by Ethanol. *Journal of Neuroscience*, *42*(9), 1738–1751. https://doi.org/10.1523/JNEUROSCI.1548-21.2021

Roberts, B. M., Lopes, E. F., & Cragg, S. J. (2021a). Axonal Modulation of Striatal Dopamine Release by Local γ-Aminobutyric Acid (GABA) Signalling. *Cells*, *10*(3), Article 3. https://doi.org/10.3390/cells10030709

Roberts, B. M., Lopes, E. F., & Cragg, S. J. (2021b). Axonal Modulation of Striatal Dopamine Release by Local γ-Aminobutyric Acid (GABA) Signalling. *Cells*, *10*(3), 709. https://doi.org/10.3390/cells10030709

Robinson, T. E., & Berridge, K. C. (1993). The neural basis of drug craving: An incentive-sensitization theory of addiction. *Brain Research Reviews*, *18*(3), 247–291. https://doi.org/10.1016/0165-0173(93)90013-P

Rocha, G. S., Freire, M. A. M., Britto, A. M., Paiva, K. M., Oliveira, R. F., Fonseca, I. A. T., Araújo, D. P., Oliveira, L. C., Guzen, F. P., Morais, P. L. A. G., & Cavalcanti, J. R. L. P. (2023). Basal ganglia for beginners: The basic concepts you need to know and their role in movement control. *Frontiers in Systems Neuroscience*, *17*. https://doi.org/10.3389/fnsys.2023.1242929

Rodriguez-Menchaca, A. A., Solis Jr, E., Cameron, K., & De Felice, L. J. (2012). S(+)amphetamine induces a persistent leak in the human dopamine transporter: Molecular stent hypothesis. *British Journal of Pharmacology*, *165*(8), 2749–2757. https://doi.org/10.1111/j.1476-5381.2011.01728.x

Rojas, G., Orellana, I., Rosales-Rojas, R., García-Olivares, J., Comer, J., & Vergara-Jaque, A. (2020). Structural Determinants of the Dopamine Transporter Regulation Mediated by G Proteins. *Journal of Chemical Information and Modeling*, *60*(7), 3577–3586. https://doi.org/10.1021/acs.jcim.0c00236

Rosahl, T. W., Geppert, M., Spillane, D., Herz, J., Hammer, R. E., Malenka, R. C., & Südhof, T. C. (1993). Short-term synaptic plasticity is altered in mice lacking synapsin I. *Cell*, *75*(4), 661–670. https://doi.org/10.1016/0092-8674(93)90487-b

Rotermund, N., Winandy, S., Fischer, T., Schulz, K., Fregin, T., Alstedt, N., Buchta, M., Bartels, J., Carlström, M., Lohr, C., & Hirnet, D. (2018). Adenosine A1 receptor activates background potassium channels and modulates information processing in olfactory bulb mitral cells. *The Journal of Physiology*, *596*(4), 717–733. https://doi.org/10.1113/JP275503

Sah, P. (1996). Ca2+-activated K+ currents in neurones: Types, physiological roles and modulation. *Trends in Neurosciences*, *19*(4), 150–154. https://doi.org/10.1016/S0166-2236(96)80026-9

Sah, P., & Louise Faber, E. S. (2002). Channels underlying neuronal calcium-activated potassium currents. *Progress in Neurobiology*, *66*(5), 345–353. https://doi.org/10.1016/S0301-0082(02)00004-7

Sah, P., & McLachlan, E. M. (1991). Ca2+-activated K+ currents underlying the afterhyperpolarization in guinea pig vagal neurons: A role for Ca2+-activated Ca2+ release. *Neuron*, *7*(2), 257–264. https://doi.org/10.1016/0896-6273(91)90264-Z

Sahu, G., & Turner, R. W. (2021). The Molecular Basis for the Calcium-Dependent Slow Afterhyperpolarization in CA1 Hippocampal Pyramidal Neurons. *Frontiers in Physiology*, *12*. https://doi.org/10.3389/fphys.2021.759707

Salmasi, M., Loebel, A., Glasauer, S., & Stemmler, M. (2019). Short-term synaptic depression can increase the rate of information transfer at a release site. *PLOS Computational Biology*, *15*(1), e1006666. https://doi.org/10.1371/journal.pcbi.1006666

Sands, L. P., Jiang, A., Liebenow, B., DiMarco, E., Laxton, A. W., Tatter, S. B., Montague, P. R., & Kishida, K. T. (2023). *Sub-second fluctuations in extracellular dopamine encode reward and punishment prediction errors in humans* (p. 2023.02.24.529709). bioRxiv. https://doi.org/10.1101/2023.02.24.529709

Sauvola, C. W., & Littleton, J. T. (2021). SNARE Regulatory Proteins in Synaptic Vesicle Fusion and Recycling. *Frontiers in Molecular Neuroscience*, *14*. https://doi.org/10.3389/fnmol.2021.733138

Schall, T. A., Wright, W. J., & Dong, Y. (2021). Nucleus Accumbens Fast-spiking Interneurons in Motivational and Addictive Behaviors. *Molecular Psychiatry*, *26*(1), 234–246. https://doi.org/10.1038/s41380-020-0683-y

Schein, J. C., Hunter, D. D., & Roffler-Tarlov, S. (1998). Girk2 Expression in the Ventral Midbrain, Cerebellum, and Olfactory Bulb and Its Relationship to the Murine Mutation*weaver*. *Developmental Biology*, *204*(2), 432–450. https://doi.org/10.1006/dbio.1998.9076

Schmidt, S. G., Malle, M. G., Nielsen, A. K., Bohr, S. S.-R., Pugh, C. F., Nielsen, J. C., Poulsen, I. H., Rand, K. D., Hatzakis, N. S., & Loland, C. J. (2022). The dopamine transporter antiports potassium to increase the uptake of dopamine. *Nature Communications*, *13*(1), 2446. https://doi.org/10.1038/s41467-022-30154-5

Schmidt-Hieber, C., Jonas, P., & Bischofberger, J. (2008). Action potential initiation and propagation in hippocampal mossy fibre axons. *The Journal of Physiology*, *586*(7), 1849–1857. https://doi.org/10.1113/jphysiol.2007.150151

Schmitt, K. C., & Reith, M. E. A. (2010). Regulation of the dopamine transporter. *Annals of the New York Academy of Sciences*, *1187*(1), 316–340. https://doi.org/10.1111/j.1749-6632.2009.05148.x

Schmitt, K. C., & Reith, M. E. A. (2011). The Atypical Stimulant and Nootropic Modafinil Interacts with the Dopamine Transporter in a Different Manner than Classical Cocaine-Like Inhibitors. *PLOS ONE*, *6*(10), e25790. https://doi.org/10.1371/journal.pone.0025790

Schmitz, Y., Schmauss, C., & Sulzer, D. (2002a). Altered Dopamine Release and Uptake Kinetics in Mice Lacking D2 Receptors. *Journal of Neuroscience*, *22*(18), 8002–8009. https://doi.org/10.1523/JNEUROSCI.22-18-08002.2002

Schmitz, Y., Schmauss, C., & Sulzer, D. (2002b). Altered Dopamine Release and Uptake Kinetics in Mice Lacking D2 Receptors. *Journal of Neuroscience*, *22*(18), 8002–8009. https://doi.org/10.1523/JNEUROSCI.22-18-08002.2002

Schuler, V., Lüscher, C., Blanchet, C., Klix, N., Sansig, G., Klebs, K., Schmutz, M., Heid, J., Gentry, C., Urban, L., Fox, A., Spooren, W., Jaton, A.-L., Vigouret, J.-M., Pozza, M., Kelly, P. H., Mosbacher, J., Froestl, W., Käslin, E., … Bettler, B. (2001). Epilepsy, Hyperalgesia, Impaired Memory, and Loss of Pre- and Postsynaptic GABAB Responses in Mice Lacking GABAB(1). *Neuron*, *31*(1), 47–58. https://doi.org/10.1016/S0896-6273(01)00345-2

Schultz, W. (1998). Predictive Reward Signal of Dopamine Neurons. *Journal of Neurophysiology*, *80*(1), 1–27. https://doi.org/10.1152/jn.1998.80.1.1

Schultz, W. (2007). Behavioral dopamine signals. *Trends in Neurosciences*, *30*(5), 203–210. https://doi.org/10.1016/j.tins.2007.03.007

Schultz, W. (2013). Updating dopamine reward signals. *Current Opinion in Neurobiology*, *23*(2), 229–238. https://doi.org/10.1016/j.conb.2012.11.012

Schultz, W. (2016). Dopamine reward prediction-error signalling: A two-component response. *Nature Reviews Neuroscience*, *17*(3), 183–195. https://doi.org/10.1038/nrn.2015.26

Schultz, W., Dayan, P., & Montague, P. R. (1997). A Neural Substrate of Prediction and Reward. *Science*, *275*(5306), 1593–1599. https://doi.org/10.1126/science.275.5306.1593

Schultz, W., Ruffieux, A., & Aebischer, P. (1983). The activity of pars compacta neurons of the monkey substantia nigra in relation to motor activation. *Experimental Brain Research*, *51*(3), 377–387. https://doi.org/10.1007/BF00237874

Scott, S., & Aricescu, A. R. (2019). A structural perspective on GABAA receptor pharmacology. *Current Opinion in Structural Biology*, *54*, 189–197. https://doi.org/10.1016/j.sbi.2019.03.023

Sesack, S. R., Hawrylak, V. A., Guido, M. A., & Levey, A. I. (1997). Cellular and Subcellular Localization of the Dopamine Transporter in Rat Cortex. In D. S. Goldstein, G. Eisenhofer, & R. McCarty (Eds.), *Advances in Pharmacology* (Vol. 42, pp. 171–174). Academic Press. https://doi.org/10.1016/S1054-3589(08)60720-6

Shan, Q., Fang, Q., & Tian, Y. (2022). Evidence that GIRK Channels Mediate the DREADD-hM4Di Receptor Activation-Induced Reduction in Membrane Excitability of Striatal Medium Spiny Neurons. *ACS Chemical Neuroscience*, *13*(14), 2084–2091. https://doi.org/10.1021/acschemneuro.2c00304

Sharp, T., & Barnes, N. M. (2020). Central 5-HT receptors and their function; present and future. *Neuropharmacology*, *177*, 108155. https://doi.org/10.1016/j.neuropharm.2020.108155

Sharpe, A. L., Varela, E., Bettinger, L., & Beckstead, M. J. (2015). Methamphetamine Self-Administration in Mice Decreases GIRK Channel-Mediated Currents in Midbrain Dopamine Neurons. *International Journal of Neuropsychopharmacology*, *18*(5), pyu073. https://doi.org/10.1093/ijnp/pyu073

Shields, B. C., Kahuno, E., Kim, C., Apostolides, P. F., Brown, J., Lindo, S., Mensh, B. D., Dudman, J. T., Lavis, L. D., & Tadross, M. R. (2017). Deconstructing behavioral neuropharmacology with cellular specificity. *Science*, *356*(6333), eaaj2161. https://doi.org/10.1126/science.aaj2161

Shields, B. C., Yan, H., Lim, S. S. X., Burwell, S. C. V., Cammarata, C. M., Fleming, E. A., Yousefzadeh, S. A., Goldenshtein, V. Z., Kahuno, E. W., Vagadia, P. P., Loughran, M. H., Zhiquan, L., McDonnell, M. E., Scalabrino, M. L., Thapa, M., Hawley, T. M., Field, G. D., Hull, C., Schiltz, G. E., … Tadross, M. R. (2024). DART.2: Bidirectional synaptic pharmacology with thousandfold cellular specificity. *Nature Methods*, *21*(7), 1288–1297. https://doi.org/10.1038/s41592-024-02292-9

Shin, J. H., Goldbach, H. C., Burke, D. A., Authement, M. E., Swanson, E. S., Bocarsly, M. E., Hernandez, S., Kwon, H. B., Cerveny, S. E., Mehr, J. B., Plotnikova, A. S., Mohanty, A., Cummins, A. C., Pelkey, K. A., McBain, C. J., Khaliq, Z. M., Eldridge, M. A. G., Averbeck, B. B., & Alvarez, V. A. (2025). Local Regulation of Striatal Dopamine Release Shifts from Predominantly Cholinergic in Mice to GABAergic in Macaques. *Journal of Neuroscience*, *45*(11). https://doi.org/10.1523/JNEUROSCI.1692-24.2025

Shink, E., Bevan, M. D., Bolam, J. P., & Smith, Y. (1996). The subthalamic nucleus and the external pallidum: Two tightly interconnected structures that control the output of the basal ganglia in the monkey. *Neuroscience*, *73*(2), 335–357. https://doi.org/10.1016/0306-4522(96)00022-X

Shoaib, M., Swanner, L. S., Beyer, C. E., Goldberg, S. R., & Schindler, C. W. (1998). The GABAB agonist baclofen modifies cocaine self-administration in rats. *Behavioural Pharmacology*, *9*(3), 195–206.

Shu, Y., Hasenstaub, A., Duque, A., Yu, Y., & McCormick, D. A. (2006). Modulation of intracortical synaptic potentials by presynaptic somatic membrane potential. *Nature*, *441*(7094), 761–765. https://doi.org/10.1038/nature04720

Silva, J. (2014). Slow Inactivation of Na+ Channels. In P. C. Ruben (Ed.), *Voltage Gated Sodium Channels* (pp. 33–49). Springer. https://doi.org/10.1007/978-3-642-41588-3_3

Simon, J., Wakimoto, H., Fujita, N., Lalande, M., & Barnard, E. A. (2004). Analysis of the Set of GABAA Receptor Genes in the Human Genome*. *Journal of Biological Chemistry*, *279*(40), 41422–41435. https://doi.org/10.1074/jbc.M401354200

Simonds, W. F. (1999). G protein regulation of adenylate cyclase. *Trends in Pharmacological Sciences*, *20*(2), 66–73. https://doi.org/10.1016/S0165-6147(99)01307-3

Smarr, B., & Kriegsfeld, L. J. (2022). Female mice exhibit less overall variance, with a higher proportion of structured variance, than males at multiple timescales of continuous body temperature and locomotive activity records. *Biology of Sex Differences*, *13*(1), 41. https://doi.org/10.1186/s13293-022-00451-1

Smith, Y., Bevan, M. D., Shink, E., & Bolam, J. P. (1998). Microcircuitry of the direct and indirect pathways of the basal ganglia. *Neuroscience*, *86*(2), 353–387. Scopus. https://doi.org/10.1016/S0306-4522(98)00004-9

Snutch, T. P. (2009). Voltage-Gated Calcium Channels. In L. R. Squire (Ed.), *Encyclopedia of Neuroscience* (pp. 427–441). Academic Press. https://doi.org/10.1016/B978-008045046-9.01370-X

Söllner, T., Whiteheart, S. W., Brunner, M., Erdjument-Bromage, H., Geromanos, S., Tempst, P., & Rothman, J. E. (1993). SNAP receptors implicated in vesicle targeting and fusion. *Nature*, *362*(6418), 318–324. https://doi.org/10.1038/362318a0

Sonders, M. S., Zhu, S.-J., Zahniser, N. R., Kavanaugh, M. P., & Amara, S. G. (1997). Multiple Ionic Conductances of the Human Dopamine Transporter: The Actions of Dopamine and Psychostimulants. *Journal of Neuroscience*, *17*(3), 960–974. https://doi.org/10.1523/JNEUROSCI.17-03-00960.1997

Sørensen, G., Rickhag, M., Leo, D., Lycas, M. D., Ridderstrøm, P. H., Weikop, P., Lilja, J. H., Rifes, P., Herborg, F., Woldbye, D., Wörtwein, G., Gainetdinov, R. R., Fink-Jensen, A., & Gether, U. (2021). Disruption of the PDZ domain–binding motif of the dopamine transporter uniquely alters nanoscale distribution, dopamine homeostasis, and

reward motivation. *Journal of Biological Chemistry*, *297*(6), 101361. https://doi.org/10.1016/j.jbc.2021.101361

Sossi, V., de la Fuente-Fernández, R., Nandhagopal, R., Schulzer, M., McKenzie, J., Ruth, T. J., Aasly, J. O., Farrer, M. J., Wszolek, Z. K., & Stoessl, J. A. (2010). Dopamine turnover increases in asymptomatic LRRK2 mutations carriers. *Movement Disorders*, *25*(16), 2717–2723. https://doi.org/10.1002/mds.23356

Spano, P., Govoni, S., & Trabucchi, M. (1978). Studies on the pharmacological properties of dopamine receptors in various areas of the central nervous system. *Advances in Biochemical Psychopharmacology*. https://www.semanticscholar.org/paper/Studies-on-the-pharmacological-properties-of-in-of-Spano-Govoni/bb9b01a4d92847d5907d1a4faea2cd945b408ebe

Specht, C. G., & Schoepfer, R. (2001). Deletion of the alpha-synuclein locus in a subpopulation of C57BL/6J inbred mice. *BMC Neuroscience*, *2*(1), 11. https://doi.org/10.1186/1471-2202-2-11

Spruston, N. (2009). Dendritic Signal Integration. In L. R. Squire (Ed.), *Encyclopedia of Neuroscience* (pp. 445–452). Academic Press. https://doi.org/10.1016/B978-008045046-9.01648-X

Spruston, N., Stuart, G., Häusser, M., Stuart, G., Spruston, N., & Häusser, M. (Eds.). (2016). Principles of dendritic integration. In *Dendrites* (p. 0). Oxford University Press. https://doi.org/10.1093/acprof:oso/9780198745273.003.0012

Srivastava, D. K., Navratna, V., Tosh, D. K., Chinn, A., Sk, M. F., Tajkhorshid, E., Jacobson, K. A., & Gouaux, E. (2024). Structure of the human dopamine transporter and mechanisms of inhibition. *Nature*, *632*(8025), 672–677. https://doi.org/10.1038/s41586-024-07739-9

Stamford, J. A., Kruk, Z. L., & Millar, J. (1986). Sub-second striatal dopamine release measured by in vivo voltammetry. *Brain Research*, *381*(2), 351–355. https://doi.org/10.1016/0006-8993(86)90087-9

Stedehouder, J., Roberts, B. M., Raina, S., Bossi, S., Liu, A. K. L., Doig, N. M., McGerty, K., Magill, P. J., Parkkinen, L., & Cragg, S. J. (2024). Rapid modulation of striatal cholinergic interneurons and dopamine release by satellite astrocytes. *Nature Communications*, *15*(1), 10017. https://doi.org/10.1038/s41467-024-54253-7

Steinecker, B., Rosker, C., & Schreibmayer, W. (2007). The GIRK1 Brain Variant GIRK1d and Its Functional Impact on Heteromultimeric GIRK Channels. *Journal of Receptors and Signal Transduction*. https://doi.org/10.1080/10799890701713073

Stensrud, M. J., Puchades, M., & Gundersen, V. (2014). GABA is localized in dopaminergic synaptic vesicles in the rodent striatum. *Brain Structure and Function*, *219*(6), 1901–1912. https://doi.org/10.1007/s00429-013-0609-4

St-Pierre, F., Marshall, J. D., Yang, Y., Gong, Y., Schnitzer, M. J., & Lin, M. Z. (2014). High-fidelity optical reporting of neuronal electrical activity with an ultrafast fluorescent voltage sensor. *Nature Neuroscience*, *17*(6), 884–889. https://doi.org/10.1038/nn.3709

Stuart, G., & Häusser, M. (1994). Initiation and spread of sodium action potentials in cerebellar purkinje cells. *Neuron*, *13*(3), 703–712. https://doi.org/10.1016/0896-6273(94)90037-X

Stuart, G. J., & Spruston, N. (2015). Dendritic integration: 60 years of progress. *Nature Neuroscience*, *18*(12), 1713–1721. https://doi.org/10.1038/nn.4157

Stuart, G., & Sakmann, B. (1995). Amplification of EPSPs by axosomatic sodium channels in neocortical pyramidal neurons. *Neuron*, *15*(5), 1065–1076. https://doi.org/10.1016/0896-6273(95)90095-0

Stuber, G. D., Hnasko, T. S., Britt, J. P., Edwards, R. H., & Bonci, A. (2010). Dopaminergic Terminals in the Nucleus Accumbens But Not the Dorsal Striatum Corelease

Glutamate. *Journal of Neuroscience*, *30*(24), 8229–8233. https://doi.org/10.1523/JNEUROSCI.1754-10.2010

Südhof, T. C. (2013). Neurotransmitter Release: The Last Millisecond in the Life of a Synaptic Vesicle. *Neuron*, *80*(3), 675–690. https://doi.org/10.1016/j.neuron.2013.10.022

Südhof, T. C., & Rothman, J. E. (2009). Membrane Fusion: Grappling with SNARE and SM Proteins. *Science*, *323*(5913), 474–477. https://doi.org/10.1126/science.1161748

Sulzer, D., Cragg, S. J., & Rice, M. E. (2016). Striatal dopamine neurotransmission: Regulation of release and uptake. *Basal Ganglia*, *6*(3), 123–148. https://doi.org/10.1016/j.baga.2016.02.001

Sulzer, D., & Galli, A. (2003). Dopamine transport currents are promoted from curiosity to physiology. *Trends in Neurosciences*, *26*(4), 173–176. https://doi.org/10.1016/S0166-2236(03)00063-8

Sun, F., Zeng, J., Jing, M., Zhou, J., Feng, J., Owen, S. F., Luo, Y., Li, F., Wang, H., Yamaguchi, T., Yong, Z., Gao, Y., Peng, W., Wang, L., Zhang, S., Du, J., Lin, D., Xu, M., Kreitzer, A. C., … Li, Y. (2018). A Genetically Encoded Fluorescent Sensor Enables Rapid and Specific Detection of Dopamine in Flies, Fish, and Mice. *Cell*, *174*(2), 481-496.e19. https://doi.org/10.1016/j.cell.2018.06.042

Swant, J., Goodwin, J. S., North, A., Ali, A. A., Gamble-George, J., Chirwa, S., & Khoshbouei, H. (2011). α-Synuclein Stimulates a Dopamine Transporter-dependent Chloride Current and Modulates the Activity of the Transporter. *The Journal of Biological Chemistry*, *286*(51), 43933–43943. https://doi.org/10.1074/jbc.M111.241232

Takagi, H. (2000). Roles of ion channels in EPSP integration at neuronal dendrites. *Neuroscience Research*, *37*(3), 167–171. https://doi.org/10.1016/S0168-0102(00)00120-6

Tariq, K., & Luikart, B. W. (2021). Striking a balance: PIP2 and PIP3 signaling in neuronal health and disease. *Exploration of Neuroprotective Therapy*, *1*(2), Article 2. https://doi.org/10.37349/ent.2021.00008

Tepper, J. M., Abercrombie, E. D., & Bolam, J. P. (2007). Basal ganglia macrocircuits. In J. M. Tepper, E. D. Abercrombie, & J. P. Bolam (Eds.), *Progress in Brain Research* (Vol. 160, pp. 3–7). Elsevier. https://doi.org/10.1016/S0079-6123(06)60001-0

Tepper, J. M., Koós, T., Ibanez-Sandoval, O., Tecuapetla, F., Faust, T. W., & Assous, M. (2018). Heterogeneity and Diversity of Striatal GABAergic Interneurons: Update 2018. *Frontiers in Neuroanatomy*, *12*. https://doi.org/10.3389/fnana.2018.00091

Tepper, J. M., Tecuapetla, F., Koos, T., & Ibanez-Sandoval, O. (2010). Heterogeneity and Diversity of Striatal GABAergic Interneurons. *Frontiers in Neuroanatomy*, *4*. https://doi.org/10.3389/fnana.2010.00150

Terunuma, M. (2018). Diversity of structure and function of GABAB receptors: A complexity of GABAB-mediated signaling. *Proceedings of the Japan Academy, Series B*, *94*(10), 390–411. https://doi.org/10.2183/pjab.94.026

Thompson, S. M., & Gähwiler, B. H. (1992). Comparison of the actions of baclofen at pre- and postsynaptic receptors in the rat hippocampus in vitro. *The Journal of Physiology*, *451*(1), 329–345. https://doi.org/10.1113/jphysiol.1992.sp019167

Thomson, A. M. (2000). Molecular frequency filters at central synapses. *Progress in Neurobiology*, *62*(2), 159–196. https://doi.org/10.1016/S0301-0082(00)00008-3

Threlfell, S., Lalic, T., Platt, N. J., Jennings, K. A., Deisseroth, K., & Cragg, S. J. (2012). Striatal Dopamine Release Is Triggered by Synchronized Activity in Cholinergic Interneurons. *Neuron*, *75*(1), 58–64. https://doi.org/10.1016/j.neuron.2012.04.038

Threlfell, S., Mohammadi, A. S., Ryan, B. J., Connor-Robson, N., Platt, N. J., Anand, R., Serres, F., Sharp, T., Bengoa-Vergniory, N., Wade-Martins, R., Ewing, A., Cragg, S. J., & Brimblecombe, K. R. (2021). Striatal Dopamine Transporter Function Is Facilitated by

Converging Biology of α-Synuclein and Cholesterol. *Frontiers in Cellular Neuroscience*, *15*. https://doi.org/10.3389/fncel.2021.658244

Toib, A., Lyakhov, V., & Marom, S. (1998). Interaction between Duration of Activity and Time Course of Recovery from Slow Inactivation in Mammalian Brain Na+Channels. *Journal of Neuroscience*, *18*(5), 1893–1903. https://doi.org/10.1523/JNEUROSCI.18-05-01893.1998

Tol, H. H. M. V., Wu, C. M., Guan, H.-C., Ohara, K., Bunzow, J. R., Civelli, O., Kennedy, J., Seeman, P., Niznik, H. B., & Jovanovic, V. (1992). Multiple dopamine D4 receptor variants in the human population. *Nature*, *358*(6382), 149–152. https://doi.org/10.1038/358149a0

Tritsch, N. X., Ding, J. B., & Sabatini, B. L. (2012). Dopaminergic neurons inhibit striatal output through non-canonical release of GABA. *Nature*, *490*(7419), 262–266. https://doi.org/10.1038/nature11466

Tritsch, N. X., Oh, W.-J., Gu, C., & Sabatini, B. L. (2014). Midbrain dopamine neurons sustain inhibitory transmission using plasma membrane uptake of GABA, not synthesis. *eLife*, *3*, e01936. https://doi.org/10.7554/eLife.01936

Turner, R. W., Kruskic, M., Teves, M., Scheidl-Yee, T., Hameed, S., & Zamponi, G. W. (2015). Neuronal expression of the intermediate conductance calcium-activated potassium channel KCa3.1 in the mammalian central nervous system. *Pflügers Archiv - European Journal of Physiology*, *467*(2), 311–328. https://doi.org/10.1007/s00424-014-1523-1

Tyurikova, O., Kopach, O., Zheng, K., Rathore, D., Codadu, N., Wu, S.-Y., Shen, Y., Campbell, R. E., Wykes, R. C., Volynski, K., Savtchenko, L. P., & Rusakov, D. A. (2025). Astrocyte Kir4.1 expression level territorially controls excitatory transmission in the brain. *Cell Reports*, *44*(2). https://doi.org/10.1016/j.celrep.2025.115299

Ueda, T., & Greengard, P. (1977). Adenosine 3':5'-monophosphate-regulated phosphoprotein system of neuronal membranes. I. Solubilization, purification, and some properties of an endogenous phosphoprotein. *Journal of Biological Chemistry*, *252*(14), 5155–5163. https://doi.org/10.1016/S0021-9258(17)40170-0

Um, K. B., Hahn, S., Kim, S. W., Lee, Y. J., Birnbaumer, L., Kim, H. J., & Park, M. K. (2021). TRPC3 and NALCN channels drive pacemaking in substantia nigra dopaminergic neurons. *eLife*, *10*, e70920. https://doi.org/10.7554/eLife.70920

Vallone, D., Picetti, R., & Borrelli, E. (2000). Structure and function of dopamine receptors. *Neuroscience & Biobehavioral Reviews*, *24*(1), 125–132. https://doi.org/10.1016/S0149-7634(99)00063-9

Vandael, D. H. F., Ottaviani, M. M., Legros, C., Lefort, C., Guérineau, N. C., Allio, A., Carabelli, V., & Carbone, E. (2015). Reduced availability of voltage-gated sodium channels by depolarization or blockade by tetrodotoxin boosts burst firing and catecholamine release in mouse chromaffin cells. *The Journal of Physiology*, *593*(Pt 4), 905–927. https://doi.org/10.1113/jphysiol.2014.283374

Vandecasteele, M., Glowinski, J., Deniau, J.-M., & Venance, L. (2008). Chemical transmission between dopaminergic neuron pairs. *Proceedings of the National Academy of Sciences*, *105*(12), 4904–4909. https://doi.org/10.1073/pnas.0703121105

Vandecasteele, M., Glowinski, J., & Venance, L. (2005). Electrical synapses between dopaminergic neurons of the substantia nigra pars compacta. *The Journal of Neuroscience: The Official Journal of the Society for Neuroscience*, *25*(2), 291–298. https://doi.org/10.1523/JNEUROSCI.4167-04.2005

Vaughan, R. A., & Foster, J. D. (2013). Mechanisms of dopamine transporter regulation in normal and disease states. *Trends in Pharmacological Sciences*, *34*(9), 489–496. https://doi.org/10.1016/j.tips.2013.07.005

Venton, B. J., Seipel, A. T., Phillips, P. E. M., Wetsel, W. C., Gitler, D., Greengard, P., Augustine, G. J., & Wightman, R. M. (2006). Cocaine Increases Dopamine Release by Mobilization of a Synapsin-Dependent Reserve Pool. *Journal of Neuroscience*, *26*(12), 3206–3209. https://doi.org/10.1523/JNEUROSCI.4901-04.2006

Verma, V. (2015). Classic Studies on the Interaction of Cocaine and the Dopamine Transporter. *Clinical Psychopharmacology and Neuroscience*, *13*(3), 227–238. https://doi.org/10.9758/cpn.2015.13.3.227

Victoria, N. C., Marron Fernandez de Velasco, E., Ostrovskaya, O., Metzger, S., Xia, Z., Kotecki, L., Benneyworth, M. A., Zink, A. N., Martemyanov, K. A., & Wickman, K. (2016). G Protein-Gated K+ Channel Ablation in Forebrain Pyramidal Neurons Selectively Impairs Fear Learning. *Biological Psychiatry*, *80*(10), 796–806. https://doi.org/10.1016/j.biopsych.2015.10.004

Villette, V., Chavarha, M., Dimov, I. K., Bradley, J., Pradhan, L., Mathieu, B., Evans, S. W., Chamberland, S., Shi, D., Yang, R., Kim, B. B., Ayon, A., Jalil, A., St-Pierre, F., Schnitzer, M. J., Bi, G., Toth, K., Ding, J., Dieudonné, S., & Lin, M. Z. (2019). Ultrafast Two-Photon Imaging of a High-Gain Voltage Indicator in Awake Behaving Mice. *Cell*, *179*(7), 1590-1608.e23. https://doi.org/10.1016/j.cell.2019.11.004

Voorn, P., Vanderschuren, L. J. M. J., Groenewegen, H. J., Robbins, T. W., & Pennartz, C. M. A. (2004). Putting a spin on the dorsal–ventral divide of the striatum. *Trends in Neurosciences*, *27*(8), 468–474. https://doi.org/10.1016/j.tins.2004.06.006

Wanat, M. J., Hopf, F. W., Stuber, G. D., Phillips, P. E. M., & Bonci, A. (2008). Corticotropin-releasing factor increases mouse ventral tegmental area dopamine neuron firing through a protein kinase C-dependent enhancement of Ih. *The Journal of Physiology*, *586*(8), 2157–2170. https://doi.org/10.1113/jphysiol.2007.150078

Wang, J., Su, M., Zhang, D., Zhang, L., Niu, C., Li, C., You, S., Sang, Y., Zhang, Y., Du, X., & Zhang, H. (2024). The cation channel mechanisms of subthreshold inward

depolarizing currents in the mice VTA dopaminergic neurons and their roles in the chronic-stress-induced depression-like behavior. *eLife*, *12*, RP88319. https://doi.org/10.7554/eLife.88319

Watanabe, M., Maemura, K., Kanbara, K., Tamayama, T., & Hayasaki, H. (2002). GABA and GABA Receptors in the Central Nervous System and Other Organs. In K. W. Jeon (Ed.), *International Review of Cytology* (Vol. 213, pp. 1–47). Academic Press. https://doi.org/10.1016/S0074-7696(02)13011-7

White, J. H., Wise, A., Main, M. J., Green, A., Fraser, N. J., Disney, G. H., Barnes, A. A., Emson, P., Foord, S. M., & Marshall, F. H. (1998). Heterodimerization is required for the formation of a functional GABAB receptor. *Nature*, *396*(6712), 679–682. https://doi.org/10.1038/25354

Williams, S. R., & Atkinson, S. E. (2008). Dendritic synaptic integration in central neurons. *Current Biology*, *18*(22), R1045–R1047. https://doi.org/10.1016/j.cub.2008.08.060

Wilson, C. J., Groves, P. M., & Fifková, E. (1977). Monoaminergic synapses, including dendro-dendritic synapses in the rat substantia nigra. *Experimental Brain Research*, *30*(2–3), 161–174. https://doi.org/10.1007/BF00237248

Wise, R. A. (2004). Dopamine, learning and motivation. *Nature Reviews Neuroscience*, *5*(6), 483–494. https://doi.org/10.1038/nrn1406

Wolfart, J., Neuhoff, H., Franz, O., & Roeper, J. (2001). Differential Expression of the Small-Conductance, Calcium-Activated Potassium Channel SK3 Is Critical for Pacemaker Control in Dopaminergic Midbrain Neurons. *Journal of Neuroscience*, *21*(10), 3443–3456. https://doi.org/10.1523/JNEUROSCI.21-10-03443.2001

Wright, S. N., Wang, S. Y., Kallen, R. G., & Wang, G. K. (1997). Differences in steady-state inactivation between Na channel isoforms affect local anesthetic binding affinity. *Biophysical Journal*, *73*(2), 779–788. https://doi.org/10.1016/S0006-3495(97)78110-4

Wu, Q., Reith, M. E. A., Walker, Q. D., Kuhn, C. M., Carroll, F. I., & Garris, P. A. (2002). Concurrent Autoreceptor-Mediated Control of Dopamine Release and Uptake during Neurotransmission: An In Vivo Voltammetric Study. *Journal of Neuroscience*, *22*(14), 6272–6281. https://doi.org/10.1523/JNEUROSCI.22-14-06272.2002

Xu, L., & Chen, L. Y. (2020). Identification of a New Allosteric Binding Site for Cocaine in Dopamine Transporter. *Journal of Chemical Information and Modeling*, *60*(8), 3958–3968. https://doi.org/10.1021/acs.jcim.0c00346

Yamashita, A., Singh, S. K., Kawate, T., Jin, Y., & Gouaux, E. (2005). Crystal structure of a bacterial homologue of Na+/Cl—Dependent neurotransmitter transporters. *Nature*, *437*(7056), 215–223. https://doi.org/10.1038/nature03978

Yang, J., Ye, M., Tian, C., Yang, M., Wang, Y., & Shu, Y. (2013). Dopaminergic modulation of axonal potassium channels and action potential waveform in pyramidal neurons of prefrontal cortex. *The Journal of Physiology*, *591*(13), 3233–3251. https://doi.org/10.1113/jphysiol.2013.251058

Yu, F. H., & Catterall, W. A. (2003). Overview of the voltage-gated sodium channel family. *Genome Biology*, *4*(3), 207. https://doi.org/10.1186/gb-2003-4-3-207

Yung, K. K. L., Bolam, J. P., Smith, A. D., Hersch, S. M., Ciliax, B. J., & Levey, A. I. (1995). Immunocytochemical localization of D1 and D2 dopamine receptors in the basal ganglia of the rat: Light and electron microscopy. *Neuroscience*, *65*(3), 709–730. https://doi.org/10.1016/0306-4522(94)00536-E

Zaltieri, M., Grigoletto, J., Longhena, F., Navarria, L., Favero, G., Castrezzati, S., Colivicchi, M. A., Della Corte, L., Rezzani, R., Pizzi, M., Benfenati, F., Spillantini, M. G., Missale, C., Spano, P., & Bellucci, A. (2015). α-synuclein and synapsin III cooperatively regulate synaptic function in dopamine neurons. *Journal of Cell Science*, *128*(13), 2231–2243. https://doi.org/10.1242/jcs.157867

Zhang, H., & Sulzer, D. (2004). Frequency-dependent modulation of dopamine release by nicotine. *Nature Neuroscience*, *7*(6), 581–582. https://doi.org/10.1038/nn1243

Zhang, M., & Augustine, G. J. (2021). Synapsins and the Synaptic Vesicle Reserve Pool: Floats or Anchors? *Cells*, *10*(3), Article 3. https://doi.org/10.3390/cells10030658

Zhang, S. J., & Jackson, M. B. (1995). GABAA receptor activation and the excitability of nerve terminals in the rat posterior pituitary. *The Journal of Physiology*, *483*(3), 583–595. https://doi.org/10.1113/jphysiol.1995.sp020608

Zhao, Y., Gameiro-Ros, I., Glaaser, I. W., & Slesinger, P. A. (2021). Advances in Targeting GIRK Channels in Disease. *Trends in Pharmacological Sciences*, *42*(3), 203–215. https://doi.org/10.1016/j.tips.2020.12.002

Zhou, F.-M., Liang, Y., & Dani, J. A. (2001). Endogenous nicotinic cholinergic activity regulates dopamine release in the striatum. *Nature Neuroscience*, *4*(12), 1224–1229. https://doi.org/10.1038/nn769

Zucker, R. S., & Regehr, W. G. (2002). Short-Term Synaptic Plasticity. *Annual Review of Physiology*, *64*(Volume 64, 2002), 355–405. https://doi.org/10.1146/annurev.physiol.64.092501.114547

Żuk, J., Bartuzi, D., Matosiuk, D., & Kaczor, A. A. (2020). Preferential Coupling of Dopamine D2S and D2L Receptor Isoforms with Gi1 and Gi2 Proteins—In Silico Study. *International Journal of Molecular Sciences*, *21*(2), Article 2. https://doi.org/10.3390/ijms21020436

Zych, S. M., & Ford, C. P. (2022). Divergent properties and independent regulation of striatal dopamine and GABA co-transmission. *Cell Reports*, *39*(7), 110823. https://doi.org/10.1016/j.celrep.2022.110823